

NPS ARCHIVE
1968
GARRITSON, G.

LIBRARY
NAVAL POSTGRADUATE SCHOOL
MONTEREY, CALIF. 93940



ABSOLUTE PAIR CREATION CROSS SECTIONS
USING MONOENERGETIC PHOTONS

DISSERTATION

Submitted to the Graduate School of the
University of Notre Dame in Partial Fulfillment
of the Requirements for the Degree of
Doctor of Philosophy

By

Lieutenant Grant R. Garritson, U. S. Navy, B. S.

ACKNOWLEDGEMENTS

I would like to thank Doctor W. C. Miller for his patience and untiring assistance during the course of this research. Also, thanks go to Doctor Sperry E. Darden and Doctor Paul R. Chagnon for the use of experimental apparatus.

Particular thanks go to the members of the Electron Group for unremitting assistance and helpful advice in preparing and performing the research: R. J. Foust, for his tolerant patience and probing questions; James M. Piowaty, for valuable discussion on theory and electronics; Dennis L. Friesel, for countless invaluable tasks ably carried out; and Dennis A. Justice, for assistance in collecting the data. To my fellow graduate students in the Nuclear Structure Laboratory, I express my gratitude for their encouragement.

Special thanks are extended to Brother Cosmos, C.S.C., and the members of the Physics Department Shop for their construction of much of the apparatus used and their prompt and expert attention to the smallest detail.

I also take this opportunity to thank the United States Navy which, through the Junior Line Officer Advanced Scientific Educational Program (Burke Program), has made this research possible.

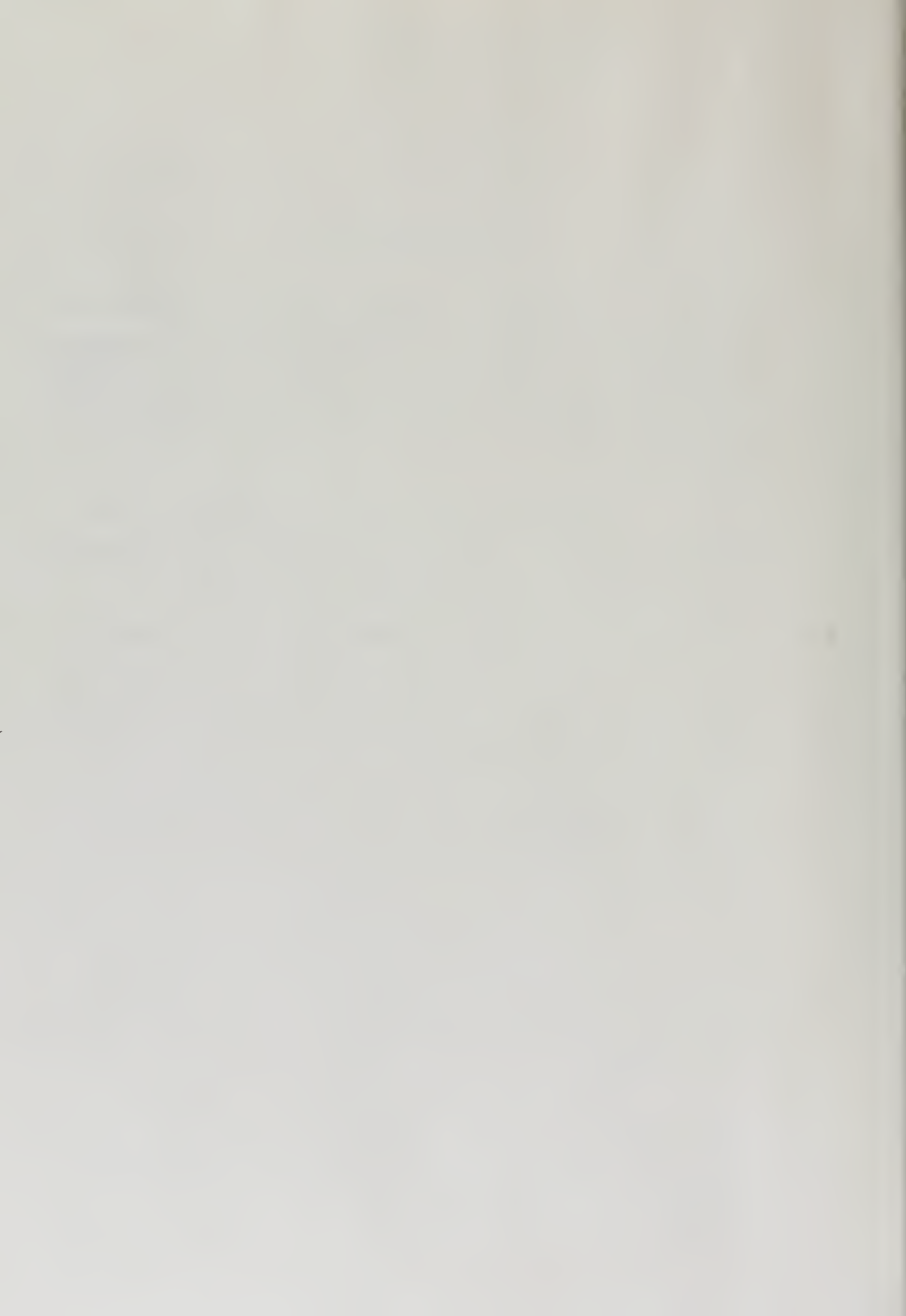
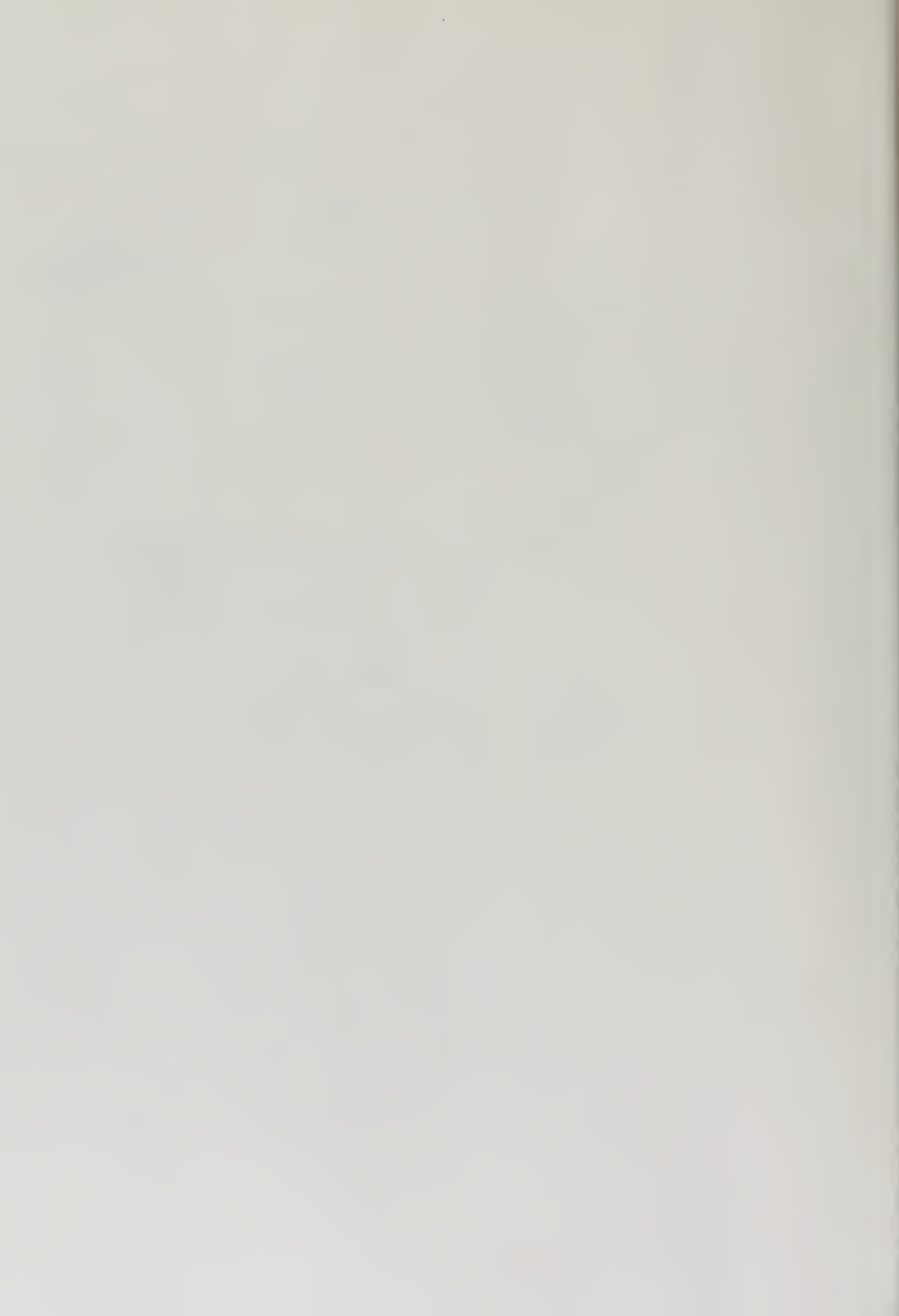
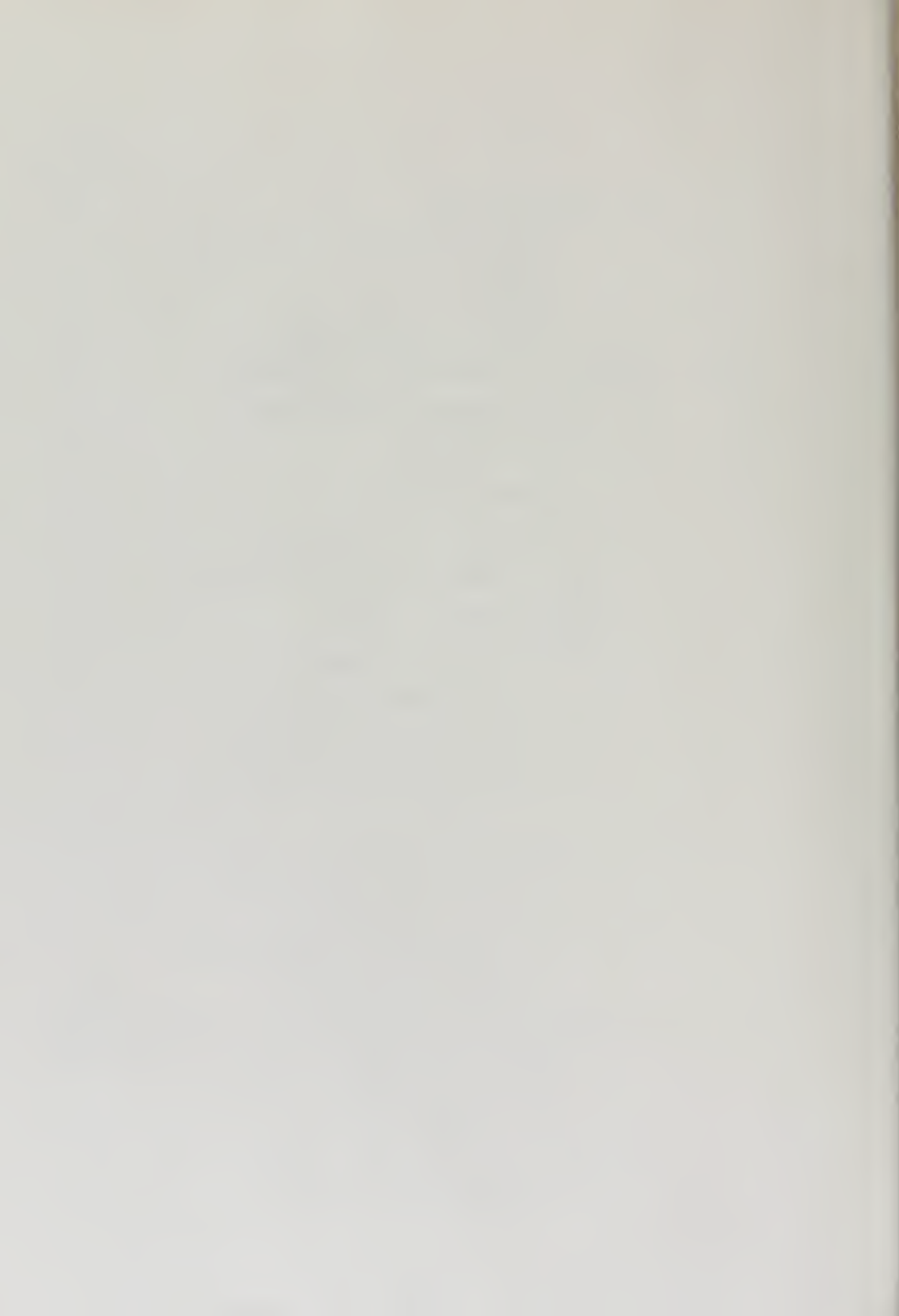


TABLE OF CONTENTS

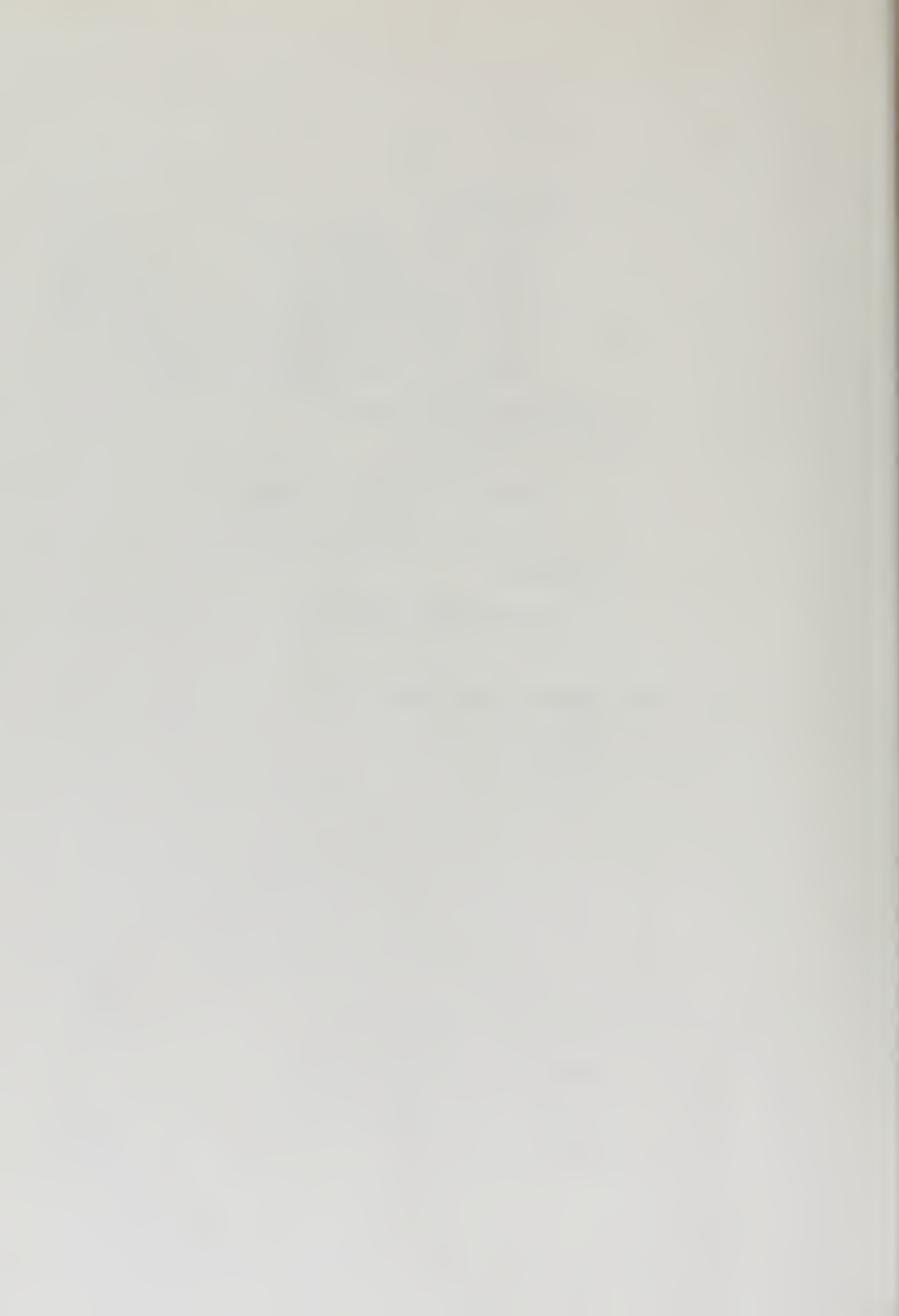
	Page
I. INTRODUCTION	1
A. Pair Creation	1
B. The Monochromatic Principle	10
C. Bremsstrahlung	15
II. THEORY	20
A. Pair Creation	
1. The Cross Section for Pair Creation	20
a. Cross Sections Due to Bethe and Heitler	21
b. Cross Section Due to Jaeger and Hulme and Jaeger	24
c. Other Approximate Pair Creation Cross Sections	25
2. The Yield Expression	27
a. Small Thin Target	28
b. Small Thick Target	30
c. Large Thick Target	31
3. Competing Processes	34
a. Inelastic Processes	34
b. Elastic Processes	36
c. Background Effects	37



B.	Bremsstrahlung	40
1.	Cross Section Due to Bethe and Heitler	40
2.	Other Approximate Theories	42
III.	EXPERIMENTAL APPARATUS AND PROCEDURE	45
A.	General Equipment and Procedure	45
B.	The Monochromator	45
1.	Theory and Design	46
2.	Parameters of Performance	56
a.	Transmission and Resolution	57
b.	Figure of Merit	59
c.	Electron Scattering	60
1.	Elastic Scattering	61
1i.	Inelastic Scattering	65
11i.	The Excessive Electron Count rate	66
3.	Monochromator Configurations	67
a.	Initial Configuration	67
b.	Intermediate Configuration	68
c.	Final Configuration	69
C.	Bremsstrahlung and Pair Creation Targets	70
1.	Bremsstrahlung Target Foils	70
2.	Pair Creation Targets	70
D.	Detection and Counting Systems	72
1.	The Experimental Layout	72



2.	Electronics	74
a.	The Fast Electron Arm	76
b.	The Fast Photon Arm	76
c.	Intrinsic Circuit Resolving Time	77
d.	Overall Circuit Resolving Time	78
E.	Detection Efficiencies	79
F.	Photon Shielding	81
1.	Electron Detector Shielding	82
2.	The Photon Detectors Shielding	84
G.	Procedure	
1.	The Bremsstrahlung Cross Sections	86
2.	Pair Creation	87
IV.	DATA REDUCTION AND ANALYSIS	91
A.	Monoenergetic Photons	91
B.	Evaluation of the Yield Expression	91
1.	Target Volume Summation	92
2.	Effects of Target Thickness and Area	93
a.	Effects Due to Target Thickness	93
b.	Effects Due to Target Area	95
C.	Pair Creation	96
V.	CONCLUSIONS AND SUMMARY	100
A.	Monochromatic Technique and Bremsstrahlung Cross Sections	100
B.	Pair Creation	101



APPENDICES

A. The Accelerator	104
B. The Beam Handling System	108
C. Energy Calibration	111
1. The 60° Analyzing Magnet	111
2. The Monochromator Magnet	113
D. Analog Ray Tracing Device	116
E. Evaluation of the Monochromatic Technique	119
1. Nuclear Resonance Fluorescence	119
2. (γ ,n) Reactions	120
3. Bremsstrahlung Cross Section Measurements	121
4. Possible Technique Improvements	121
a. Pole Piece Design	123
b. System Size	125
c. Detection System and Electronics	126
F. Transmission and Resolution	128

REFERENCES

130



ABSTRACT

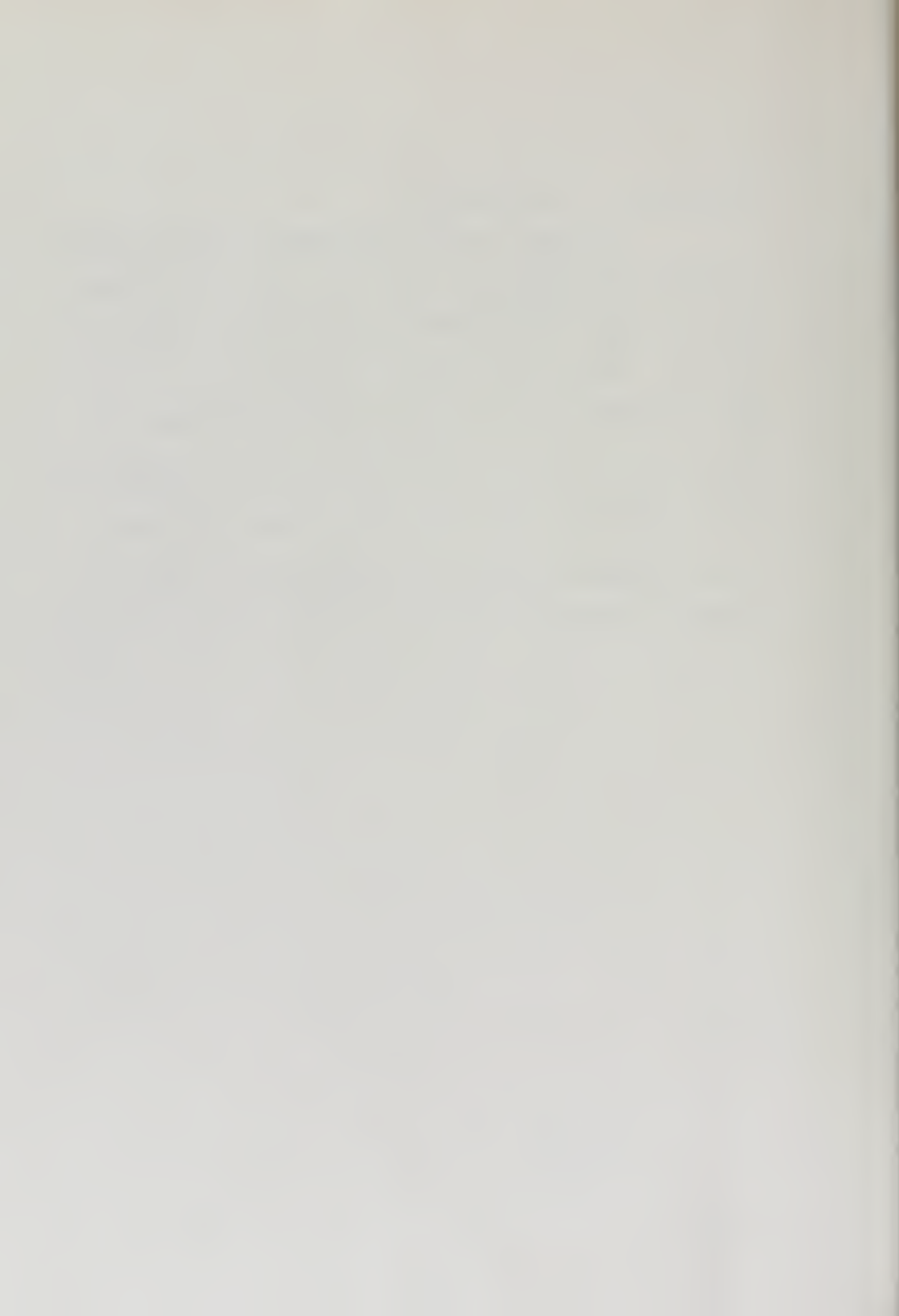
The photon monochromator, designed and built in this laboratory by Walter and Shea and also studied by Malaker, has been further developed in the course of the present research. The transmission of the device has been improved by a factor of 2.6 and the electron count rate reduced by a factor of three. Monoenergetic photons produced by the monochromatic technique have been studied at incident electron energies of 1.54, 2.30, and 2.86 MeV. These studies reveal that the monoenergetic photon production equals that predicted by theory and measured in previous experiments over the energy range of interest. The monoenergetic photons, with an energy spread of less than two percent, have been used to study the pair creation cross section over the incident photon energy range of 1.2 to 2.0 MeV for the elements tin and lead.

Particular attention has been given to the pair creation cross section for tin and lead at the incident photon energy 1.533 MeV since the exact calculations of Jaeger and Hulme are available. Use of the monochromatic technique enables a study of the pair creation process, variable over incident photon energy, to be made. The cross sections measured are absolute values which are not normalized to any other pair creation cross section,



theoretical or experimental.

The cross section measurements, made at photon energies of 1.20, 1.533, 1.57, 1.71, 1.85, and 2.0 MeV, give the ratio of experiment to the theory of Bethe and Heitler, $\sigma_{\text{PAIR}}(\text{EXP}) / \sigma_{\text{PAIR}}(\text{B-H})$, as $2.60 \pm .7$ at 1.20 MeV decreasing to $1.53^{+.19}_{-.17}$ at 2.00 MeV for lead. The same ratio for tin is $1.52^{+.44}_{-.35}$ at 1.20 MeV decreasing to $1.33^{+.23}_{-.21}$ at 2.00 MeV. The ratio of the experimental cross sections to the exact calculations of Jaeger and Hulme at 1.533 MeV are $1.14 \pm .14$ for lead and $1.05^{+.12}_{-.10}$ for tin.



I. INTRODUCTION

A. Pair Creation

As one of the most fundamental and important of the electromagnetic interactions, the process of electron-positron pair creation by photons has been the subject of intensive theoretical and experimental investigation. Among the first theoretical studies was the work of Heitler and Sauter¹ who provided a calculation of the total cross section at a photon energy of 2.657 MeV.

The earliest comprehensive study of the pair creation cross section was formulated by H. Bethe and W. A. Heitler² in 1934. Their Born approximation calculation produced expressions for the cross section differential in positron energy for a given incident photon energy, the total cross section for a given incident photon energy, and for the screening effects of the orbital electrons.

H. R. Hulme and J. C. Jaeger,³ in 1936, conducted exact calculations at the photon energies of 1.533 and 2.657 MeV for the element lead. J. C. Jaeger^{4,5} later extended this calculation to include the total cross section for tin and terbium at the incident photon energy 1.533 MeV. These papers also reported computation of the asymmetry factor, a measure of positron energy

distribution shift due to nuclear Coulombic repulsion, for the cross section differential in positron energy. Other theoretical calculations have been conducted to study specific details of the pair creation process. These generally use approximation techniques best suited to the region of interest and often study finer details of the process such as angular distributions and energy distributions at back angles. Examples of interest are the works of Davies et al.,⁶ Bethe and Maximon,⁷ and Moroi and Hammer.⁸

To a great extent, the experimental measurements are compared with the results due to Bethe and Heitler (hereafter referred to as the B-H pair result) and, where applicable, with the exact results due to Jaeger and Hulme (hereafter referred to as the JH result).

The earliest experimental measurements were made with the use of cloud chambers and naturally occurring radioactive sources, notably ThC". The first reported results were due to Chadwick, Blackett, and Occhialini,^{9,10} using photons of energy 2.657 MeV. The analyzed data resulted in a corrected pair production total cross section, at photon energy $k = 2.657$ MeV, of 2.8 barns. This result compared quite favorably with the value of 2.5 barns predicted by Heitler and Sauter. At this same time, Meitner and Philipp¹¹ and Curie and



Joliot¹² reported successful measurements of the pair creation cross section. A later effort by Simons and Zuber,¹³ using the same cloud chamber technique, studied the energy distribution of the electron-positron pair, the total kinetic energy carried off by the pair, and the angular distribution of the outgoing pair, using an argon gas target and an incident photon energy of 2.657 MeV. The results of this experiment apparently confirmed the prediction of the B-H pair result for this energy. Other experiments of this genre were conducted using krypton¹⁴ and xenon and krypton¹⁵ gas targets.

In the late 1940's and early 1950's, another series of experiments based on measurements of the absorption of gamma-rays in matter was conducted. These measurements derived the pair creation cross section from the measured total absorption cross section by subtraction of the well known Compton effect cross section and photoelectric effect cross section. Among the first such experiments of this type was the work of Adams^{16,17} using the continuous bremsstrahlung spectrum as a photon source. Using threshold detectors to provide a band of photon energies near the maximum, studies at photon energies of 11.04, 13.73, and 19.10 MeV for the elements Cu, Fe, and C were conducted. The measured cross sections were 5 to 10 percent lower than theory predicted. Walker,¹⁸ using

the 17.6 MeV line from the $\text{Li}^7(\text{p}, \gamma)\text{Be}^8$ reaction and a pair magnetic spectrometer, confirmed the deviation from the B-H pair result noted by Adams for five atomic numbers, 6 to 82. Lawson¹⁹ and Dewire et al.,²⁰ using betatron x-rays and pair magnetic spectrometers to isolate the desired energy band, extended the measurements to 88.0 MeV and 280 MeV for six elements of atomic numbers 4 through 92. These authors also noted a decreased cross section relative to the Bethe-Heitler prediction. Using a cloud chamber technique, Emigh²¹ used betatron x-rays and a pair spectrometer to study the Z-dependence, total cross section and positron energy distributions of elements in the $Z = 13$ to $Z = 90$ region over an energy range of 50 to 300 MeV. Reported relative cross sections deviated from the B-H pair result as noted in previous experiments. Since the exact calculations of Jaeger and Hulme predict a ratio $\sigma_{\text{PAIR}}/\sigma_{\text{B-H}}$ greater than unity for photon energies less than 2.7 MeV and the research just described measures the same ratio as being less than unity if the photon energy is greater than 10 MeV, Rosenblum et al.²² studied the pair creation cross section over the energy range 5 to 18 MeV since the value of the cross section must crossover unity in this region in order to satisfy these requirements. Using betatron x-rays and the magnetic pair spectrometer, the resultant



measurements demonstrated the predicted and measured behaviours with $\sigma_{\text{EXP}} / \sigma_{\text{BH}} \approx 1$ at 6 MeV for high Z targets.

Another prominent method of measuring pair creation cross sections involves the use of artificial radioactive sources in an effort to measure the Z-dependence of the cross section and the relative total cross section. In these experiments the gamma-rays from the source impinge on the target sample causing pair creation. The positive member of the pair then annihilates and the resulting two .511 MeV photons are detected by two detectors placed at 180 degrees relative to one another, forming the so-called pair scintillation spectrometer. These counters count in time coincidence the annihilation photons and thus the number of pairs created (after appropriate corrections for detection efficiency, geometry, source strength, etc.). These studies were initiated by Hahn et al.²³ who investigated the cross sections for twelve atomic numbers over the range $Z = 13$ to $Z = 83$ for the energy range 1.17 MeV to 2.657 MeV. The measured cross sections, normalized to either the B-H pair result or the JH result at 2.657 MeV, were in qualitative agreement with the predictions of Jaeger and Hulme showing an increasing deviation from the B-H pair result with decreasing photon energy and

increasing atomic number, Z . Experimental studies on the pair phenomenon at low energies were continued by a number of investigators (Dayton, Schmid and Huber, West, Standil and Moore, Standil and Shkolnik, Singh, Dasso, and Griffiths).²⁴

In an apparent effort to coalesce and unify the existing measurements, Rama Roa et al.^{25,26} have effectively repeated and extended the previous measurements in a study of the pair creation cross sections for eight elements, $Z = 29$ through $Z = 82$, over the incident photon energy range 1.12 MeV to 2.0 MeV. Relative total cross sections and empirical Z -dependence formulae have been determined. For incident photon energies greater than about 1.2 MeV, the data, as a function of Z , could be fit using the empirical formula

$$\sigma = \sigma_{B-H} [1 + d \cdot Z^2]$$

where d is an empirical energy dependent fitting parameter with a value of the order 2×10^{-4} . The data at 1.12 MeV, however, could only be fit by a modified Z -dependence equation of the form

$$\sigma = \sigma_{B-H} [1 + d \cdot Z^2 \exp(-bZ)]$$

where the empirical fitting parameters b and d have values of 3×10^{-2} and 2×10^{-3} , respectively. The

relative total cross sections measured, however, were quite inconsistent with the extrapolated JH result being about a factor of two low in the energy region 1.17 to 1.33 MeV.

In the previous experiments conducted using radioactive sources, the major number of these sources provide several photon energy lines which result in measured pair creation cross sections which are the sum of the cross sections for all the photon energies which exceed the 1.022 MeV threshold energy. In order to compare these experiments with theory it is then necessary to fold together the various contributions in the ratio of the intensities of the various spectral lines, thereby gaining a calculated theoretical cross section for a given source. Since each laboratory does not use the same normalization procedure and since each experimenter uses his version of the JH result extrapolated over energy and Z , it is not surprising that discrepancies between theory and experiment as great as a factor of two are reported. Nor is it surprising that experiments performed in different laboratories provide discrepant results relative to one another of greater than 30 percent, far beyond the quoted measurement accuracies of less than 12 percent.

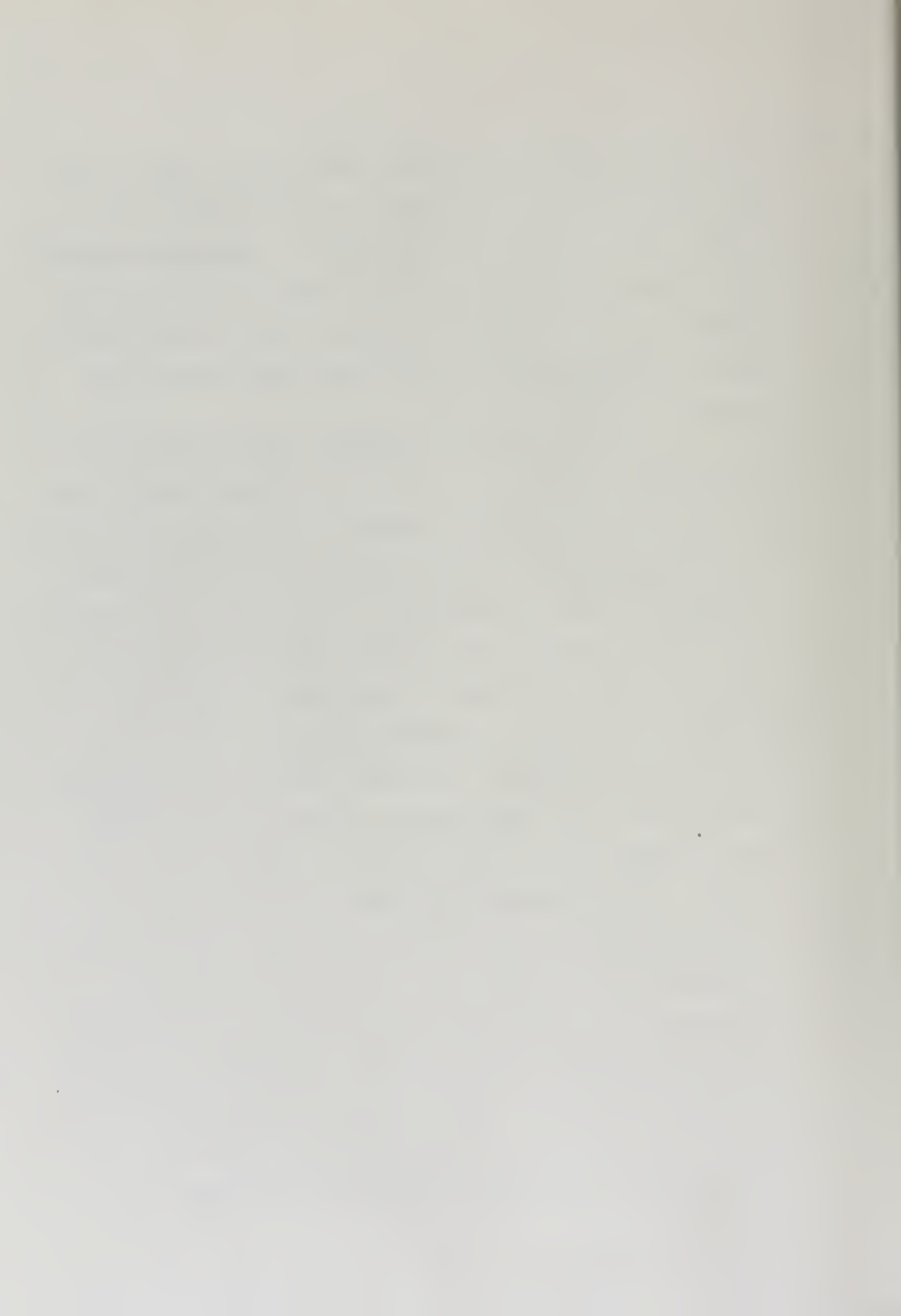
Using a modified form of the pair scintillation spectrometer which effectively considers only one photon

energy at a time, Yamazaki and Hollander²⁷ have recently completed a determination of the total pair creation cross section for germanium at thirteen photon energies ranging from 1.077 MeV to 2.754 MeV using radioactive sources. By requiring a triple time coincidence between the creation of the pair in a Ge(Li) detector (the double escape peak) and the detection of the annihilation radiation, these experimenters were able to study the effects of a single photon energy. The resultant cross sections indicated a more conspicuous deviation from theory (B-H pair result) than was expected on the basis of the exact calculations conducted by Jaeger and Hulme. Yamazaki and Hollander normalized their data to agree with the extrapolated JH result curve at 2.754 MeV. This technique allows only one atomic number to be studied and, in this case, the Z considered was not close to the available exact calculations. It is significant to note that the reported results are about twenty percent higher than theory (the JH result) and 30 percent higher than the measurements of Dayton and Hahn et al. in the region 1.33 to 1.50 MeV.

In view of the relative nature of many of the previous experiments, the lack of a measurement for lead and tin corresponding to the results of Jaeger and Hulme at $3 m_0 c^2$, and the discrepant nature of the results of preceeding measurements, most notably the consistently high values reported by Yamazaki and Hollander, a study

of absolute pair creation cross sections for lead, $Z = 82$, and tin, $Z = 50$, was conducted for photon energies of 1.2, 1.533, 1.57, 1.71, 1.85, and 2.00 MeV. Particular emphasis was placed on the measurement at 1.533 MeV for these elements since the JH result provides an exact calculation at this energy and no results have been reported for this energy.

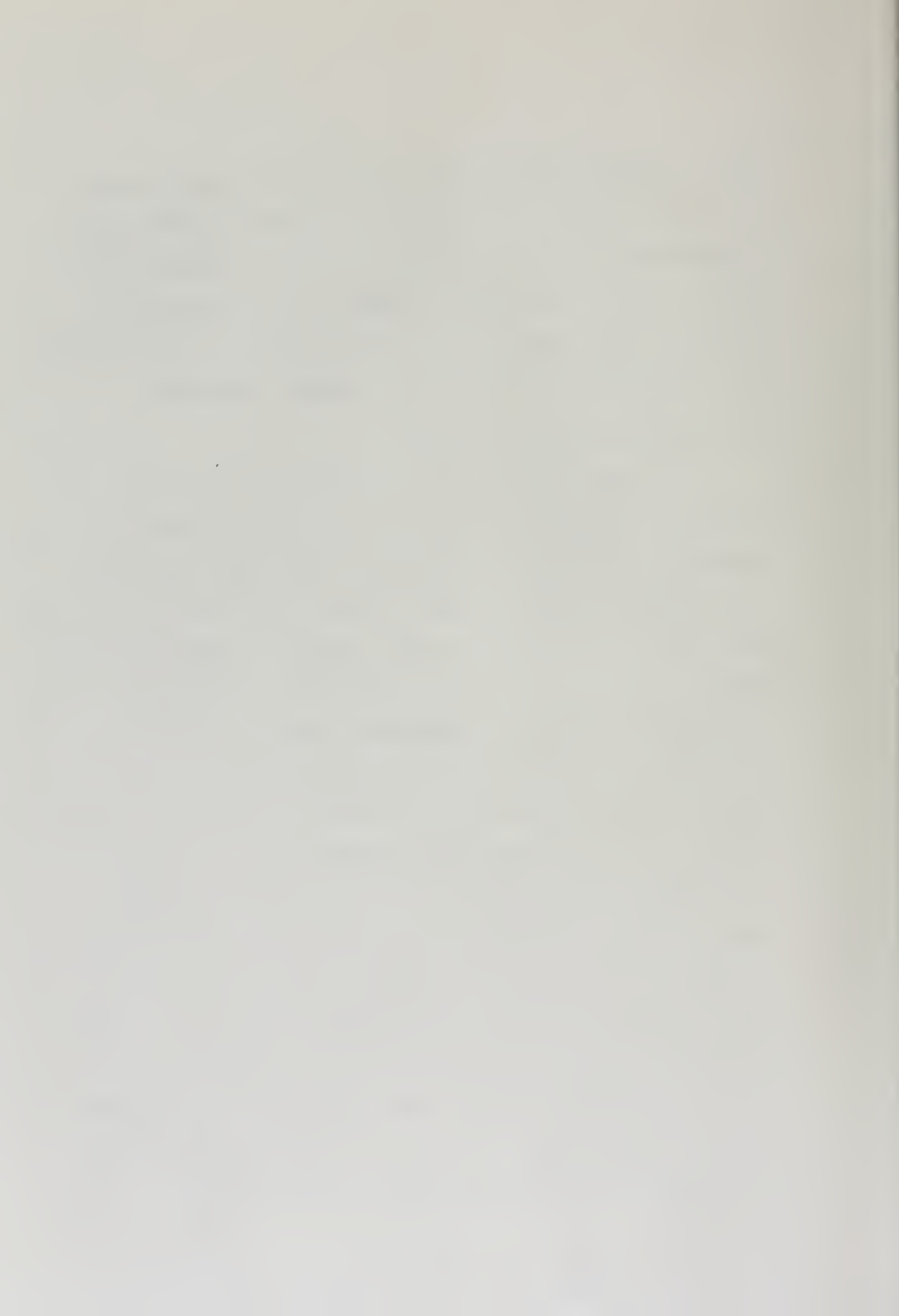
The desired pair creation cross sections were measured by detecting the .511 MeV radiation arising from annihilation of a created positron in the target sample in time coincidence with a post-bremsstrahlung electron corresponding to the monoenergetic photon which initiated the pair creation event. The required monoenergetic photons were produced by the photon monochromator using the monochromatic principle to be described in the next section. Accurate determination of the pair creation cross sections required not only monochromatic photons but also a knowledge of the flux of these photons incident on the target sample. It was, therefore, important to measure the number of these monoergic photons incident on the target and to determine, by comparison with predicted and measured bremsstrahlung cross sections, the efficacy of the monochromator in producing the desired radiation. As will be described in Section (I.C.), available measurements of the bremsstrahlung cross sections over the energy region of interest for this experiment show that the Bethe and



Heitler bremsstrahlung cross sections are approximately valid and can be used to provide a figure of merit useful in demonstrating the success of the monochromatic principle in providing the proper number of the proper energy photons. Measurement of the bremsstrahlung cross sections was a necessary corollary to the present research.

B. The Monochromatic Principle

The production of bremsstrahlung in a thin target by a beam of monoenergetic electrons creates a spectrum of photons, the energy of which ranges from T_0 , the incident electron energy, to near zero energy. In most cases, the desired photons comprise a small range of photon energy, k to $k + \Delta k$, where k is the desired energy of the photons. Therefore, the vast majority of the photons produced are extraneous background which complicates the analysis of the experimental data. Since the work of C. E. Dick²⁸ which demonstrated the existence of a finite cross section at the high frequency limit (tip) of the bremsstrahlung spectrum, some reduction in background difficulties is afforded by using tip energy photons as the source of the desired radiation. It would be useful, however, to be able to take advantage of the higher bremsstrahlung cross sections at photon energies, $k < T_0$, without the necessity of considering the effects of the continuous bremsstrahlung spectrum. The



development of an efficacious monochromator would allow such a procedure to be used.

The monochromatic principle is based on the fact that when a monoergic electron beam of initial energy T_0 interacts with a nucleus of atomic number Z producing the bremsstrahlung spectrum, there exists for every photon of energy k , a degraded post-bremsstrahlung electron of energy, $T_0 - k$. (This arises since the nucleus carries off a negligible amount of energy in the interaction.) Thus, since the electron of energy $T_1 = T_0 - k$ is in time coincidence with the photon of energy k , the electron can serve as a gate or identifier for the photon itself or for the products of photon-induced reactions.

The first use of the monochromatic principle was made by Weil and McDaniel.^{29,30} This experiment consisted of a study of the (γ, p) reaction in carbon using 190 MeV monoergic photons produced by an electron beam at the Cornell 300 MeV synchrotron. The guide field of the synchrotron was utilized to momentum analyze the energy degraded post-bremsstrahlung electrons and a resolution of 50 MeV was determined by a measurement of the energy spread of the 190 MeV photons. Cence³¹ then repeated, essentially, the work of Weil and McDaniel at 245 MeV using the Berkeley 342 MeV synchrotron. Goldemberg,³²

using a 180° permanent magnet beta-ray spectrometer, conducted experiments with monochromatic photons which studied the absorption of gamma-rays by carbon over the energy range 13.5 to 16.5 MeV. This device provided a resolution of 8%.

In 1961, O'Connell, Tipler and Axel³³ reported the successful use of a photon monochromator in conjunction with the University of Illinois 25 MeV betatron. The device used was a rectangular inclined plane pole-face spectrometer which was designed to use advantageously the focusing properties of the field by utilizing as many as six electron detectors placed on the locus line of horizontal foci. Since each detector was positioned at the focal point for a unique electron energy, six different photon energies could be used simultaneously. The initial experiment at Illinois used the monochromator for the study of elastic photon scattering from gold. The Illinois design is particularly adapted for high energy incident electron energies since the mean angular divergence of the post-bremsstrahlung electrons is sufficiently small to allow the transmission properties of the rectangular design to be adequate for the collection of the majority of the desired post-bremsstrahlung electrons. At lower energies, a shaped profile pole is necessary to collect a comparable percentage of the desired electrons.



O'Connell et al. reported an initial energy resolution of approximately one percent at 15 MeV. This figure was improved to a reported .67% by Tipler, Axel, Stein and Sutton³⁴ in experiments on the scattering of 11 to 19 MeV monoenergetic gamma-rays from ¹⁶⁵Ho. The device was also used by Kuchnir³⁵ in the study of neutron spectra from monoenergetic photons on bismuth. An energy resolution of 1.7 percent was reported as the best value attained.

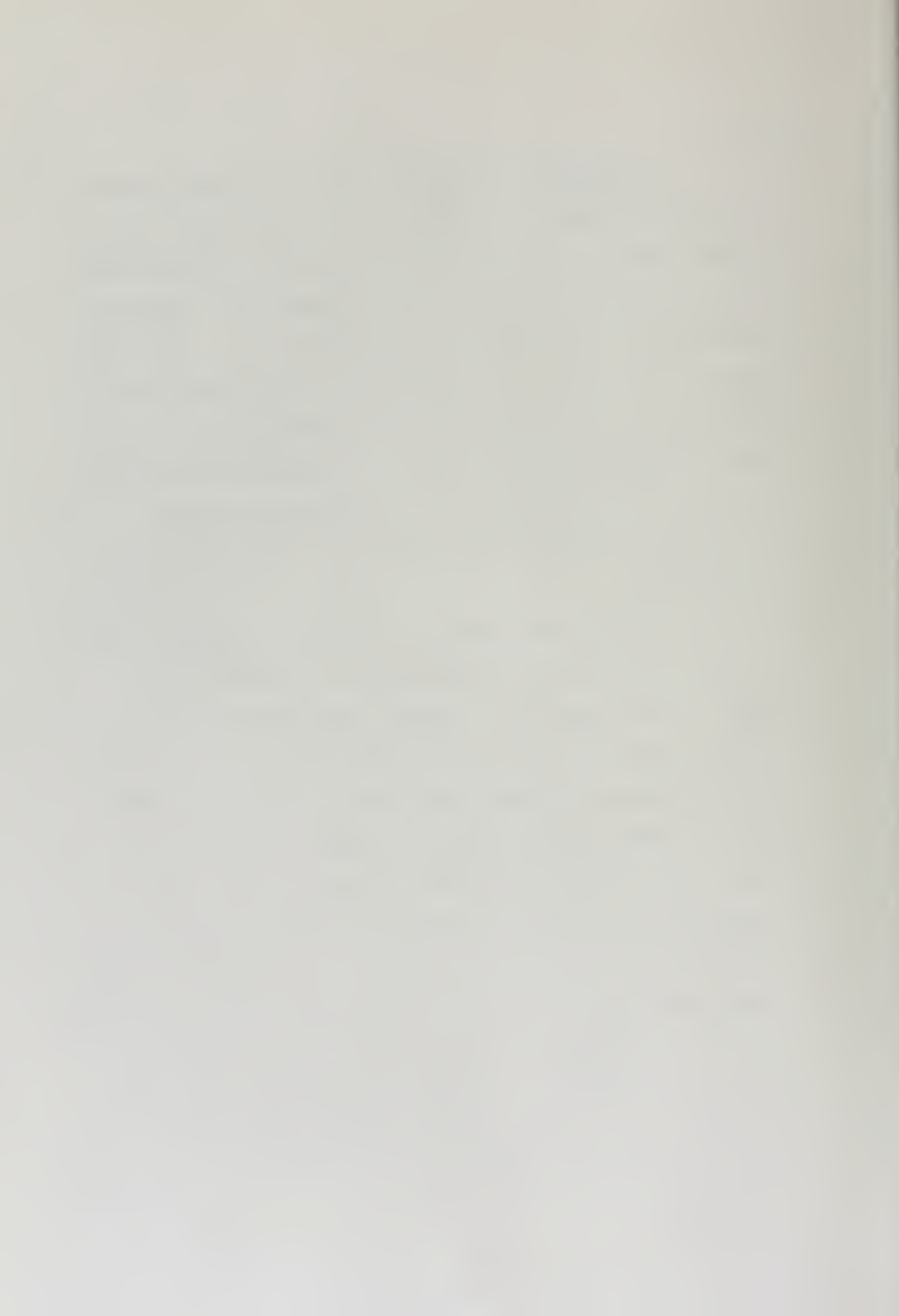
The initial monochromator effort in this laboratory was undertaken by Walter, Shea, and Miller in 1959.³⁶ The spectrometer was designed from the principles used by Kofoed-Hansen, Lindhard, and Nielsen^{37,38} in their development of a six-gap beta-ray spectrometer. This design utilizes a specially shaped pole piece leading edge profile in order to focus the maximum number of beta-rays from an isotropic source. Use of the special profile shape allows the fringe field effects of the magnet to contribute to optimum transmission and resolution parameters. No transmission values were reported but a momentum resolution of .7 percent was achieved. Excessive electron counting rates of the order of 10^6 greater than expected limited the magnitude of the usable incident electron beam to the several nanoampere region and rendered the device unsuitable for the intended use in photo-neutron reaction measurements.



D. L. Malaker³⁹ reduced this excessive electron count rate by a factor of about 10^5 and improved the resolving time of the "fast-slow" coincidence circuit from about 100 nanoseconds to about 10 nanoseconds. Malaker reported a transmission of .17 percent of 4π with a momentum resolution of 1.2 percent at electron energies of .625 MeV. The low value of the transmission and the remaining excess factor of ten in the electron count rate ruled out the proposed use of the monochromator for studies of nuclear excited states by nuclear resonance fluorescence.

The present research examines in further detail the performance of the monochromator in order that it might be developed into a useful experimental device. Relocation of the plastic scintillator used to detect post-bremsstrahlung electrons plus improved baffle systems, thinner target foils, and standardized electronics provided the required improvement in performance. The transmission was measured to be .44 percent, with a resolution of 2 percent at .625 MeV. The excess electron count rate was reduced by approximately a factor of three.

As noted previously, the criterion for success in developing the monochromator was taken to be the production of the proper number of monoenergetic photons for use in experimental studies of the pair creation phenomenon.



The figure of merit, defined as the ratio of the measured bremsstrahlung cross section to the theoretical value due to Bethe and Heitler, was measured at a number of photon energies between .500 MeV and 2.00 MeV. Use of this figure of merit as a parameter requires consideration of the theoretical and measured values of bremsstrahlung cross sections over the energy range of interest and these will be discussed in the next section.

C. Bremsstrahlung

The loss of energy by electrons in interacting with matter is a physical process of considerable interest. In particular, the loss of energy by electrons in the Coulomb field of either a nucleus or an electron by the emission of radiation, the bremsstrahlung process, plays a salient role in this research. While of fundamental importance itself, the process of bremsstrahlung also assumes great significance due to the availability of the resultant photons as "projectiles" in the conduct of photo-reactions of various kinds.

As was the case in the study of pair production, the initial comprehensive study of the theory of bremsstrahlung was provided by Bethe and Heitler.² Employing the Born approximation, equations for the cross section differential in photon energy, photon emission angle, and the electron emission angle and the cross section

integrated over angles, both relativistic and non-relativistic, were derived. In addition, the effects of screening and energy loss by the electrons were considered.

Sauter,⁴⁰ Schiff,⁴¹ Gluckstern and Hull⁴² and numerous others have studied the phenomenon using various approximation techniques. A compilation of the various theories and resulting expressions has been prepared by Koch and Motz (see Reference 67).

Only a few measurements have been made of the bremsstrahlung cross sections. For the most part, this paucity of measurements has been attributed to the inherent difficulties involved with such an experiment in which the information is spread over a very wide energy range. Experimental data have been obtained over the incident electron energy range 34 keV to 22 MeV by a variety of workers. In all cases, the data were obtained for the cross section integrated over all electron emission angles.

The data available have been taken at the following incident electron energies: 34 keV by Amrehn⁴³ and Ross⁴⁴; 50 keV by Motz and Placious⁴⁵; .5 and 1.0 MeV by Motz⁴⁶; 1.0, 1.7, and 2.5 MeV by Rester and Dance⁴⁷; 2.72, 4.54, and 9.66 MeV by Starfelt and Koch⁴⁸; and 22 MeV by Weinstock and Halpern⁴⁹. The Sauter theory and

the Schiff theory were often used for comparison with the experimental results. For the case of low incident electron energies, $T_0 \ll m_0 c^2$, the Sauter predictions underestimated the cross section by approximately 20 percent. Over the energy range, 4 to 25 MeV, both theories agreed with measurement to within about 10 percent.

Over the incident electron energy range of 1 to 3 MeV (the available range for the Notre Dame monochromator), some elements of the measurements by Motz, Rester and Dance, and Starfelt and Koch are of greatest interest. The discussion to follow will consider the pertinent fractional photon energy range, $k/T_0 = .5$ to $k/T_0 = .75$, which was used in the present research.

Motz has measured the spectral distribution of the bremsstrahlung at photon angles of 0, 30, 60, and 90 degrees for incident electron energies of .5 and 1.0 MeV using a target of atomic number $Z = 79$. Using the predictions of Sauter for comparison, the data at 1.0 MeV incident electron energy and 0° emission angle agreed with theory within 5 percent over the range of fractional photon energy, .5 to .65. For $k/T_0 = .65$ to .75, agreement with theory was within 10 percent.

Starfelt and Koch measured spectral and angular distributions of the bremsstrahlung photons at incident

electron energies of 2.72, 4.54, and 9.66 MeV using targets of Be, Al, and Au. The measurement at $T_0 = 2.72$ MeV for gold at a photon emission angle of 0 degrees is most pertinent. Once again the Sauter theory was used as a reference. These results can be most clearly presented in tabular form as:

INCIDENT ELECTRON ENERGY = 2.72 MeV
 TARGET ATOMIC NUMBER, $Z = 79$

<u>Fractional Photo Energy</u>	<u>$\sigma_B(\text{EXP})/\sigma_{\text{SAUTER}}$</u>
.5	.9 \pm .1
.6	.9 \pm .1
.7	.9 \pm .1
.8	.9 \pm .2

Rester and Dance conducted measurements, at incident electron energies of 1.0, 1.7, and 2.5 MeV using targets of atomic number $Z = 13, 19, 50,$ and 79 , of the spectral and angular distributions of the bremsstrahlung cross section. Data were taken at photon emission angles of 0, 4, 10, 20, 30, 40, and 60 degrees. The experimental results for $T_0 = 1$ MeV, at emission angle 0 degrees for the target with $Z = 79$, gave a value for

$\sigma_B(\text{EXP})/\sigma_{\text{SAUTER}}$ equal to unity, within 7 percent, over the fractional photon energy range of .5 to .7. For

$k/T_0 = .75$, the ratio $\sigma_E(\text{EXP})/\sigma_{\text{SAUTER}} = 1.2 \pm .1$.
 At an incident electron energy of 1.7 MeV (using the same target and emission angle), the ratio of experimental cross section to theory was about .85 at $k/T_0 = .5$, was equal to unity at $k/T_0 = .7$, and was within 6 percent of unity for $k/T_0 = .8$ with a quoted measurement accuracy of ± 7 percent. At $T_0 = 2.5$ MeV, the 0 degree data gave $\sigma_E(\text{EXP})/\sigma_{\text{SAUTER}} = .72 \pm 7\%$ at $k/T_0 = .5$ with the ratio increasing with increasing photon energy until $k/T_0 = .75$ at which point $\sigma_E(\text{EXP})/\sigma_{\text{SAUTER}} = 1.0 \pm 7\%$.

For larger photon angles (4° , 10° , etc.) over the fractional photon energy range of .5 to .75, the ratio $\sigma_E(\text{EXP})/\sigma_{\text{SAUTER}}$ is equal to or greater than unity for all measured incident electron energies. As a result, the measured cross section integrated over the full photon emission solid angle is within 10 percent of theory over the k/T_0 range of .5 to .75. In general, the agreement between theory and experiment is fairly good with the notable exception of the Rester and Dence measurement at $T_0 = 2.5$ MeV.

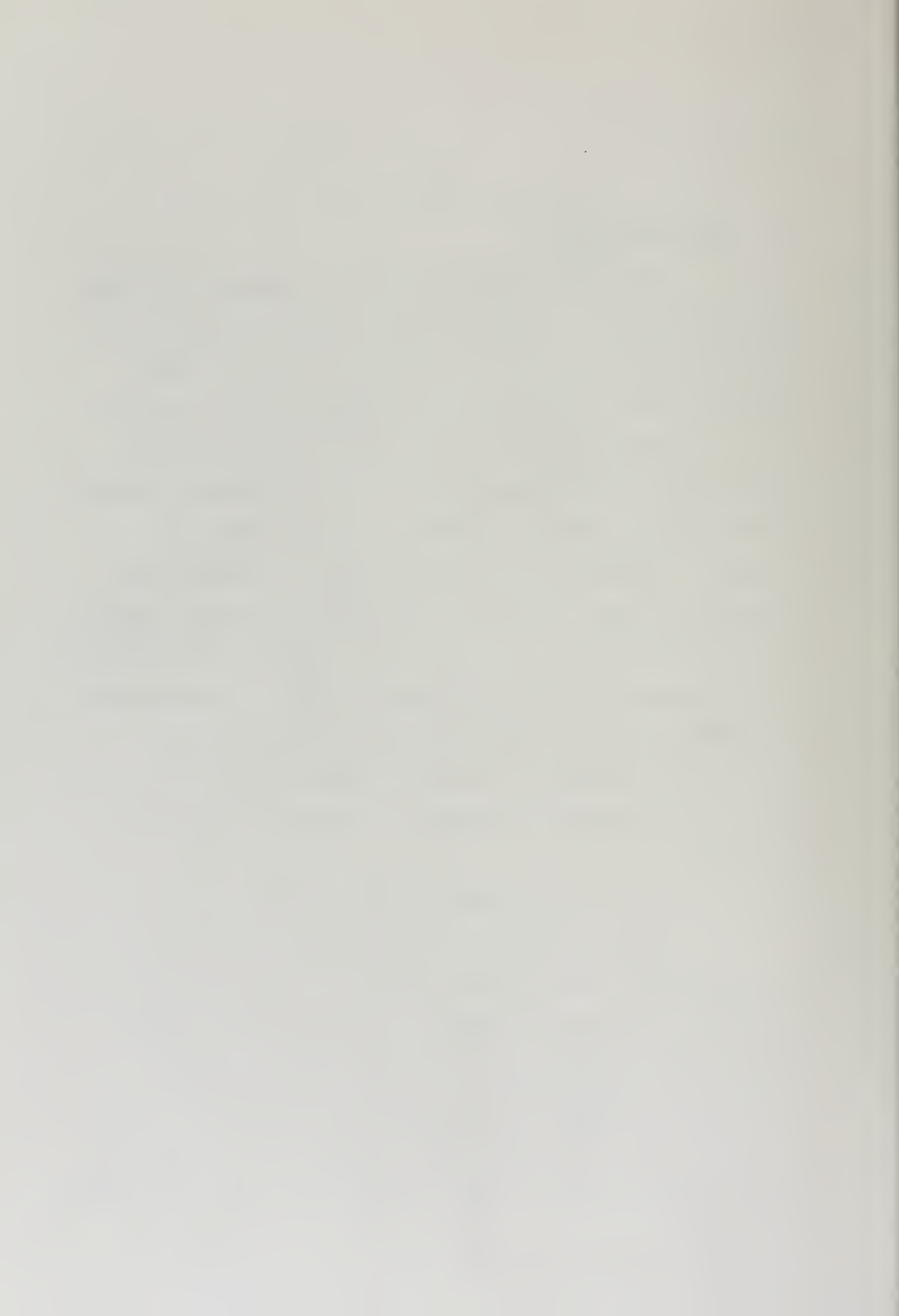
II. THEORY

A. Pair Creation

Production of a positive and negative electron pair by photons can take place in either the field of a nucleus or the field of an electron. The well known threshold for the process in the field of the nucleus is $2 m_0 c^2$, where $m_0 c^2$ is the rest energy of the electron, while Perrin⁵⁰ has demonstrated that the threshold for the effect taking place in the field of the electron is $4 m_0 c^2$. The process of interest here is coherent pair production which occurs when the atomic electrons play no role in the process other than to screen the Coulomb field of the nucleus. Pair production is related to the bremsstrahlung process in which the post-bremsstrahlung electrons are left in a negative energy state and generally the two processes are treated in concert in theoretical analyses.

1. The Cross Section for Pair Creation

The derivation of an exact expression for the pair creation cross section requires a description of the positive and negative electrons in the screened nuclear Coulomb field using exact wave functions. In general it is not possible to solve the Dirac wave equation in such a form since the required wave functions are represented by an infinite series. For the most part, then, a variety



of approximation techniques have been used in the calculation of pair creation cross sections.

a) Cross Sections Due to Bethe and Heitler

The pioneer effort in the study of the pair creation process was conducted by Bethe and Heitler.² This theory was presented in a classic paper putting forth the theory of both bremsstrahlung and pair creation. The Born approximation was used in the development of the theory. The validity conditions for this approximation can be written as

$$2\pi\alpha Z/\beta_+ \ll 1 \quad ; \quad 2\pi\alpha Z/\beta_- \ll 1$$

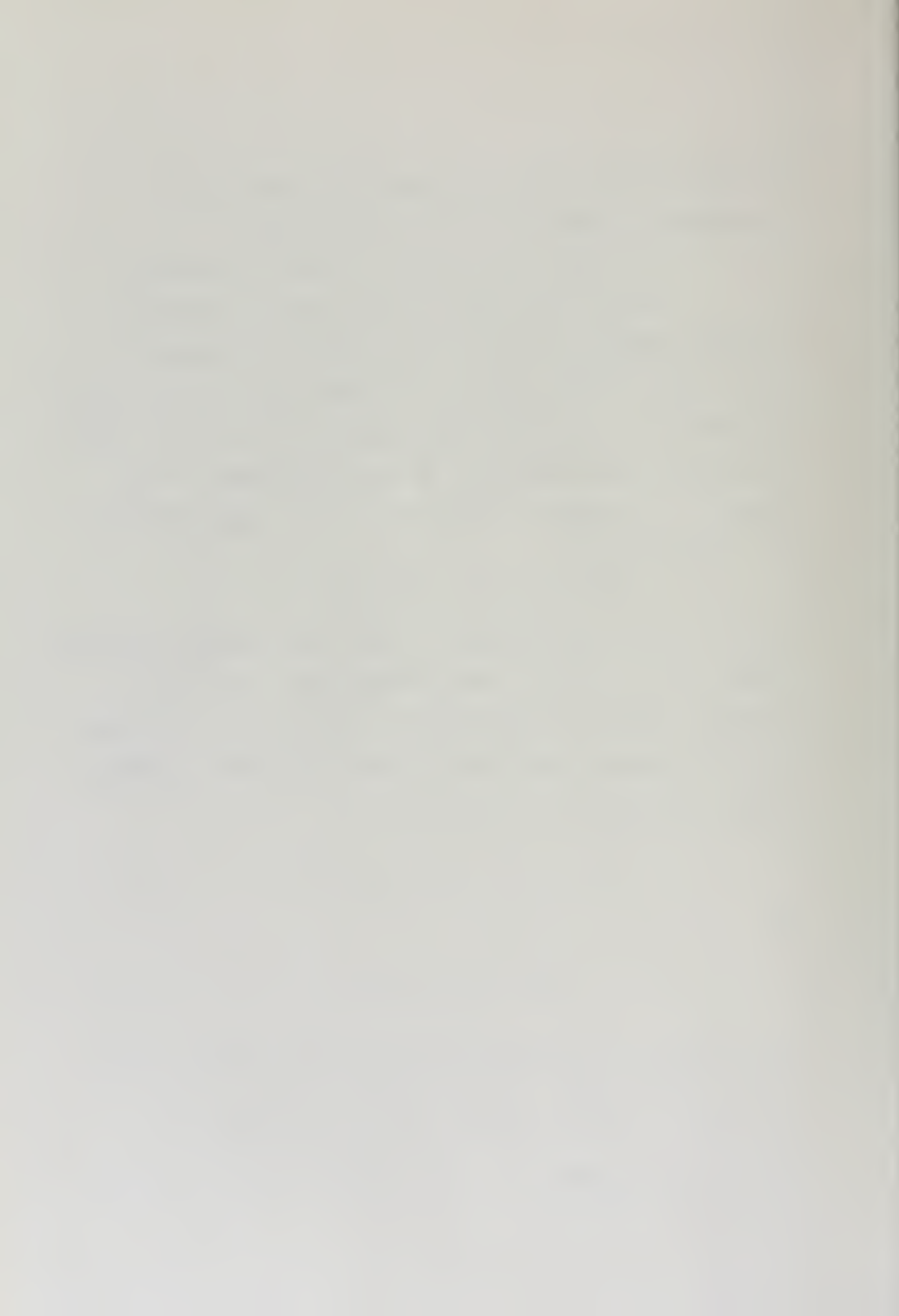
where Z is the atomic number of the target element and the quantities β_+ and β_- are, respectively, the ratio of positron velocity to the speed of light and the same ratio for the negatron, and α is the fine structure constant. These conditions can be rewritten as

$$E_+(\alpha E_-) \gg 1/[1 - (\alpha Z)^2]^{1/2} \quad (\text{II-1})$$

or

$$k \gg 2/[1 - (\alpha Z)^2]^{1/2} \quad (\text{II-2})$$

where $E_+(E_-)$ is the positron (negatron) total energy and k is the photon energy, both in units of m_0c^2 . It follows from these conditions that the Born approximation becomes less reliable as, (a) the atomic number, Z , of the



target element is increased, and (b) the momentum and energy of the emergent particles decreases or, more simply stated, as the incident photon energy decreases to near the threshold value.

The Born approximation calculation as conducted by Bethe and Heitler, neglecting screening, yields for the cross section differential in photon energy the expression

$$\frac{d\sigma}{dE_+} = \bar{\Phi} \frac{R_P}{k^3} \left\{ -\frac{4}{3} - 2E_+E_- \left(\frac{P_+^2 + P_-^2}{P_+^2 P_-^2} \right) + \mu^2 \left(\frac{E_+E_-}{P_-^3} + \frac{E_+E_-}{P_+^3} - \frac{E_+E_-}{P_+P_-} \right) + \right. \\ \left. L \left[\frac{k^2}{P_+^3 P_-^3} (E_+^2 E_-^2 + P_+^2 P_-^2) - \frac{8}{3} \frac{E_+E_-}{P_+P_-} - \frac{\mu^2 k}{2 P_+P_-} \left(\frac{E_+E_- P_-^2 E_-}{P_-^3} + \right. \right. \right. \\ \left. \left. \left. \frac{E_+E_- P_+^2 E_+}{P_+^3} + \frac{2k E_+E_-}{P_+^2 P_-^2} \right) \right] \right\} \quad (\text{II-3})$$

where the following definitions have been used.

$$\bar{\Phi} = \alpha Z^2 r_0^2$$

where r_0 is the classical electron radius,

$$E_{\pm} = 2 \ln \left(\frac{E_{\pm} + P_{\pm}}{\mu} \right)$$

$$L = 2 \ln \left(\frac{E_+E_- + P_+P_- + \mu^2}{\mu k} \right)$$

$$\mu = m \cdot c^2.$$

The symmetry of this result with respect to the interchange of the positron and the electron results from the



use of the Born approximation. As the photon energy approaches the threshold value the symmetry noted above is destroyed by the approximate correction factor⁵¹

$$f(\xi_+, \xi_-) = \frac{2\pi \xi_+ 2\pi \xi_-}{(e^{2\pi \xi_+} - 1)(1 - e^{-2\pi \xi_-})} \quad (\text{II-4})$$

where

$$\xi_{\pm} = \frac{Z e^2}{\hbar v_{\pm}} = \frac{Z \mu}{137 p_{\pm}}.$$

This correction factor is only valid under the condition $v_{\pm} \ll c$.

Neglect of the screening effects of the atomic electrons is only valid if the total energies of both particles are sufficiently low such that the condition

$$\frac{2E_+ + E_-}{\hbar \mu} \ll 137 Z^{-1/3} \quad (\text{II-5})$$

is satisfied. Since the conditions of the present measurements do not completely satisfy Equation (II-5), the B-H pair result can only be used as a basis for comparison if the screening corrections can be shown to be small for the energies and atomic numbers studied. Bethe and Heitler point out that for heavy elements screening effects are not significant for photon energies less than $15 m_0 c^2$.

The total cross section has been calculated by Bethe and Heitler and, more recently, Yamazaki and

Hollander by numerically integrating Equation (II-3). The results of the latter calculation are tabulated as Table III in Reference 27 and are plotted in Figures (IV-13) and (IV-15) in this dissertation.

b) Cross Section Due to Jaeger and Hulme and Jaeger

In the low photon energy range Jaeger and Hulme and, later, Jaeger used Dirac wave functions to calculate the total pair creation cross section for photon energies of 1.533 MeV and 2.657 MeV. This rigorous treatment of the problem, using spherical wave functions and without employing any approximations other than numerical ones, should yield exact total cross sections. These calculations employ a technique, used by Jaeger and Hulme⁵² in an earlier work on internal pair creation, in which the gamma-ray was treated as a perturbation acting on an electron state of negative energy in the Coulomb field of a nucleus.

The results of these calculations are given in Table (II-1), along with the computed asymmetry factor,

$$(\bar{E}_+ - \mu) / (\bar{E}_- - \mu)$$

which measures the shift in the energy distribution of positrons (negatrons) due to Coulombic repulsion (attraction) effects due to the positive nuclear charge.

TABLE (II-1)

Pair production cross sections from the calculations of Jaeger
and Hulme³ and Jaeger^{4,5}

Z	$h\nu = 3 m_0 c^2$			$h\nu = 5.2 m_0 c^2$
	50	65	82	82
$\sigma_{\text{PAIR}} (10^{-24}) \text{ cm}^2$	0.17	0.34	0.67	3.1
$(\bar{E}^+ - \mu) / (\bar{E}^- - \mu)$.	2.0	1.4

For the photon energy 1.533 MeV, Jaeger derives an extrapolation formula for obtaining the pair creation cross section for any element of atomic number, Z,

$$\sigma(Z) \times 10^{24} = 0.95 (Z/137)^2 + 2.54 (Z/137)^4 \quad (\text{II-6})$$

C. Other Approximate Pair Creation Cross Sections

Bethe and Maximon, in Reference (7), have conducted an extensive calculation, without using the Born approximation, over the energy region in which both electrons have energies large compared to the electron rest mass. The result was the B-H pair result modified by a multiplicative factor and an additive factor. This result is in good agreement with experiment above photon energies of 10 MeV but is not expected to be reliable for lower energies.

Calculations for high energy, taking screening into account, have been carried out by Bethe⁵³ using the Thomas-Fermi distribution for the orbital electrons. This result can be written

$$\frac{d\sigma}{dE_+} = \frac{1}{k^3} \left\{ (E_+^2 + E_-^2) \left[Q_1(\gamma) - \frac{4}{3} \ln Z \right] + \frac{2}{3} E_+ E_- \left[Q_2(\gamma) - \frac{4}{3} \ln Z \right] \right\} \quad (\text{II-7})$$

where

$$\gamma = (100 m_0 c^2 h\nu) / (E_+ E_- Z^{-1/3})$$



and $\Phi_1(\gamma)$ and $\Phi_2(\gamma)$ are functions of the parameter γ , the values of which are obtained by numerical integration, for $0 < \gamma < 2$, since these functions include the Fermi form factor which is only known numerically. For smaller energies such that $2 < \gamma < 15$, the result

$$\frac{d\sigma}{dE_+} = \frac{4\bar{\Phi}}{k^3} (E_+^2 + E_-^2 + \frac{2}{3} E_+ E_-) \left[\ln \left(\frac{2E_+ E_-}{k m_0 c^2} - \frac{1}{2} - C(\gamma) \right) \right] \quad (\text{II-8})$$

can be written. Curves of the parameters $\Phi_1(\gamma)$, $\Phi_2(\gamma)$, and $C(\gamma)$ are given by Bethe and Heitler² and Bethe and Ashkin.⁵⁴ Since this screening correction is valid for high photon energies ($\geq 15 m_0 c^2$), Equations (II-7 and 8) are useful only in the extreme relativistic case. Hough⁵⁵ has given a formula for the cross section differential in positron energy, without consideration of screening effects, which approximates Equation (II-3), and is valid for $k < 20 m_0 c^2$. This expression can be written as

$$\frac{d\sigma}{dE_+} = \left(\frac{d\sigma}{dE_+} \right)_m z \left\{ 1 + 0.135 \left[\left(\frac{d\sigma}{dE_+} \right)_m / \bar{\Phi} - .52 \right] z (1-z) \right\} \quad (\text{II-9})$$

where

$$\left(\frac{d\sigma}{dE_+} \right)_m$$

is the differential cross section from Equation (II-3) for $E_+ = E_- = k/2$; i.e., for equipartition of energy between the two members of the pair; and,



$$Z = 2 [x(1-x)]^{1/2}$$

where

$$x = (E_+ - m_0 c^2) / (k - 2m_0 c^2) .$$

The second term in the curly bracket must be dropped whenever it assumes a negative value. Equation (II-9) agrees with the Bethe-Heitler result for $.05 < x < .95$ to within 1%.

Integrated cross sections equivalent to the integrated B-H pair result have been obtained by Racah⁵⁶ and Jost et al.⁵⁷ but these forms are not given in terms of tabulated functions.

At incident photon energies in the range 1.022 MeV to 6.13 MeV, Zerby and Moran⁵⁸ give the empirical formula

$$\sigma = \sigma_{B-H} [1 + (7.824 \times 10^{-4}) Z \exp(-0.612 k)] \quad (II-10)$$

based on the analysis of available experimental results, where k is in units of $m_0 c^2$ and σ_{B-H} is obtained by integrating either Equation (II-3) or (II-9) over positron energy. Calculations indicate that Equation (II-10) can be used to fit experimental data in the energy range 2.7 to 6 MeV to within 10 percent.

2. The Yield Expression

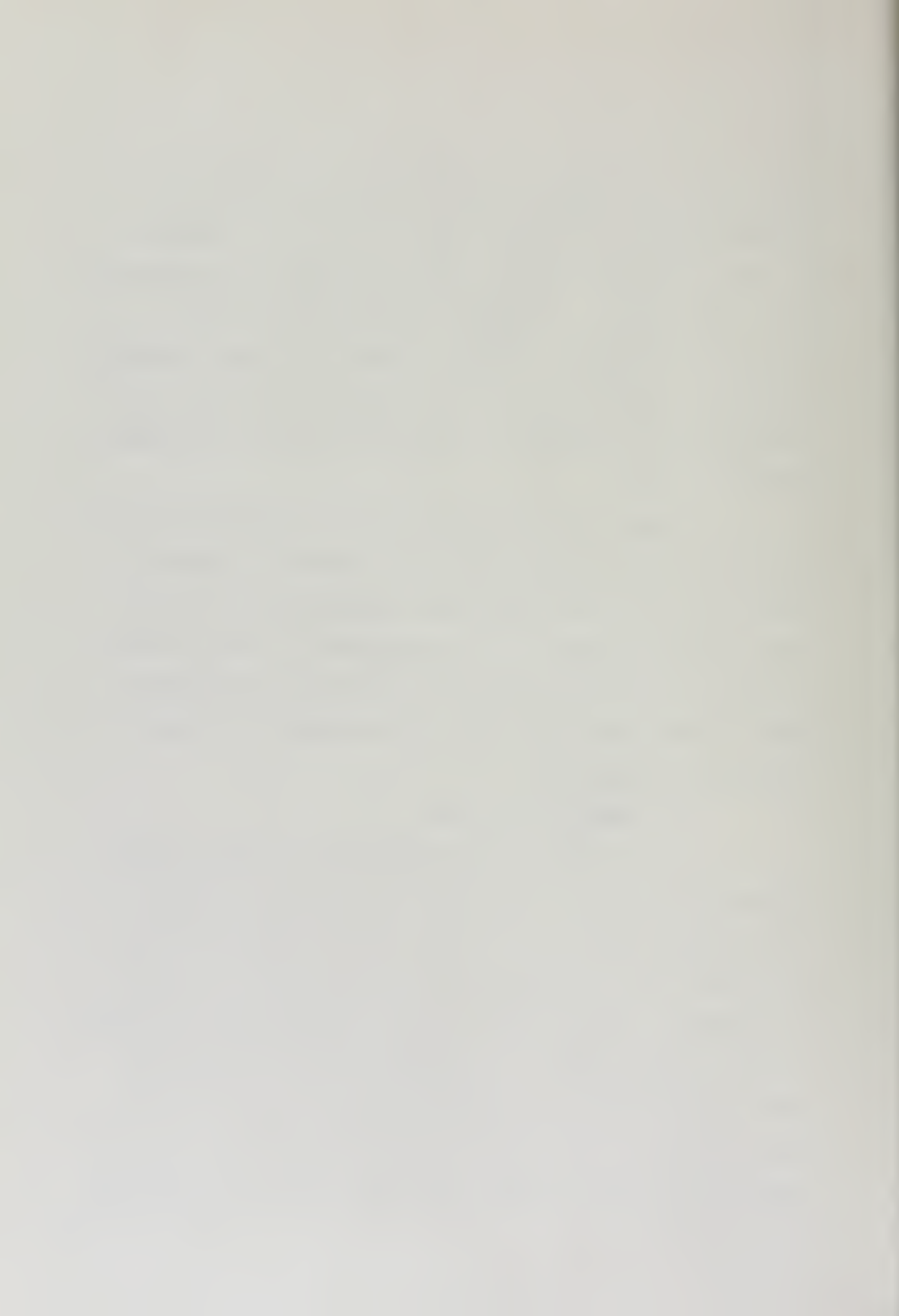
The experimentally measured quantity in this research is the number of annihilation radiation quanta

produced in the target sample by the annihilation of created positrons and detected by the NaI(Tl) detector in time coincidence with a post-bremsstrahlung electron of the proper energy. In order to determine the cross section for the pair creation process from this quantity, referred to as the yield, it is necessary to form an expression which relates the cross section to the measured number of counts.

There are three expressions which can be used to relate the known yield to the cross section. Each derives its particular form from considerations of target size and the geometry of the experimental layout as well as from the physical principles involved in the experiment. These expressions will be considered in order of increasing complexity.

a) Small Thin Target

If the dimensions of the target sample perpendicular to the beam direction are very small relative to the distance between the target position and the bremsstrahlung foil and relative to the distance from target to detector, then the pair creation target sample subtends a small solid angle at the bremsstrahlung foil and acts as a point source of annihilation radiation relative to the detector. Additionally, if the target is so thin that absorption of the incident radiation and the annihilation



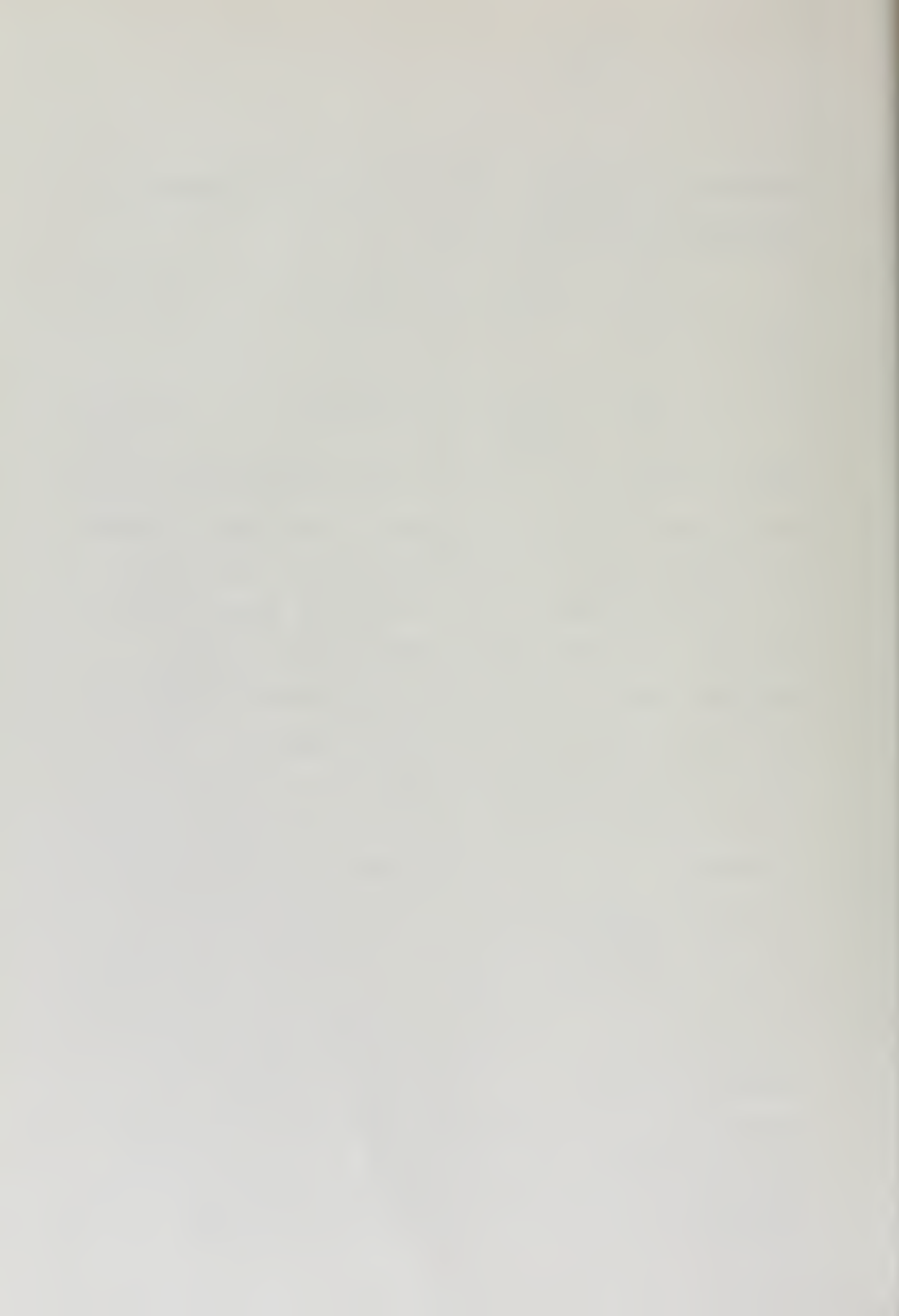
radiation is negligible, the yield expression assumes an especially simple form given by

$$Y = N(k) \sigma_{\text{PAIR}} \rho T \bar{\eta} P W(\theta) \sec \phi \quad (\text{II-11})$$

with

$$N(k) = \left(\frac{d^2 \sigma_{\text{BREMS}}}{dk d\Omega_k} \right) \Delta k \Delta \Omega_k n_{\text{DENSITY}} Q \quad (\text{II-11a})$$

where $(d^2 \sigma_{\text{BREMS}}/dk d\Omega_k)$ is the cross section for production of a photon of energy k by electrons collected in a solid angle $\Delta \Omega$ in the monochromator with energy $T_0 - k$ ($\text{cm}^2/\text{MeV-Str}$); Δk is the energy uncertainty of the photon deriving from the resolution of the monochromator (MeV); $\Delta \Omega_k$ is the solid angle subtended by the target at the foil (Steradians); n_{DENSITY} is the areal density of the bremsstrahlung foil (Atms/cm^2); and Q is the number of incident electrons accumulated (# of electrons). Thus, $N(k)$ is the number of photons incident on the pair creation target in the energy interval $k \pm \Delta k/2$ and in the solid angle subtended by the sample at the bremsstrahlung target; σ_{PAIR} is the cross section for pair creation (cm^2/atom); ρ is the target sample density (atoms/cm^3); T is the target thickness; $\bar{\eta}$ is the average source full energy peak detection efficiency for .511 MeV photons; P is the probability factor for annihilation of the positron in the target sample; $w(\theta)$ is



the angular distribution function for the annihilation radiation; and φ is the angle between the normal to the face of the target and the incident beam direction.

In this simple case, the pair production cross section is just

$$\sigma_{\text{PAIR}} = Y/N(k) \rho T \sec \varphi \bar{\eta} PW(\theta) \quad (\text{II-11b})$$

b) Small Thick Target

If the "zero-thickness" approximation is not valid, it becomes necessary to reformulate the relationships between σ_{PAIR} and the measured yield. The absorption effects of the target on the incident photon flux and the outgoing annihilation radiation must be considered.

The yield expression, differential in target thickness, can now be written as

$$dY = N(k) \rho \sigma_{\text{PAIR}} \bar{\eta} PW(\theta) \exp\{-\mu x\} \exp\{-(\mu_c + \sigma_{\text{PAIR}}) \rho x\} dx \quad (\text{II-12})$$

where $x = t \sec \varphi$ (cm.), μ is the absorption coefficient for .511 MeV photons (cm.²/atom), and μ_c is the Compton and photo effect absorption coefficient for the incident photons of energy k (cm.²/atom).

Carrying out the integration over thickness, the resulting expression is

$$\begin{aligned}
 Y &= N(k) \rho \sigma_{\text{PAIR}} \bar{\eta} P W(\theta) \int_0^X \exp\{-\mu_f x\} \exp\{-(\mu_c + \sigma_{\text{PAIR}}) \rho x\} dx \\
 &= N(k) \sigma_{\text{PAIR}} \bar{\eta} P \frac{W(\theta)}{(\mu + \mu_c + \sigma_{\text{PAIR}}) \rho} [1 - \exp\{-(\mu + \mu_c + \sigma_{\text{PAIR}}) \rho X\}]
 \end{aligned}
 \tag{II-13}$$

where $X = T \sec \phi$, with T the total thickness of the target.

c) Large Thick Target

In this final case for consideration, the target size is so large that none of the previous geometrical simplifying assumptions is completely valid. The target sample now subtends a finite solid angle at the bremsstrahlung foil and the detector subtends a large finite but complex solid angle at the target sample. The yield expression must be modified to include these effects. This expression for a large thick target divided into differential volume elements \mathcal{T} can be written as

$$\begin{aligned}
 dY &= N(k) \frac{\rho \mathcal{T}}{S} P \sigma_{\text{PAIR}} W(\theta_{\mathcal{T}}) \exp\{-\mu_f \delta_{\mathcal{T}}'\} \exp\{-(\mu_c + \sigma_{\text{PAIR}}) \rho \delta_{\mathcal{T}}\}^x \\
 &\quad \eta_{\mathcal{T}} C_0 \exp\{-\alpha_{\mathcal{T}}^2/q^2\} d\mathcal{T}
 \end{aligned}
 \tag{II-14}$$

where

$$N(k) = \left(\frac{d\sigma_{\text{BREMS}}}{dk} \right) \Delta k n_{\text{DENSITY}} Q F_M
 \tag{II-14a}$$

$$\frac{d\sigma_{\text{BREMS}}}{dk} = \int_{\Delta\Omega_p} \int_{\Delta\Omega_k} \frac{d^3\sigma_{\text{BREMS}}}{dk d\Omega_p d\Omega_k} d\Omega_p d\Omega_k \quad (\text{II-14b})$$

Ω_p is the effective solid angle at the beam spot subtended by the exit slit of the monochromator, Ω_k is the solid angle subtended by the target at the bremsstrahlung foil, F_M is the ratio

$$(d\sigma_{\text{BREMS}}/dk)^{\text{EXP}} / (d\sigma_{\text{BREMS}}/dk)^{\text{THEORY}},$$

and the other terms in Equation (II-14a) have been defined. For Equation (II-14), τ is $\sec\phi$, S is the frontal area of the target sample which is included to cancel the integration over the area implied by the differential volume element $d\tau$, $W(\theta_\tau)$ is the angular distribution factor for radiation from volume element τ which in the pair creation process is unity, δ'_τ is the distance within the target of element τ measured along the direction of the outgoing radiation, δ_τ is a similar distance measured in the direction of the incoming beam,

η_τ is the efficiency for detection of the .511 MeV photons emanating from volume element τ ,

$$C_0 \exp \left\{ -\alpha^2/q^2 \right\}$$

is an expression which approximates the angular distribution of the incident monoenergetic photons and is a

Gaussian of revolution with a half-width at half-maximum equal to q , the parameter $\alpha_{\mathcal{T}}$ measures the angular displacement of volume element \mathcal{T} from the incident beam direction at the foil. C_0 is a normalization constant. All other terms have been defined previously.

The integration necessary to evaluate the yield, Y , requires analytic representation of the factors in equation (II-14) which depend on the position of the elemental $d\mathcal{T}$; e.g., $\eta_{\mathcal{T}}$, $\alpha_{\mathcal{T}}$, $\delta_{\mathcal{T}}$, etc. However, division of the target sample into incremental volume elements, $\Delta\mathcal{T}$, each so small that any variation in the factors just mentioned over the size of the volume element is negligible, allows the integral to be replaced by a sum. For each volume element, $\Delta\mathcal{T}$, the value of the required parameters can be replaced by their values at the center of $\Delta\mathcal{T}$. The final yield is then determined by summing the contribution due to each volume element. The summation form of the yield expression can be written as

$$Y = N(k) \rho \frac{T}{N} P \sigma_{\text{PAIR}} \sum_{\substack{\text{VOL.} \\ \text{ELEMENTS}}} \exp\{-\mu \rho \delta_{\mathcal{T}}'\} \exp\{-(\mu_c + \sigma_{\text{PAIR}}) \rho \delta_{\mathcal{T}}\} \eta_{\mathcal{T}} C_0 \exp\left\{-\frac{\alpha_{\mathcal{T}}^2}{q^2}\right\} \quad (\text{II-15})$$

where the integration over $d\mathcal{T}$ is replaced by a sum over $\Delta\mathcal{T}$, with $\Delta\mathcal{T} = ST/N$ and N is the number of volume elements in the target.

3. Competing Processes

The existence of extraneous .511 MeV photons at the position of the photon detector posed the major background problem in this research. Due to the presence of the continuous bremsstrahlung flux, these .511 MeV photons could arise via inelastic scattering of higher energy photons plus elastic scattering of those .511 MeV photons produced by the bremsstrahlung process. The inelastic processes of interest are Compton scattering, pair creation at photon energies other than the monochromatic energy, and secondary bremsstrahlung produced by "knock-on" electrons in the target. The elastic processes to be considered are Rayleigh scattering, nuclear Thomson scattering, and Delbrück scattering.

a) Inelastic Processes

In the energy range used in the present experiments, Compton scattering accounts for the major share of the photons inelastically scattered into the detector. The cross section for incident unpolarized radiation is given by the Klein-Nishina⁵⁹ formula,

$$\frac{d\sigma_e}{d\Omega} = \frac{r_0^2}{2} \left\{ \frac{1}{\left[1 + \frac{k}{\mu}(1 - \cos\theta)^2\right]} \right\} \left\{ 1 + \cos^2\theta + \frac{\left(\frac{k}{\mu}\right)^2(1 - \cos\theta)^2}{1 + \left(\frac{k}{\mu}\right)(1 - \cos\theta)} \right\} \quad (\text{II-17})$$



where θ is the angle through which the photon is scattered. In the energy region near threshold for pair creation, this cross section is relatively large even for scattering angles greater than 90 degrees. However, the energy of the scattered quanta is given by

$$k' = k \left(1 + \frac{k}{m_0 c^2} (1 - \cos \theta) \right)^{-1} \quad (\text{II-18})$$

and for the maximum incident photon energy used in this experiment, the scattered radiation has a maximum energy considerably less than .511 MeV (for $k_{\text{INC}} = 2.86$ MeV, $k' = .266$ MeV at a 120 degree scattering angle). Therefore, the Compton scattered photons make no contribution to the annihilation radiation data. The contribution of .511 MeV bremsstrahlung produced by Compton scattered electrons in the target sample has been estimated to be less than one part in 10^4 at an angle of 120 degrees.

The annihilation radiation which arises due to pair creation by photons of other than monochromatic energy will contribute to the full energy peak in the spectrum of the scintillation spectrometer detector. Using Equation (II-9) and the corrected bremsstrahlung cross sections of Starfelt and Koch, the full energy peak can be expected to contain, on the average, a 60 percent contribution from this source. This effect will occur to the same magnitude in the total (true plus chance) and

chance coincidence data and can therefore be accounted for experimentally.

b) Elastic Processes

The previously mentioned elastic processes are known to occur with only a small loss in energy taken up by recoil of the scattering atom or nucleus. Rayleigh scattering; i.e., scattering from bound electrons without removal of the electron from a bound state, has been treated by Franz⁶⁰ by extending the earlier work of Debye⁶¹ into the gamma ray energy region. Franz assumed a Thomas-Fermi distribution for the atomic electrons.

For scattering angles greater than or equal to 90 degrees and for photon energies of order $\approx_0 c^2$, the expression

$$\frac{d\sigma_R}{d\Omega} = 8.67 \times 10^{-33} \left(\frac{Z m_0 c^2}{k} \right)^3 \frac{1 + \cos^2 \theta}{2 \sin^3 \frac{\theta}{2}} \quad \frac{\text{cm}^2}{\text{Ster.}} \quad (\text{II-19})$$

results, where Z is the atomic number of the scattering atom, k is the incident photon energy, and θ is the angle of scattering. The work of Brown et al.⁶² indicates that Equation (II-19) is valid over the energy range 1 to 3 MeV.

The nuclear Thomson scattering cross section may be obtained from the expression⁶³ for the scattering of x-rays by electrons by using the nuclear mass, M , in

place of the electronic mass, m_0 , and the nuclear charge, Ze , in place of the electronic charge, e , resulting in

$$\frac{d\sigma_{Th}}{d\Omega} = \frac{Z^4 e^4}{2M^2 c^4} (1 + \cos^2 \theta) \frac{\text{cm}^2}{\text{Ster.}} \quad (\text{II-20})$$

which may be rewritten as

$$\frac{d\sigma_{Th}}{d\Omega} = 2.39 \times 10^{-32} \frac{Z^4}{A^2} \frac{(1 + \cos^2 \theta)}{2} \frac{\text{cm}^2}{\text{ster.}} \quad (\text{II-20a})$$

Delbruck scattering, the elastic scattering of photons in the Coulomb field of the nucleus, is reported to have cross sections proportional to $(\alpha Z)^4 r_0^2$.⁶⁴ While numerous theoretical studies⁶⁵ have been conducted on this process, there exists no experimental evidence to show that the process can be detected below 9 MeV⁶⁶ and any contribution from this source was considered to be negligible.

c) Background Effects

It is of interest to consider the effects due to the competing processes at the annihilation radiation energy (and at an angle of 120 degrees). If the number of background .511 MeV photons detected is denoted by the parameter B_g , the expression

$$B_g = N_{PAIR}(k'') + N_{Th} + N_R \quad (\text{II-21})$$

can be written. In this equation, $N_{\text{PAIR}}(k'')$ is the number of annihilation radiation quanta detected which are produced by incident photons of other than the monochromat energy, N_{Th} is the number of .511 MeV bremsstrahlung quanta detected after being scattered by nuclear Thomson scattering, and N_{R} is a similar number for the Rayleigh scattering process.

The number of background quanta detected for the two elastic processes can be expressed as

$$N_{\text{R}} = \mathcal{N}(k') n \bar{\eta} \Omega \frac{d\sigma_{\text{R}}}{d\Omega} \quad (\text{II-22})$$

for the Rayleigh process, and

$$N_{\text{Th}} = \mathcal{N}(k') n \bar{\eta} \Omega \frac{d\sigma_{\text{Th}}}{d\Omega} \quad (\text{II-23})$$

where $\mathcal{N}(k')$ is the number of .511 MeV bremsstrahlung photons incident on the target sample and previous notation is used for the other factors.

The pair creation contribution due to non-monoergic photons is more complex in form and is approximated by a numerical sum of contributions

$$N_{\text{PAIR}}(k'') = \sum_{\substack{k' \\ k' \neq k''}} \mathcal{N}(k') n \bar{\eta} \sigma_{\text{PAIR}}(k') \quad (\text{II-24})$$

which are calculated using the "zero-thickness"



approximation. The factor B_g can now be written as

$$B_g = n\bar{n} \left[\mathcal{N}(k') \left\{ \frac{d\sigma_m}{d\Omega} + \frac{d\sigma_R}{d\Omega} \right\} \Omega + \sum_i \mathcal{N}(k') \sigma_{PAIR}(k') \right] \quad (II-25)$$

but recalling Equation (II-11a), write

$$\mathcal{N}(k) = n'Q \Delta\sigma_B(k) \quad (II-26)$$

which allows the final expression for B_g to be expressed as

$$B_g = n\bar{n} n'Q \left[\Delta\sigma_B(k') \Omega \left\{ \frac{d\sigma_m}{d\Omega} + \frac{d\sigma_R}{d\Omega} \right\} + \sum_i \Delta\sigma_B(k') \sigma_{PAIR}(k') \right] \quad (II-27)$$

This expression provides a means to estimate the total number of background .511 MeV quanta which will be detected in the scintillation spectrometer detector.

In a double coincidence measurement, the final estimate of the background effect must be determined by

$$B_g^{ch} = 2\mathcal{T} B_g N_e \quad (II-28)$$

where $2\mathcal{T}$ is the full width at half-maximum value for the resolving time curve and N_e is the average counting rate for the detection of post-bremsstrahlung electrons.

The background effects present in this research were measured and, therefore, were accounted for



experimentally. The estimated value of the background, as developed, showed that if the pair creation cross section was equal to the predictions of Jaeger and Hulme, the cross section could be measured for an incident photon energy of 1.533 MeV using the monochromatic technique.

B. Bremsstrahlung

As in the case of pair creation studies, the derivation of an exact expression for the bremsstrahlung cross section requires use of Dirac wave functions obtained from solution of the Dirac wave equation. For reasons previously noted in Section (II.A.1), the major portion of analytical expressions for the bremsstrahlung cross section has been derived using some appropriate approximation technique. This discussion will include only those derivations which have some relevancy for the present research.

1. Cross Section Due To Bethe and Heitler

In the same paper which laid the fundamental groundwork for pair creation cross section predictions, these authors provided a comprehensive study of the bremsstrahlung phenomenon using the Born approximation technique. In this formulation, the assumptions

$$2\pi \alpha Z/\beta \ll 1, \quad 2\pi \alpha Z/\beta \ll 1$$

were made, where β_0 and β refer to the incident and outgoing electron, respectively. Thus, for high Z , atomic number, targets, for electrons of low initial kinetic energy, and for the case where the photon carries off almost all of the available energy, the prediction becomes less reliable.

The Bethe and Heitler calculation (hereafter referred to as the B-H result) gave the bremsstrahlung cross section differential in photon energy, photon emission angle, and electron emission angle. This result was integrated over all angles to provide a cross section differential in photon energy. Calculations were also conducted to predict the effect of screening at high energies such that $E, E_0 \gg m_0 c^2$.

The B-H result is often used as a starting point in other more specific investigations of the bremsstrahlung phenomenon. Of primary interest for this research is the work of Koch and Motz⁶⁷ who have compiled a compendium of theoretical analyses with the corresponding analytical expressions and compared these theories to existing experimental cross sections. These authors have presented a form of the B-H result given by

$$\frac{d^3\sigma_B}{dk d\Omega_k d\Omega_p} = \frac{Z^2}{137} \left(\frac{r_0}{2\pi}\right)^2 [1 - F(q, Z)]^2 \frac{1}{k} \frac{p}{P} \frac{1}{q^4} \times \quad (\text{II-29})$$



$$\left\{ \frac{p^2 \sin^2 \theta}{(E - p \cos \theta)^2} (4E_o^2 - q^2) + \frac{p_o^2 \sin^2 \theta_o}{(E_o - p_o \cos \theta_o)^2} (4E^2 - q^2) - \frac{2pp_o \sin \theta \sin \theta_o \cos \phi (4EE_o - q^2)}{(E - p \cos \theta)(E_o - p_o \cos \theta_o)} \right. \\ \left. + \frac{2k^2 (p^2 \sin^2 \theta + p_o^2 \sin^2 \theta_o - 2pp_o \sin \theta \sin \theta_o \cos \phi)}{(E - p \cos \theta)(E_o - p_o \cos \theta_o)} \right\} \quad (\text{II-29})$$

where

$$\cos \theta = \frac{\vec{p} \cdot \vec{k}}{|\vec{p}| |\vec{k}|} \quad (\text{II-29a})$$

$$\cos \theta_o = \frac{\vec{p}_o \cdot \vec{k}}{|\vec{p}_o| |\vec{k}|} \quad (\text{II-29b})$$

$$q^2 = p^2 + p_o^2 + k^2 - 2p_k \cos \theta_o + 2pk \cos \theta - 2p_p (\cos \theta \cos \theta_o + \sin \theta \sin \theta_o \cos \phi) \quad (\text{II-29c})$$

and ϕ is the angle between the planes (\vec{p}, \vec{k}) and (\vec{p}_o, \vec{k}) , $F(q, Z)$ is an atomic form factor which accounts for screening effects, and the other terms have been previously defined. This expression has been integrated over various electron and photon solid angles and the result for one given set of energy parameters is presented in Figure (II-1).

2. Other Approximate Theories

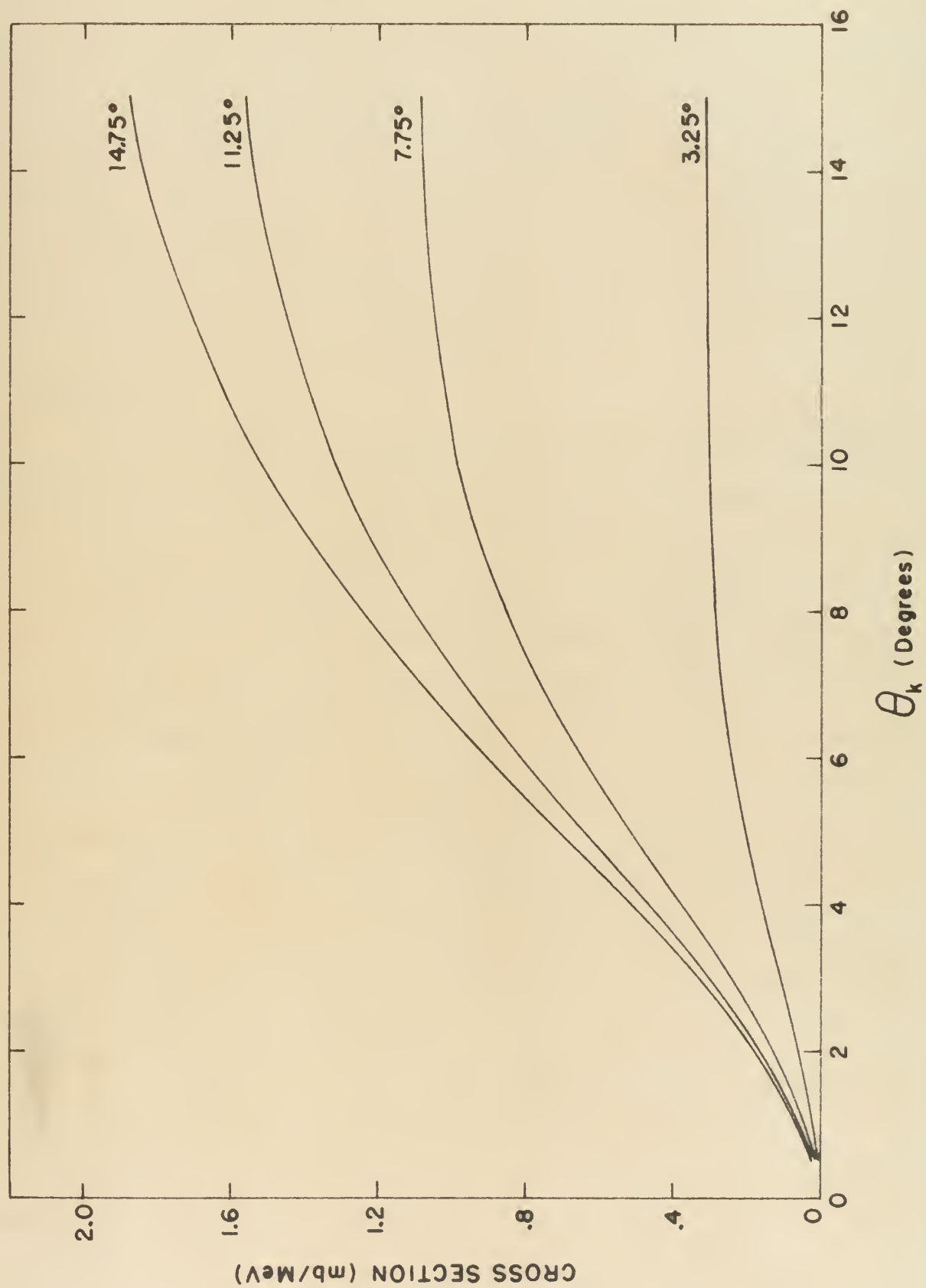
Sauter⁴⁰ has formulated an expression for the



Figure (II-1)

Evaluation of the Bethe-Heitler bremsstrahlung cross section differential in photon energy, photon emission angle, and electron emission angle. Shown are four curves corresponding to electron emission cones of half-angle 3.25° , 7.75° , 11.25° , and 14.75° for an incident electron energy of 2.3 MeV and a photon energy of 1.2 MeV. Each curve represents the cross section (mb/MeV) for photon emission into the cone of half-angle θ_k plotted as a function of θ_k .





bremssstrahlung cross section differential in photon energy and photon emission angle using the Born approximation. However, the development omitted the effects of screening which causes the expression to be of questionable validity unless the condition for no screening

$$1/(\alpha Z^{1/3}) \gg E_0 E / k$$

obtains.

Schiff⁴¹ integrated the B-H result over electron emission angles for the extreme relativistic case ($E_0, E, k \gg m_0 c^2$) using the approximate screening potential correction $V(r) = (Ze/r) \exp(-r/a)$, where $a = 111 Z^{-1/3}$. The expression obtained, differential in photon energy and photon emission angle, is valid only for small forward angles.

Gluckstern and Hull⁴² obtained the Sauter expression for low photon energies in an independent Born approximation calculation. Using the same approximate screening potential expression as Schiff, the result included a correction for screening of the nuclear Coulomb field by the atomic electrons.

Racah⁶⁸ and, independently, McCormick, Kieffer, and Parzen⁶⁹ provided a bremsstrahlung cross section differential in electron energy and emission angle by integrating the B-H result over photon emission angle. Neglect of screening effects reduced the reliability of



these results at small forward angles.

III. EXPERIMENTAL APPARATUS AND PROCEDURE

A. General Equipment and Procedure

The accelerator, beam handling system, and calibrations of the 60 degree analyzing magnet and monochromator magnet have been considered in some detail in previous theses.^{39,70,71} For the sake of completeness, an up-to-date discussion of the present system is included in Appendices A, B, and C, respectively. A brief description of the procedure is in order here, however.

The electron beam is extracted from the Notre Dame 4.5 MeV electrostatic accelerator and steered via the beam handling system through a set of defining slits into the 60 degree analyzing magnet. After passing through this calibrated magnetic field and a set of image slits, the beam undergoes a further 45 degree deflection in a magnetic field which focuses it onto a thin self-supporting gold foil in which the photons used in photon-induced reactions are produced. The 60 degree analyzing magnet field provides knowledge of the incident electron beam energy while signals from the image slits of this magnet are used in a negative feedback system to provide energy stabilization of the accelerator terminal potential.

B. The Monochromator

Figure (III-1) is presented prior to discussion of the monochromator in order to assist in the visualization of many of the quantities referred to in the text.

1. Theory and Design

The study of the inclined plane pole-face type magnet was initiated by H. O. W. Richardson^{72,73} in a study of the orbit trajectories, focusing conditions, and momentum dispersion properties of such a magnetic spectrometer with the source position located in the magnetic field. The magnet envisioned consisted of a plane face magnet with the pole-faces inclined at an angle of 2ϕ relative to one another. The resultant magnetic field between the pole pieces is then similar to the field due to a current carrying wire running along the axis of intersection of the inclined poles (extended) with each $\phi = \text{constant}$ plane being a magnetic equipotential plane. The field between the pole pieces carries a $1/r$ dependence, where r is the distance from the Z-axis.

The mathematical theory used by Richardson led to orbit equations given as

$$r = A e^{K \cos \psi} \quad (\text{III-1})$$

where, for a point source,

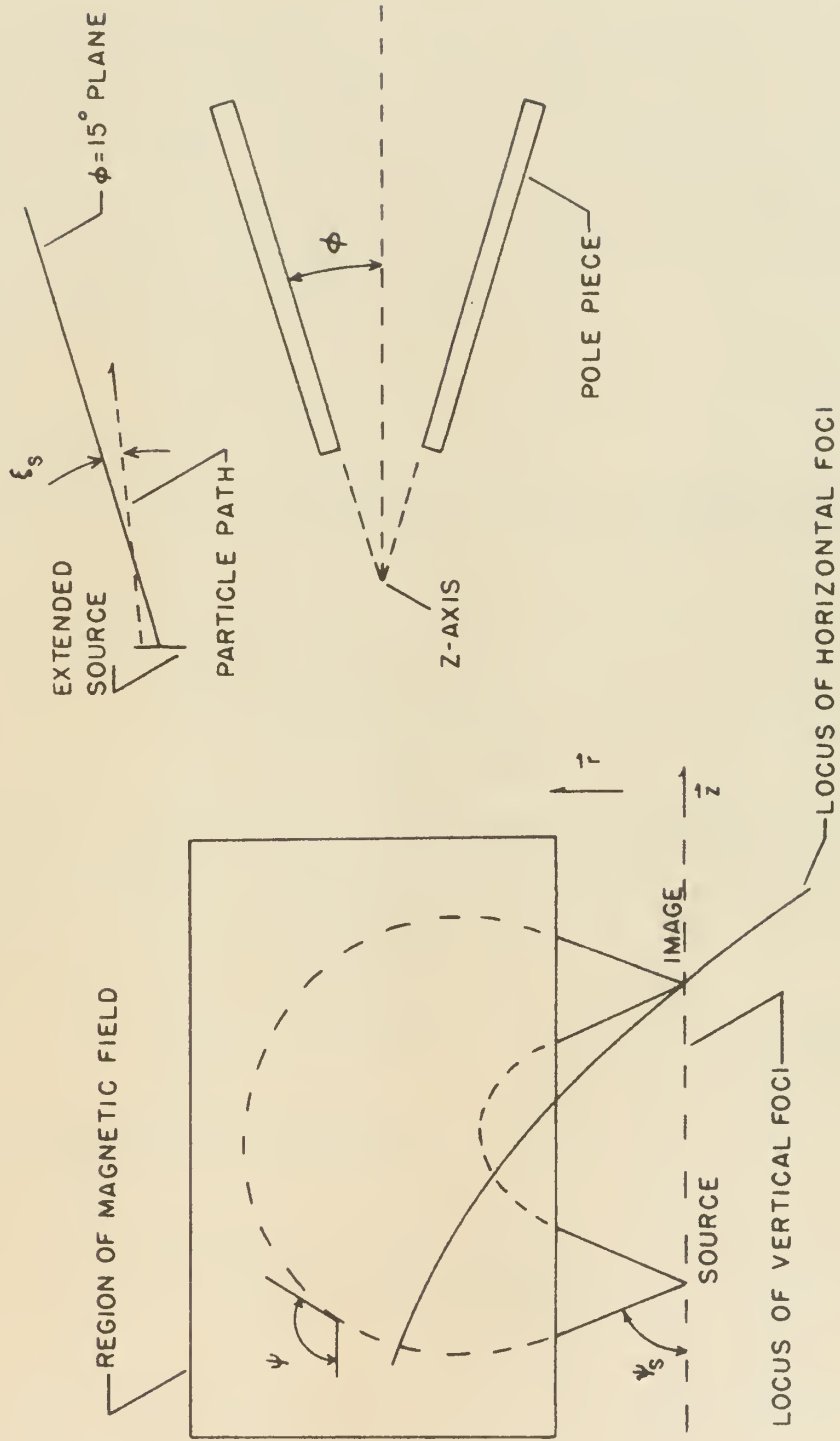
$$A = r_s e^{-K \cos \psi_s} \quad (\text{III-1a})$$



Figure (III-1)

Typical inclined plane pole-face
magnet including nomenclature and
variables.





with r_s being the distance of the source position from the Z-axis, ψ_s is the angle of emission of the source particles, ψ is the angle between the velocity vector of the particle at any point in its orbit and the Z-axis, and K is a momentum parameter defined by

$$K = \frac{mv}{B_1 c} ; \quad B_1 \quad (\text{III-1b})$$

is the magnetic field value at $r = 1$.

The equation of the Z-component of the trajectory is given by

$$z = -AK \int \frac{e^{K \cos \psi} \cos \psi d\psi}{\sqrt{1 - \frac{a_0^2 e^{-2K \cos \psi}}{A^2 \sin^2 \psi}}} , \quad (\text{III-2})$$

with a_0 given by $r_s \sin \xi_s$, ξ_s being the angle between the velocity vector at emission and a plane of angle $\phi = \text{const}$; a_0 can also be given by

$$p\phi/mv = r \sin \xi . \quad (\text{III-2a})$$

The equation for ϕ is given by

$$\phi = -\frac{a_0 K}{A} \int \frac{e^{-K \cos \psi} d\psi}{\sqrt{1 - \frac{a_0^2 e^{-2K \cos \psi}}{A^2 \sin^2 \psi}}} . \quad (\text{III-3})$$

The Equations (III-1), (III-2), and (III-3) form the orbit equations for the general case.

If conditions are simplified to consideration of orbits from a point source lying in the mid-plane, these



equations are reduced to

$$r = r_s e^{K(\cos \psi - \cos \psi_s)} \quad (\text{III-4a})$$

$$z = -K r_s e^{-K \cos \psi_s} \int \cos \psi e^{K \cos \psi} d\psi \quad (\text{III-4b})$$

$$\phi = \text{Constant} (=0 \text{ for midplane}), \quad (\text{III-4c})$$

if the inclination i is small or zero. These relatively simple equations were used by Richardson to determine orbits in the mid-plane using numerical integration techniques.

Richardson pointed out that since the orbits are symmetric about $\psi = 0$ (in this reference system), a particle emitted from the source point at an angle ψ_s will return to the radius r_s at $\psi = -\psi_s$. Therefore, the image point can be found from

$$z_i = -2K r_s e^{-K \cos \psi_s} \int_{\psi_s}^0 \cos \psi e^{K \cos \psi} d\psi \quad (\text{III-5})$$

for orbits in the mid-plane.

For orbits out of the mid-plane, the expression

$$z_i = -2K r_s e^{-K \cos \psi_s} \int_{\psi_s}^{\psi_m} \frac{\cos \psi e^{K \cos \psi} d\psi}{\sqrt{1 - \frac{b^2 e^{-2K \cos \psi}}{\sin^2 \psi}}} \quad (\text{III-6})$$



was given where

$$b = \sin \xi_s e^{K \cos \psi s} . \quad (\text{III-6a})$$

The upper limit on the integral is, effectively, the limiting angle beyond which the particle will not return to the $r = r_s$ axis.

From detailed considerations of slit size, maximum ψ value, range of ψ values collected at the image point, source to image distance, Z_1 , and other factors, Richardson concluded that the theoretical solid angle for collection was 16.5 times that available to a parallel pole spectrometer of similar size. By studying the momentum dispersion and resolving power properties of the device, he claimed an increase in dispersion of a factor of 4.24 over a semi-circular spectrometer of the same path length.

In their development of an inclined plane pole-face spectrometer, Kofoed-Hansen, Lindhard, and Nielsen re-examined the motion of the electrons in the Z - r plane obtaining essentially the same results as Richardson. The family of trajectories was re-expressed as

$$z = a K U(K, \psi) + z_0 \quad (\text{III-7a})$$

$$r = a e^{-K \cos \psi} \quad (\text{III-7b})$$

$$\phi = \text{Constant} , \quad (\text{III-7b})$$

where a is the value of r at the point where $\psi = \pi/2$ and K is the momentum parameter as given by Richardson. The function $U(K, \psi)$ defined as

$$U(K, \psi) = \int_{\pi}^{\psi_s} \cos \psi e^{-K \cos \psi} d\psi$$

was developed in a series of Bessel functions as

$$U(K, \psi) = i J_1(iK) (\pi - \psi) - \sum_{n=1}^{\infty} \frac{1}{n} (i)^{n-1} (J_{n-1}(iK) - J_{n+1}(iK)) \sin \psi. (\text{III-8})$$

The authors pointed out that for $K \lesssim 1$, only four to six terms in the sum over n are necessary to obtain $U(K, \psi)$ to about four decimal places.

By limiting the analysis to the angular range, $0 \leq \psi \leq 2\pi$, possible multi-loop trajectories were avoided. Unsymmetric orbit arrangements were considered by introduction of a parameter

$$\rho(a) \equiv z(r = r_{\max.}),$$

where, for symmetric orbits, $\rho(a) = 0$. The orbit Equations (III-7) were then rewritten as

$$z = a K U(K, \psi) + \rho(a) \quad (\text{III-9a})$$

$$r = a e^{-K \cos \psi} \quad (\text{III-9b})$$

$$\phi = \text{Constant} . \quad (\text{III-9c})$$

The shape of the magnet profile was then determined using Equations (III-9) and the condition that focusing was to take place at the conjugate point on the image side of the magnet. Using a simple relationship for $\rho(a)$ given by $\rho(a) = C \cdot a$, the profile was constructed from the equations

$$z = z_s \frac{K U(K, \psi) + C}{K U(K, \psi) + C - \cot \psi \exp \{-K \cos \psi\}} \quad (\text{III-10a})$$

$$r = z_s \frac{\exp \{-K \cos \psi\}}{K U(K, \psi) + C - \cot \psi \exp \{-K \cos \psi\}} . \quad (\text{III-10b})$$

In 1961, O'Connell et al. considered in detail the electron trajectories, vertical and horizontal focusing conditions, image width, image location, energy dispersion, and magnification of the inclined plane pole-face magnet using a simplified procedure. Their method was based on the rectangular pole piece without shaping of the profile. Thus, no compensation for fringe field effects was included. These results were consistent with those of Richardson and Kofoed-Hansen et al. though much simplified in nature. This type of a device is particularly



suitied for use as a high energy (> 6 MeV) monochromator.

A very definitive study of the properties of the shaped profile inclined plane pole-face magnetic sector spectrometers, including the effects due to fringe fields, has been reported by Jaffey et al.⁷⁴ Almost every conceivable problem associated with this type of spectrometer was anticipated and treated, to some degree, in this exhaustive presentation. Only the salient points will be mentioned here.

Using the mathematical theory applied by both Richardson and Kofoed-Hansen et al. plus including the possible multi-loop trajectories, these authors obtain as trajectory equations

$$r = a e^{-K \cos \psi} \quad (\text{III-11a})$$

$$z = aK [U(K, \psi) + 2\pi n i J_1(iK)] + Z_M, \quad (\text{III-11b})$$

where

$$Z_M = z_m (= z @ \psi = \pi)$$

if n is integer

$$Z_M = z_m - aK i J_1(iK) \pi (= z @ \psi = 0)$$

if n is half-integer and the inclusion of multi-loop trajectories causes the more complex structure of these equations to arise. Important facts to be considered were pointed out as

- (1) Vary a , K and Z_M constant. Families of similar trajectories result differing only in scale factor; thus $(a-Z_M)$ and r are proportional to a . This is a symmetric family.
- (2) Vary Z_M by ΔZ_M , K and a constant. A displacement parallel to the z axis in the trajectory results. The point on the trajectory (z_1, r_1) becomes $(z_1 + \Delta Z_M, r_1)$.
- (3) Vary K , a and Z_M constant. A variation in the form of the trajectory results.

The most general family of trajectories was given by (with K constant)

$$z = aK [U(K, \psi) + 2\pi ni J_1(aK)] + Z_M(a) \quad (\text{III-12a})$$

$$r = a e^{-K \cos \psi} \quad (\text{III-12b})$$

in a form similar to Equations (III-9). This family provides the property of complete focusing since, in this case, the magnetic field acts on particles of the same momentum but with different initial conditions.

In the case where $p_\phi \neq 0$, i.e., there exists a momentum component parallel to the flux lines, the authors gave the following trajectory equations (assuming p_ϕ is so small that $a_0 \approx \delta a_0$)



$$Z = aK \int \cos \psi e^{-K \cos \psi} \left[1 - \frac{1}{2} \left(\frac{\delta a_0}{a} \right)^2 e^{2K \cos \psi} (1 + K \cos \psi) \right] d\psi + Z_M \quad (\text{III-13a})$$

$$r = a e^{-K \cos \psi} \left[1 + \frac{1}{2} \left(\frac{\delta a_0}{a} \right)^2 K \cos \psi e^{2K \cos \psi} \right] \quad (\text{III-13b})$$

$$\phi = K V(K, \psi) \frac{\delta a_0}{a} + \phi_m \quad (\text{III-13c})$$

where

$$V(K, \psi) = \int_{-\pi}^{\psi} e^{K \cos \gamma} d\gamma = J_0(iK)(\psi - \pi) + \sum_{l=1}^{\infty} \frac{2}{l} (-i)^l J_l(iK) \sin l\psi \quad (\text{III-14})$$

The functions $U(K, \psi)$ and $V(K, \psi)$ are provided in tabular form by the authors.

Using these equations as elements of a boundary value problem, the entrance and exit profiles of the magnetic field region can be determined. The problems of ghost peaks, dispersion, resolution, transmission, etc. were treated with and without the effects of fringing and techniques were presented for simplified application of the theory to any practical design for a spectrometer. As well, all necessary functions useful in the calculations were tabulated.

In brief, the fringe field effects were shown to have generally deleterious effects on the properties of this type of magnet. In total, the effects were proven



to reduce the available transmission³⁹ and resolving power³⁹ of the device although the device was still potentially superior to any other spectrometer in terms of transmission available. The major contribution of these authors lay in the complete analysis of the total problem, thus demonstrating methods to be used to minimize the problems of the fringe field effects.

The design and construction of the Notre Dame monochromator predated the complete development of the theory as related by Jaffey et al. The Notre Dame design was adapted from the Kofoed-Hansen et al. design, the major difference being the use of the 120 degree entrance angle rather than the 90 degree angle of the Swedish device. This change was necessitated by the requirement on bending the main electron beam, as well as the post-bremsstrahlung electrons, through angles greater than 90 degrees. The various theoretical developments just traced were used by the present author to verify the expected operating parameters of the spectrometer.

The primary concern in the initial theoretical tests was the determination of the correct entrance (or source) position and the correct exit slit position. The proper location of these positions would serve to ensure attainment of the optimum operating parameters. The determination of the theoretical electron trajectories was



carried out in two ways, each independent of the other.

The first method utilized an analog ray-tracing device, known as the "Bug", which was built in this laboratory. This device will be considered in some detail in Appendix (D). Using the analog ray-tracing device, trajectories were determined for a range of electron energies large enough to include non-focused high and low energy electrons and the proper energy electrons to check the focusing properties with and without the fringe field. Repeatability of the resultant trajectories was checked and found to be within two or three percent deviation in the region of the magnetic field.

These analog results were checked by computer calculations using the theoretical expressions discussed previously. Some trajectories obtained are shown in Figure (III-2) and verify that the positions of the source and exit slits are conjugate points.

The positions of the source and exit slit, as well as the proper shape for the exit slit aperture, were experimentally determined by Walter, Shea, and Miller and the method used was discussed in Reference (36).

2. Parameters of Performance

The disappointing performance of the monochromator as reported by Malaker forced a complete re-evaluation of the device and necessitated an experimental

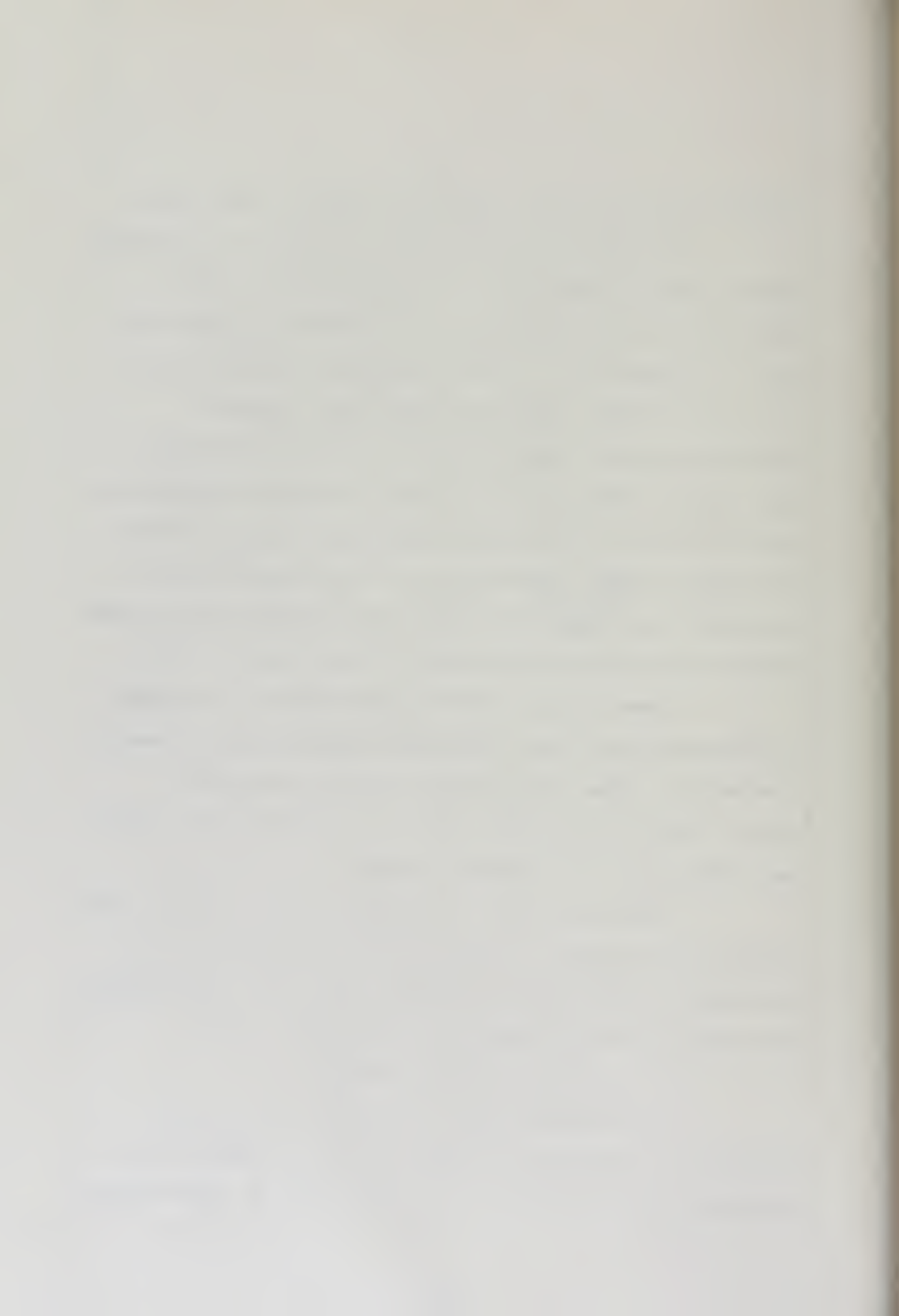
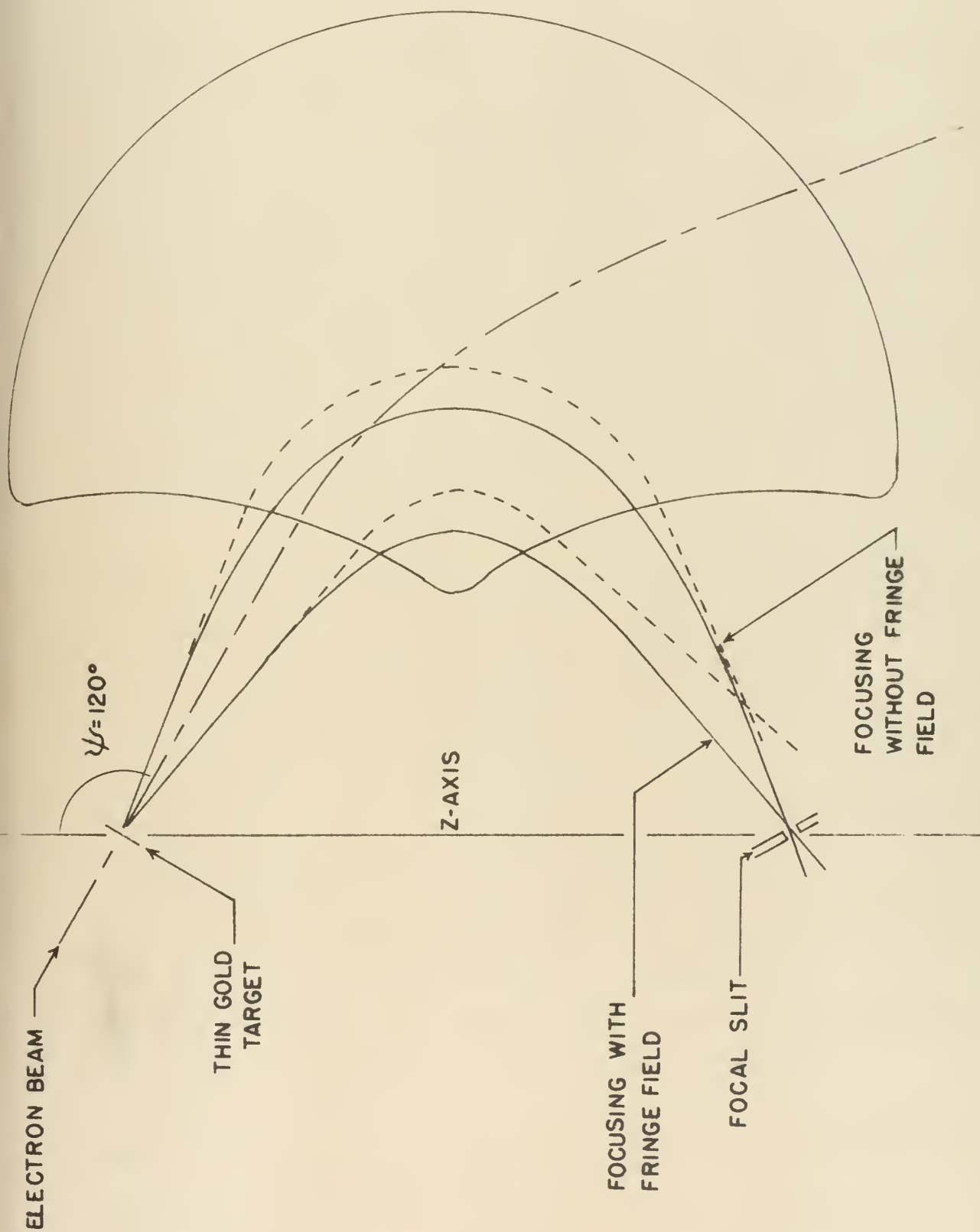


Figure (III-2)

Electron trajectories in the monochromator.



examination of the effects of source position, exit slit position and shape, and the effects due to baffles.

a) Transmission and Resolution

Due to the insertion of a rotating coil used to measure the magnetic field, the available geometric solid angle was approximately 2.65 percent of 4π rather than the 4 percent figure which was available to Kofoed-Hansen et al. Thus, the probability of achieving the desired transmission value of 2 percent was severely reduced before any tests were conducted.

The initial procedure used was to test the monochromator in the original configuration as set up by Malaker, described in detail in a later section, in order to improve the performance or, at the very least, to explain the low transmission measured by Malaker. The test procedure used was as follows: a calibrated ^{137}Cs source was moved in the median plane normal to the Z-axis. Electrons were detected with a plastic scintillator placed behind the exit slit. For each source position, the exit slit was sequentially (a) changed in size, then (b) repositioned in the median plane normal to the Z-axis, then (c) moved parallel to the Z-axis. Changing the position of the source affected the transmission by, at most, 10 percent. Changes in exit slit position, both parallel and normal to the Z-axis, caused a general



deterioration in the transmission and resolution parameters. The salient feature of these tests was a failure to improve the transmission by more than 25 percent as a result of changes in both source position and slit shape. The optimum transmission measured was .21 percent compared to the .17 percent measured by Malaker. (In fact, the transmission without slits or baffles was only .9 percent of 4π !)

The problem of the low transmission was resolved by moving the plastic scintillator closer to the exit slit. When this change was made, the transmission, without baffles or slits, was raised to 2.4 percent or 90.5 percent of the available geometric solid angle. Introduction of a baffle to eliminate direct transmission between the source and the exit slit, reduced the transmission to 1.8 percent, 69 percent of the geometric solid angle, at a resolution, $\Delta P/P$, of 9.2 percent. The tests described above were then repeated using the new position of the scintillator. These tests demonstrated an optimum transmission of .7 percent (corresponding to an electron acceptance cone of half-angle 9.5 degrees) with an associated resolution of 1.98 percent. It was also determined in the course of this investigation that the electron acceptance cone was right elliptical in nature, with the major axis parallel to the Z-axis,



rather than right circular as had been previously assumed. However, computer evaluation of the bremsstrahlung cross sections using a right elliptical electron acceptance cone of the measured size showed a negligible error was introduced by assuming this cone to be right circular in form.

The introduction of an exit baffle, described further in Section (III.B.2.c), was necessary in order to reduce the excessive electron count rate in the electron detector. This added restriction resulted in a final set of parameters which were a transmission of .44 percent and a resolution of 2 percent. These parameters were considered adequate for the pair creation measurements.

b) Figure of Merit

In previous evaluations of the Notre Dame monochromator, the criterion for acceptable performance was taken to be the ratio of the number of monoenergetic photons produced to the number of electrons detected in the electron detector. Thus, if the electron count rate was higher than expected the relative performance of the monochromator appeared to be unsatisfactory. Since all previous checks had indicated an excessive electron count rate, it was necessary to determine a parameter which was a measure of the efficiency of the system for producing monochromatic photons in a given solid angle for a



measured post-bremsstrahlung electron acceptance solid angle, without regard for the accompanying electron count rate. The figure of merit was defined as the ratio of the measured bremsstrahlung cross section, to be described, to the calculated cross section (calculated using Equation (II-29)) for the same photon emission solid angle and electron emission solid angle. The ratio is given by

$$F_M = \left(\frac{d\sigma_B}{dk} \right)_{\text{EXP}} / \int_{\Delta\Omega_p} \int_{\Delta\Omega_k} \frac{d^3\sigma}{dk d\Omega_p d\Omega_k} d\Omega_p d\Omega_k$$

Numerous tests using foils of various thicknesses and atomic numbers were conducted. Over the fractional photon energy range .4 to .6 using a thin (1.16 mg/cm²) Ni foil, an average figure of merit of $1.07 \pm .07$ was measured. Final tests with a gold foil (1.41 mg/cm²) over the fractional photon energy range of .5 to .75 gave an average figure of merit of $1.00 \pm .06$. The conclusion is therefore clear that the monochromator is very efficient in the production of monoenergetic photons.

c) Electron Scattering

The major problem experienced in the continuing development of the monochromator has been the existence of extraneous electrons, nominally of the correct energy, $T_0 - k$, but not corresponding to the production of monoenergetic photons. In the work of Walter and Shea,



inelastically scattered electrons were found to give a factor of 10^6 too many electrons. The introduction of a 45 degree bending magnet between the energy control slits and the gold foil eliminated the slit scattered electrons (a factor of 10^5) but there remained a factor of ten times too many electrons. This difficulty was sufficient to obviate the use of the monochromatic technique in nuclear resonance fluorescence studies. As a result of this experience, Malaker suggested the existence of an extra factor of ten in the inelastic electron scattering cross section.

In order to gain insight into the possible sources of the excess electron rate, consideration of the electron scattering phenomenon is important. Bremsstrahlung is not considered in the following discussion.

When electrons interact with matter, the particles can lose energy and can be deflected from their original trajectory. In the energy range of 1 to 3 MeV, the deflection of the electrons is almost entirely due to elastic interaction with the atomic nucleus. The energy loss results from interaction with the atomic electrons. It is possible to consider these two phenomena separately although they occur together.

1) Elastic Scattering

Elastic scattering can be considered in four



classes as: (1) Single Scattering, (2) Plural Scattering, (3) Multiple Scattering, and (4) Diffusion. The criterion for determining which process takes place is expressed in terms of the areal density of the foil and the cross section for the scattering process. For the foils used in the present research, the condition $n \sigma_{\text{SCATT.}} \approx 1$ is satisfied and multiple scattering is the dominant process. Generally speaking, multiple scattering indicates that the target is so thick that the mean number of scattering processes which take place in the foil is larger than about twenty. The angular distribution function is approximately Gaussian unless the mean angle of scattering is greater than approximately 20 degrees.⁷⁵

Theoretical investigations of multiple scattering have been carried out by Bothe⁷⁶, Williams⁷⁷, Molière⁷⁸, and by Snyder and Scott.⁷⁹ For small values of the scattering angle ($\theta < 20$ degrees), Molière obtains relatively simple, and experimentally confirmed, angular distributions for the probability that an electron passing through a foil of thickness d will be scattered through an angle θ into the solid angle $d\Omega = 2\pi \sin\theta d\theta$. His expression is given by

$$W(\theta)2\pi\sin\theta d\theta = [2\exp(-\theta^2) + F_1(\theta)/B + F_2(\theta)/B^2 + \dots] \theta d\theta \quad (\text{III-15})$$



where

$$\Theta = \bar{\Theta} / \chi_c \sqrt{B} \quad ; \quad \chi_c = \frac{44.8 Z}{\left(\frac{T + m_0 c^2}{m_0 c^2} - \frac{m_0 c^2}{T + m_0 c^2} \right)} \sqrt{\frac{n}{A}} \quad \text{degrees}$$

with n being the foil areal density (g/cm^2), Z is the atomic number of the atoms of the foil and A is the atomic weight, T and m_0 are the kinetic energy and rest mass of the incident electron. The parameter B is related to the mean number of collisions, C , given by Molière as

$$\log_{10} C = 8.215 + \log_{10} \left[\frac{n}{AZ^{2/3}} \frac{\gamma^2}{1.13 + 3.76 \gamma^2} \right] \quad (\text{III-16})$$

with $\gamma = \alpha Z / \beta$.

Projecting the distribution of Equation (III-15) onto a plane parallel to the incident beam direction results in a "projected angular distribution" given by

$$W(\Phi) d\Phi = [\pi^{-1/2} \exp(-\Phi^2) + f_1(\Phi)/B + f_2(\Phi)/B^2 + \dots] d\Phi \quad (\text{III-17})$$

where

$$\Phi = \bar{\Phi} / \chi_c \sqrt{B}$$

B is tabulated in References 75 and 78, for various values of C . The functions F_1 , F_2 , f_1 , and f_2 have also been tabulated by Molière.

The mean value of the scattering angle, $\bar{\Theta}$, is given by Molière as



$$\frac{2}{\pi} \bar{\Theta} = \bar{\Phi} = \chi_c \sqrt{B} (1 + 0.982/B - 0.117/B^2 + \dots). \quad (\text{III-18})$$

Hanson et al.⁸⁰ give an expression for the 1/e th angle as

$$\Theta_{1/e} = \chi_c (1.007B - 1.33)^{1/2}. \quad (\text{III-19})$$

Experimental studies by Kulchitsky and Latyshev,⁸¹ with 2 MeV incident electrons, confirms, for a large number of elements, the theory as presented by Molière.

A series of calculations on the distributions and mean scattering angles in a variety of target foils was carried out. The results of this study indicated that the dependence of the mean scattering angle on the areal density of the foil (through the B parameter) might play an important role in accounting for the excess electron count rate. This circumstance arises due to the possibility of widely scattered electrons interacting with the baffles and pole pieces of the monochromator magnet in inelastic collisions after the scattered electrons had passed the foil. For a gold foil of areal density 2.56 mg/cm² and an incident kinetic energy of 2.86 MeV, the mean value of the scattering angle is 7.6 degrees indicating that a finite percentage of the electrons is



elastically scattered to larger angles. Thus, since the angle between the median plane and a pole piece is 15 degrees, and also since the effect of the magnetic fringe field is to bend off-axis particles towards the pole pieces, a finite percentage of the beam might hit the baffles and pole pieces. A simple calculation shows that if only 16 electrons per million in the main electron beam were thus scattered from the baffles and pole pieces such that their trajectories terminated in the electron detector, the excess electron rate would be accounted for. The use of a 1.41 mg/cm^2 foil at the same energy reduces the mean scattering angle to a value of 3.8 degrees. More importantly, the use of thinner target foils, coupled with a new exit baffle, did reduce the excessive electron count rate by about a factor of three.

11) Inelastic Scattering

Since the majority of theoretical and experimental studies of energy loss by electrons in matter are concerned with the most probable energy loss and the mean energy loss per unit path length, it was difficult to determine the value of the relative cross section for energy losses of the order of $.5T_0$ or greater. The excellent papers by Paul et al.,⁸² Knop et al.,⁸³ and Febal et al.⁸⁴ allow at least an approximate determination of the relative magnitudes of the bremsstrahlung and



inelastic processes. From the former papers, it can be deduced that, for large energy losses, the contribution to the electron count rate would be of the order of 1.3 electrons per million in the main electron beam for foils of areal density 2.2 mg/cm^2 . This is roughly one order of magnitude less than the value needed to account for the excess detected electron rate.

111) The Excessive Electron Count Rate

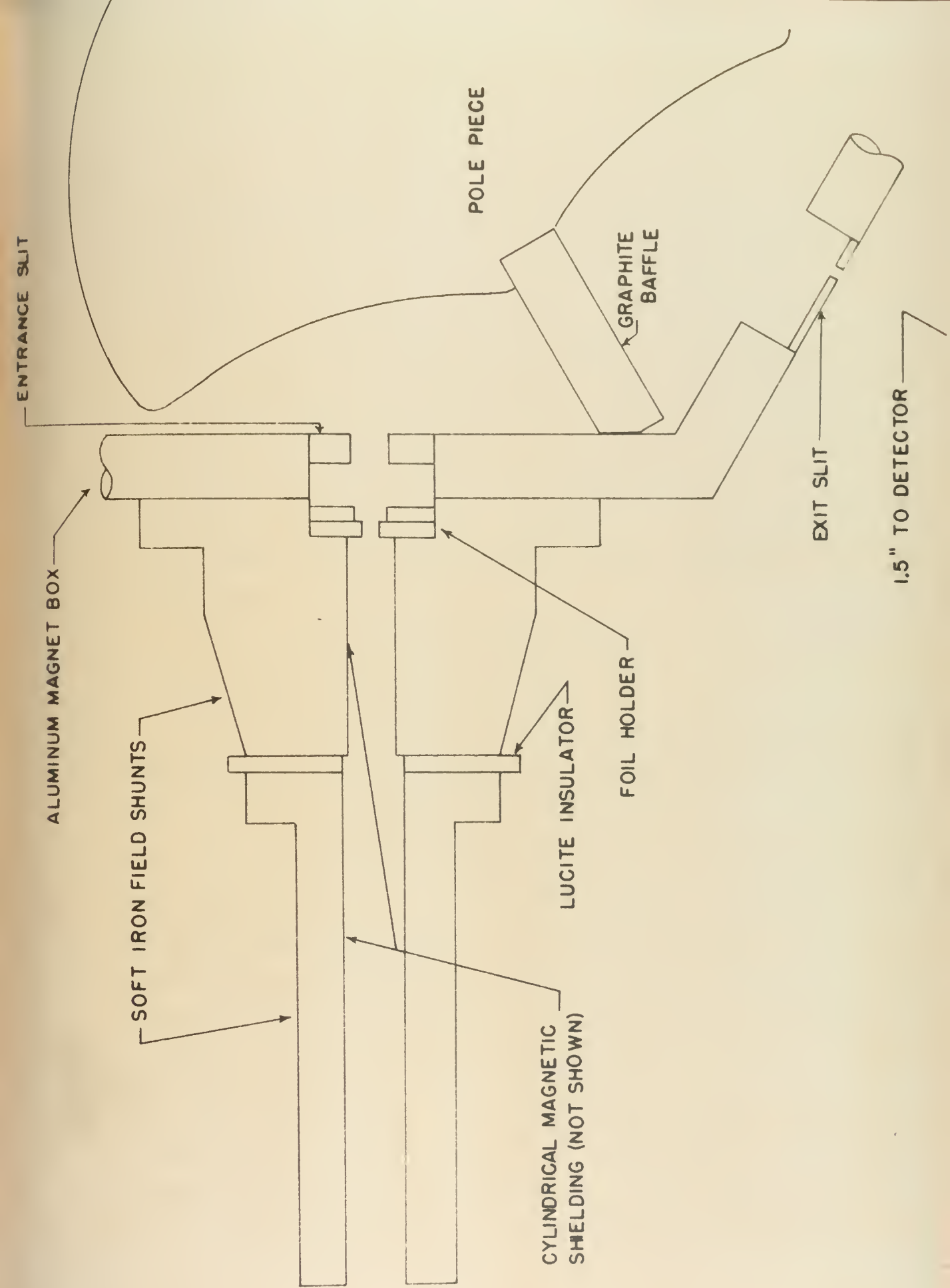
From the discussion of the former two subsections, it is possible to reach at least some qualitative conclusions as to the origin of the electrons detected which do not correspond to monoenergetic photons. The inelastic electron scattering contribution seems to be a factor of ten too low to account for the extra electrons if they are assumed to arise from processes in the foil. On the other hand, the use of thicker foils (2.56 mg/cm^2) gave rise to higher count rates than did the thinner foils (1.41 mg/cm^2), the difference being unaccountable solely in terms of inelastic processes in the two foils. The difference could be understood in terms of a reduced number of interactions in the vacuum chamber corresponding to the smaller mean scattering angle for the elastic process in the thin foil.

At the same time that the thin foils were introduced into the system, an exit baffle was positioned



Figure(III-3)

Initial monochromator configuration
showing positions of baffles and
beam defining slits.

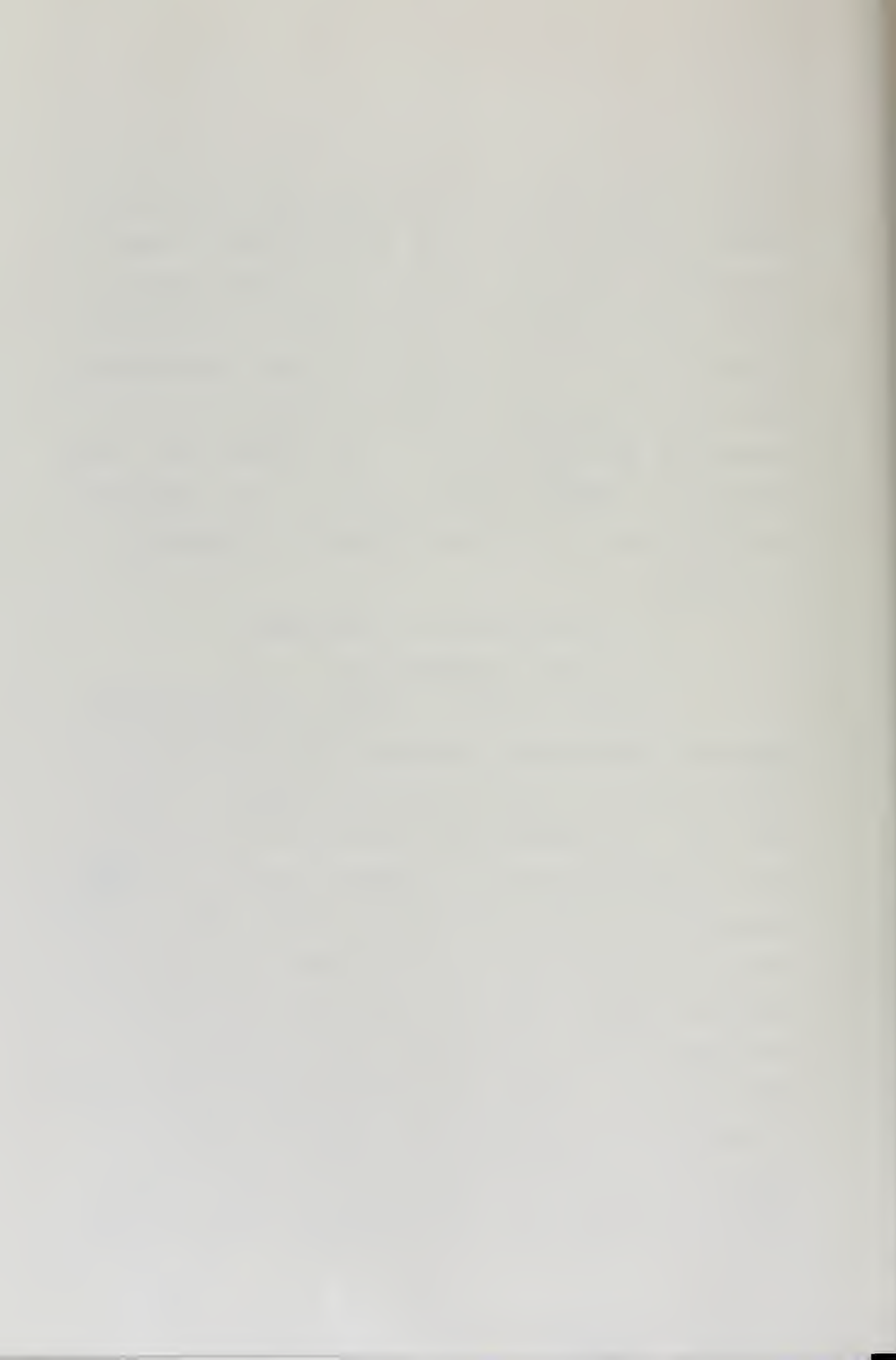


in the vacuum chamber in such a manner that part of the graphite collection box, which monitors the main beam, was masked. Since this part of the collector box was nearest the exit slit and could no longer be reached by the main beam, it is not possible to state unequivocally that the use of the thin foils or the baffle alone was responsible for the reduction in the electron rate. The reduction was deemed evidence enough that the processes in the foil were not the sole cause of the excessive count rate.

3. Monochromator Configurations

a) Initial Configuration

As shown in Figure (III-3), the initial monochromator configuration consisted of an entrance slit, a baffle between the entrance and exit apertures, and an exit slit. The entrance slit consisted of a circular disc of graphite one inch in diameter having a centered three-sixteenth inch diameter hole drilled into it. The side of the slit towards the exit side of the system was grooved in order to pass the beam which was deflected in the fringe field of the magnet as soon as it left the soft iron shunt flange. The vertical baffle, which stood at the apex of the pole-face in the fringe field of the magnet, was constructed of one-half inch thick graphite. The exit slit consisted of a one-eighth inch thick lead



disc with a one-sixteenth inch wide by one inch high quarter moon slit located one quarter-inch off center. The long dimension of this aperture was vertical and the precise shape of the slit was determined from the electron beam photographs of Walter and Shea. The plastic scintillator was positioned about one and one-half inches away from the exit slit. This configuration gave a transmission of .17 percent.

b) Intermediate Configuration

Tests conducted on the monochromator while in the above configuration indicated that some major changes were necessary if the performance of the device was to be improved. Transmission measurements indicated that the circular exit slit tended to cut off electrons due to the unexpectedly strong effects of the fringe field. Also, the entrance slit did not prevent the scattered electrons from striking the aluminum rotating coil holder so that the possibility of the beam interacting with this object was present. For these reasons, the entrance slit was replaced by an entrance baffle constructed of one-half inch thick graphite. The aperture of this baffle was constructed so that at least ± 14 degrees of the ϕ -angle and a range of entrance angles, ψ_s , from 90 degrees to 150 degrees were available. The vertical baffle was redesigned and constructed from one-half inch thick lead.

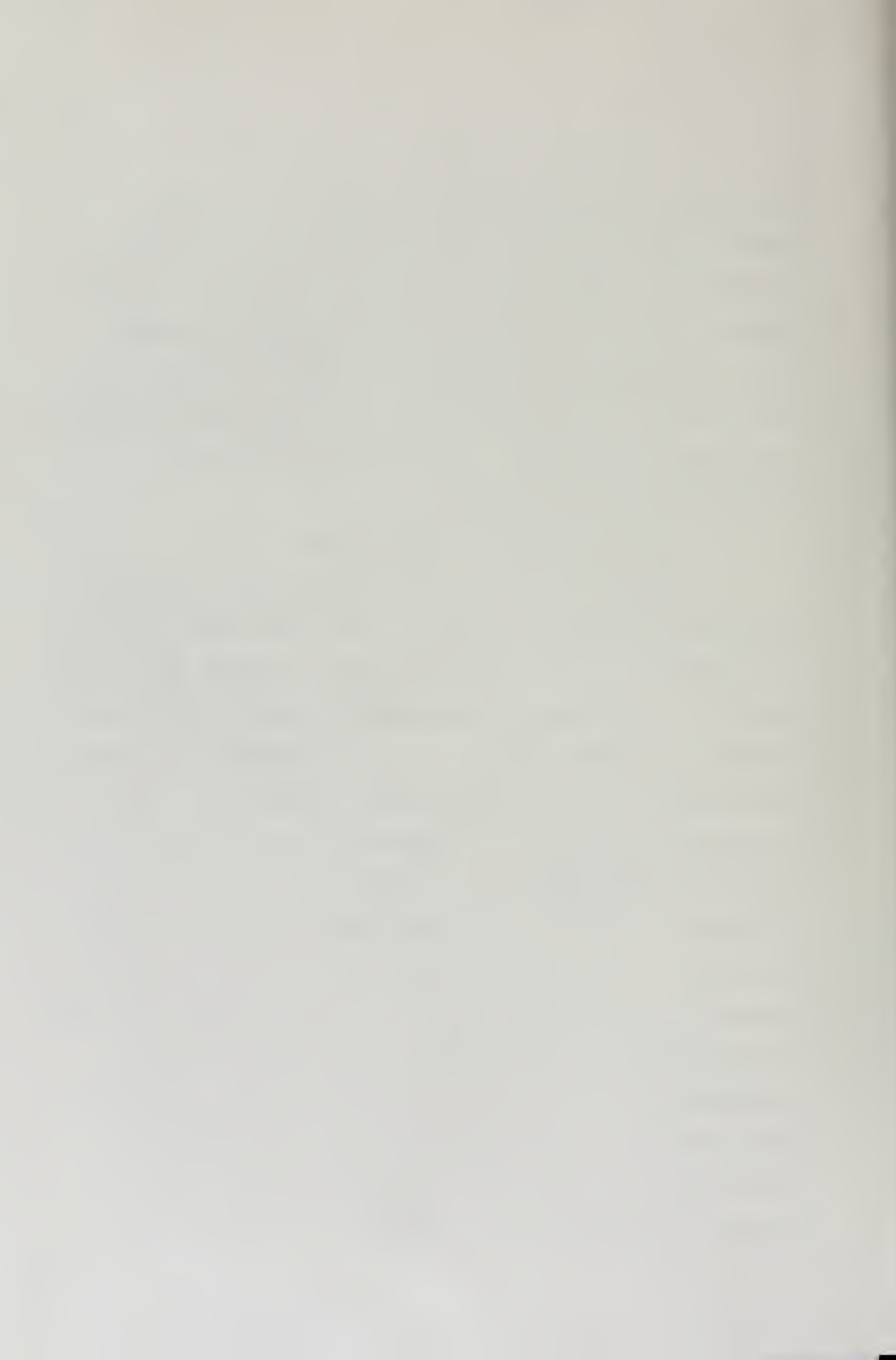
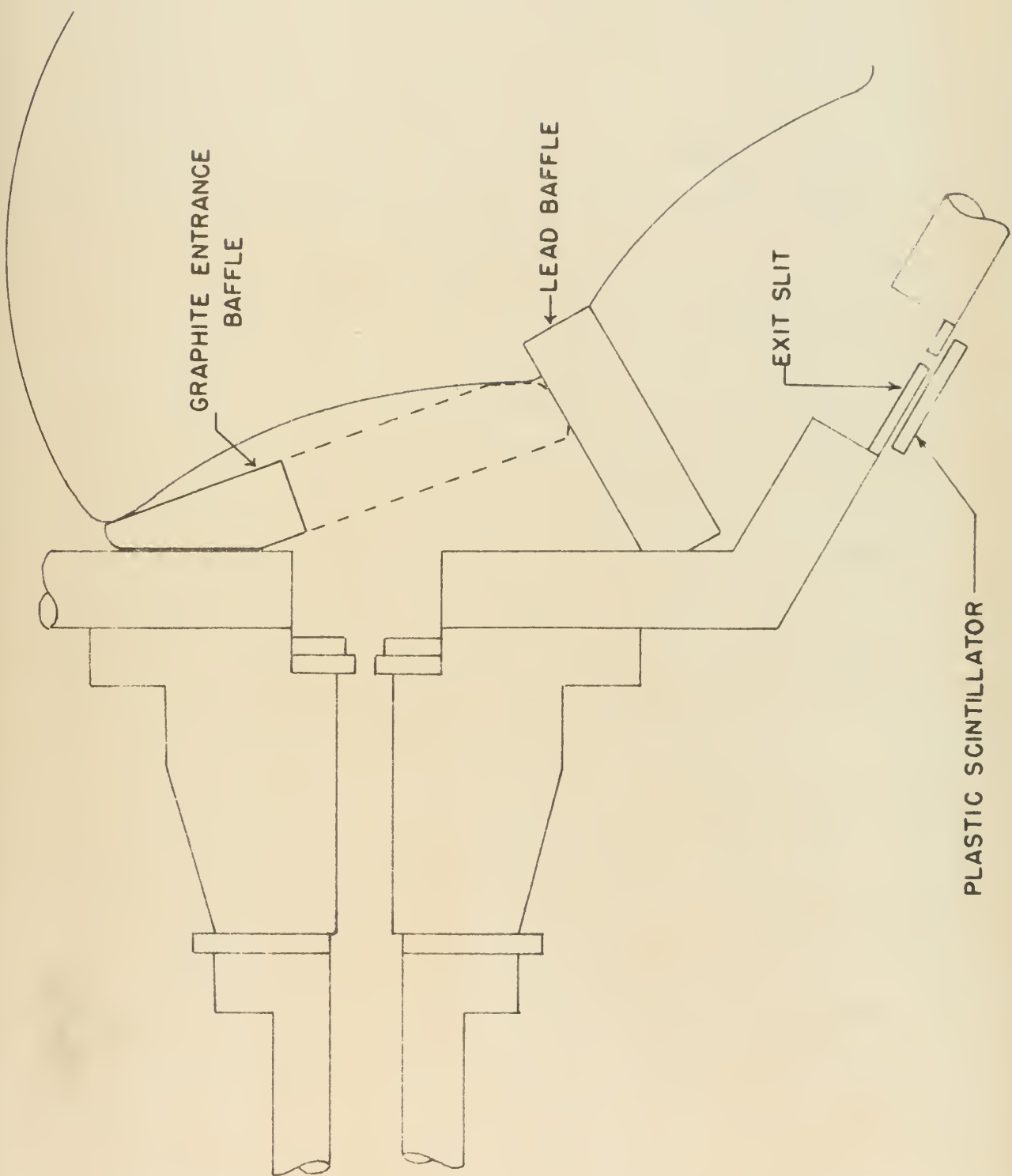


Figure (III-4)

Intermediate monochromator configuration
showing entrance baffle and relocated
plastic scintillator.





GRAPHITE ENTRANCE
BAFFLE

← LEAD BAFFLE

EXIT SLIT

PLASTIC SCINTILLATOR



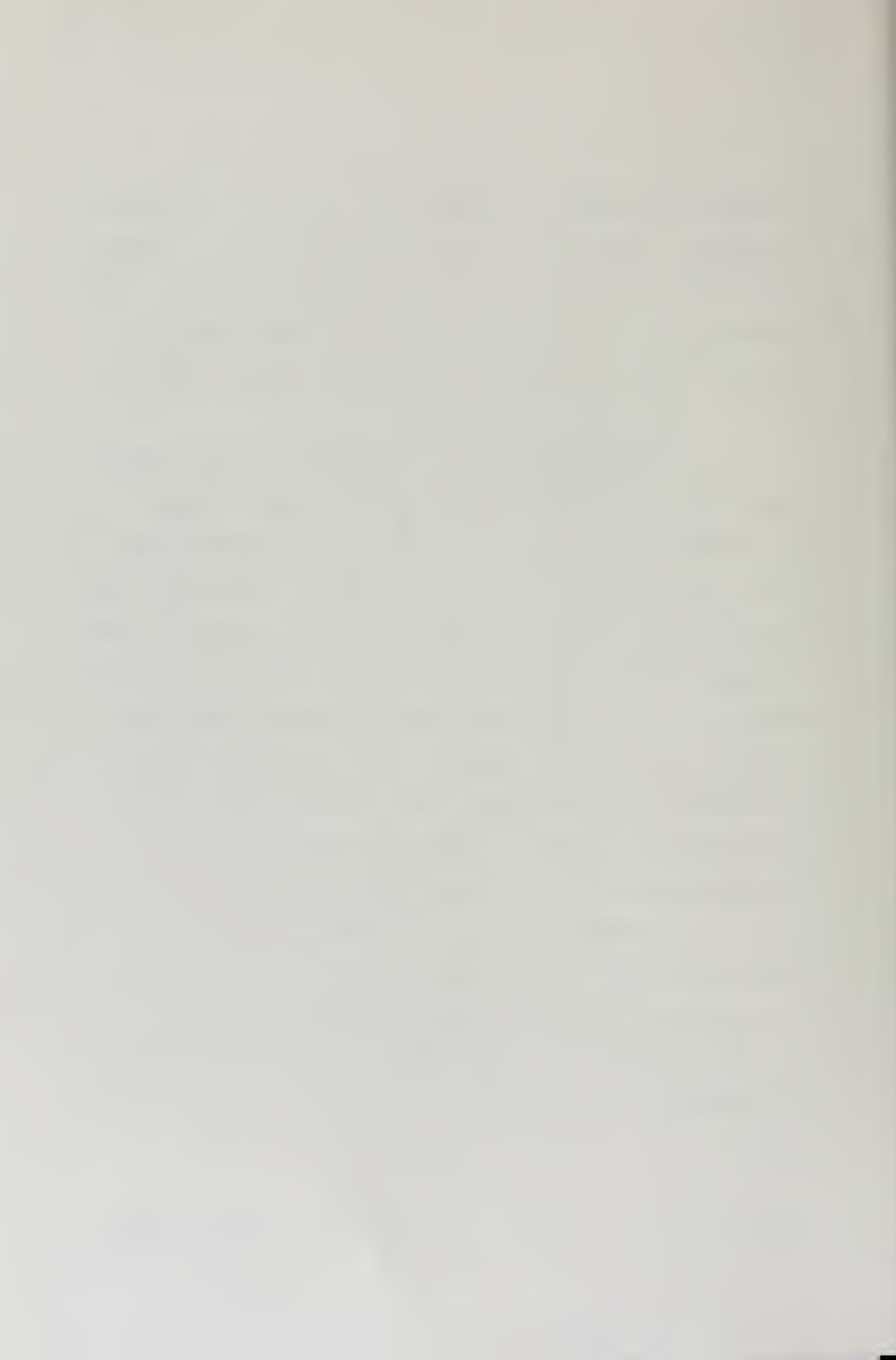
The exit slit remained essentially unchanged in position and shape. The plastic scintillator was moved to within three-thirty-seconds of an inch of the exit slit. The transmission in this configuration was measured to be .7 percent. This configuration is shown in Figure (III-4).

c) Final Configuration

Difficulties with an excessive electron count rate led to the introduction of yet another baffle. This baffle, constructed of one-half inch graphite, was placed onto the exit side of the magnetic field and was placed close to the pole edge in a manner similar to the entrance baffle. The aperture of this baffle allowed acceptance of ϕ -angles less than ± 14 degrees and restricted the range of entrance angles to approximately 100 degrees to 150 degrees. This reduced the available geometric solid angle to about 2.24 percent of 4π . The entrance baffle, vertical baffle, exit slit, and plastic scintillator were left unchanged. The exit baffle was positioned in such a manner as to mask part of the collector box used to monitor the main electron beam current. It was therefore necessary to limit the range of available photon energies according to the relationship

$$k = \frac{C-1}{C} T_0 ,$$

where $C > 1.5$, in order to keep the main beam away from



the exit baffle. The measured transmission for this final configuration was .44 percent. The set-up is depicted in Figure (III-5).

C. Bremsstrahlung and Pair Creation Targets

1. Bremsstrahlung Target Foils

A number of thin self-supporting gold foils have been used in the tests of the monochromator and in the pair creation study. These foils, obtained from J. M. Ney Company, are cut by a machined die of known area. The areal density is then determined by weighing the foil section. The gold foil used in the investigation of the pair creation process had an areal density of $1.41 \pm .01 \text{ mg/cm}^2$ and was shown to be free of holes and visible flaws by microscopic inspection.

2. Pair Creation Targets

The target samples used in this experiment were positioned at a distance of 69 centimeters from the bremsstrahlung foil. The target was rotated so that the normal to its front face bisected the angle formed at the intersection of the incident beam direction and the center line of the detector. The geometrical center of the target was placed at the intersection of the beam line and detector center line. Repeatability of this set-up was ensured by use of a target stand, the location of which was measured with a precision transit.

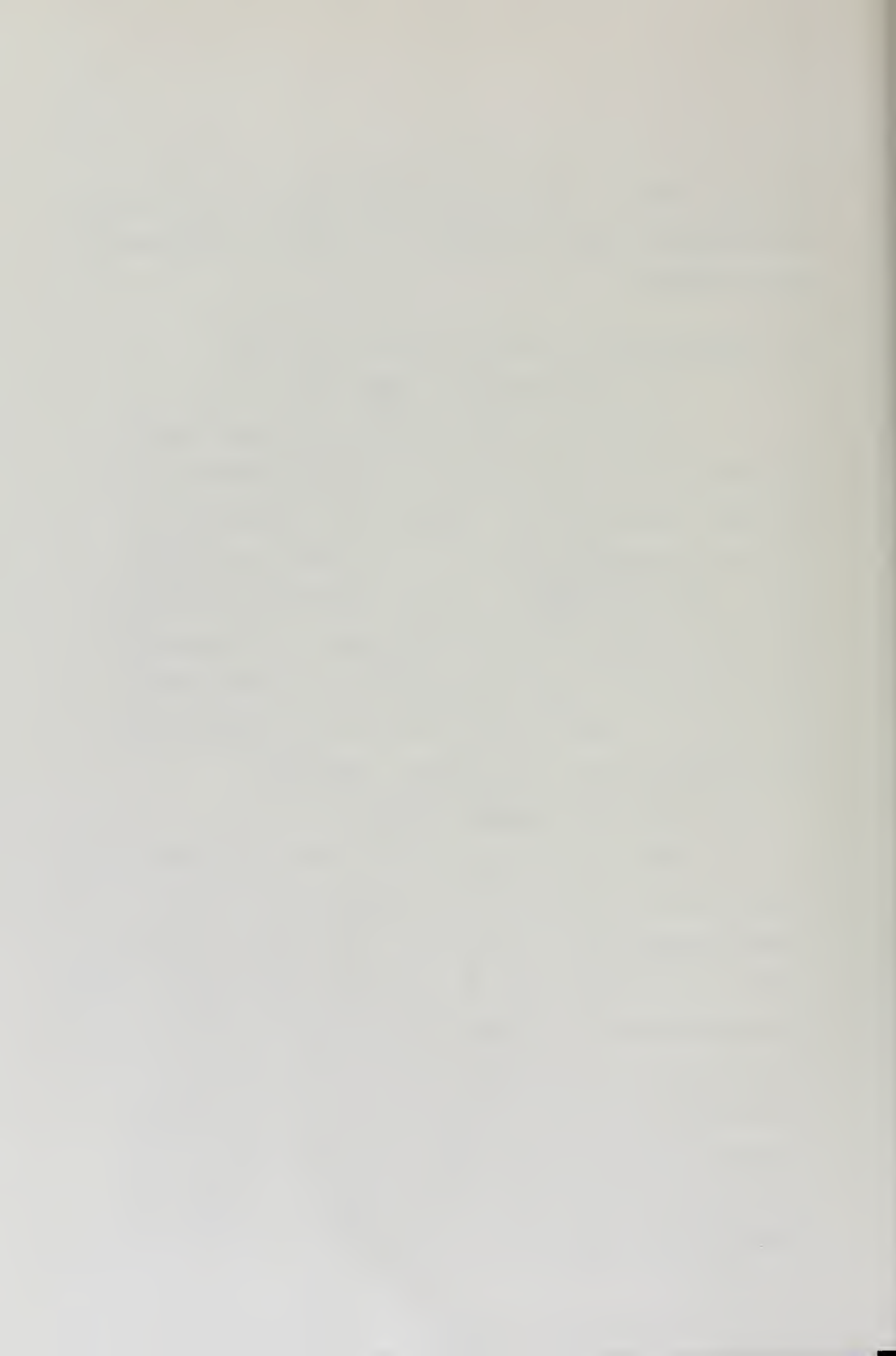
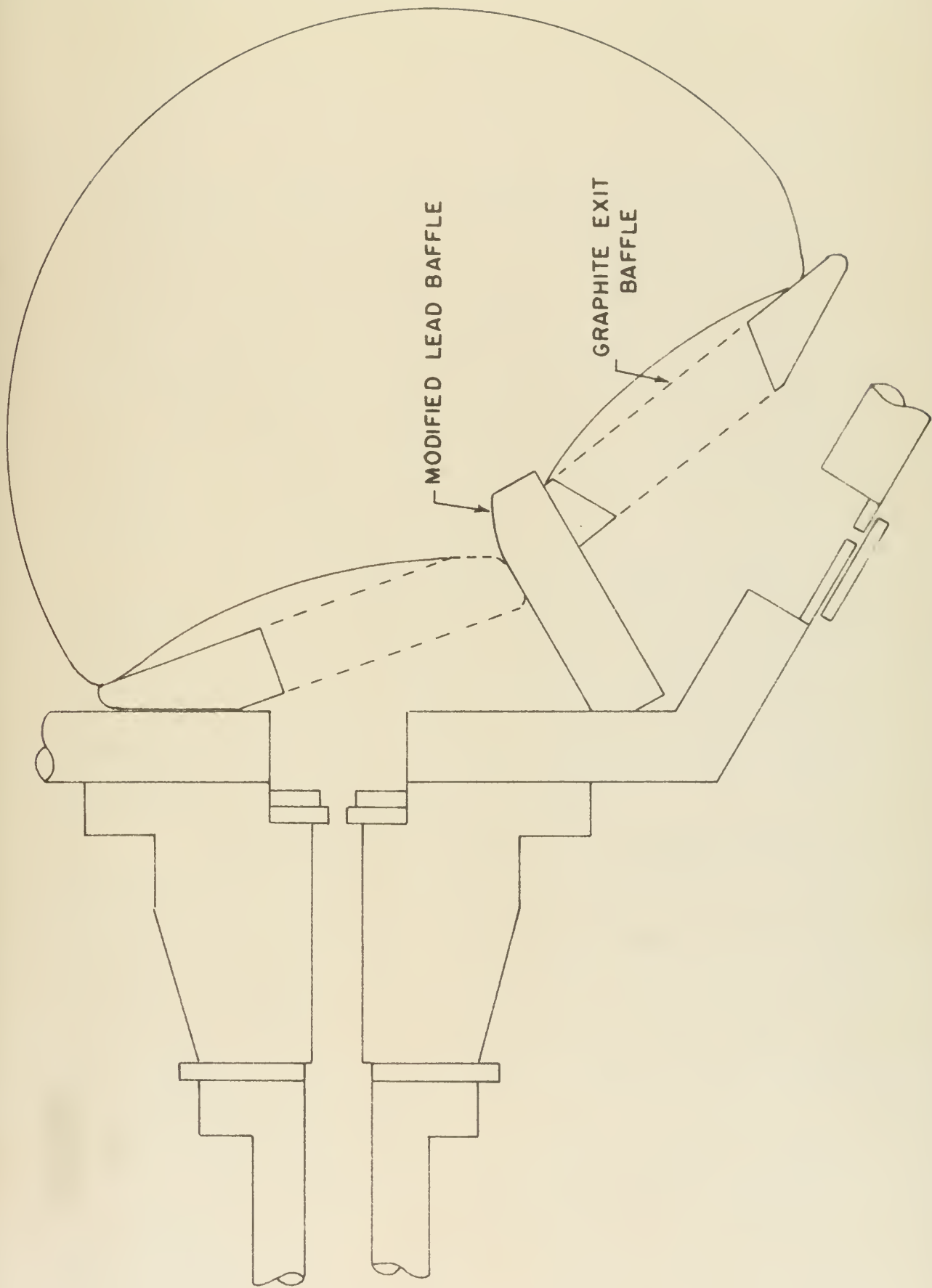


Figure (III-5)

Final monochromator configuration showing
exit baffle.



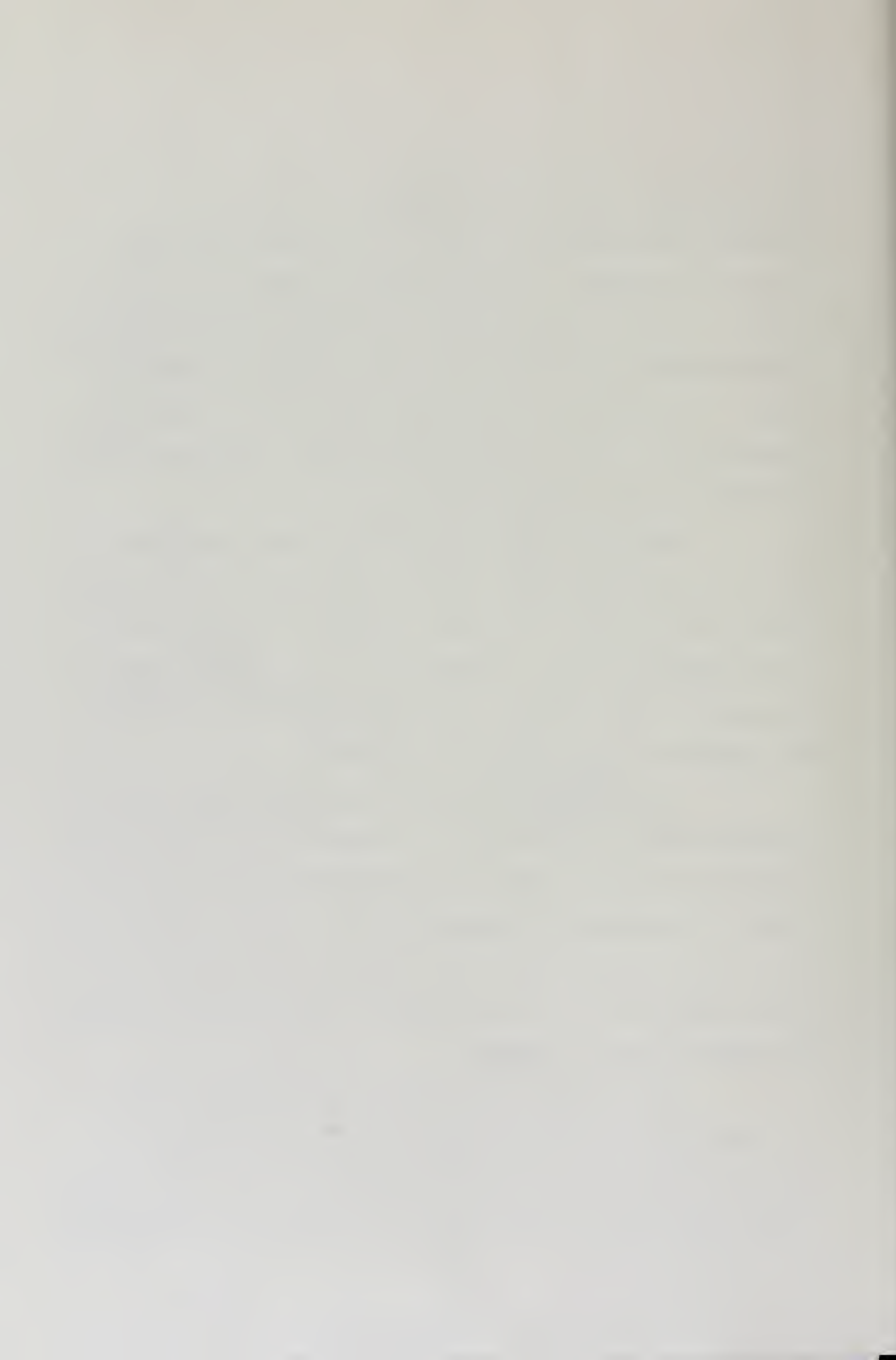


The rotatable target stand rested on a lucite disc inscribed with alignment marks at 30 degrees and multiples of 45 degrees. Proper angular alignment was ensured by lining up the 30 degree reference mark with a beam direction line inscribed on the immovable aluminum table. The height of the target holder itself was made such that the center of the target sample would be at the altitude of the bremsstrahlung source.

The lead target consisted of four matching natural lead sheets, each four inches high by four inches long by one-eighth inch thick, arranged to form one piece with dimensions eight inches wide by four inches high by one-quarter inch thick. The areal density of the target was measured to be $6.985 \pm 0.07 \text{ gm/cm}^2$.

The tin target was made up of sixteen sheets of lead-free natural tin, each six inches wide by four inches high by one-sixty-fourth inch thick, arranged to form one piece of dimensions 6 inches wide by 4 inches high by one-fourth inch thick. The areal density of this target was determined to be $4.47 \pm .04 \text{ gm/cm}^2$. The tin was supplied by Fisher Chemical Company.

Both targets were initially encased in sheets of lucite, one-sixteenth inch thick, front and back in order to ensure that any positrons escaping from the target would annihilate in the lucite. Experimental measurements



indicate that, within the statistical uncertainty of the data, the effect of the lucite was negligible. The lucite was used for support, however.

D. Detection and Counting Systems

1. The Experimental Layout

Annihilation radiation arising from pairs created in the target samples was detected at 120 degrees relative to the incident beam direction, as indicated in Figure (III-6). The scintillator used was a two inch diameter by two inch thick NaI(Tl) detector, obtained from the Harshaw Chemical Company. This crystal was mounted, using Dow Corning type C-2-0057 silicone coupling compound, on an RCA-6342A multiplier phototube. The phototube was wrapped with Netic and Conetic magnetic shielding material obtained from Perfection Mica Company.

Monochromatic photons were detected at zero degrees, as indicated in Figure (III-7), using a second two inch by two inch NaI(Tl). This crystal was also mounted on an RCA-6342 multiplier phototube but with Dow Corning "200" coupling fluid. Magnetic shielding material also protected this phototube.

Recommended⁸⁵ voltage dividers were used for both tubes such that the application of -1500 volts to the photocathode provided the correct dynode potentials. The power supply used was a Power Designs Supply Model

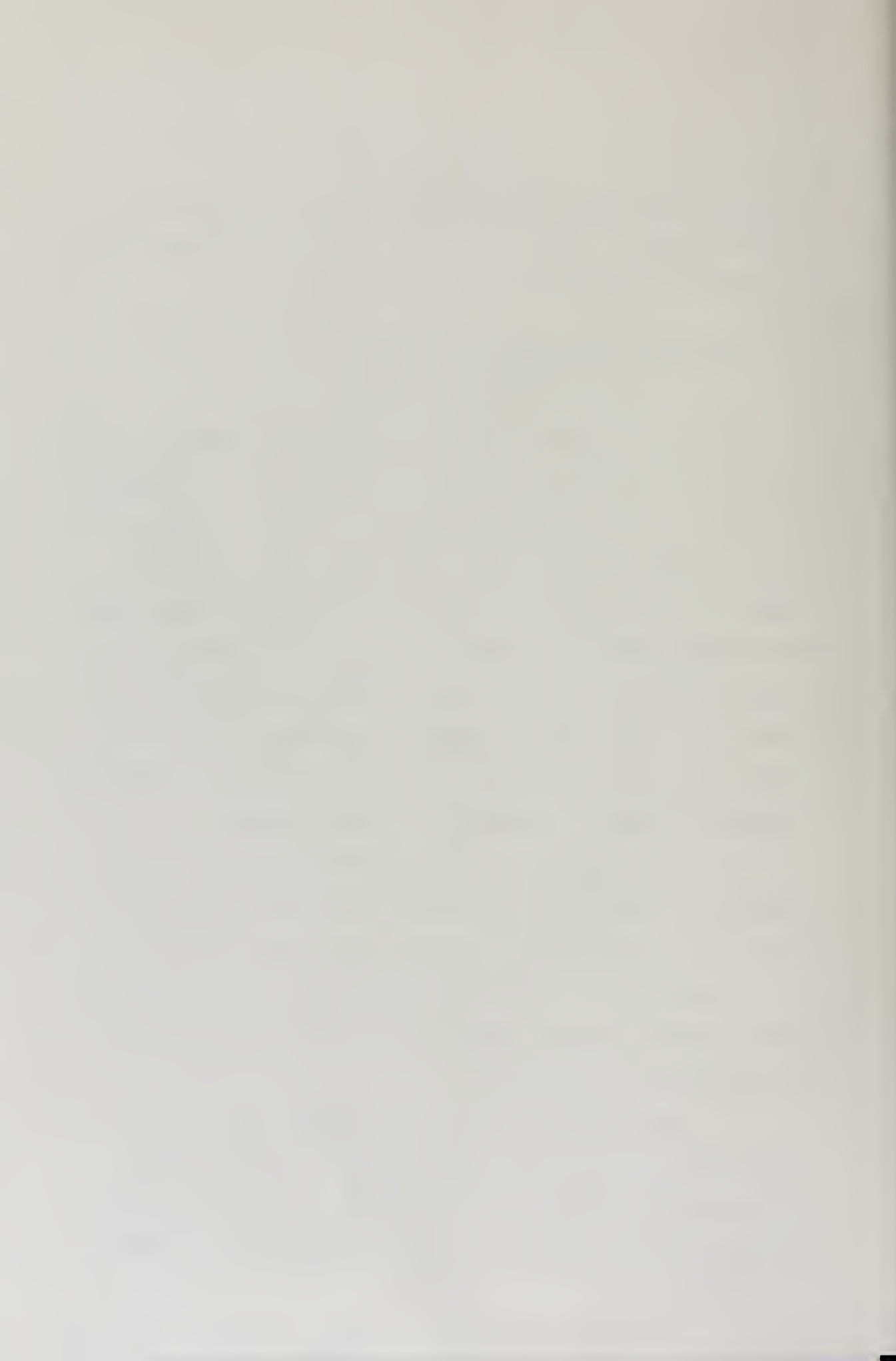
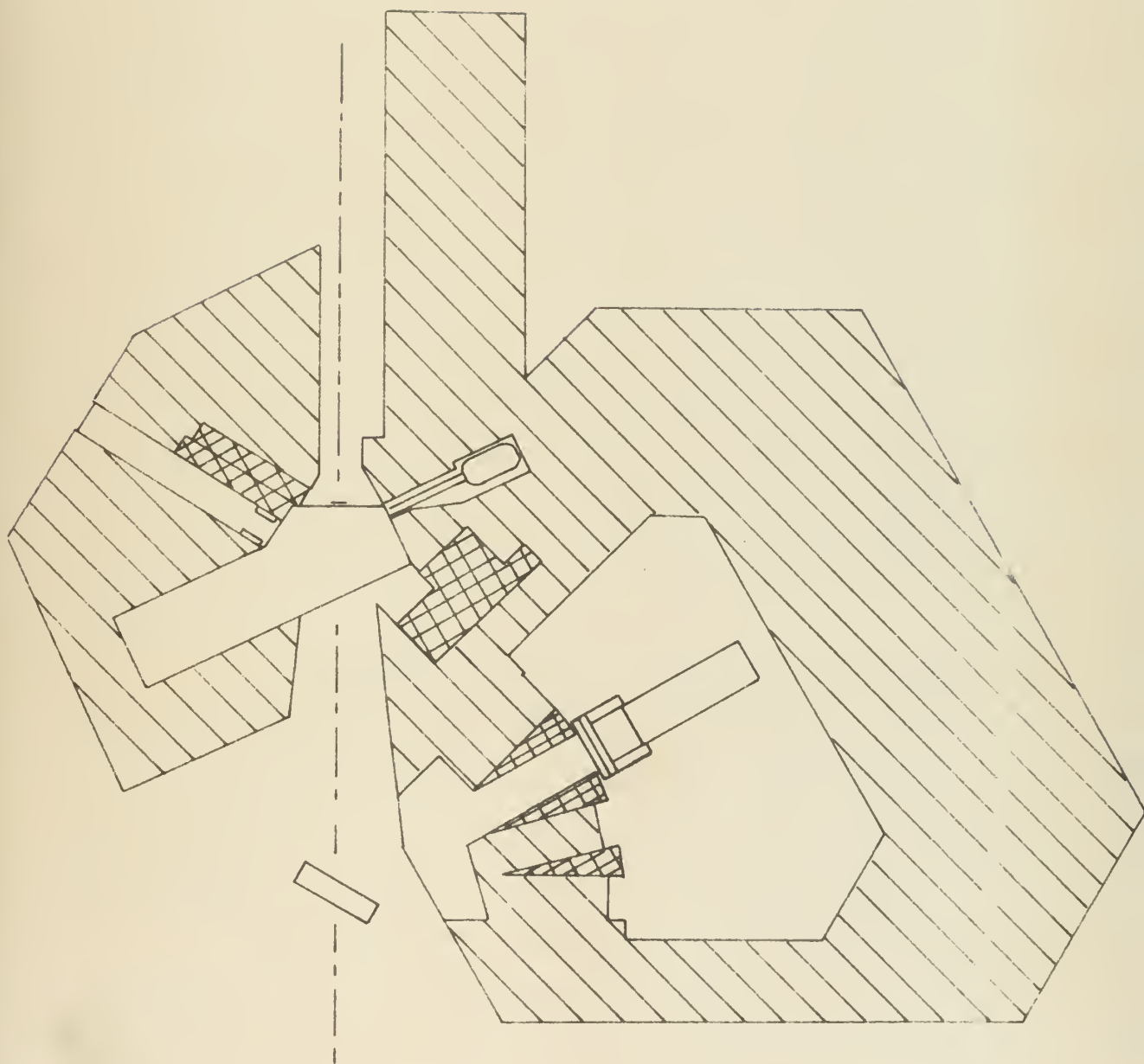


Figure (III-6)

Experimental layout showing 120° photon
detector and electron detector, with
photon shielding.





LEAD



MALLORY-2000





(1565).

The post-bremsstrahlung electrons corresponding to monochromatic photons were brought to a focus at a NE-102 plastic scintillator, obtained from Nuclear Enterprises Limited, of diameter one inch and three-sixteenths of an inch in thickness. The scintillator was coupled, with the Dow Corning type C-2-0057 compound, to an optically clear lucite light pipe which in turn was coupled in the same manner to an RCA-7746 multiplier phototube. This phototube was wrapped in magnetic shielding material and in an insulated layer of aluminum foil which was connected to the photocathode to provide an electrostatic shield.

A recommended voltage divider was used such that the application of between -2000 volts and -2400 volts to the photocathode provided the correct interdynode potentials. The commonly used voltage was -2000 volts being provided by a Fluke High Voltage Supply.

The use of the long light pipe in the electron detection system was necessitated by the magnetic fringe field interaction with the RCA-7746 multiplier phototube. When the photocathode of this tube was closer than 2.5 inches to the exit slit, the magnetic field in the monochromator could be set to only 60 percent of its maximum value before distortion and gain loss occurred in the

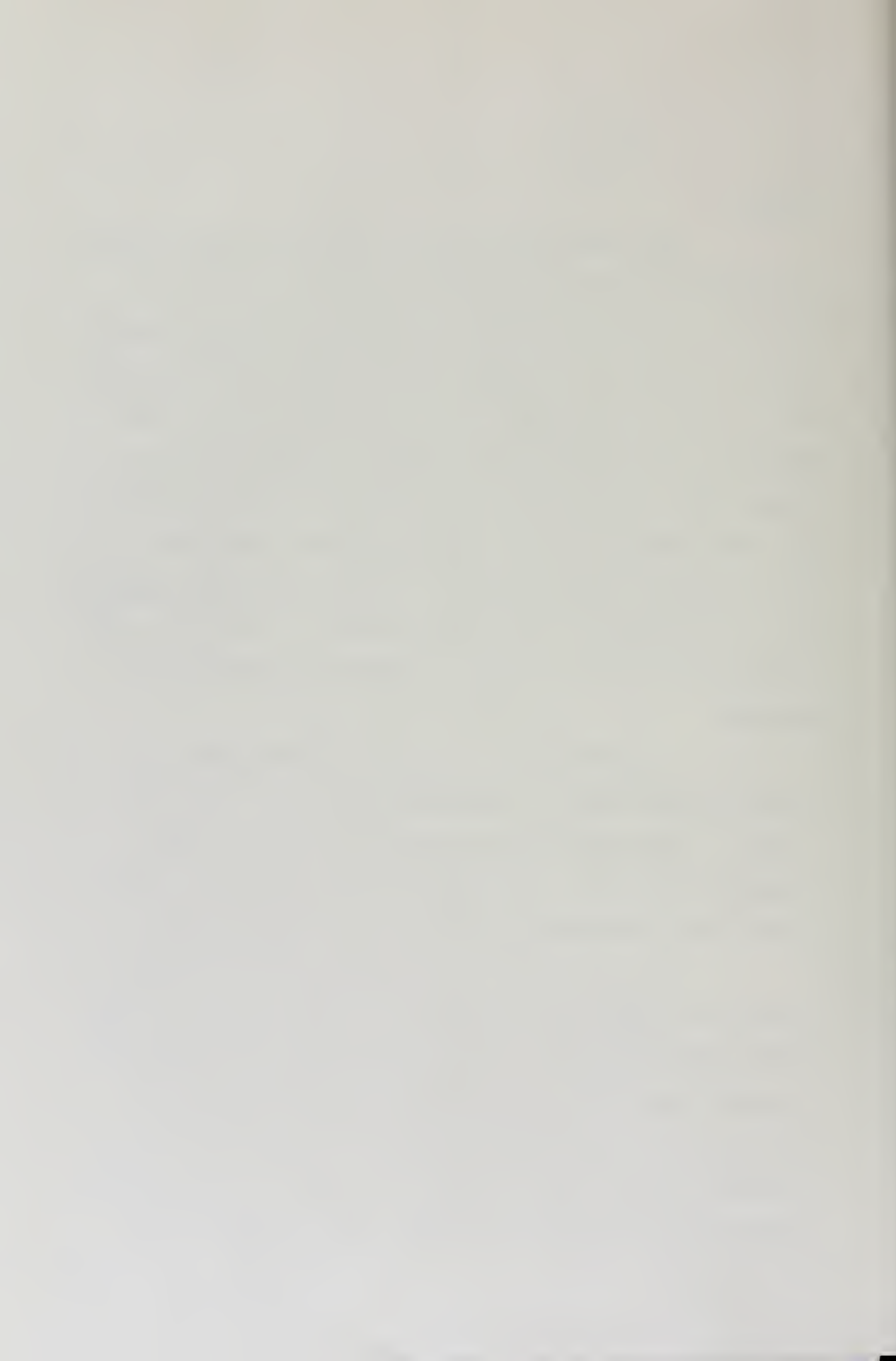
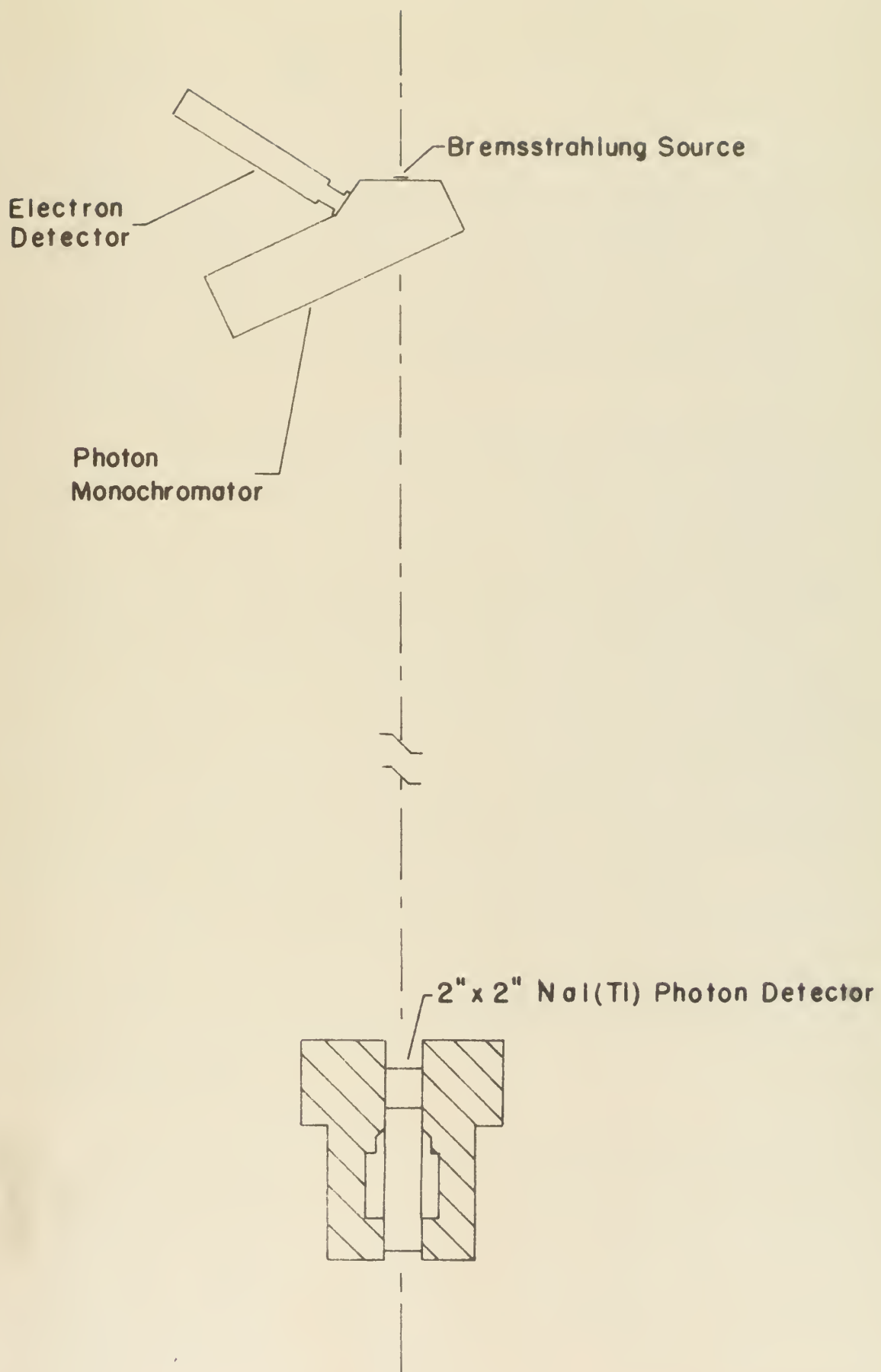


Figure (III-7)

Experimental layout for monochromats
showing photon shielding of the mono-
chromatic photon detector.







phototube output. Placing the tube in position so that the photocathode was magnetically well shielded and more than 2.5 inches from the exit slit allowed use of the full magnetic field with no detectable pulse distortion or loss in gain.

The choice of the two inch by two inch NaI(Tl) scintillators was dictated by the necessity to compromise pulse rise time and detection efficiency. A larger crystal would give better detection efficiency but a slow rising pulse while a smaller crystal would give a fast pulse but with poor detection efficiency. The rise time of the current pulse from the two inch by two inch crystal is about 25 nanoseconds while the detection efficiency is about 55 percent for .511 MeV photons. These parameters were deemed sufficient for the present studies.

The NE-102-RCA-7746 combination was selected after tests of various combinations of Pilot "B", Naton 136 and NE-102 scintillators with 7746 and 6810A multiplier phototubes.

2. Electronics

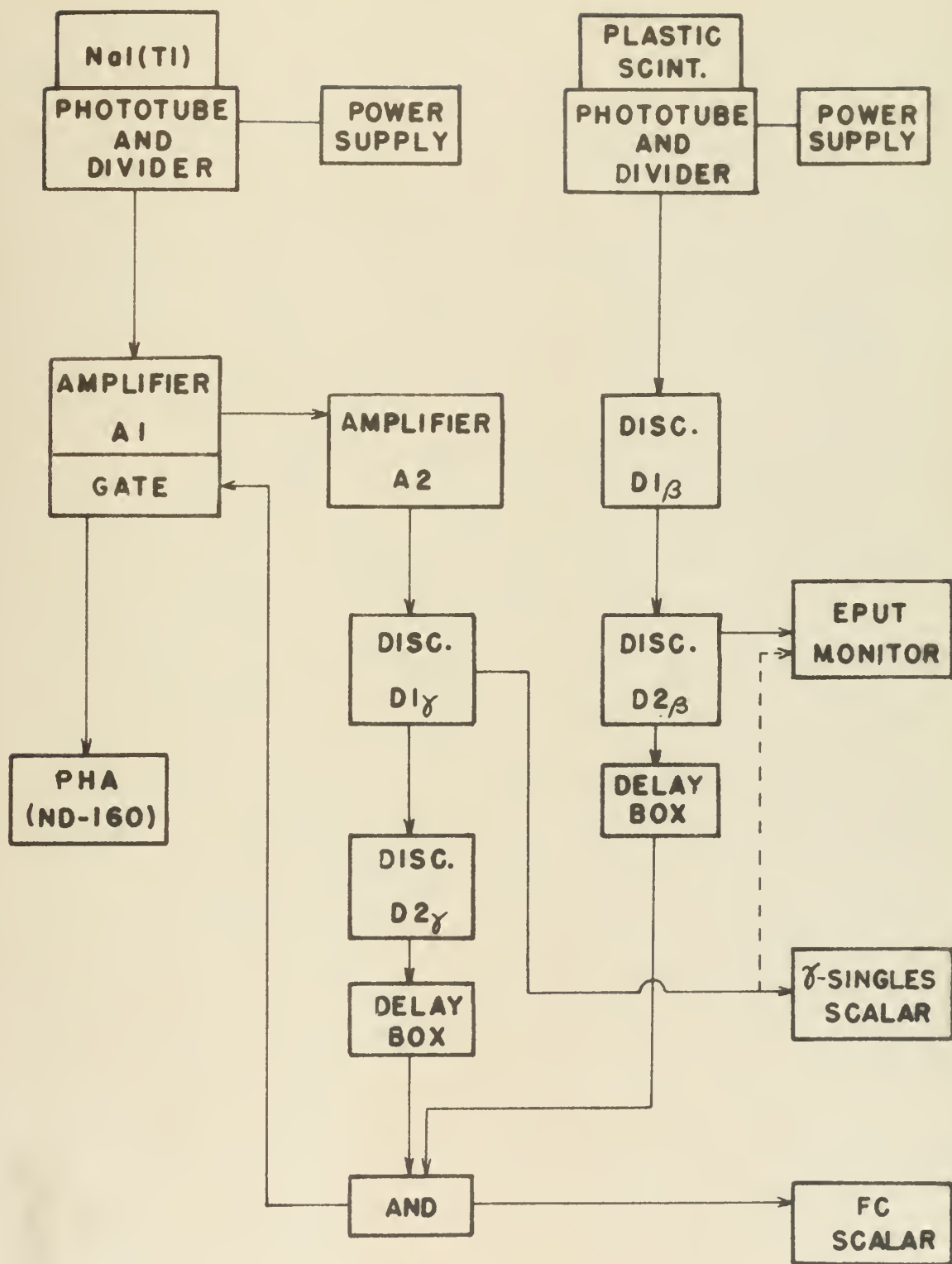
Standardized electronics modules were used in the coincidence circuitry for the investigations reported here. The Chronetics Nanologic System components were used in conjunction with an amplifier and pulse shaping circuit designed by P. R. Chagnon.⁸⁶ The amplifier

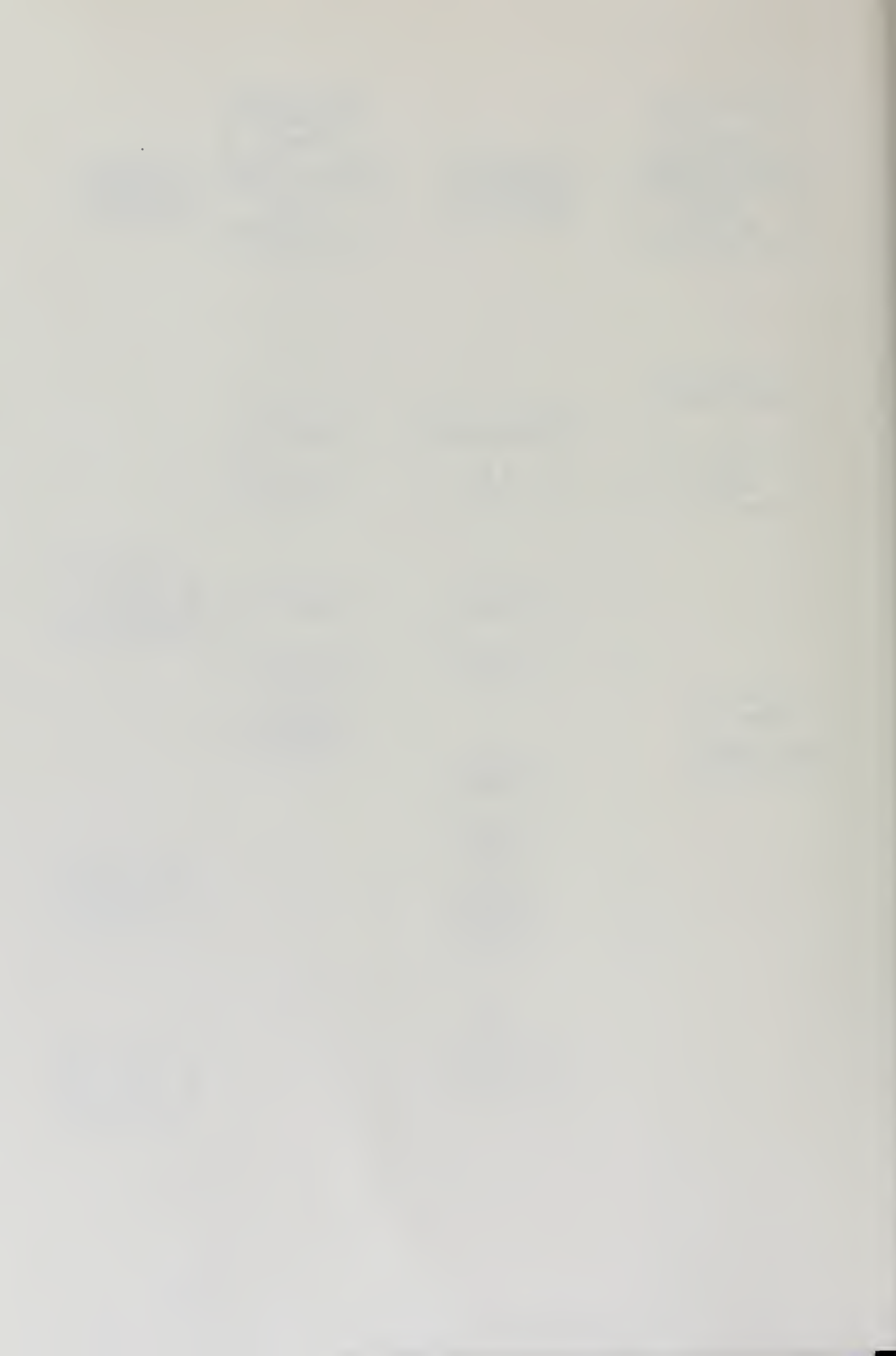


Figure (III-8)

Block diagram of the electronics
used.







circuit was used in the photon arm and allowed for flexibility and reliability in the selection and energy analysis of the gamma-ray pulse height spectrum. Figure (III-8) is a block diagram of the electronic apparatus used. The circuit labelled A1 is the Chagnon designed circuit mentioned earlier.

The purpose of the circuitry is to selectively energy analyze the pulses from the NaI(Tl) crystals. This selection is carried out by opening the gate of the circuit whenever a time coincidence occurs between a post-bremsstrahlung electron of energy $T_0 - k$ and an annihilation photon (or, in the case of monochromats, a photon of energy, k). The coincidence selection is made on the basis of a required coincidence between the output pulses of the Chronetics discriminators labelled $D2_\gamma$ and $D2_\beta$ in Figure (III-8). The occurrence of the required coincidence in a Chronetics And circuit gives an output pulse which controls the opening of the gate in the A1 circuit. Those pulses which are passed by the gate are energy analyzed in a Nuclear Data Model 160 Analyzer System.

A fast-slow coincidence technique modeled after that used by Malaker was tested extensively and found to provide no significant improvement over the fast coincidence only system finally used.



a) The Fast Electron Arm

The fast output current pulses from the RCA-7746 multiplier phototube were transmitted from the target area to the control room over approximately 150 feet of RG-62/U cable directly to the input BNC of the Chronetics Nanologic System. Continuous checks were carried out to ensure that no reflections or multiple pulsing events occurred. These checks were made using either the Tektronix type 561A oscilloscope with a 3T77 sampling unit or with a Tektronix type 581 oscilloscope with a type 82 vertical amplifier. The rise time of the former combination is 0.4 nanoseconds and for the latter 1.5 nanoseconds. No reflection problems were encountered.

b) The Fast Photon Arm

The output current pulses from the RCA-6342A multiplier phototube were transmitted over approximately 140 feet of RG-62/U cable to the control room. These pulses were inputs into the amplifier system, A1. In this circuit, the signal was split with the "slow" signal being integrated and shaped and delayed. The "fast" signal was clipped and sent into the Chronetics coincidence system. The lower level discriminator of the Nanologic discriminator triggered at a pulse height corresponding to a 100 keV photon. The resulting discriminator output pulses were monitored by a Hewlett-Packard (Model



5254L) electronic counter in order to provide continuous information on the integral photon counting rate.

In each arm, the first discriminator output pulses were used as inputs to a second Chronetics discriminator in an effort to increase reliability at high count rates. The use of the uniform output pulses of $D1_{\gamma}$ (or $D1_{\beta}$) as inputs to other discriminators ($D2_{\gamma}$ or $D2_{\beta}$) did allow an increase of a factor of 10 in the repetition rate in each arm.

The gain of the system was adjusted to place the 511 keV photons in relative channel thirty and to give a 12 keV/channel slope to the energy versus channel analyzer resolution curve. Linearity of system gain was checked using sources of ^{137}Cs and ^{60}Co . For the monochromat runs, the same system was used except that for timing checks the analyzer resolution was changed by adjustment of the voltage on the photon detector base in order to give the monoenergetic photons a pulse height corresponding to the annihilation radiation pulse height from the NaI(Tl) detector. Gain stability was checked using the sources previously noted.

c) Intrinsic Circuit Resolving Time

The intrinsic resolving time of the fast coincidence system was tested using either a Texas Instruments Company pulser (Model 6613R) or a ^{207}Bi source. In the

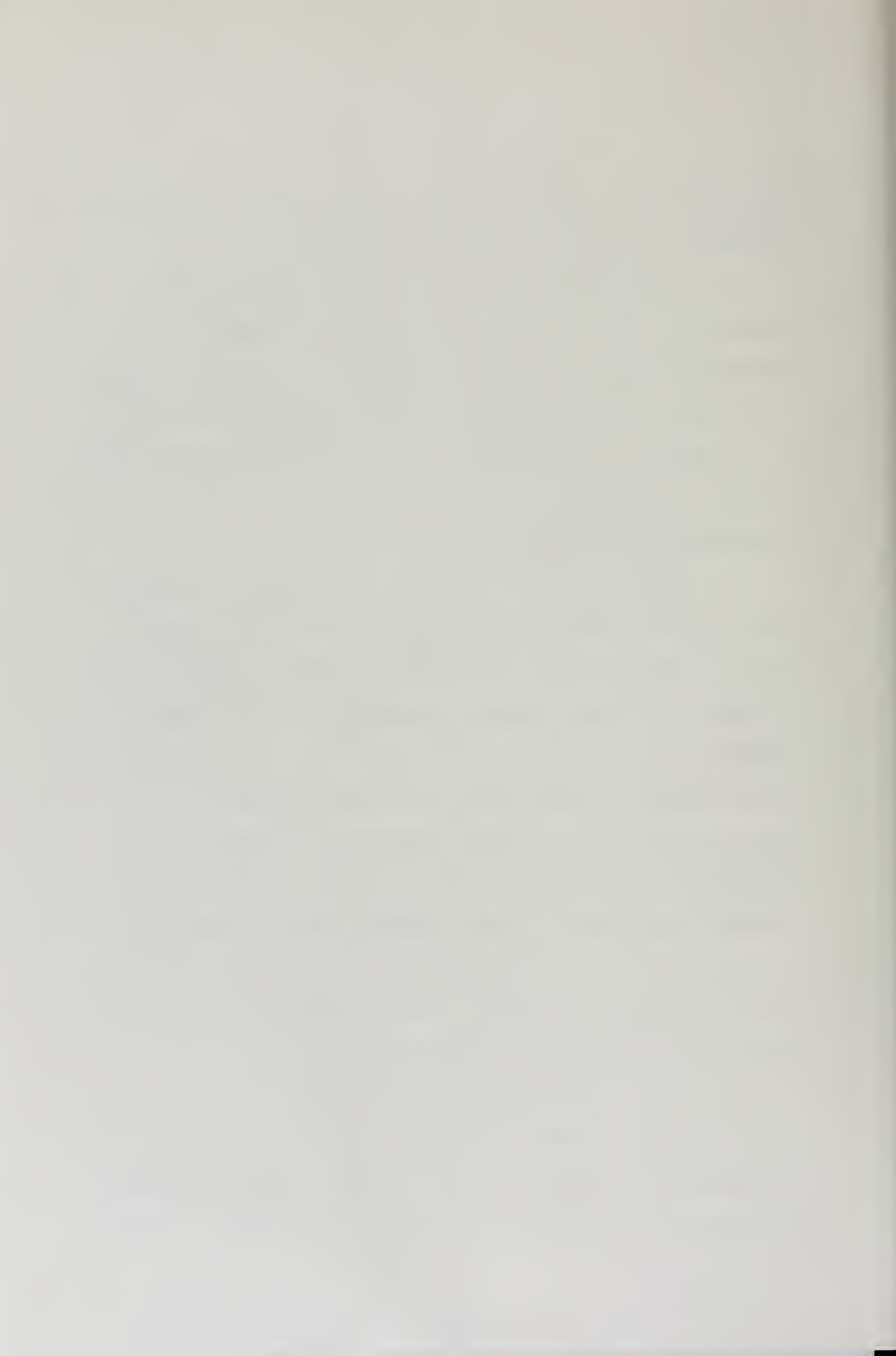
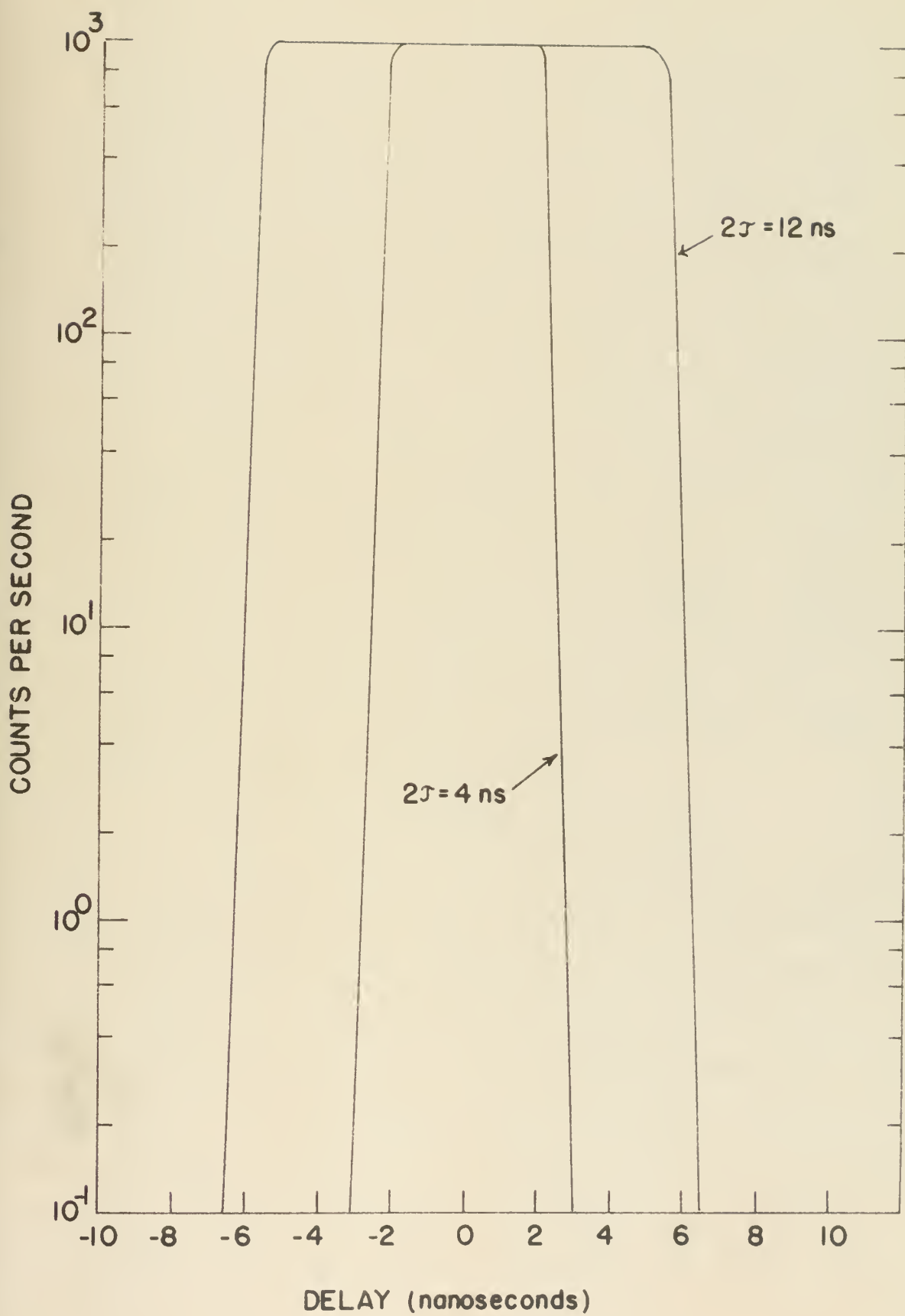


Figure (III-9)

Intrinsic resolving time delay curves as a function of delay in the electron arm.







tests with the pulser, the output pulse was shaped to approximately the form of the electron detector output pulse and was then split with one signal going to the electron side of the system unaltered while the other signal was stretched and used as an input to the photon arm of the coincidence circuit. Delay curves were then taken for various lengths of the clipping lines used with $D2\gamma$ and $D2\beta$. These curves are shown in Figure (III-9). The tests using the ^{207}Bi source were conducted with the source placed in the foil position by gating the detection of the 570 keV gamma-ray, from the first excited state transition to the ground state in ^{207}Pb , with the 970 keV K-conversion electron from the decay of the 1.634 MeV level in ^{207}Pb to the .570 MeV level. These curves are shown in Figure (III-10).

d) Overall Circuit Resolving Time

Final tests on the circuit resolving time and coincidence efficiency were conducted by measuring the yield of monoenergetic photons as a function of delay in the beta arm of the coincidence system. This curve is shown in Figure (III-11). The final resolving time, 2τ equal to 7.6 nanoseconds, was used since this set-up provided ample assurance of 100 percent coincidence efficiency. The four nanosecond wide flat-top of the curve would allow as much as a two nanosecond shift in timing

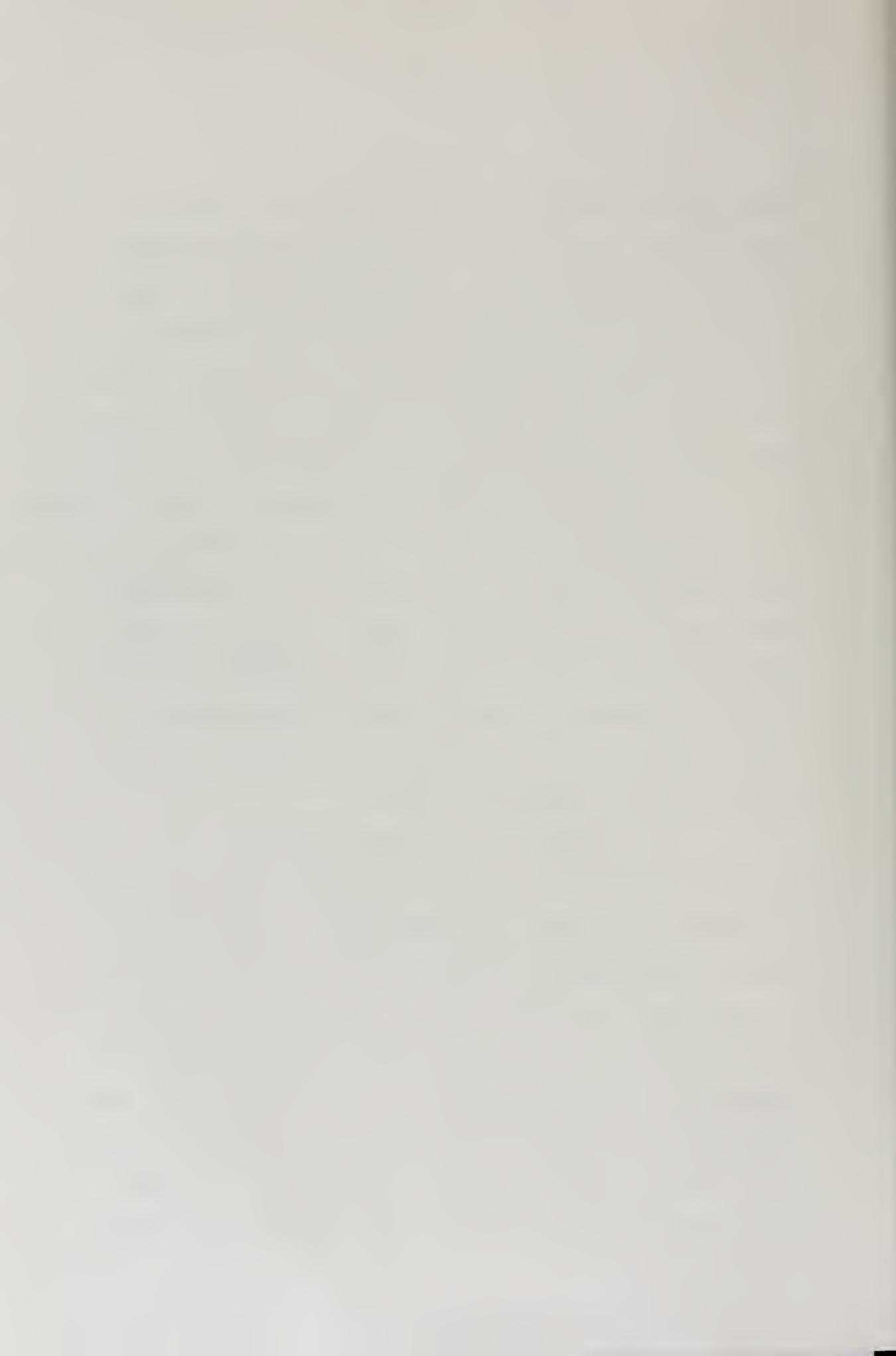
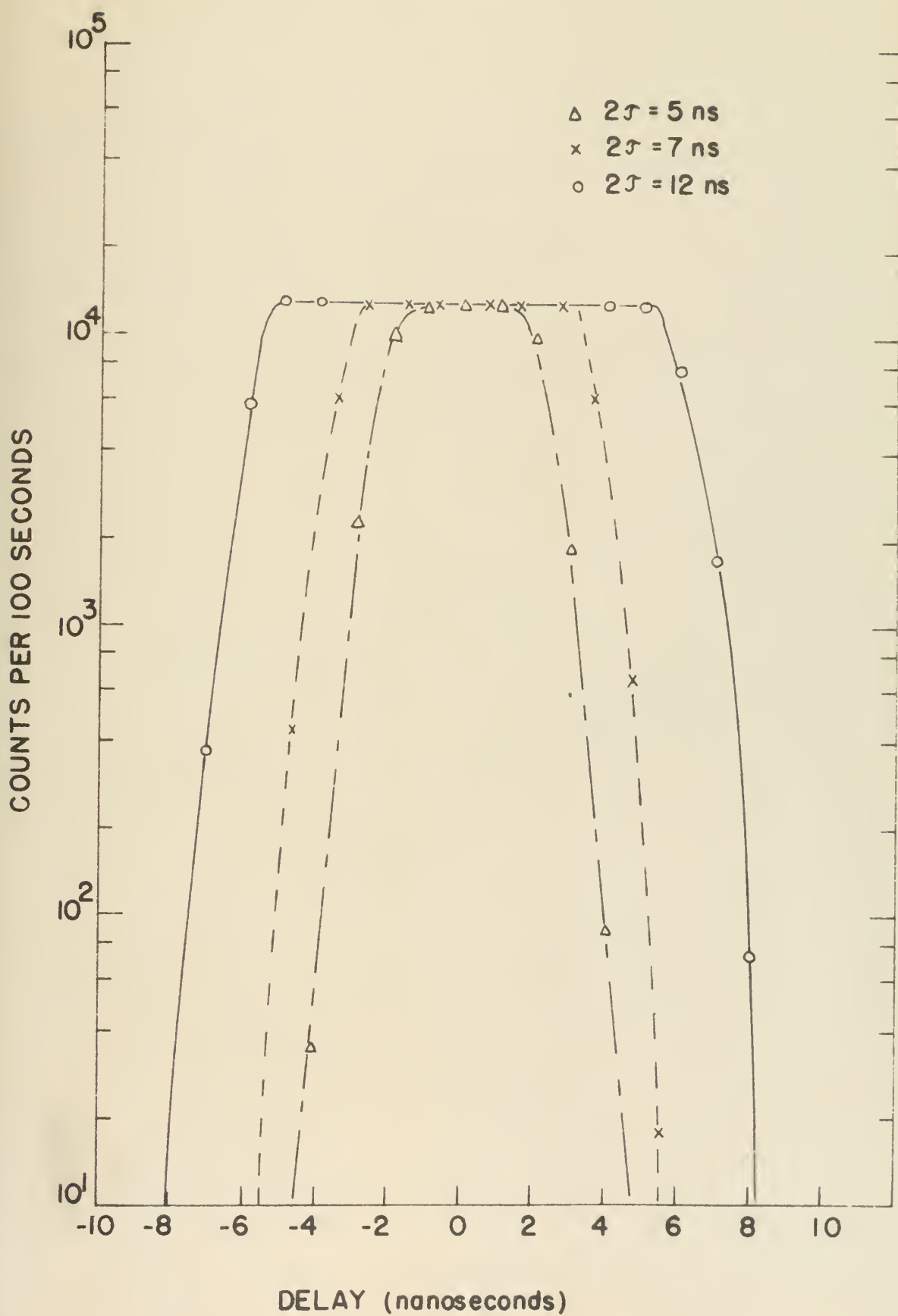


Figure (III-10)

Overall circuit resolving time as a
function of delay in the electron arm.





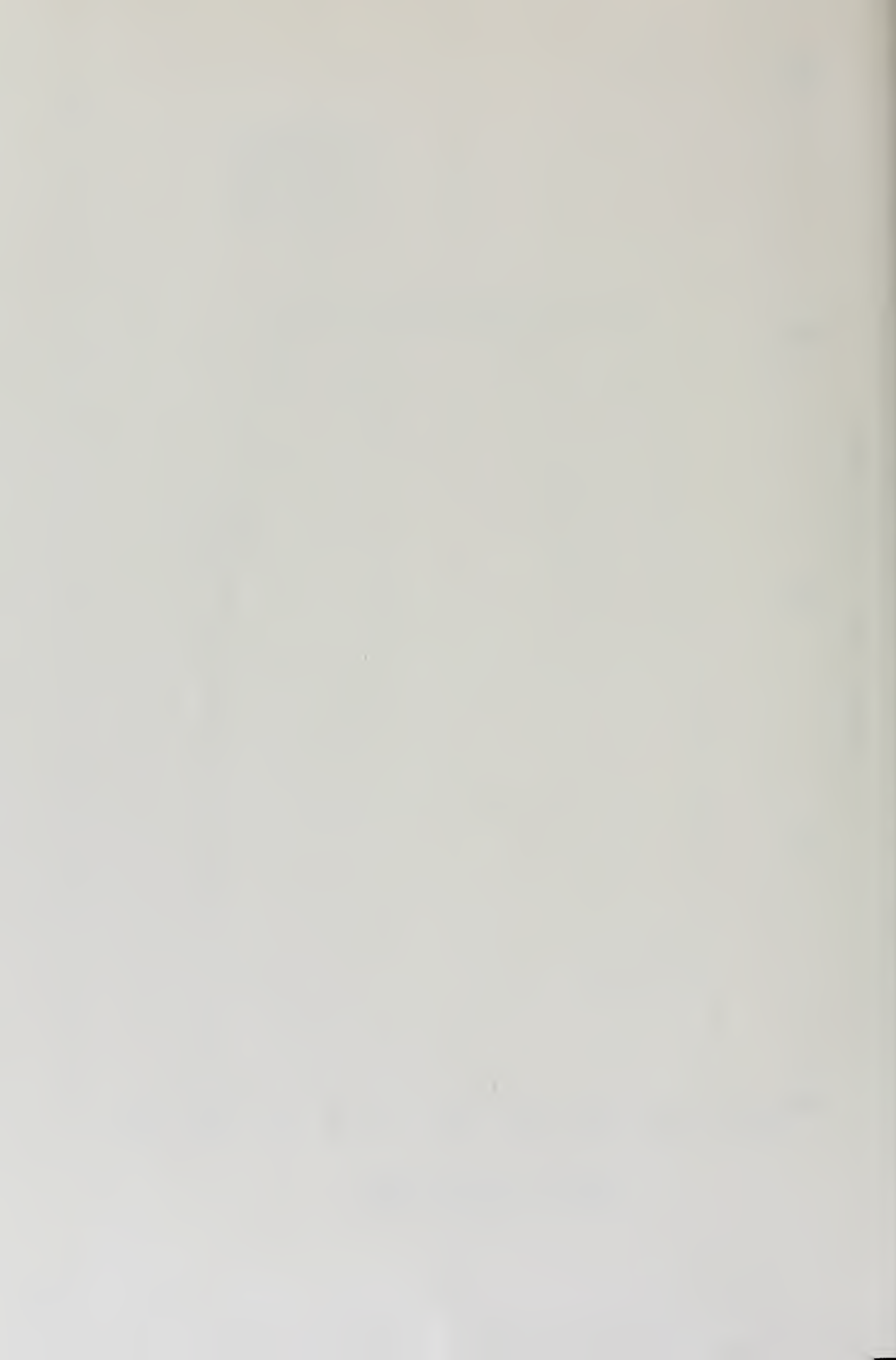
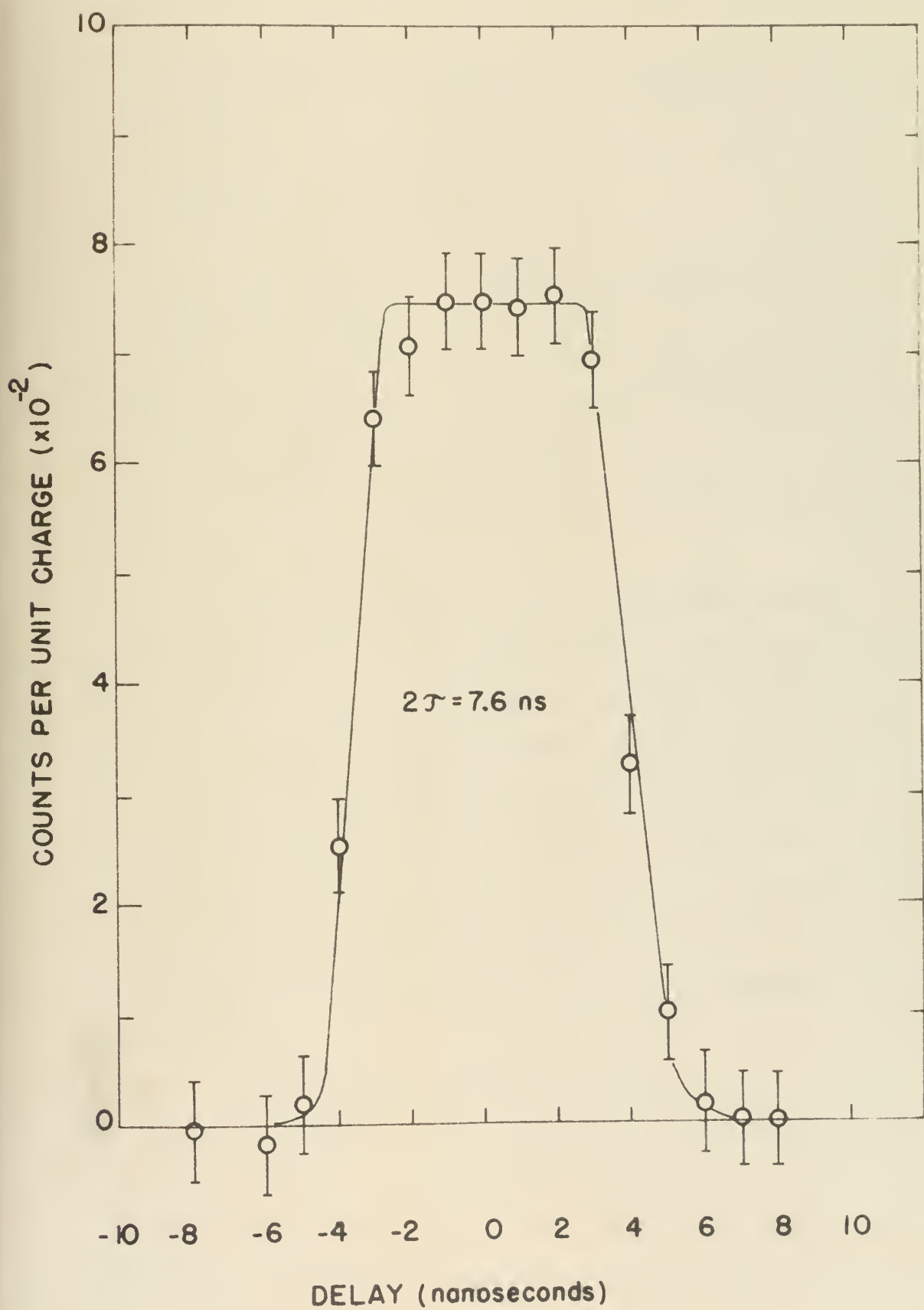


Figure (III-11)

Typical operating resolving time curve as
a function of delay in the electron arm
using monoenergetic photons.







without destroying the property of 100 percent coincidence efficiency.

E. Detection Efficiencies

The detection efficiencies for the annihilation photons were experimentally measured by use of a gamma-ray source of known strength placed successively at the center position of each of the volume elements into which the target sample had been divided (see p. 33). The number of photons was then counted at each volume element for a fixed time interval.

The same aluminum grid plate described by Loscoe was used for this measurement. The aluminum grid was placed at the target position and the IJ positions were counted. Due to the thinness of the target samples only the $k = 1$ measurement was made. The effects of the absorption in the various conceptual K layers were evaluated in the computer calculation of the yield expression since the uncertainty in target (grid) location was of the order of the uncertainties in the absorption coefficients.⁸⁷

The absolute gamma-ray emission rate of the source used in the detection efficiencies determination was measured with a three inch by three inch NaI(Tl) crystal. The source was placed along the center line of the detector at three accurately measured distances and



the number of counts in the full energy peak was determined for each distance. The solid angle subtended by the crystal at the source was calculated and the known values⁸⁸ of incident intrinsic efficiency and peak-to-total spectrum ratios were used to provide the source strength for each position. The weighted mean of these three measurements provided a measured source strength to within ± 5.0 percent.

Source full energy peak efficiency η is taken as

$$\eta = \frac{N_p}{S}$$

where S is the measured source strength and N_p is number of counts in the full energy peak. The efficiency for each volume element was determined by dividing the number of counts under the photopeak by the measured source strength. The statistical uncertainty of the measured area under the full energy peak (after a computer fit) varied from ± 3.3 percent (the worst case) to less than 1.5 percent (the best case). The variation noted resulted due to the location of the volume elements, those farthest from the center line of the detector having the greater statistical uncertainty. The corresponding source full energy peak efficiencies were thus known to within ± 6 percent and ± 5.2 percent respectively.

Due to the manner in which these efficiencies



were measured the attenuation of the annihilation quanta in the lead and graphite absorbers placed before the detector was included in the measured values of η .

Two sources were used for this measurement. The relative efficiency measurements were made using a ^{137}Cs source of high specific activity. The annihilation quanta from a ^{22}Na source of low specific activity were used to provide the reference value η_0 for the measurement. As a consistency check the ^{137}Cs data were corrected for: 1) the total absorption coefficients for the pair creation samples and the lead and graphite absorbers, 2) the incident intrinsic efficiencies⁸⁹ for the two inch by two inch NaI(Tl) crystal, and 3) the peak-to-total spectrum ratio⁹⁰ for this crystal. These corrections resulted in a corrected η_0 for this ^{137}Cs data which was in agreement with the ^{22}Na value.

F. Photon Shielding

A major experimental difficulty encountered in using the bremsstrahlung continuum in the production of monochromatic photons is the presence of a large number of extraneous photons produced in the target foil or in any part of the beam handling system struck by the main beam. Great care must be taken to provide a clean uncluttered beam path, to optimize detector locations, and to place as much shielding as possible between the



detectors and points struck by the beam.

Three major sources of bremsstrahlung flux are the energy control slits, the target foil, and the graphite collector box. Introduction of the 45 degree bending magnet allows the experimental set-up to be placed out of the direct flux of slit produced bremsstrahlung quanta. The bremsstrahlung produced in the graphite collector box is directed away from the detector since the main beam is deflected through an angle of 90 degrees or more, relative to the incident beam direction, before hitting the collector box and the resultant bremsstrahlung distribution is peaked in the forward direction. The flux produced in the target foil is attenuated over the direct path to the detectors by the use of lead and Mallory-2000 shielding, a tungsten alloy with a density of 18 g/cm^3 . These factors will be discussed in some detail in the next two sub-sections.

1. Electron Detector Shielding

The electron detector assembly is located in the flux of photons produced in the energy control slits, in the bremsstrahlung target, and in the baffles, collector box, and exit slit of the monochromator.

In the direct line between the energy control slits and the plastic scintillator were placed four inches of Mallory-2000 metal and ten inches of lead. The count

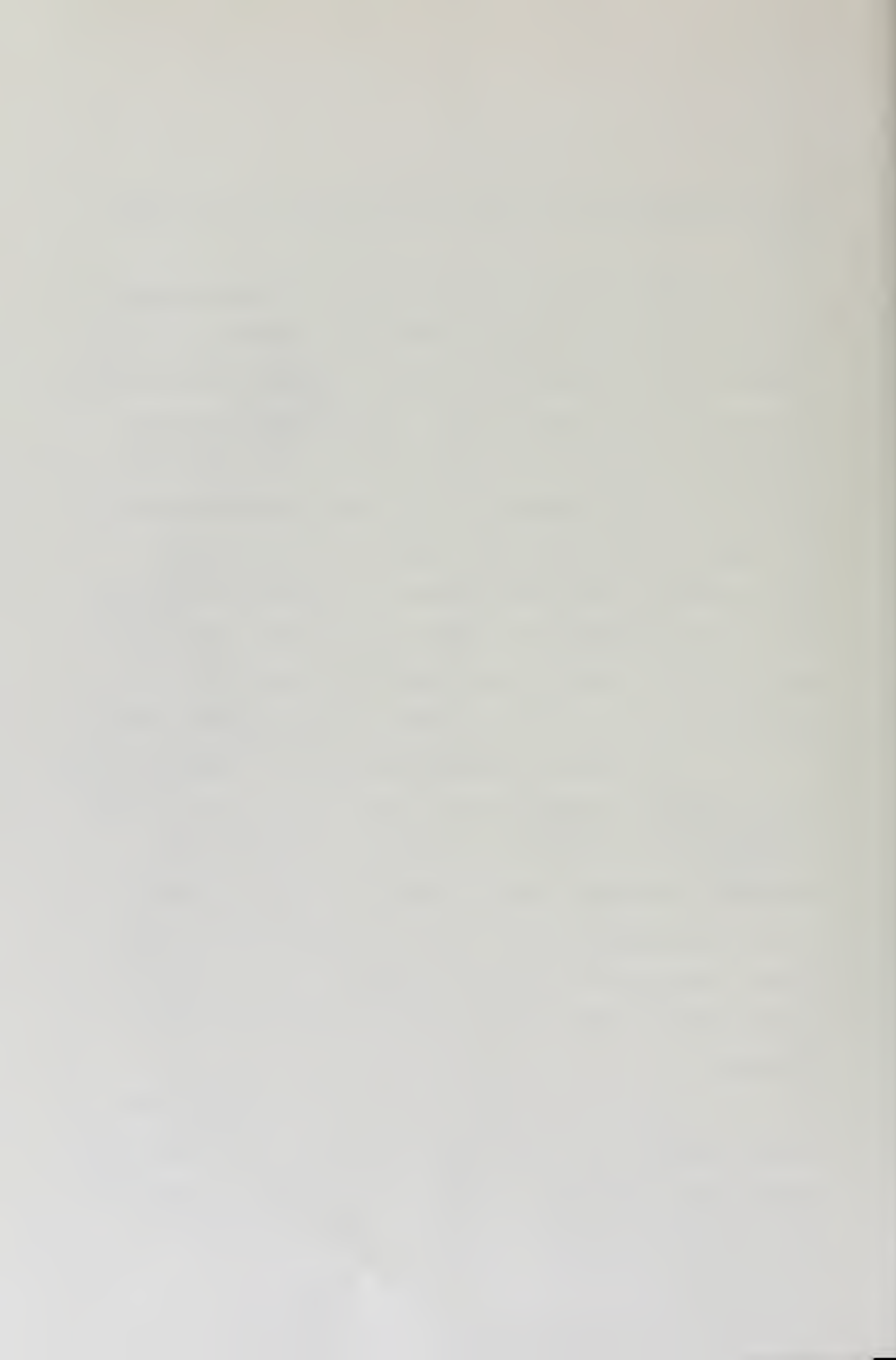


rate in the electron detector from this source is negligible.

The distance between the gold bremsstrahlung foil and the plastic scintillator was occupied to a large extent by the monochromator vacuum chamber. For this reason the vertical baffle in the monochromator was constructed of one-half inch thick lead. There was also sufficient space external to the vacuum chamber to place 2.3 inches of Mallory-2000 between the foil and the scintillator. The cross section for bremsstrahlung production at 90 degrees is small and therefore the flux of photons arising in the foil and being detected by the plastic scintillator is estimated to be negligibly small.

The number of photons produced by bremsstrahlung in the baffles, collector box, and exit slit of the monochromator and detected by the electron detector was measured by filling the exit aperture with a one-half inch thick graphite disc. Over the fractional photon energy range used in this experiment, .5 to .75, the contribution to the total count rate was less than 5 percent.

As seen in Figure (III-6), the electron detector assembly was positioned in a lead and Mallory-2000 house which provided a maximum of 14 inches of shielding and a minimum of 2 inches (top). The total amount of



shielding used was limited by the space available for the construction of the house.

The small size of the plastic scintillator coupled with a low absorption coefficient also aided in keeping the photon contribution to the total count rate small.

2. The Photon Detectors Shielding

The interlocked lead house described in detail by Loscoe was used to house the annihilation radiation detector. This set-up is shown in Figure (III-6) also. Two changes were made to the house described by Loscoe, however.

First, only the 120 degree detector position was used in the present research with the other channels being filled with approximately eight to ten inches of lead shielding. The two inch by two inch NaI(Tl) detector was further shielded by a lead collar to prevent scattering-in by photons which penetrate the lead house.

Second, the necessity to mount the drive motor for the rotating coil in the lead shielding, approximately between the target foil and the 120 degree detector, forced an approximate two inch reduction in available lead shielding. This loss was made up to some extent by repositioning the Mallory-2000 material as indicated in Figure (III-6). Previous measurements have shown that

no more than two percent of the total photon count rate arises from direct penetration of the lead house. About 182 centimeters of lead were placed between the 120 degree detector and the energy control slits. More than five tons of lead and two hundred pounds of Mallory-2000 were used in the construction of the shielding assemblies.

Another much smaller lead house was constructed for the monochromatic photon detector. This house used the lead pig assembly used by Malaker and described on page 73 of Reference 90. Additional lead bricks were used to collimate the photon flux and to shield the back of the assembly. With the exception of the entrance aperture, a minimum of two inches of lead and a maximum of six inches of lead shielded this detector. (Removal of the rear protection showed that only five percent of the total photon count rate was due to photons back-scattered from the walls of the target room.)

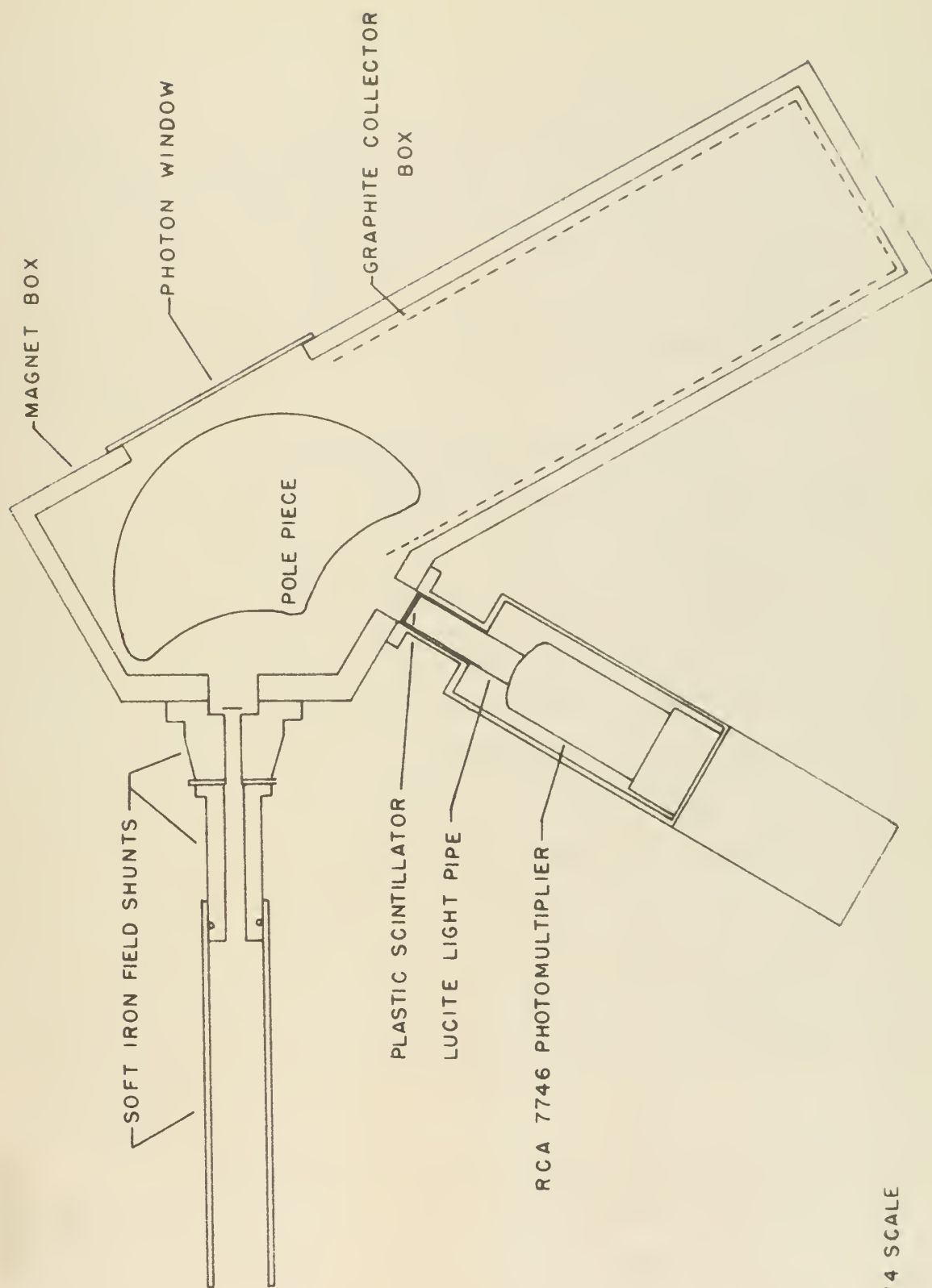
G. Procedure

In any measurement involving the use of photons from the bremsstrahlung spectrum to measure a physical process, the number of usable photons in the energy interval and solid angle of interest represents a major source of uncertainty. Therefore, the use of either well verified theoretical predictions of the cross section or experimental measurements of the cross section is

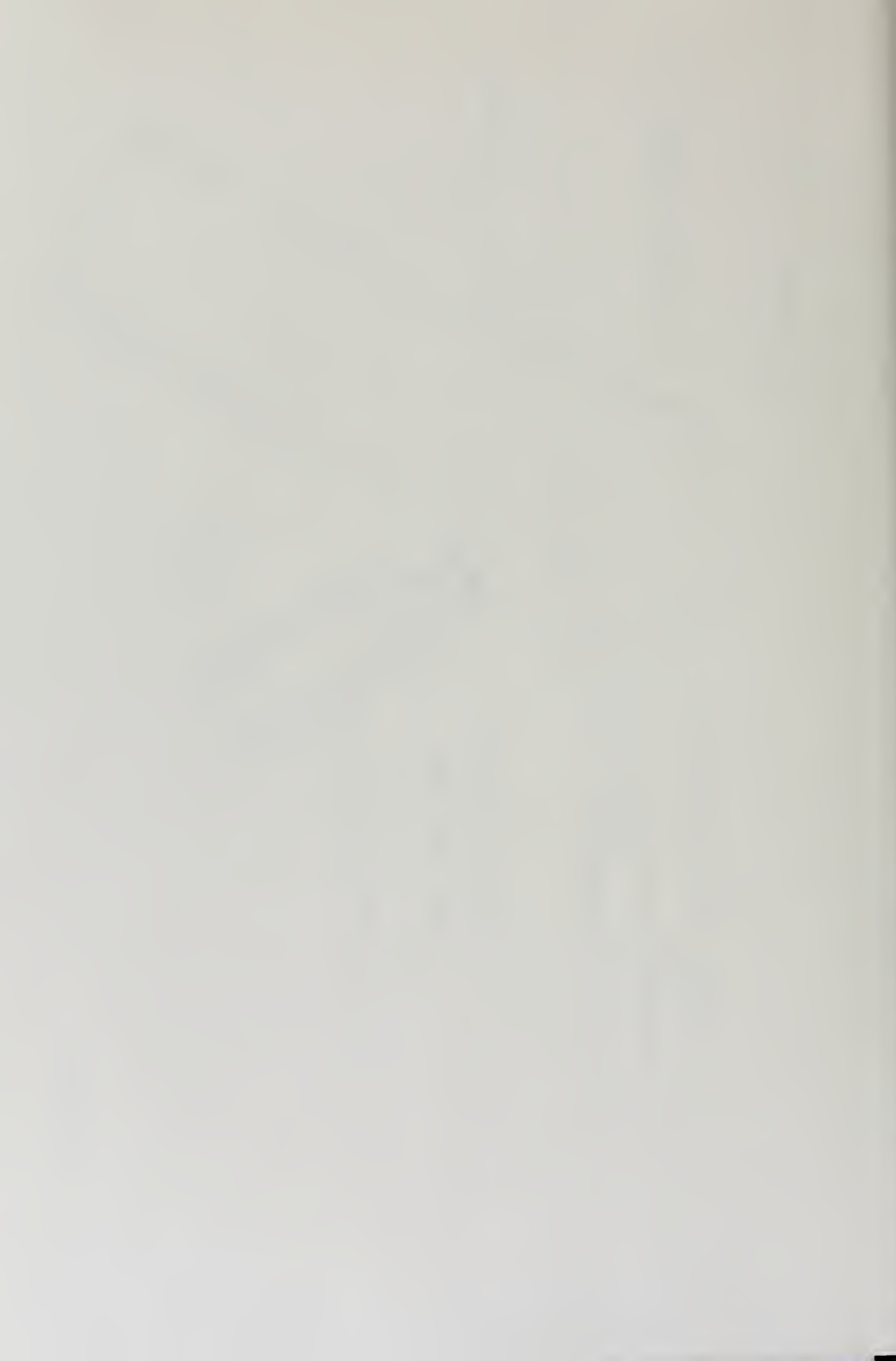


Figure (III-12)
Monochromator in detail.





1/4 SCALE

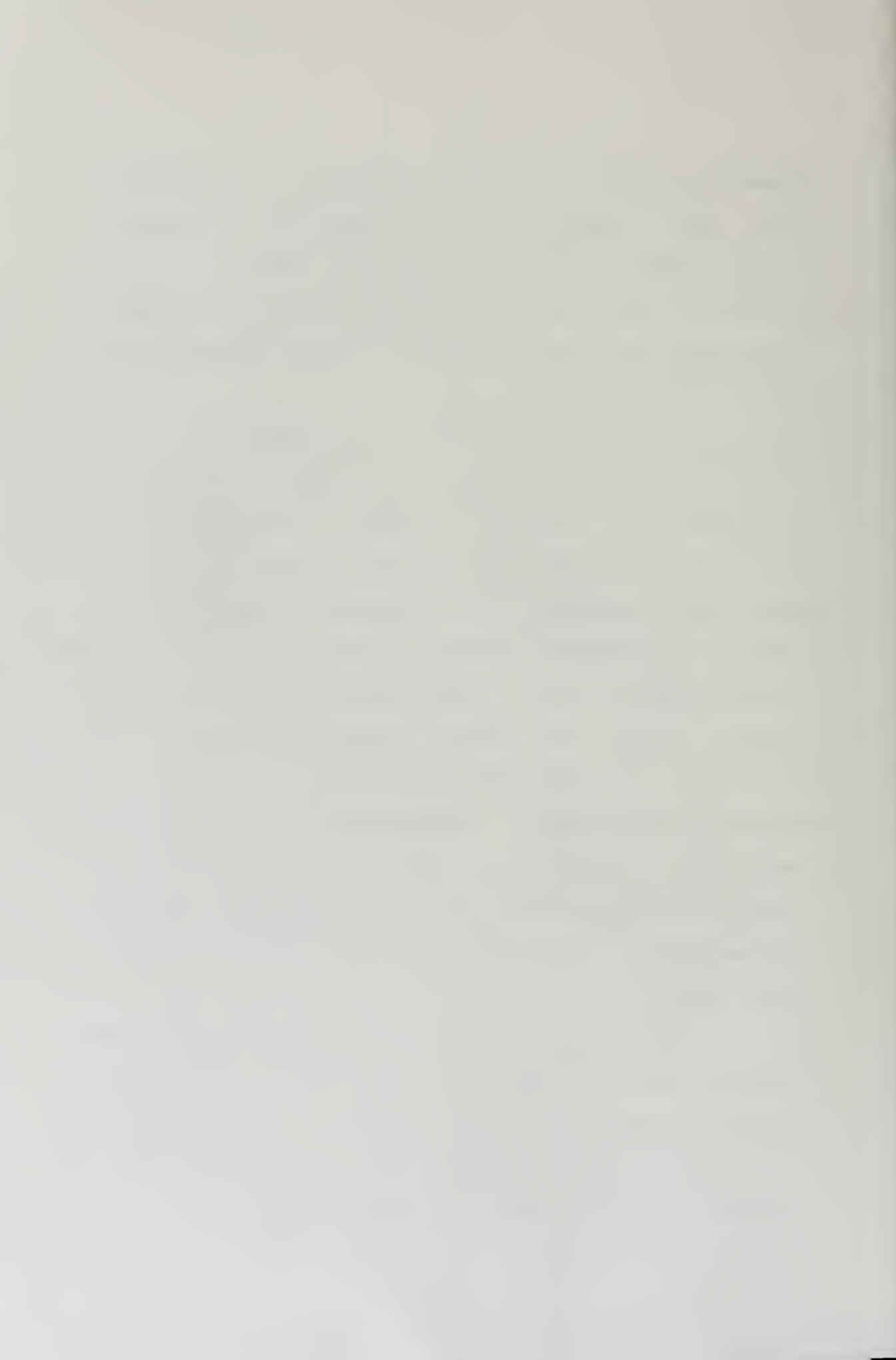


necessary to gain an accurate knowledge of the incident flux. Since no measurements have been made integrated over the small electron emission cones used in this experiment, it was necessary to carry out, as an adjunct experiment, measurements of the required bremsstrahlung cross sections.

1. The Bremsstrahlung Cross Sections

The yield of monoenergetic photons was measured by placing a well shielded two inch by two inch NaI(Tl) detector in the direct photon flux with the detector center line coincident with the incident beam direction. Ideally, the detector should be so set up that it subtends a solid angle at the foil equivalent to that of the pair creation target. For incident electron energies of 1.65 MeV or less, this procedure was possible if the beam current did not exceed 10 nanoamperes, since higher currents produced excessively high (> 20 kHz) counting rates in the photon detector. For higher incident electron energies, it was necessary to reduce the detector solid angle.

Measuring the bremsstrahlung cross section for a small photon emission solid angle raises a question of validity in extrapolating the measured cross sections to larger photon emission solid angles (such as that subtended by the pair creation target samples).



To examine this dilemma, a series of measurements was made with the detector located 25 cm. from the foil and subtending a solid angle equivalent to that of the target sample. The detector was then relocated a distance of 4.5 meters from the foil and the measurements repeated. A comparison of the resultant figures of merit indicated no significant change in the figure of merit within the statistical and geometric uncertainty of the measurement. These measurements were made at an incident electron energy of 1.54 MeV and a monoenergetic photon energy of .66 MeV. The assumption was made as a result of this test that the figure of merit measured for a small photon emission solid angle could be applied to the theoretical cross section corresponding to the target solid angle to an accuracy within the uncertainty of the measurement.

Monochromatic photon yields were measured for incident electron energies of 2.86 MeV and 2.3 MeV. At the former energy, 4×10^{-5} Coulombs of charge were collected for each of five photon energies, which were 1.533 MeV, 1.570 MeV, 1.71 MeV, 1.85 MeV, and 2.0 MeV. At the latter electron energy, 8×10^{-5} Coulombs of charge was collected at a photon energy of 1.2 MeV.

2. Pair Creation

The target sample was placed in the photon flux



in the manner described on p. 70 using the target holder assembly. The electron beam was then brought out of the accelerator and steered onto the gold foil. For both the bremsstrahlung and pair yield runs the beam was centered using the following techniques. The current through the LEFT/RIGHT coil of Steering 6 (see Appendix B) was varied until the beam struck the annular steel foil holder. The monitored photon rate increased notably and the current in the coil was then reversed and increased until the same nominal photon count rate was obtained for the oppositely directed current. The field in the 45 degree magnet was then adjusted so that equal deflections were necessary to obtain the same monitored counting rate. When this was achieved the beam was centered left/right. Vertical centering was achieved in the same manner except that the current through the UP/DOWN coil was adjusted to be half of the algebraic sum of the currents required to move the beam to the top and bottom of the foil, respectively.

The centering process was repeated whenever the incident electron energy or the monochromator magnetic field was varied. Moreover, the centering was checked before each data run to ensure that the photons being used arose only in the gold foil (experience has shown that the slightest striking of the foil holder, even if



only temporary, completely invalidates the data).

For the pair creation yield measurements, the collection of 10^{-4} Coulombs of data, with an average beam current of .1 microamperes, constituted one run. The limiting factor on the beam current was the average count rate in the electron detector, which was maintained at a level no higher than 5 MHz. This average rate was determined to arise from instantaneous rates as low as 100 kHz and as high as 12 MHz.

Checks using natural sources were made on the gain stability of the detection and counting system periodically throughout the data collection process. Unless the photon counting rate exceeded 30 kHz, no detectable drift was noted. In the annihilation radiation detector, with the electron rate at 5 MHz, the photon count rate never exceeded 1.2 kHz.

The data were taken sequentially as true plus chance coincidence runs, with proper delay in the β -arm, followed by a chance coincidence run, with a delay greater than the resolving time of the circuit in the β -arm. A timing curve was also taken at the start of each period of data collection. A typical timing curve was presented in Figure (III-11).

The data taken were normalized to the total number of electrons accumulated. The accumulated charge



was measured using the current integrator described elsewhere.³⁹

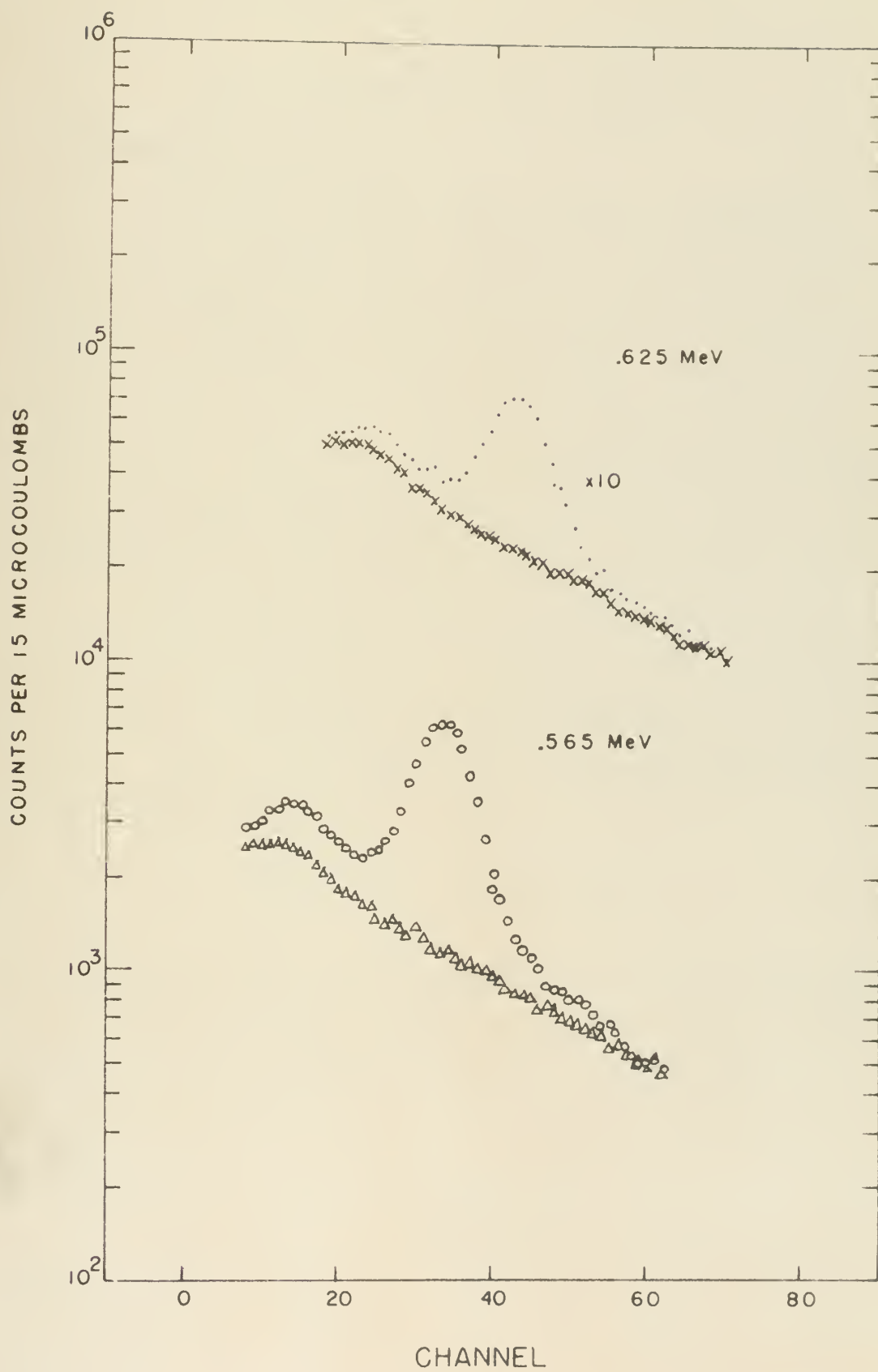
The chance coincidence runs are necessary to correct the true plus chance coincidence spectrum so that only the yield due to monoenergetic photons is considered in the cross section analysis. The chance spectrum serves, therefore, as background reduction data.



Figure (IV-1)

Typical pulse height distribution
of monoenergetic photons showing
uncorrected total and chance co-
incidence spectra.







IV. DATA REDUCTION AND ANALYSIS

A. Monoenergetic Photons

The pulse height distributions were prepared for fitting by subtraction, channel by channel, of the chance coincidence spectrum from the total coincidence spectrum. Examples of these distributions are shown in Figures (IV-1) and (IV-2) before and after subtraction, respectively. The background subtracted result was then fit to a Gaussian using the method of least squares. An example of the fitted spectrum is shown in Figure (IV-2).

The area under the fitted peak, corrected for total detection efficiency, was taken to be a measure of the number of monoenergetic photons incident on the detector. The measured cross section was then determined using Equation (II-14a).

$$\left(\frac{d\sigma_{\text{BREMS}}}{dk} \Delta k \right)_{\text{EXP}} = N(k) / nQ$$

The figure of merit, for each energy, was then determined as discussed in Section (III.B.2.b). The measured bremsstrahlung cross sections and figures of merit are presented in Table (IV-1).

B. Evaluation of the Yield Expression

The use of the bremsstrahlung radiation as a source of monoenergetic gamma-rays necessitated the use of a large target sample in order that a high percentage

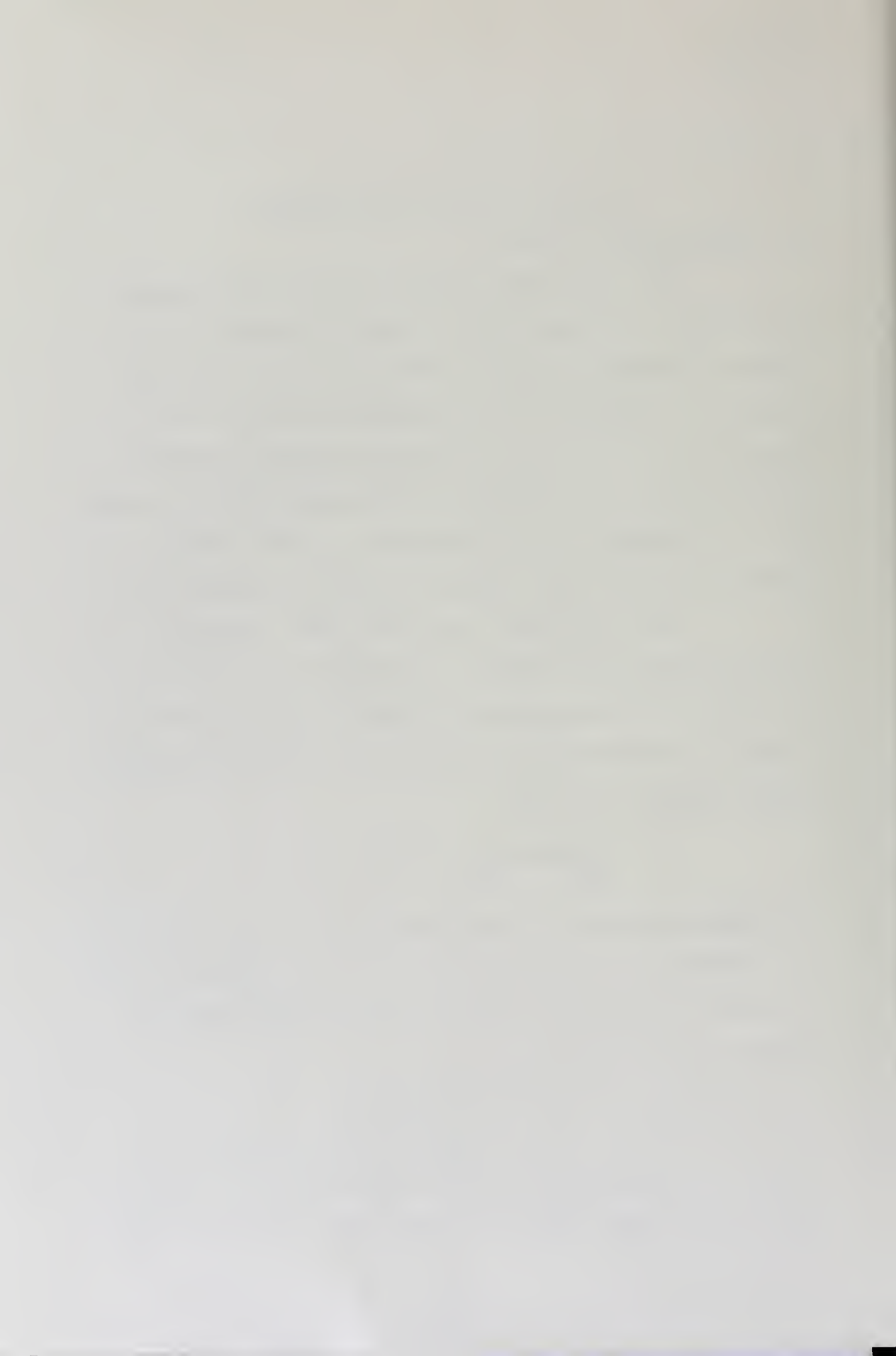


TABLE (IV-1)

Measured bremsstrahlung cross sections and figures of merit for electron emission into a cone of half-angle 7.6° and photon emission into a cone of half-angle $.5^\circ$.

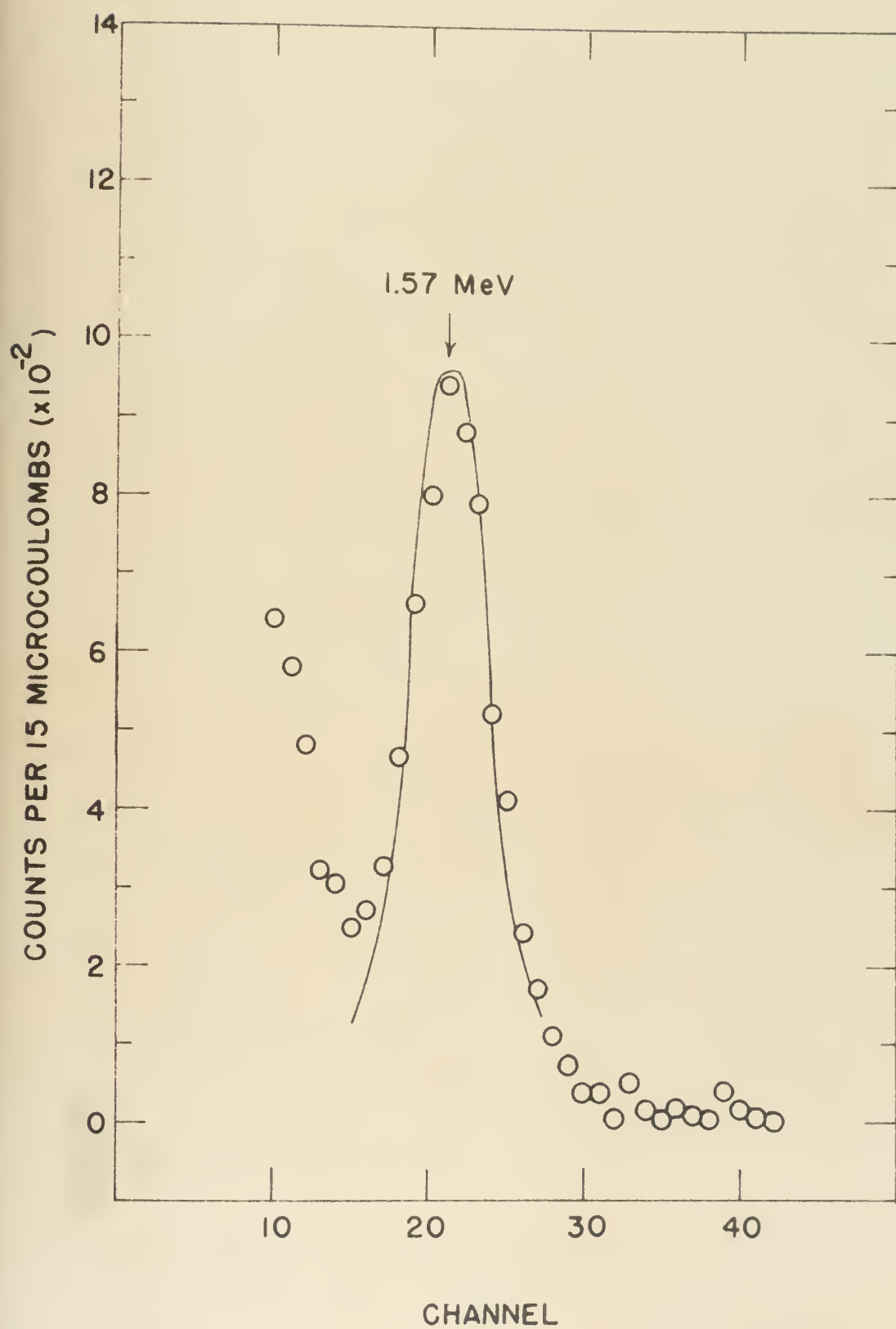
T_0 (MeV)	k (MeV)	k/T_0	$((d\sigma_s/dk)\Delta k)_{\text{exp}}$ mb	F_M
2.3	1.20	.52	$.110 \pm .006$	$1.00 \pm .05$
2.86	1.533	.54	$.151 \pm .009$	$.94 \pm .06$
2.86	1.57	.55	$.151 \pm .009$	$.99 \pm .06$
2.86	1.71	.6	$.102 \pm .006$	$1.02 \pm .06$
2.86	1.85	.65	$.068 \pm .005$	$1.09 \pm .08$
2.86	2.00	.7	$.036 \pm .002$	$1.03 \pm .07$



Figure (IV-2)

Background corrected monoenergetic photon
distribution (open circles) fit to a
Gaussian (solid line).







of the available gamma-rays would intercept the target. This procedure was further necessitated by the small cross sections for pair creation near the threshold energy.

1. Target Volume Summation

A detailed treatment of the analysis of the detection efficiencies and the incident photon distribution has been given previously⁹⁰ and only the results of this analysis will be given here.

The detection efficiencies were determined in the manner described in Section (III-E). The detection efficiency, $\epsilon_k(i,j)$, for each volume element was normalized to the value at the approximate center position of the I x J grid as

$$\eta_k(i,j) = \epsilon_k(i,j) / \eta_0$$

where η_0 is the source full energy peak efficiency at the reference grid position ($i = 4, j = 7, k = 1$).

It was necessary to evaluate the term

$$\exp \left\{ - \alpha_j^2 / q^2 \right\}$$

at each grid position in the I x J x K matrix. It has been shown⁹⁰ that α_j can be represented for such a matrix by an expression of the form

$$\alpha_k^2(i,j) = \frac{(i - \frac{I+1}{2})^2 m_i^2 + [(j - \frac{J+1}{2}) m_j - (k - \frac{K+1}{2}) m_k \tan \varphi]^2 \cos^2 \varphi}{[h + (j - \frac{J+1}{2}) m_j \sin \varphi + (k - \frac{K+1}{2}) m_k \cos \varphi]^2}$$



where m_i , m_j , m_k are the dimensions of each volume element along the i-, j-, and k- axis, respectively, h is the distance between the target sample and the bremsstrahlung source measured along the beam direction, and ϕ has been defined. The target was divided into layers along the k-axis conceptually to account for self-absorption effects in various layers of the sample. This division also allowed full use of the expression for $\alpha_k^2(i,j)$

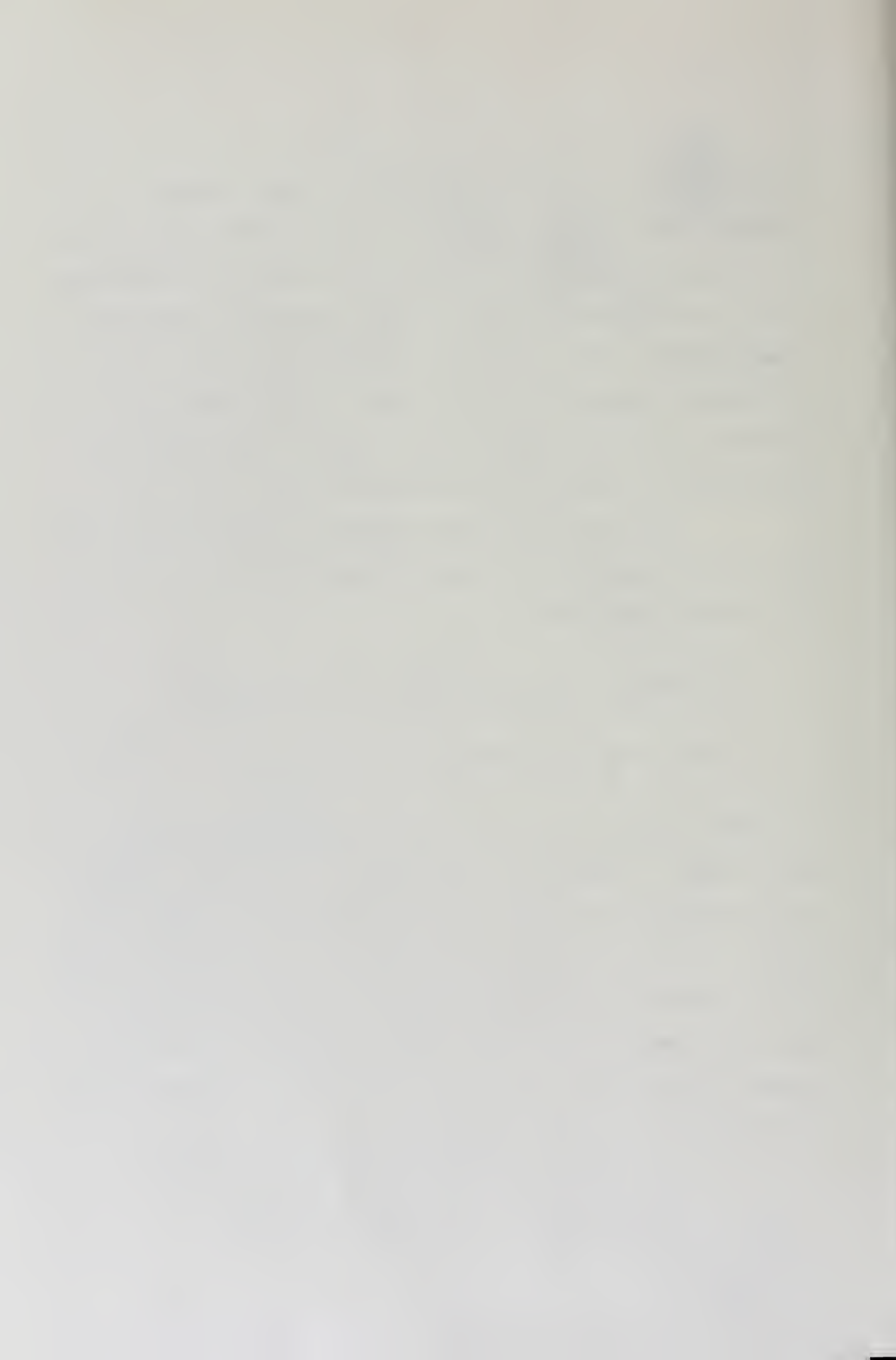
The sum over volume elements of Equation (II-15) can now be replaced by an explicit sum over i, j, and k in the following form,

$$Y = N(R) \frac{\rho T T}{I \cdot J \cdot K} P \sigma_{PAIR} \eta_0 C \cdot \sum_{k=1}^K \sum_{i=1}^I \sum_{j=1}^J \eta_R(i,j) \exp\left\{-\frac{\alpha_m^2(i,j)}{q^2}\right\} \times \\ \exp\left\{-\mu \frac{\rho T T}{K} \left(\frac{2k-1}{2}\right)\right\} \exp\left\{-(\mu_c + \sigma_{PAIR}) \frac{\rho T T}{K} \left(\frac{2k-1}{2}\right)\right\} \quad (IV-1)$$

The terms δ_f and δ_f' have been replaced by the approximation $\frac{\rho T T}{K}$. While this replacement is not exact, owing to the variation in effective thickness as the angle between incident and exiting radiation and the normal to the face of the target changes, numerical calculations show that the average reduction, over the target, for the incident and outgoing radiation is less than .5 percent and 1.2 percent, respectively.

2. Effects of Target Thickness and Area

a) Effects Due to Target Thickness



Three major factors were considered in the determination of optimum target thickness. The target must be thick enough to provide the maximum possible yield but also sufficiently thin so that self-absorption and multiple effects, i.e., Compton scattering of incident monoenergetic photons in the target followed by pair creation, do not seriously affect the data. The yield expression, including self-absorption effects, has been evaluated for various target thicknesses and is shown in Figure (IV-3) for both lead and tin.

Following the method of Yamazaki and Hollander, the contribution due to multiple effects has been approximated by a parameter, α , given by the expression

$$\alpha \approx \frac{1}{2} T \mu_{CE}(k) \frac{\int_2^k \sigma_{PAIR}(k') dk'}{(k-2) \sigma_{PAIR}(k)}$$

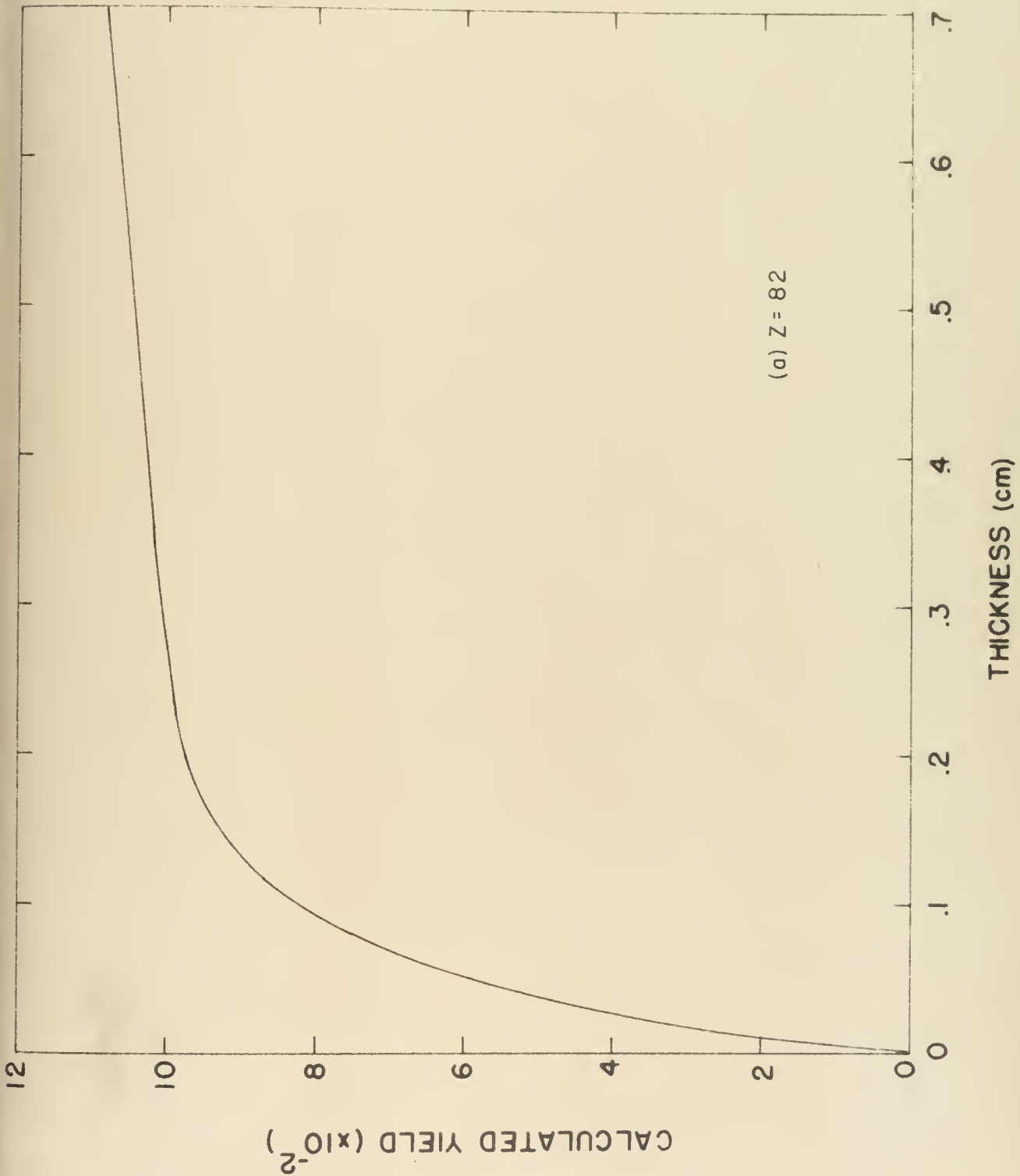
where μ_{CE} is the Compton absorption coefficient at photon energy k . Only the multiple effects due to the monoenergetic photons are considered since only these will appear in the corrected true coincidence spectrum. The parameter α is presented as a function of incident photon energy in Figure (IV-4a) for lead and in Figure (IV-4b) for tin. The choice of quarter-inch thick targets can be seen to combine the properties of high yield and low order (less than 2 percent) multiple effect contributions.



Figure (IV-3)

Calculated annihilation radiation yield
as a function of target thickness for (a)
lead (b) tin.







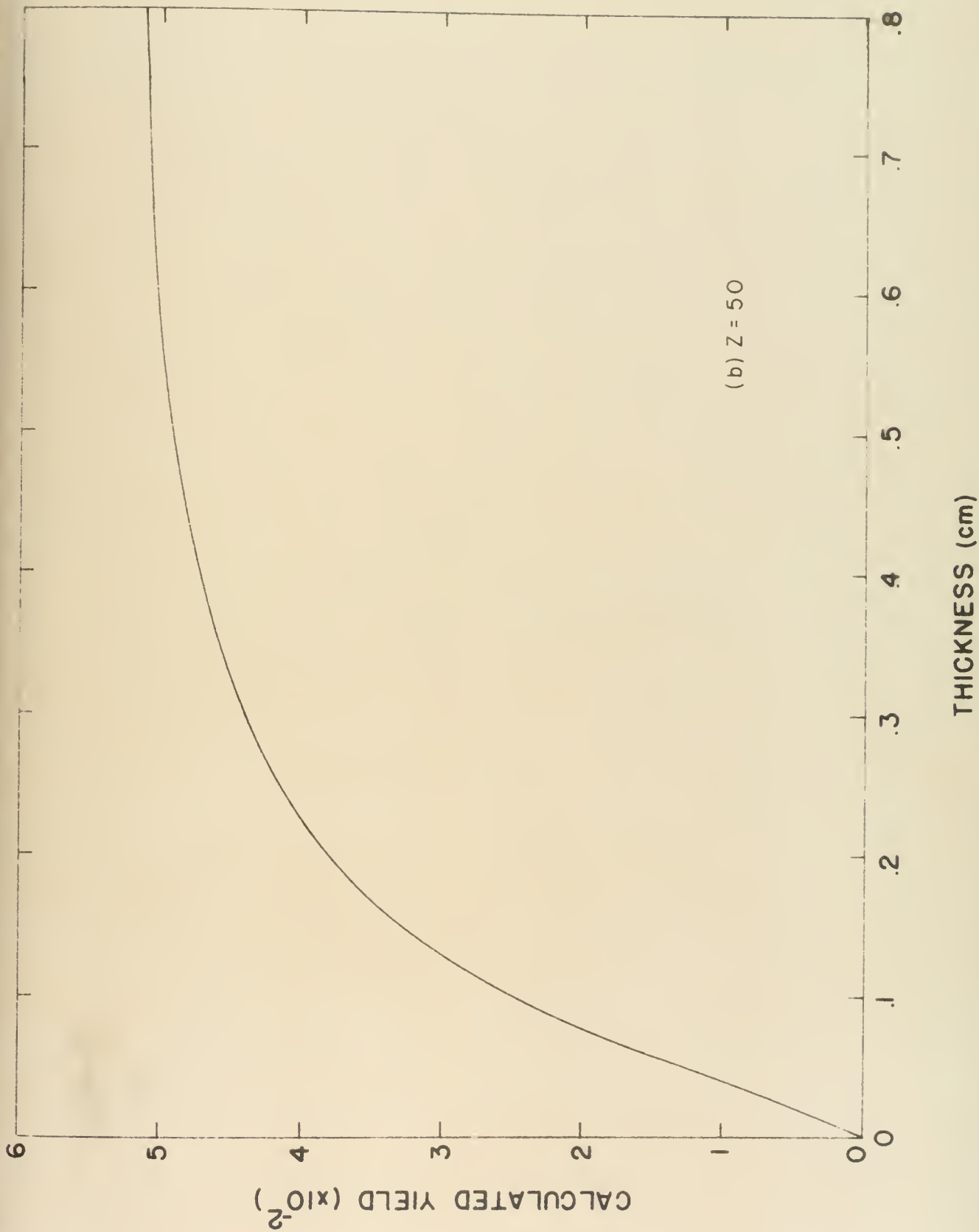
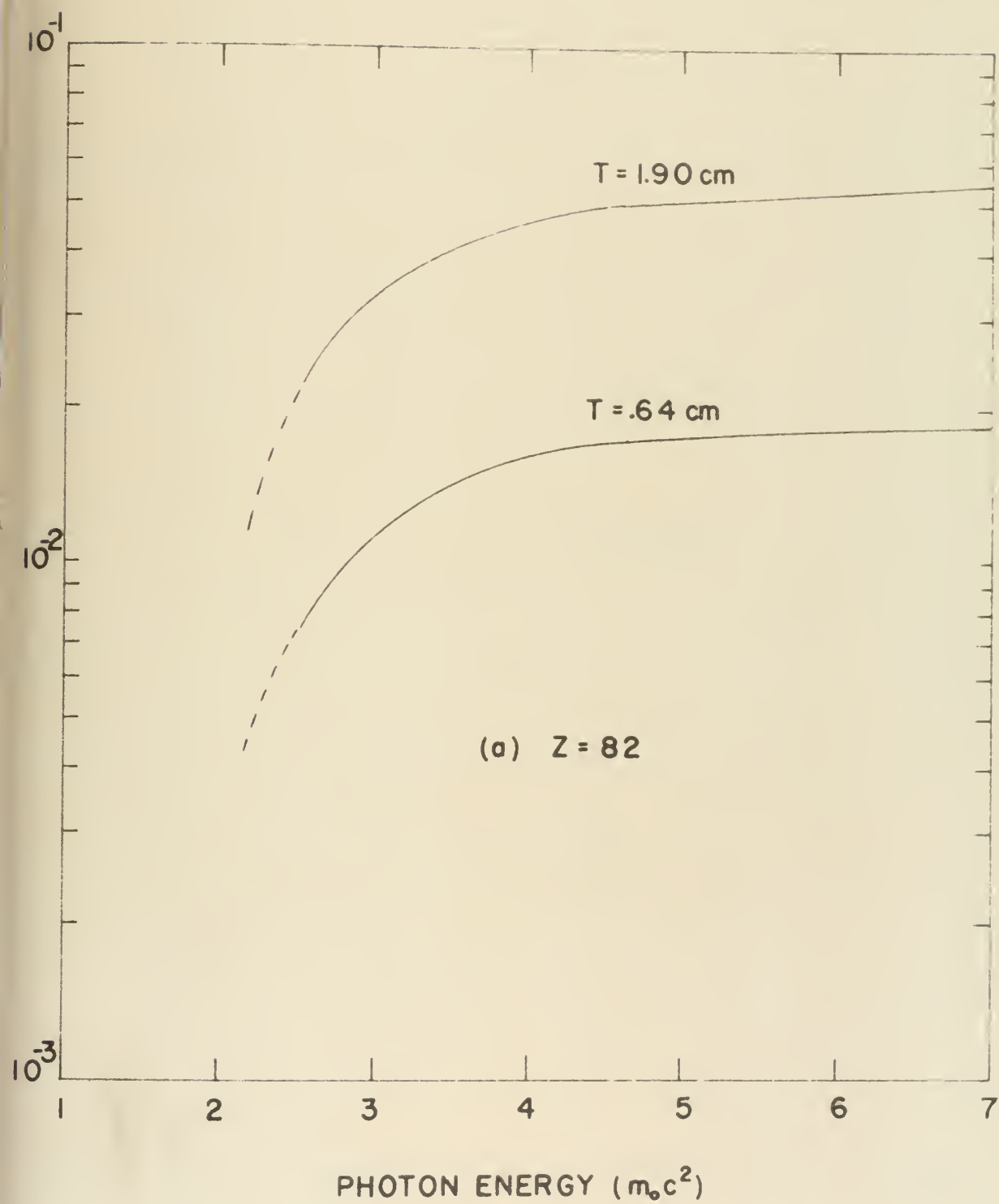




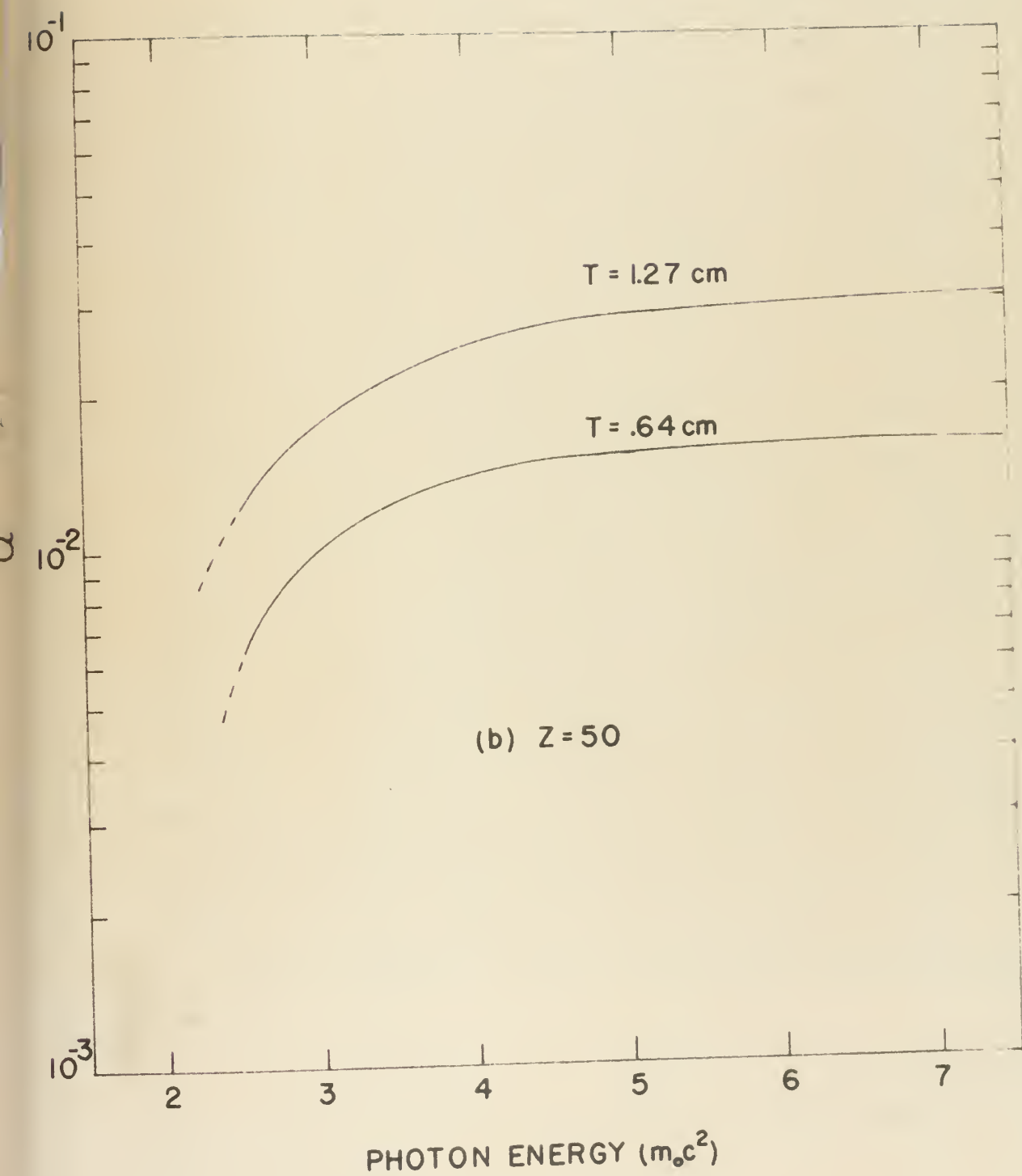
Figure (IV-4)

Multiple effect parameter, α , as a
function of incident photon energy for
(a) lead and (b) tin.











b) Effects Due to Target Area

At first sight, a target of large frontal area seems desirable in order to subtend the largest possible solid angle at the bremsstrahlung source, thereby increasing the attainable yield. For such a large target, the detector solid angle would also be increased contributing to a larger yield. These effects are offset by two other effects. As the solid angle subtended at the bremsstrahlung source increases, the number of detected photons increases non-linearly due to the approximate Gaussian nature of the incident photon distribution. Moreover, the detection efficiencies for those volume elements furthest from the center of the target sample are reduced. The net effect, then, is a leveling off of the yield as the frontal area of the target is increased. These effects have been studied by evaluation of the yield expression, Equation (IV-1), while limiting the range of the i and j indices for an assumed constant incident photon distribution. These calculated yields are plotted in Figure (IV-5) as a function of the half-angle of the solid angle subtended by the target at the bremsstrahlung source.

The effect of the parameter q in the expression for the angular distribution of the incident radiation will be considered in the next section.

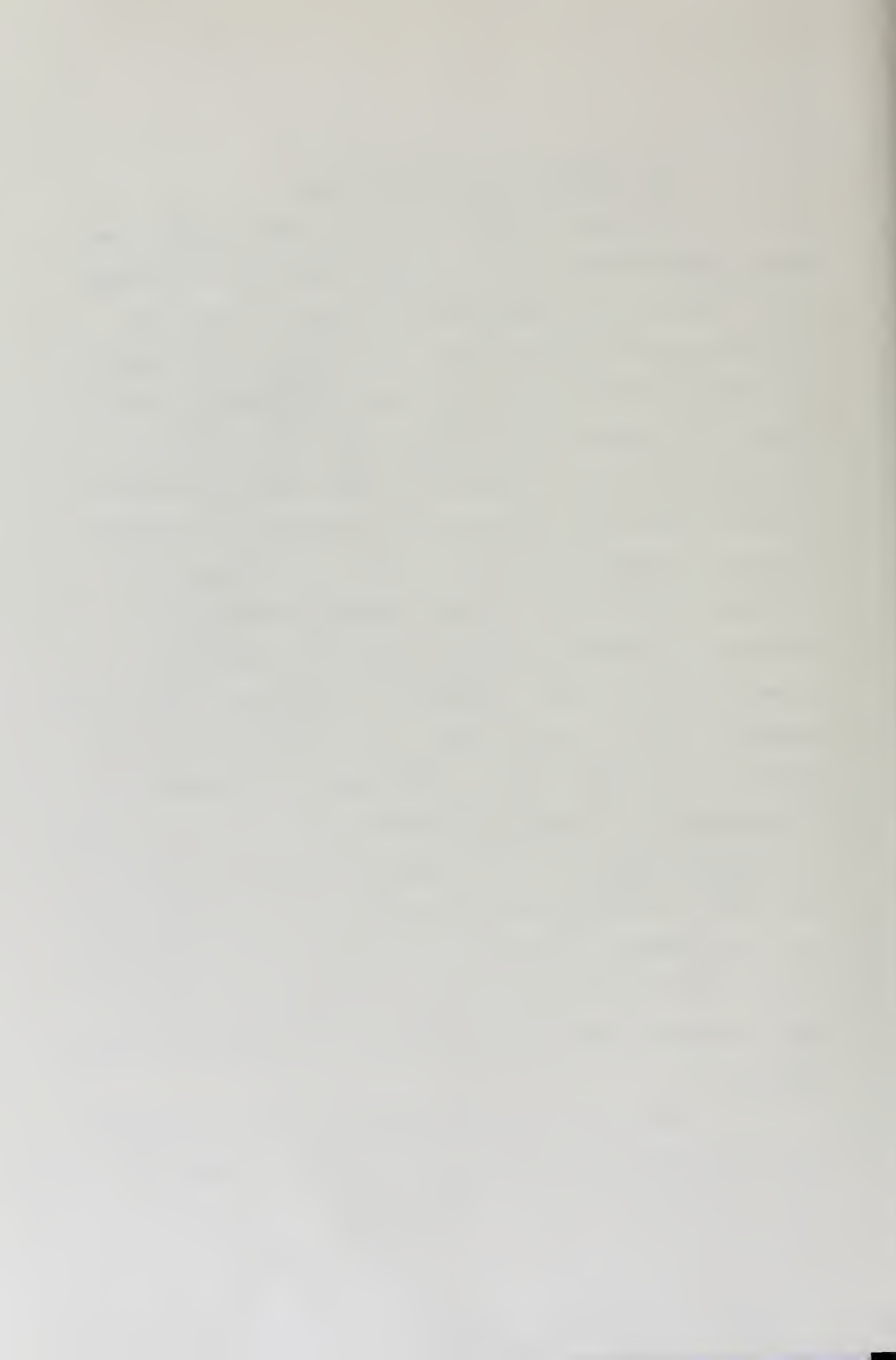
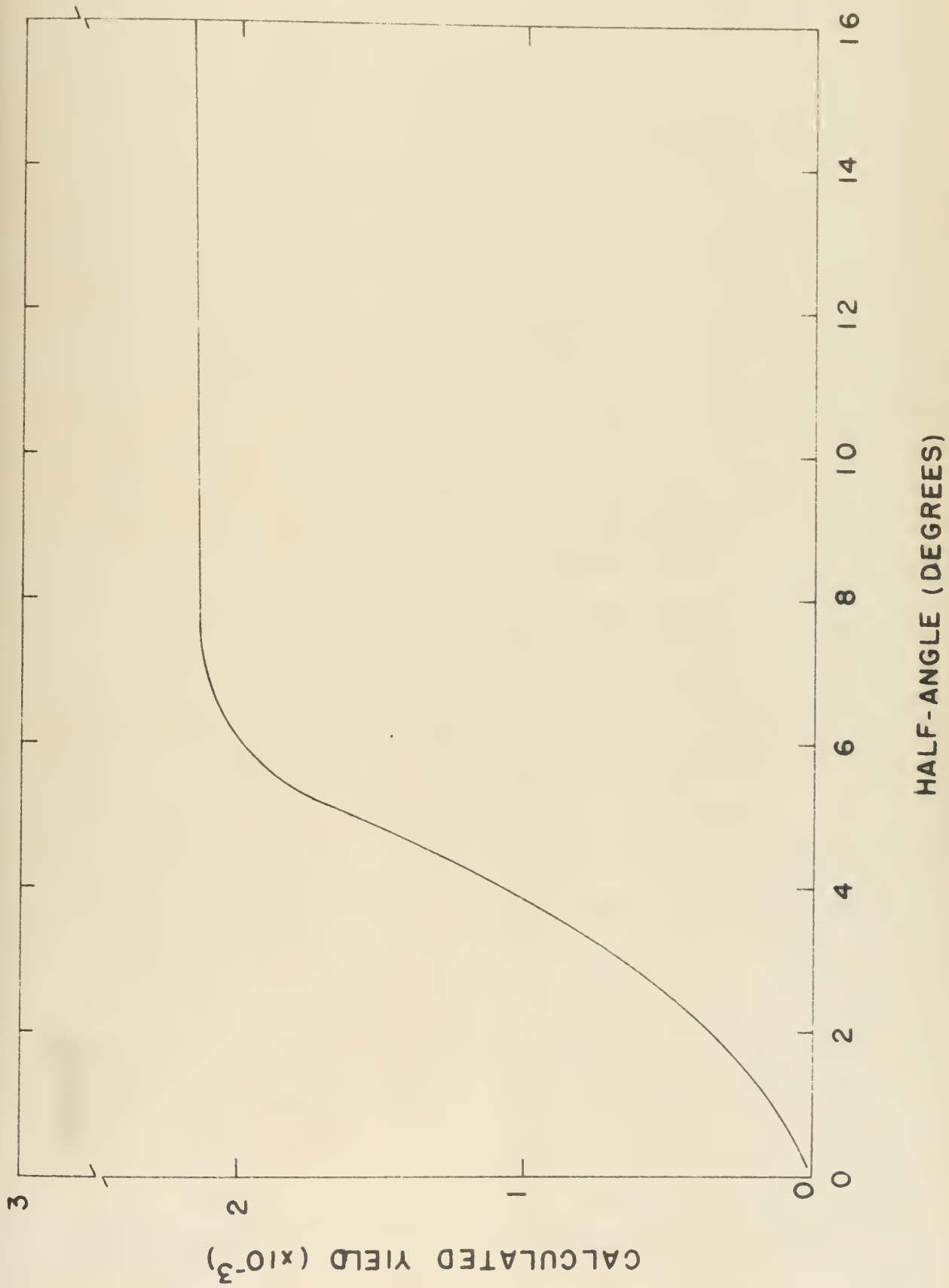


Figure (IV-5)

Calculated annihilation radiation
yield as a function of the half-
angle of the photon emission cone.







C. Pair Creation

Due to the existence of an annihilation radiation photopeak in the chance coincidence pulse height distribution, both the total coincidence and chance coincidence photopeaks were fit to Gaussian curves by the method of least squares. Two methods were used in the fitting procedure. In the first case, the photopeak in each pulse height distribution was fit and the resultant areas under the peaks were subtracted to give the yield. In the second case, the pulse height distributions were fit over the energy interval .6 MeV to .7 MeV with an assumed beam dependent background. This background was then subtracted, channel by channel, from the initial pulse height distributions. The revised spectra were then fit as in the first method. The yield was then determined by subtracting the areas under the fitted photopeaks. No significant variation existed between the yields as determined by these two fitting techniques. The level of confidence for these fits, determined by the Chi-square test, satisfied the requirement $\chi^2/F \approx 1$, where F is the number of degrees of freedom. Examples of the data and the fits for the two methods are shown in Figures (IV-6) and (IV-7).

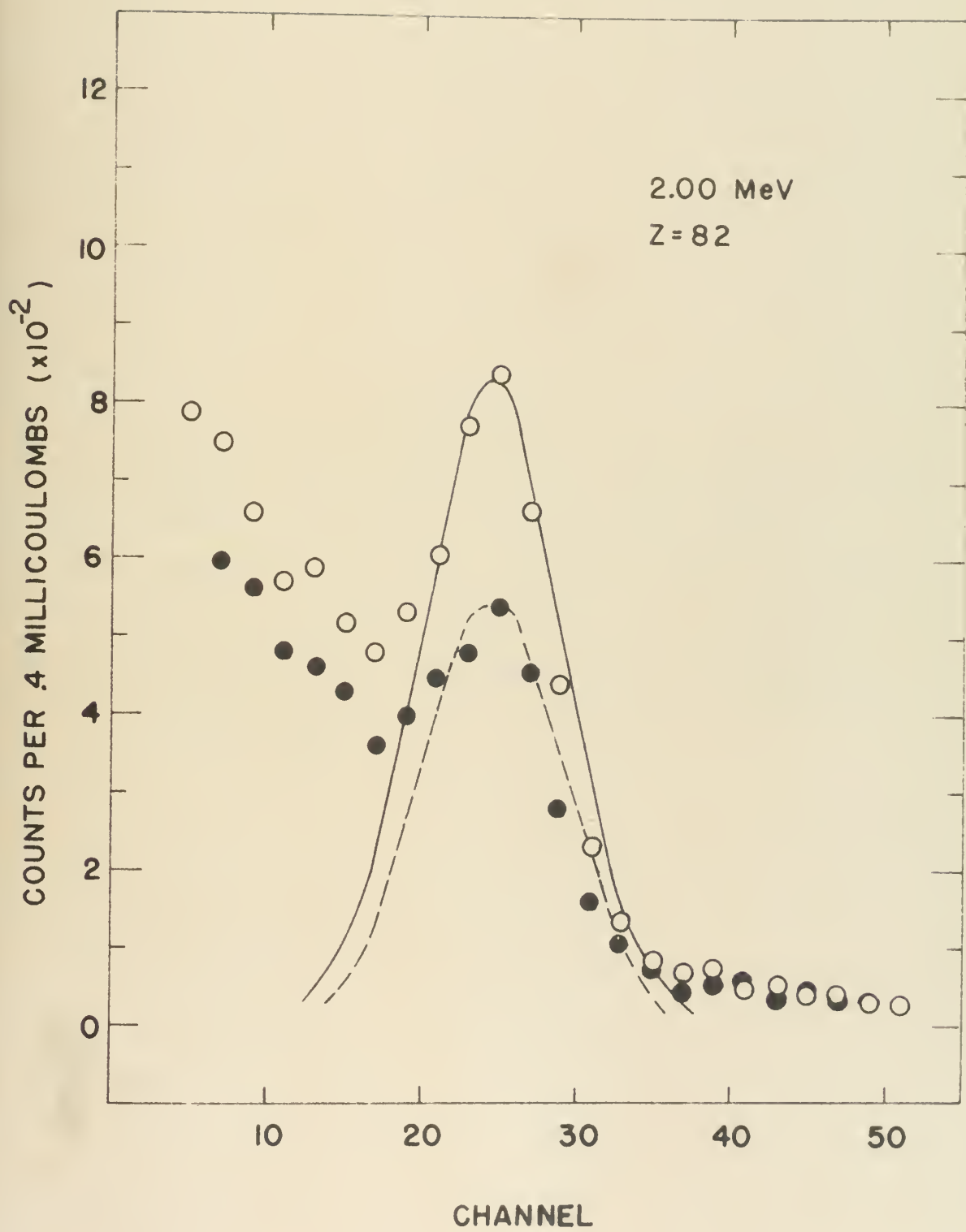
The yield, corrected for multiple effects in the target sample, was taken to be a measure of the number



Figure (IV-6)

Typical annihilation radiation pulse height distributions for total coincidence (open circles), fit to a Gaussian (solid line), and chance coincidence (dark circles), fit to a Gaussian (broken line).





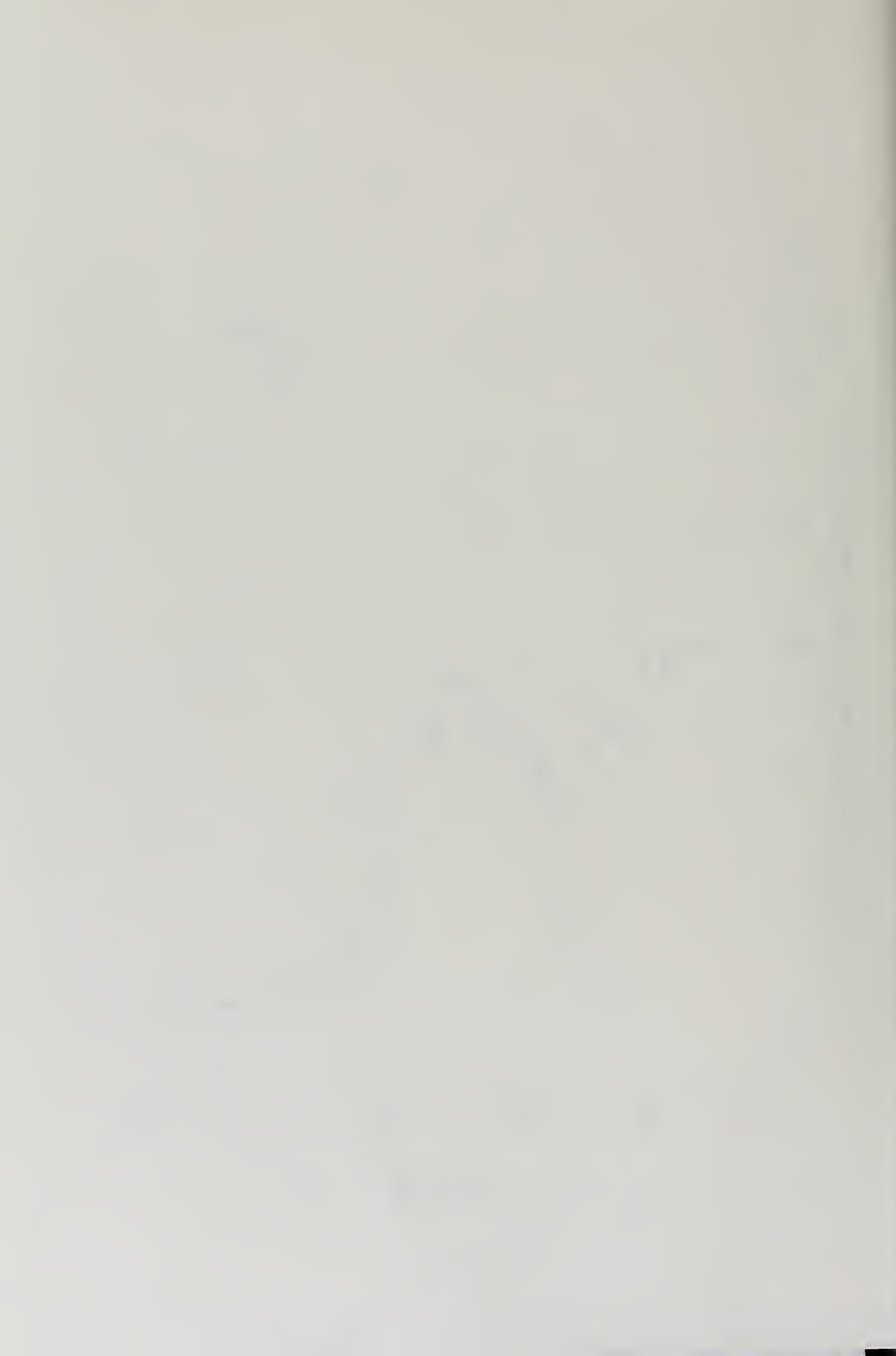
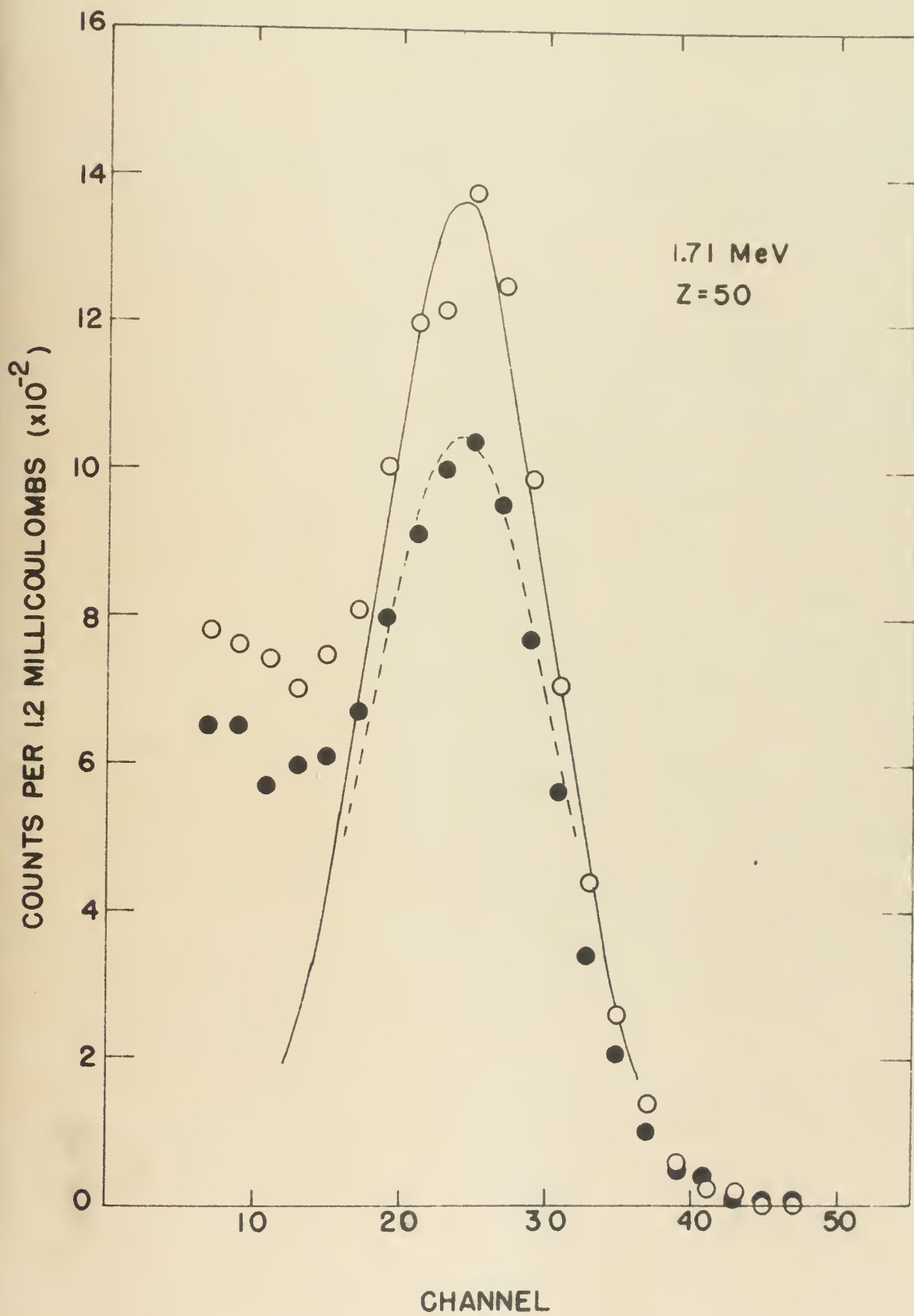
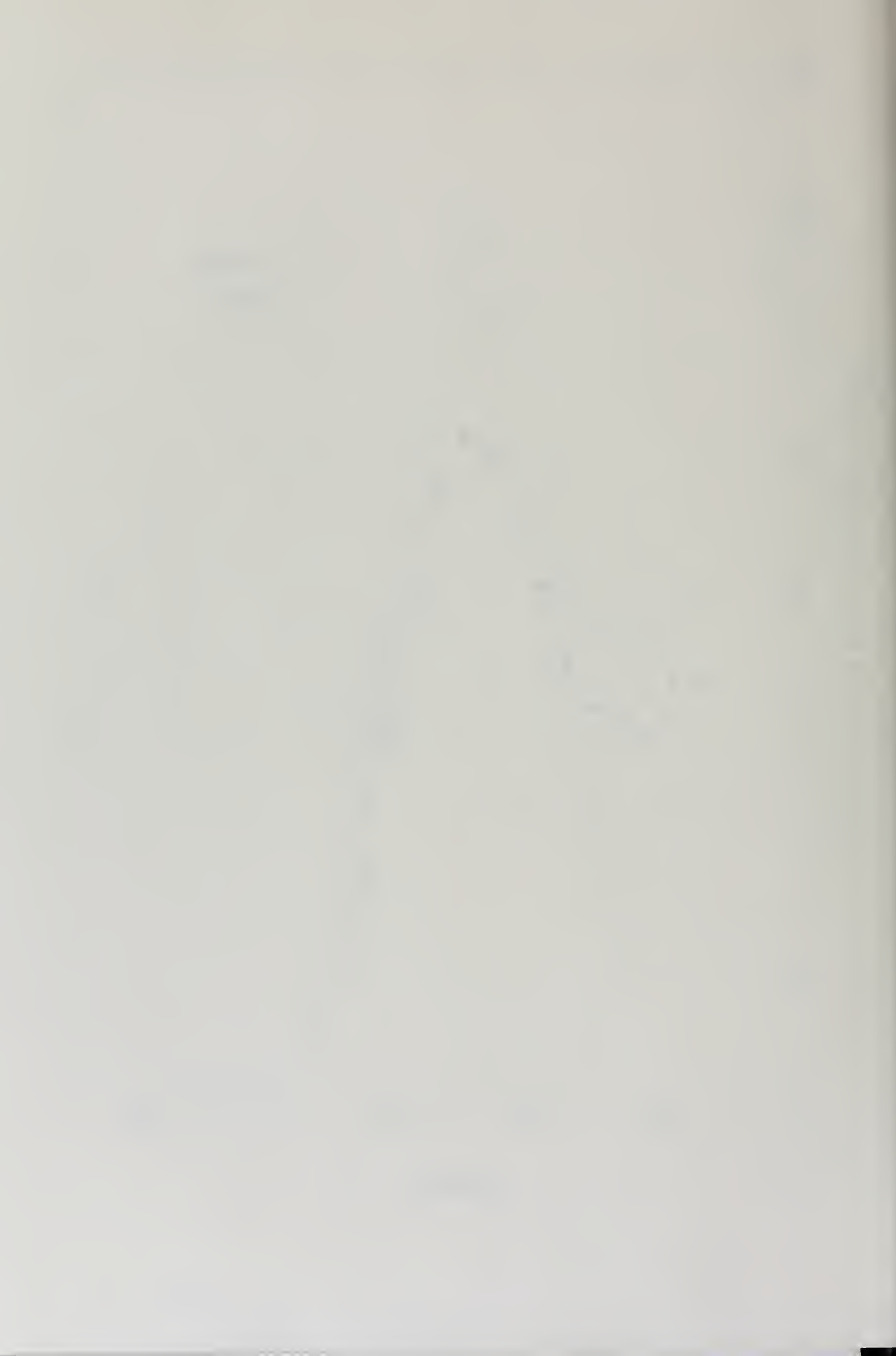


Figure (IV-7)

Typical annihilation radiation pulse height distributions, corrected for assumed beam dependent background, for total coincidence (open circles), fit to a Gaussian (solid line), and for chance coincidence (solid circles), fit to a Gaussian (broken line).







of pairs created in the target sample which annihilated in the sample and were detected by the scintillation spectrometer.

From the discussion of Section (IV.B.1), it follows that the effect of the angular distribution of the incident photon flux on the calculated yield must be considered. Since the value of $\alpha_k^2(1,j)$ is fixed by the geometry of the experimental layout, the parameter q is the major source of uncertainty in the expression.

To determine the correct value of this parameter, angular distributions calculated using Equation (II-29) and the experimental angular distributions presented by Rester and Dance have been considered. The experimental distributions were about 20 percent wider than those calculated using the B-H result and the effect of this disparity will be discussed shortly. The actual incident photon distribution differs from those mentioned due to small angle multiple scattering effects in the bremsstrahlung foil.

As discussed in Section (III.B.2.c), the electron multiple scattering effects can be accounted for by the theory of Molière and appropriate electron angular distributions calculated for scattering in thin foils. The angular distributions of electrons shown in Figures (IV-8) and (IV-9) have been so calculated. The final

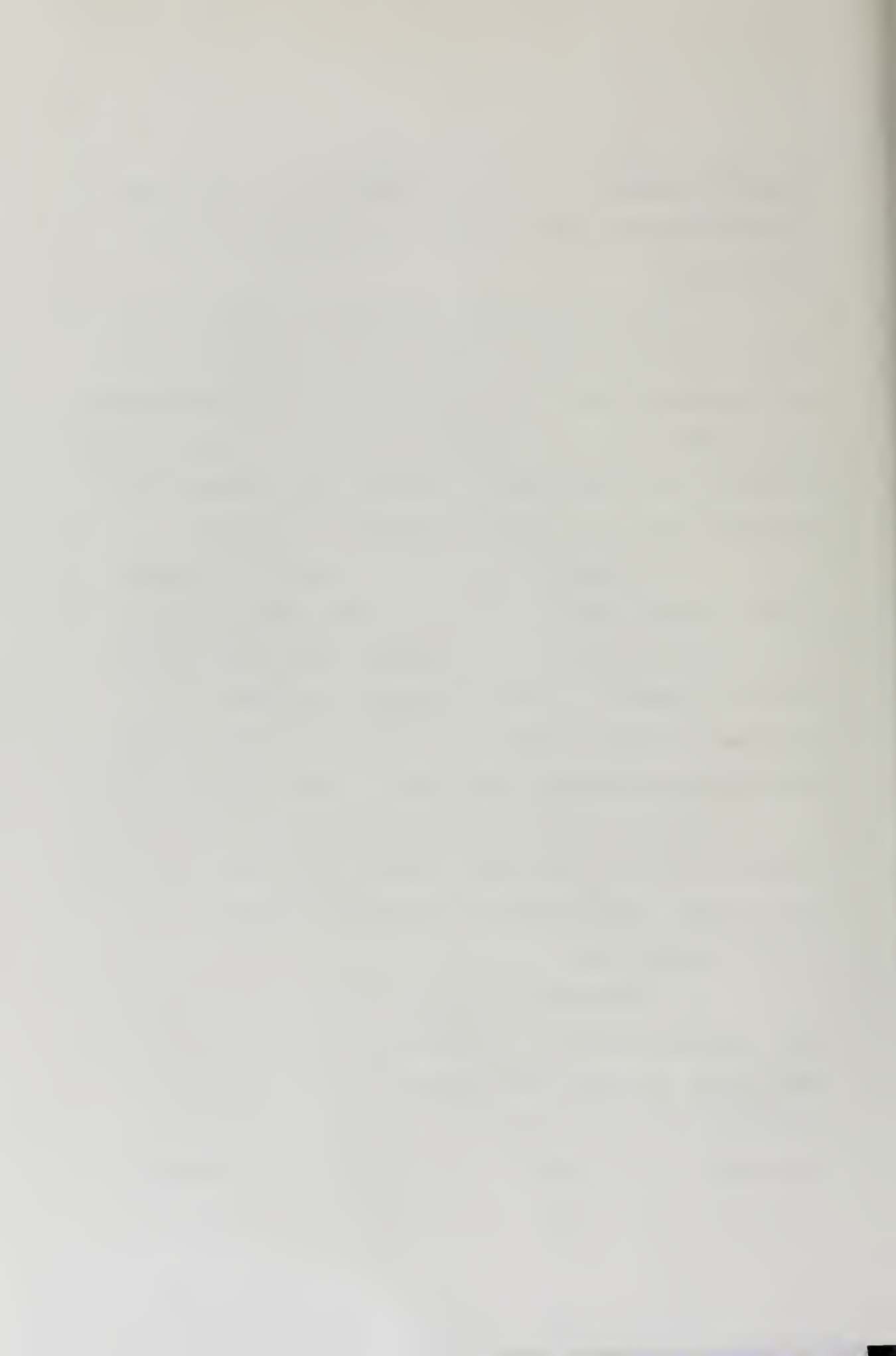
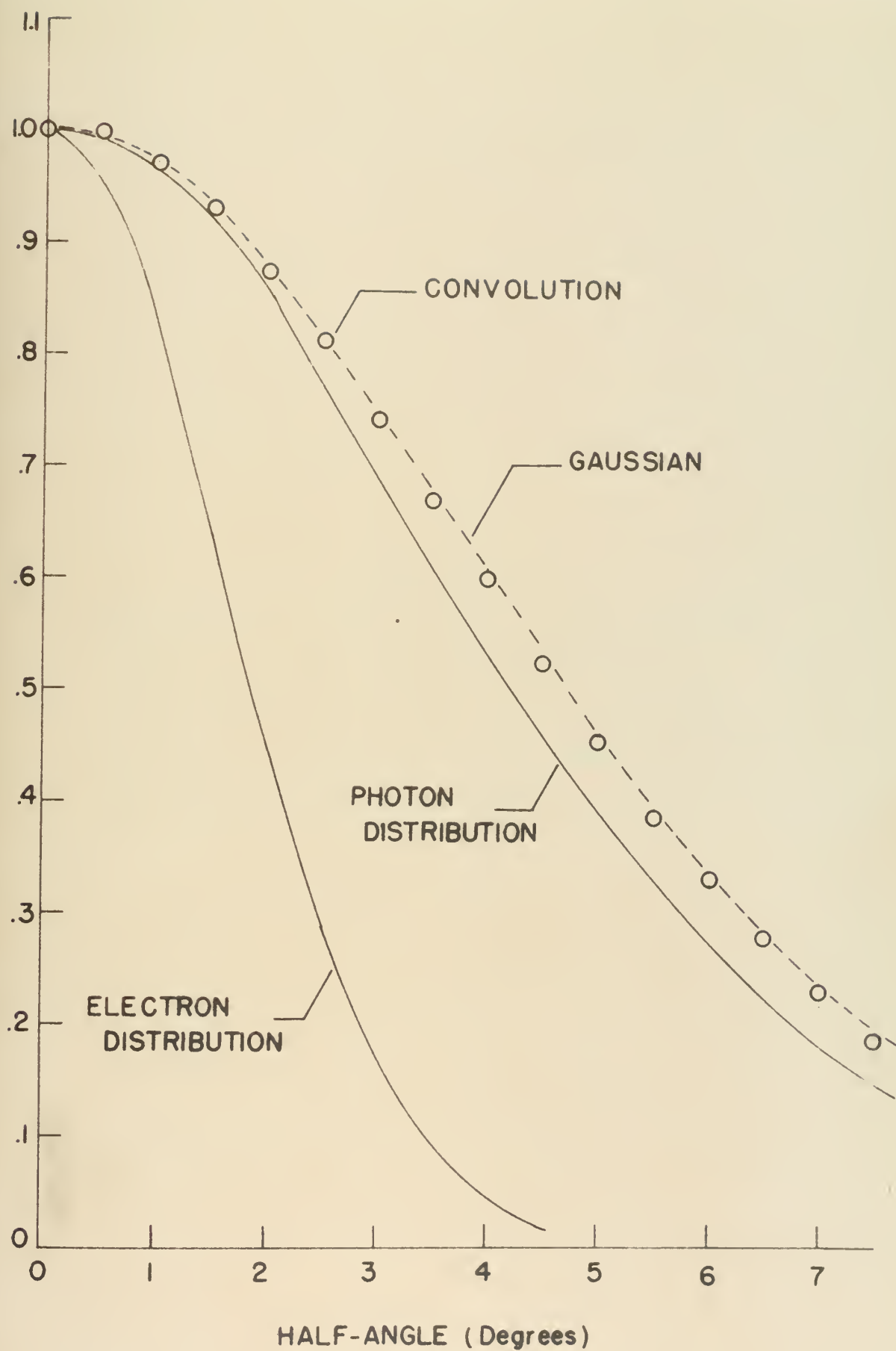


Figure (IV-8)

Electron distribution for an incident electron energy of 2.86 MeV, photon distribution for a photon energy of 1.533 MeV, the resultant convolution, and the Gaussian with which the convolution was fit, as a function of angle.





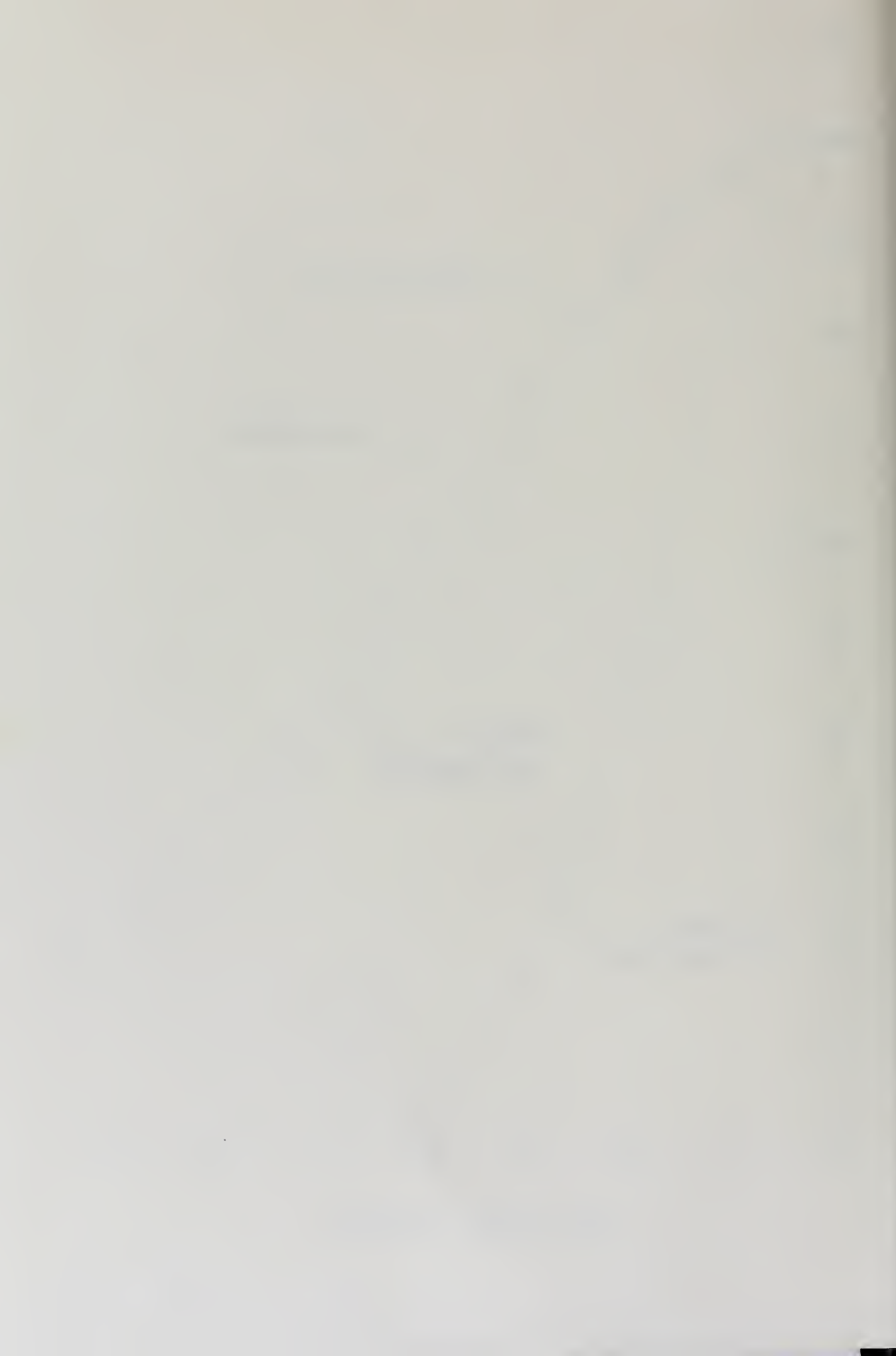


Figure (IV-9)

Electron distribution for an incident electron energy of 2.3 MeV, photon distribution for a photon energy of 1.2 MeV, the resultant convolution, and the Gaussian with which the data was fit, as a function of angle.



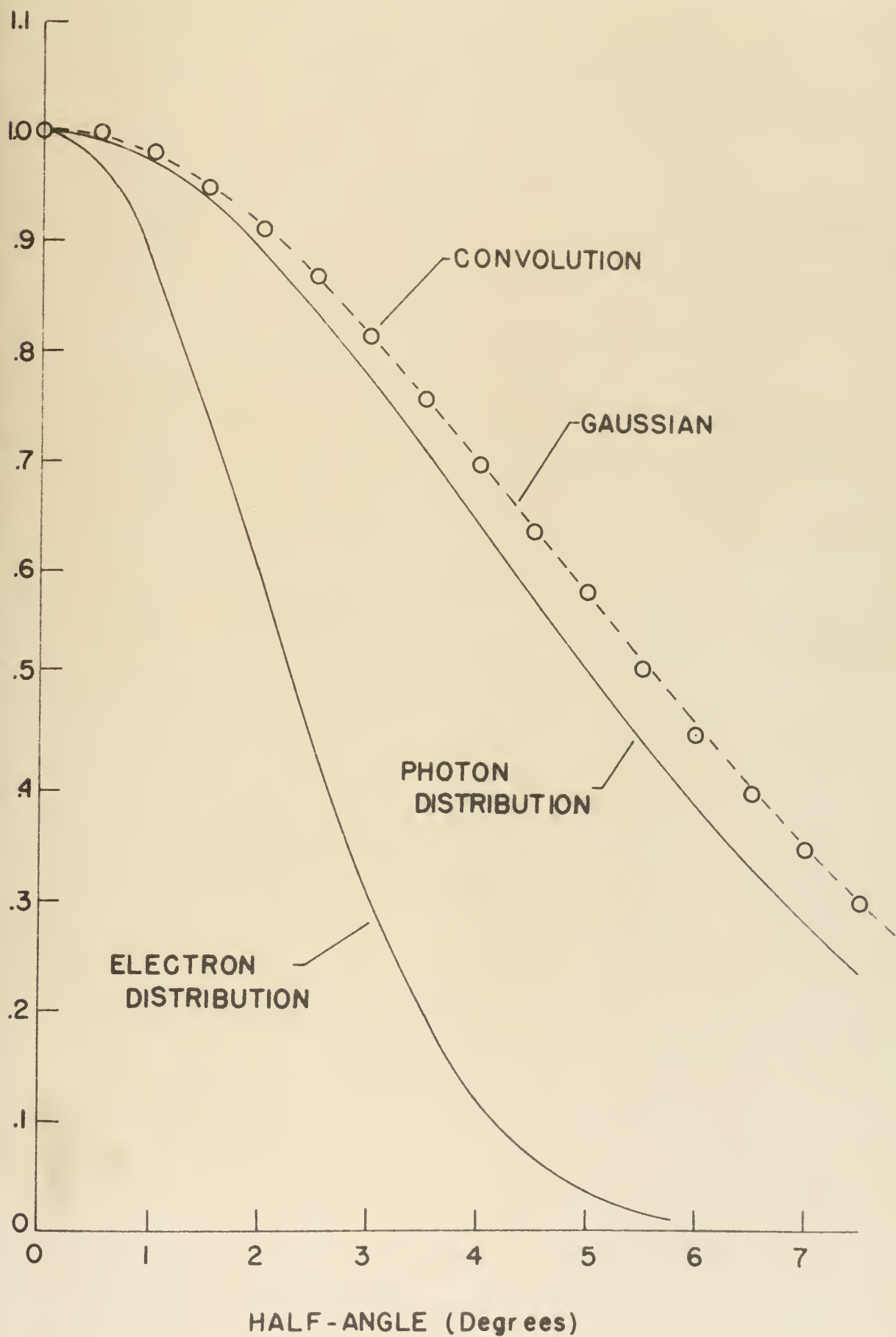


TABLE (IV-2)

Calculated half-widths at half-maximum for the distribution of multiply scattered electrons and for the Gaussian approximation to the final incident photon distribution

T_0 (MeV)	k (MeV)	Foil Thickness (mg/cm ²)	θ_e (Degrees)	q Theory (Degrees)	q Composite (Degrees)
2.30	1.20	1.41	2.28	5.60	6.85
2.86	1.533	1.41	1.85	5.02	6.15
2.86	1.57	1.41	1.85	4.94	6.05
2.86	1.71	1.41	1.85	4.85	5.93
2.86	1.85	1.41	1.85	4.80	5.86
2.86	2.00	1.41	1.85	4.70	5.75

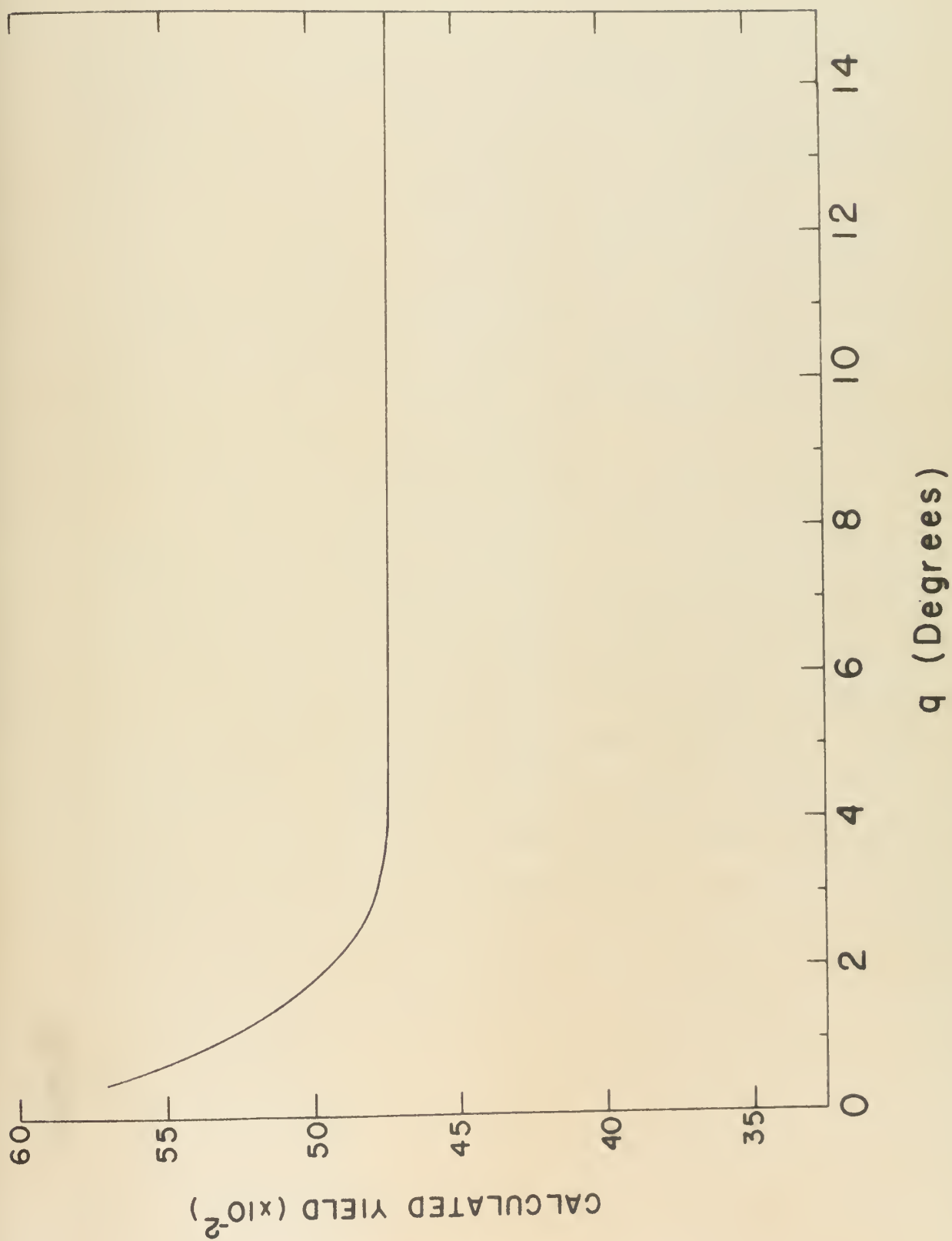
incident photon flux angular distribution can now be obtained by folding together, or convoluting, the electron and photon distributions. Convolutions based on the theoretical photon distribution are shown in Figures (IV-8) and (IV-9) also.

The convolutions were fit to a Gaussian normalized by C_0 so that the average value over the angular range subtended by the target (e.g., -6.5° to $+6.5^\circ$) was unity. The convolution for each photon energy was carried out using the calculated photon distribution since the measurements by Rester and Dance were conducted at rather large angular intervals. A composite angular distribution was constructed consisting of the theoretical distribution for half-angles less 3 degrees and the Rester and Dance result for larger half-angles. The composite convolution half-widths were approximately 20 percent wider than those obtained using the B-H result. Consideration of the effect of the q parameter on the calculated yield is, therefore, quite important.

The annihilation radiation yield has been calculated as a function of q using Equation (IV-1). By properly adjusting the C_0 parameter as q is increased, a yield curve such as that shown in Figure (IV-10) results. From this calculation, it can be determined that the variation in the yield is less than one-half percent

Figure (IV-10)

Calculated annihilation radiation yield as
a function of the half-width at half-maximum
of the Gaussian curve used to approximate the
incident photon distribution.



per degree in the region of the calculated half-widths, q (see Table (IV-2)). Thus, an error in the widths of the angular distribution of as much as a few degrees does not have a major effect on the calculated yield.

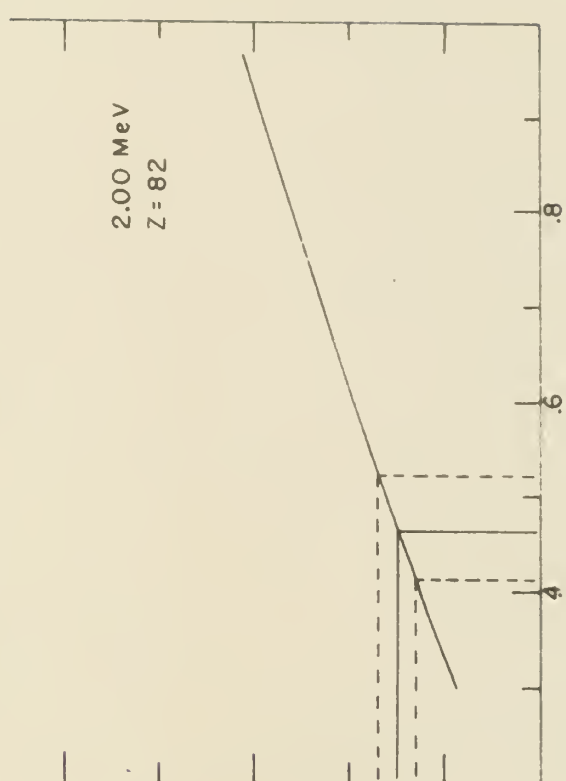
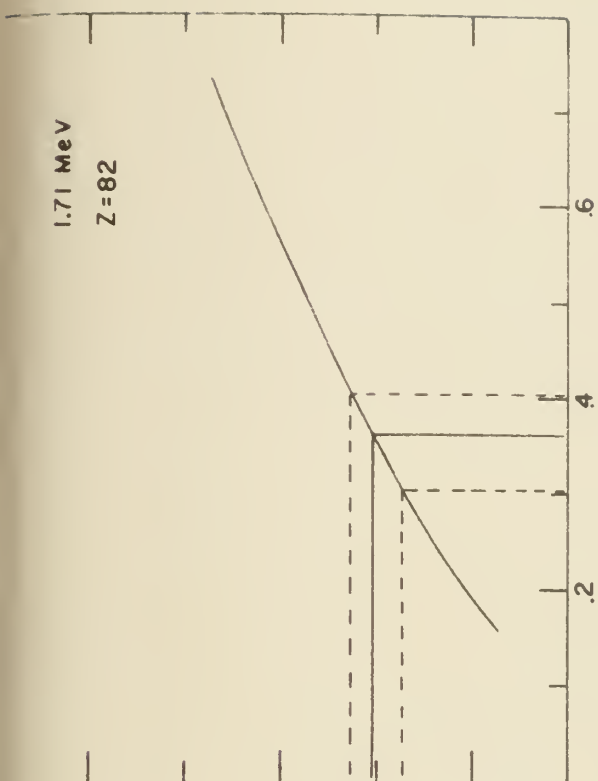
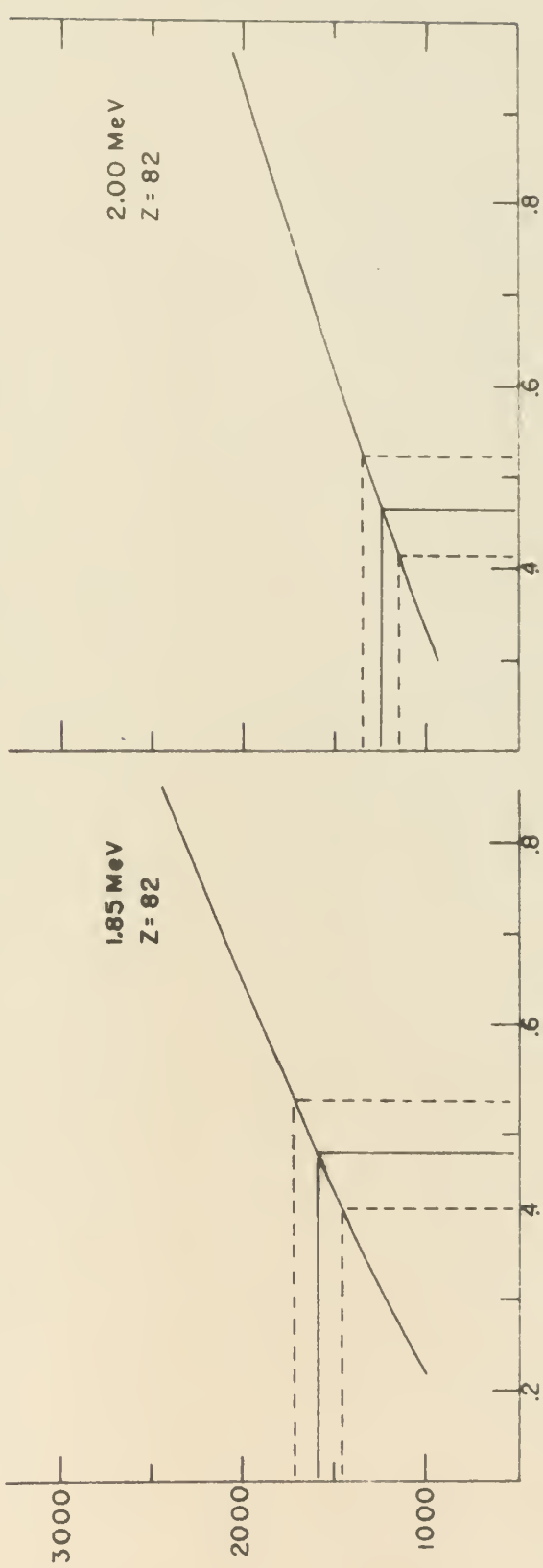
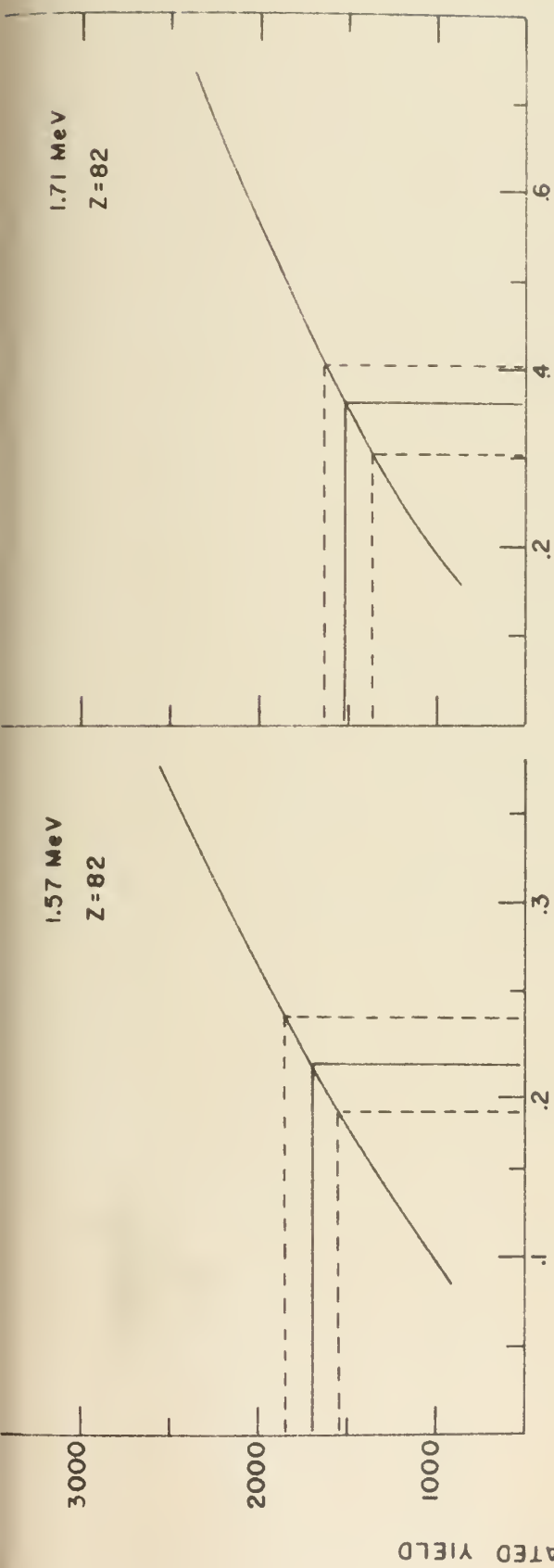
To determine the pair creation cross sections, the yield expression was evaluated as a function of the cross section and plotted versus σ_{PAIR} . The plot was then entered with the measured yield to obtain the measured pair creation cross sections.

The calculated and measured yields for the element lead are shown in Figures (IV-11) and (IV-12). The measured cross sections are tabulated in Table (IV-3) and plotted versus incident photon energy in Figure (IV-13).

Figures (IV-12) and (IV-14) show the calculated and measured yields for tin. The measured cross sections are presented in Table (IV-4) and plotted in Figure (IV-15). Parameters used in evaluation of the yield expression are presented in Table (IV-5).

Figure (IV-11)

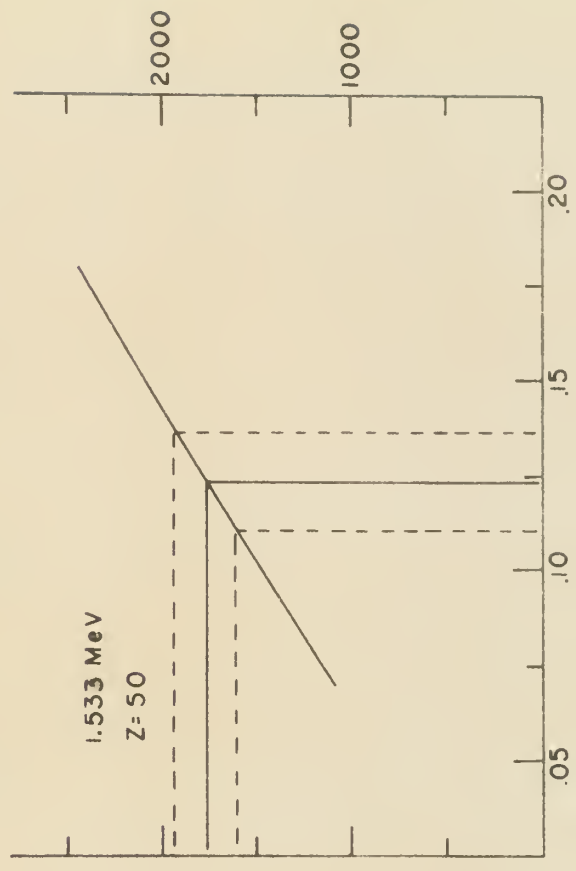
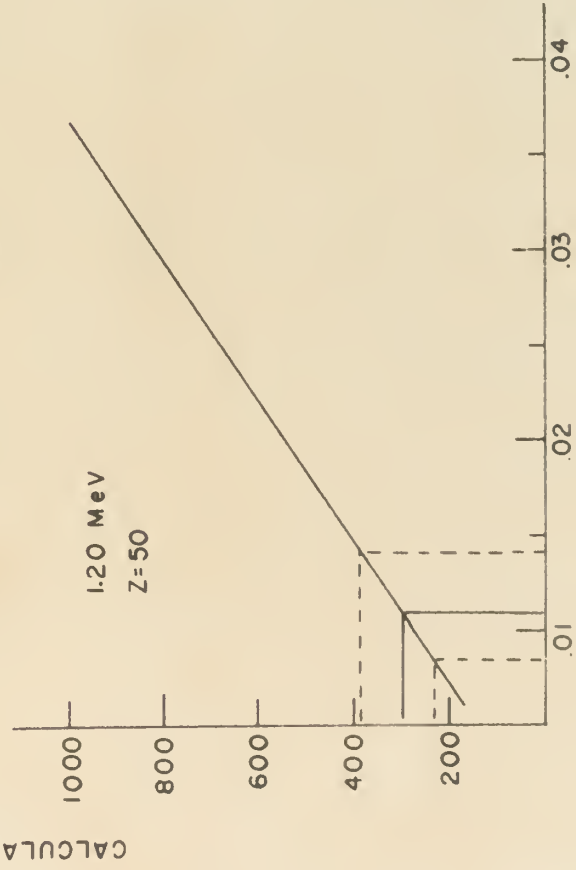
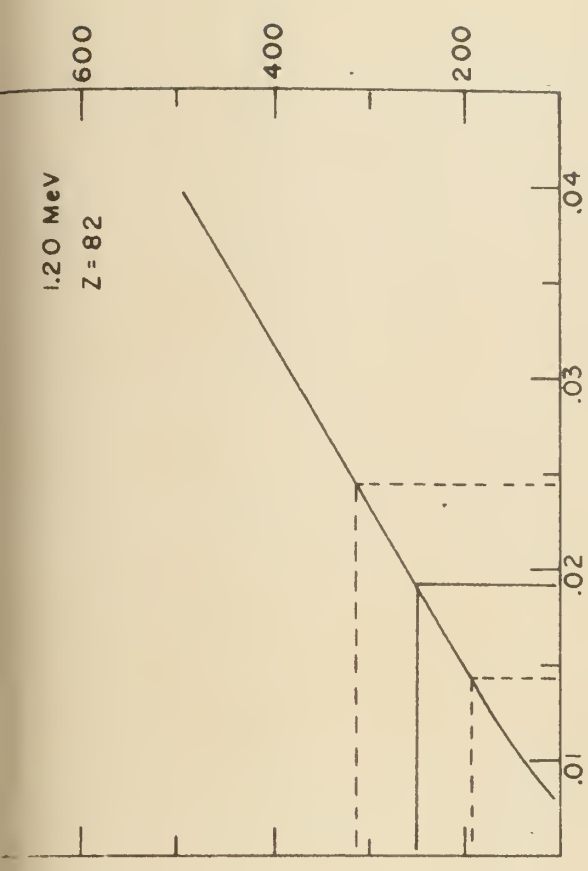
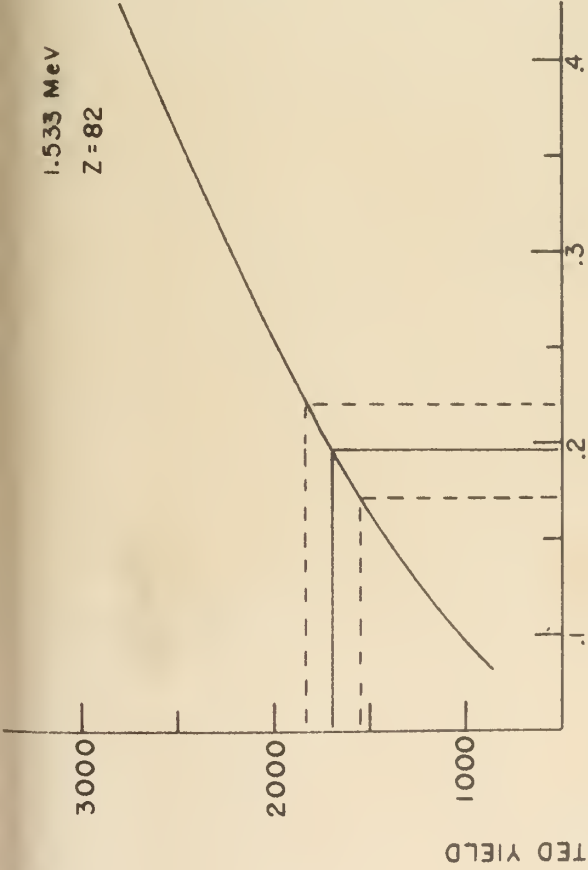
Calculated and measured pair creation yield as a function of pair creation cross section for incident photon energies 1.57, 1.71, 1.85, and 2.00 MeV for the element lead.



$\sigma_{\text{PAIR}}(\text{EXP})/\Phi$

Figure (IV-12)

Calculated and measured pair creation yields as a function of pair creation cross section for incident photon energies 1.533 and 1.20 MeV for the element lead and for 1.20 and 1.533 MeV for the element tin.



$\sigma_{\text{PAIR}}(\text{EXP})/\Phi$

Pair creation cross sections for the element lead.

k (MeV)	$\sigma_{\text{PAIR}}^{\text{(EXP)}}$ (barns)	$\sigma_{\text{PAIR}}^{\text{(EXP)}} / \sigma_{\text{PAIR}}^{\text{(JH)}}$	$\sigma_{\text{PAIR}}^{\text{(EXP)}} / \sigma_{\text{PAIR}}^{\text{(B-H)}}$
1.20	$.075 \begin{smallmatrix} + .020 \\ - .019 \end{smallmatrix}$		$2.567 \begin{smallmatrix} + .720 \\ - .678 \end{smallmatrix}$
1.533	$.764 \pm .094$	$1.14 \pm .14$	$2.242 \pm .274$
1.57	$.807 \begin{smallmatrix} + .101 \\ - .098 \end{smallmatrix}$		$2.054 \begin{smallmatrix} + .258 \\ - .248 \end{smallmatrix}$
1.71	$1.404 \begin{smallmatrix} + .164 \\ - .218 \end{smallmatrix}$		$2.244 \begin{smallmatrix} + .261 \\ - .349 \end{smallmatrix}$
1.85	$1.794 \begin{smallmatrix} + .214 \\ - .246 \end{smallmatrix}$		$2.037 \begin{smallmatrix} + .244 \\ - .279 \end{smallmatrix}$
2.00	$1.810 \begin{smallmatrix} + .226 \\ - .199 \end{smallmatrix}$		$1.531 \begin{smallmatrix} + .191 \\ - .168 \end{smallmatrix}$

Figure (IV-13)

The measured pair creation cross section as a function of incident photon energy (open circles) and the Bethe-Heitler prediction (solid line) for the element lead. The prediction of the JH result is shown as a small triangle.

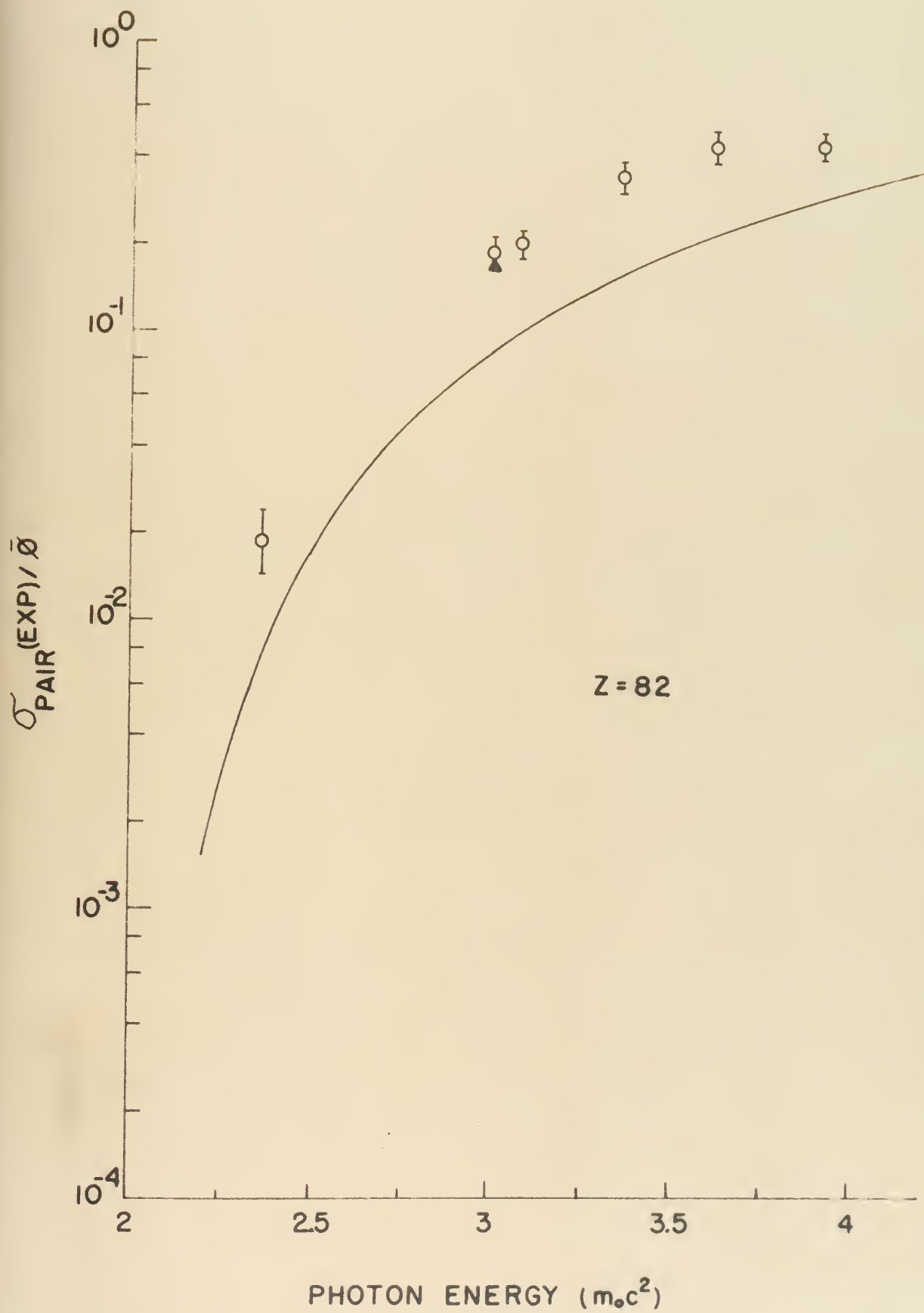
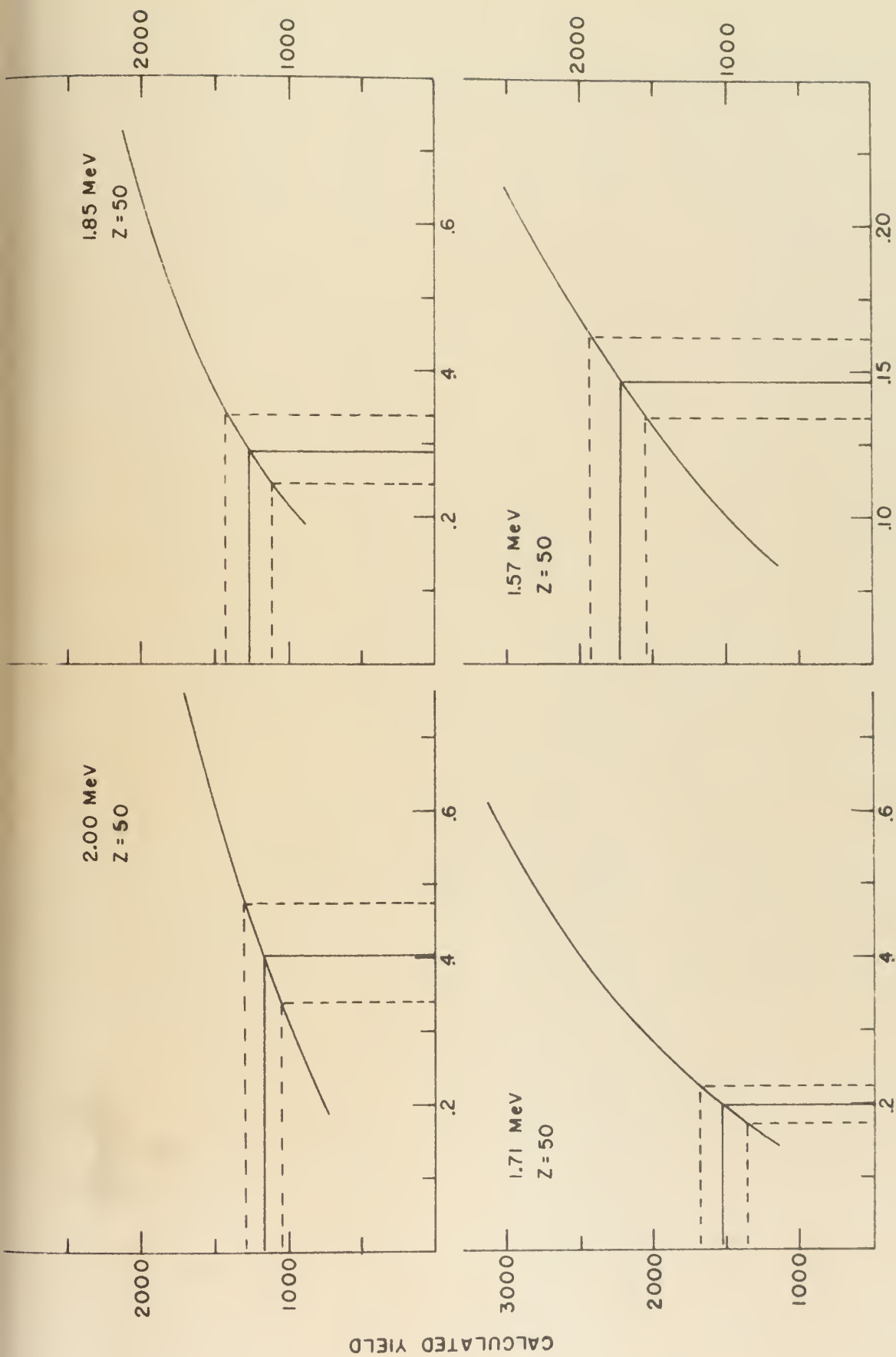


Figure (IV-14)

Calculated and measured pair creation yields as a function of pair creation cross section for incident photon energies 2.00, 1.85, 1.71, and 1.57 MeV for the element tin.



$\sigma_{\text{PAIR}}(\text{EXP})/\Phi$

TABLE (IV-4)

Pair creation cross sections for element tin.

k (MeV)	$\sigma_{\text{PAIR}}^{\text{(EXP)}}$ (barns)	$\sigma_{\text{PAIR}}^{\text{(EXP)}} / \sigma_{\text{PAIR}}^{\text{(JH)}}$	$\sigma_{\text{PAIR}}^{\text{(EXP)}} / \sigma_{\text{PAIR}}^{\text{(B-H)}}$
1.20	.016 \pm .005 - .004		1.522 \pm .433 - .346
1.533	.178 \pm .020 - .017	1.05 \pm .12 - .10	1.37 \pm .108 - .092
1.57	.213 \pm .022 - .019		1.458 \pm .149 - .129
1.71	.290 \pm .036		1.246 \pm .156
1.85	.421 \pm .072 - .067		1.284 \pm .221 - .203
2.00	.586 \pm .100 - .093		1.333 \pm .228 - .211

Figure (IV-15)

Measured pair creation cross sections as a function of incident photon energy (open circles) with the Bethe-Heitler predictions (solid line) for the element tin, $Z = 50$. The prediction of the JH result is shown as a small triangle.

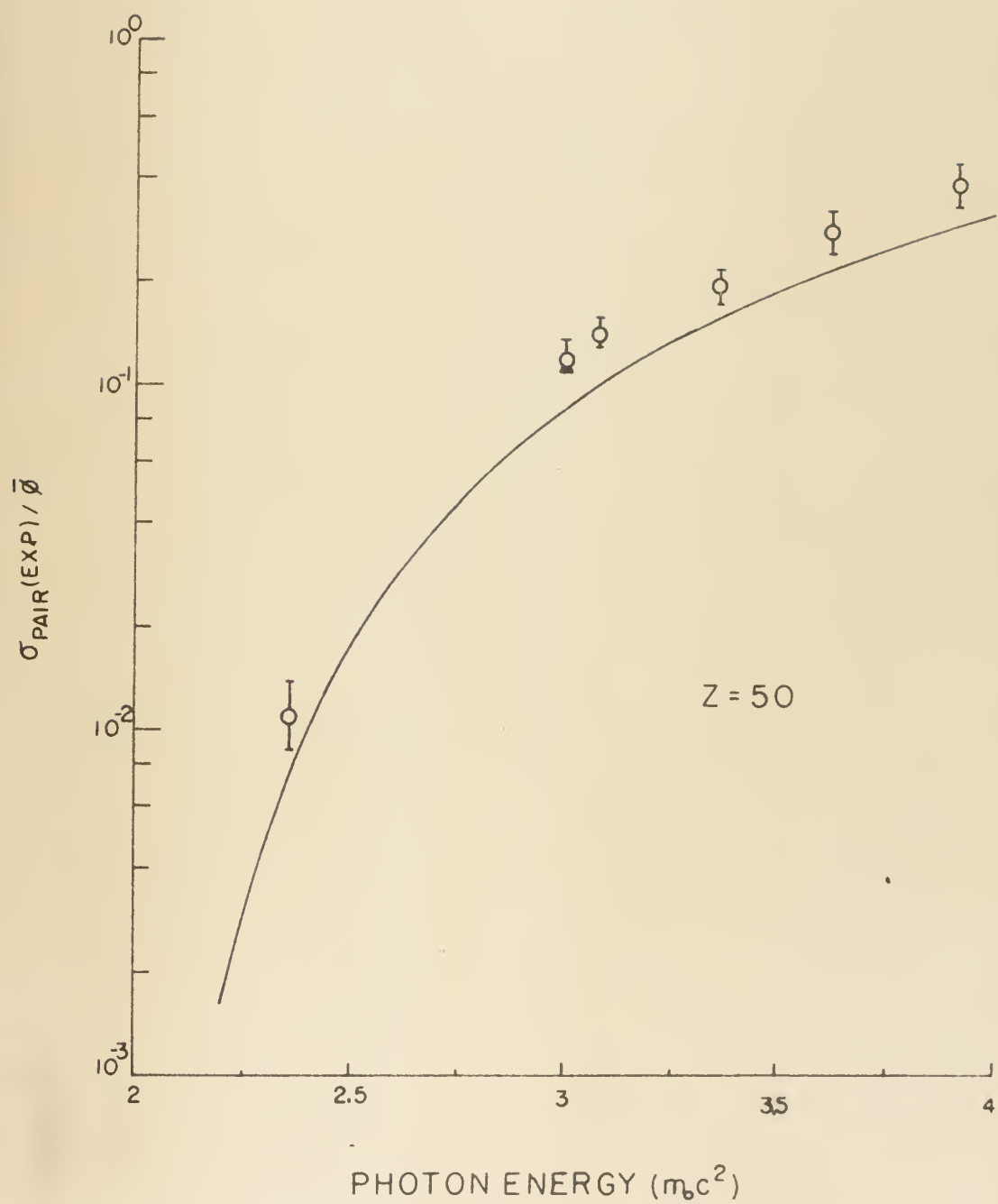


TABLE (IV-5)

Parameters used in evaluation of the yield expression.

k (Me V)	μ c (barns/atom) Z = 82 Z = 50		Δ k (Me V)	$\frac{1}{Z^2} \frac{d\sigma}{dk}$ (mb/Me V)
1.20	20.46	10.20	.024	.779
1.533	17.08	8.83	.031	.714
1.57	16.88	8.75	.030	.736
1.71	15.90	8.20	.026	.538
1.85	14.99	7.82	.023	.393
2.00	14.18	7.59	.020	.252

Z = 82

$$n = 2.03 \times 10^{22} \text{ nuclei/cm}^2$$

$$\mu = 51.2 \text{ barns/atom}$$

$$Q = 2.50 \times 10^{15} \text{ electrons}$$

$$I.J.K = 8.16.4$$

Z = 50

$$n = 2.27 \times 10^{22} \text{ nuclei/cm}^2$$

$$\mu = 17.57 \text{ barns/atom}$$

$$Q = 7.49 \times 10^{15} \text{ electrons}$$

$$I.J.K = 8.12.4$$

$$\Upsilon = 1.1547$$

$$\eta_0 = .332 \times 10^{-3}$$

$$m_i = m_j = 1.27 \text{ cm}$$

$$m_k = .159 \text{ cm}$$

$$T = .635 \text{ cm}$$

Figure (IV-16)

Comparison of present measurement to the predictions of Bethe and Heitler and Jaeger and Hulme, small triangles, for the element lead.

PHOTON ENERGY (MeV)

Z = 82

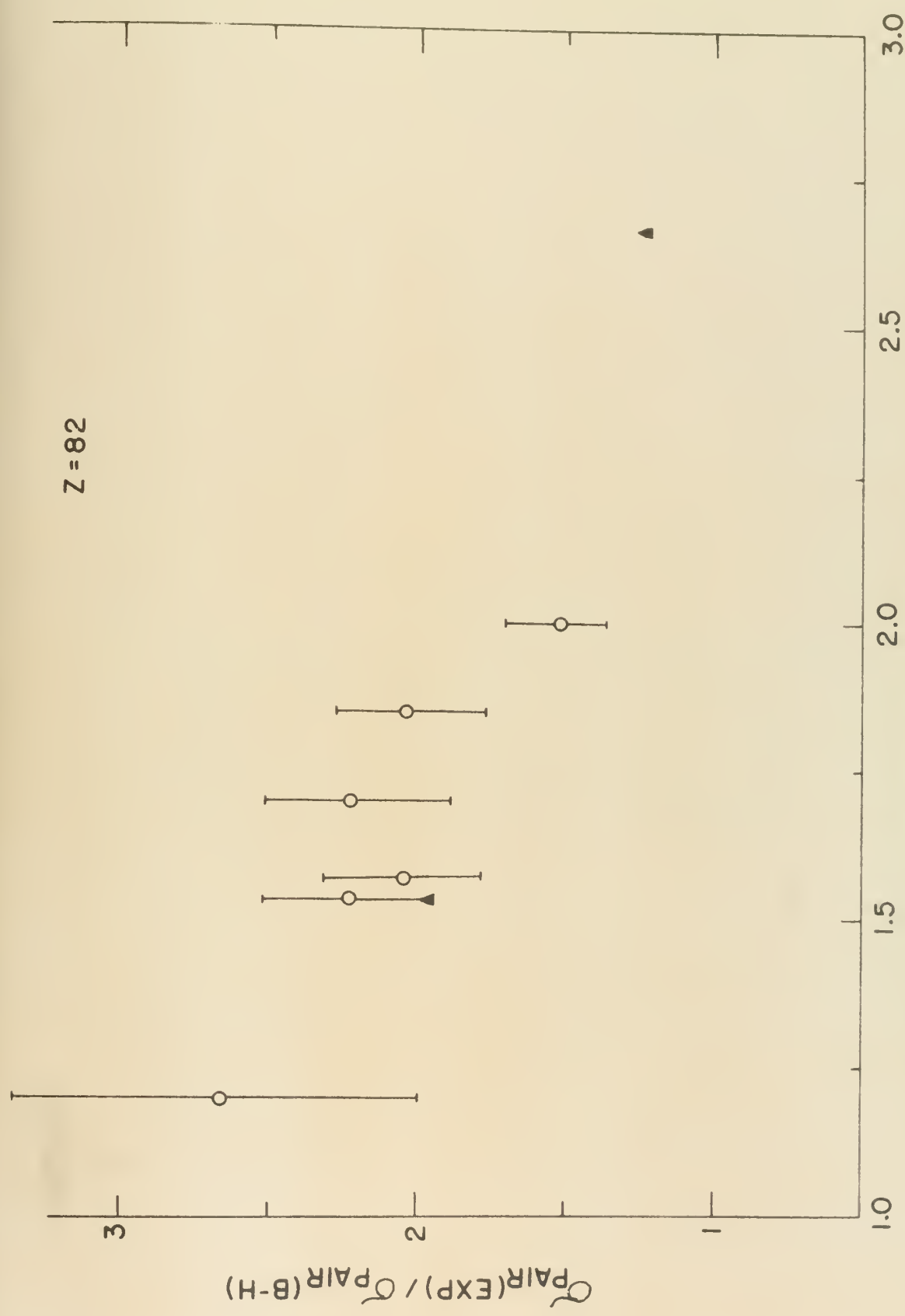


Figure (IV-17)

Comparison of the present measurement to the predictions of Bethe and Heitler and Jaeger and Hulme, small triangles, for tin. (The dotted triangle is an extrapolated value.)

Z = 50

$Q_{\text{PAIR}}(\text{EXP}) / Q_{\text{PAIR}}(\text{B-H})$

PHOTON ENERGY (MeV)

Δ





Results of some previous pair creation measurements

Author	Range of Z	Range of k (MeV)	Quoted Accuracy	Reported Agreement With JH Result
Huck ⁹¹	53	1.08 - 2.75		10% low
Jenkins ⁹²	82	1.12	± 11%	39% low
Rama Roa et al. ²⁵	29-82	1.12 - 2.00	± 5%	Pb: ~ 3% at 2.00 MeV > 100% low for k < 1.4 MeV
Shkolnik and Standil ²⁴	82	1.12	> 8%	13% low
Yamazaki and Hollander ²⁷	32	1.08 - 2.75	± 10% @ 1.08 MeV ± 5% @ 1.48 MeV	> 20% high @ 1.08 MeV 20% high @ 1.48 MeV
Dayton ²⁴	13-82	1.17 - 2.62	< ± 3% @ 2.75 MeV	Normalized @ 2.75 MeV
Hahn et al. ²³	13-82	1.17 - 2.66	< ± 3%	~10% low @ 1.17 + 1.33 MeV Agreement @ 2.62 MeV
Schmid and Huber	82	2.76	± 6%	23% low @ 1.17 + 1.33 MeV Normalized @ 2.66 MeV
Standil and Moore ²⁴	82	2.76	± 25%	13% low ~ 40% low

V. CONCLUSIONS AND SUMMARY

A. Monochromatic Technique and Bremsstrahlung Cross Sections

The monochromatic technique has been successfully developed in the course of the present research to the highest level yet attained in this laboratory. The technique has been shown to be efficacious in terms of performing certain meaningful physical experiments. In addition, possible methods of improving the technique have been discussed in Appendix E.

As adjunct experiments to the pair creation measurements, the bremsstrahlung cross section has been measured for photon energies of 1.53, 1.57, 1.71, 1.85, and 2.00 MeV at an incident electron energy of 2.86 MeV and for the photon energy 1.20 MeV at an incident electron energy of 2.30 MeV. These measurements have been compared to the theory of Bethe and Heitler and with previous experimental measurements, described in Section (I-C), over the energy range of interest. There is excellent agreement with theory and quite good agreement with the measurement of Starfelt and Koch. The Rester and Dance measurement agrees well with our measurement only in the case of the cross section differential in photon energy. The exact nature of agreement to be expected is unclear since the present measurement yields the cross section

integrated over an electron emission cone of half-angle 7.6 degrees while all previous measurements consider the cross section integrated over the entire electron emission solid angle. The importance of these measured cross sections for the pair creation experiment is clear.

B. Pair Creation

A table of pertinent previous measurements and their comparison with the JH result is presented in Table (IV-6) for easy reference. In order to use the exact calculations of Jaeger and Hulme, which, it should be recalled, gave cross sections, for tin, terbium, and lead, at 1.533 MeV and, for lead only, at 2.657 MeV, many of these experimenters have used graphical interpolation and extrapolation of the JH result to cover the area of their experiment. The resulting comparisons between theory and experiment have been neither uniform in their discrepancies nor have the measurements been consistent relative to one another.

The cross sections measured in this research can be compared directly to the JH result for the incident photon energy 1.533 MeV. For the lead measurement, the ratio of the measured cross section to the prediction of Jaeger and Hulme, $\sigma_{\text{PAIR}}(\text{EXP}) / \sigma_{\text{PAIR}}(\text{JH})$, is $1.14 \pm .14$. The tin measurement shows agreement with the JH result as indicated by the value $1.05 \pm_{-.10}^{+.12}$ for the ratio

just defined. The experimental cross sections for the photon energy 1.57 MeV have been compared with the JH result at 1.533 MeV providing ratios of $1.20 \pm .15$ for lead and $1.20^{+.12}_{-.11}$ for tin. While not strictly valid, these latter comparisons do demonstrate the increase in pair creation cross section with increasing photon energy. Since these measurements are the first absolute cross sections measured which correspond directly to the JH predictions, the agreement achieved seems quite satisfactory.

Comparison with the B-H pair result, a theory which is predicted to fail in the range of k and Z used for this research, has been made for completeness. The ratio, $\sigma_{\text{PAIR}}(\text{EXP}) / \sigma_{\text{PAIR}}(\text{B-H})$, a standard quantity in the reporting of previous pair creation measurements, is presented in Tables (IV-4) and (IV-5) as well as in Figures (IV-16) and (IV-17).

On the basis of the cross sections reported here, it can be concluded the exact calculations of Jaeger and Hulme for $k = 1.533$ MeV for lead and tin are in accord with the measured values. If one connects the results of the Jaeger and Hulme calculations in lead at $3m_0c^2$ and $5.2 m_0c^2$ with an assumed curve, or even a straight line, a "JH pair creation cross section curve" is generated. Comparing the present measurements for

lead to such a curve might be said to indicate that the measured cross sections are slightly higher than those of theory. Using the same procedure, with an extrapolated JH result at $5.2 m_0 c^2$, for tin might seem to indicate that the experimental cross sections slightly exceed theory over the complete energy range, 1.2 to 2.0 MeV. Rigorous conclusions concerning the behaviour of the measured values relative to the JH result over the entire energy range are not possible on the basis of this hypothetical curve. Such conclusions must await the extension of the exact calculations over an expanded range of energies and atomic numbers.

APPENDIX A

The Accelerator

Research conducted by the Electron Group Division of the Nuclear Structure Laboratory utilizes an electron beam from the Notre Dame 4.5 MeV electrostatic accelerator. This accelerator can be used in both the positive ion and electron accelerating modes. Introduction of a source interchanger⁹³ in 1963 allows interchange of the two modes to be made in as little as one-half hour. This machine is of horizontal construction and employs a single accelerator tube.

The electron beam is injected into the accelerator tube by an electron gun, the design of which was adapted from an early television gun,^{70,71} located in the high-voltage terminal of the accelerator. Electromagnetic steering and focusing coils, placed on the gun, provide precise steering and focusing control of the beam out of the terminal. For the present research, the gun operated at -15 kV relative to the terminal with 5.1 amperes of filament current. The latter figure is a compromise between high output current and long filament life. Maximum beam output is approximately 100 microamperes while the filament lifetime is estimated at one to two years with this arrangement.

Stabilization of the terminal potential is

provided by two essentially independent systems both of which provide compensation for high- and low- frequency fluctuations of the terminal potential. In the first system, fluctuations of the terminal potential are sensed by a generating voltmeter, placed in the field of the high-voltage terminal, which produces a signal proportional to the terminal voltage. This signal was amplified, rectified and balanced by a d.c. voltage in the voltage stabilization circuit (hereafter referred to as the VS circuit). Any deviation from the d.c. level produces error signals which are then used to control the high- and low- frequency correction circuits.

High- frequency fluctuations of the terminal potential are corrected by control of the voltage on a cylindrical metal liner which surrounds the terminal and approximately one-third of the support column assembly. This capacitive liner is able to rapidly change the voltage on the terminal simply by a correctly phased variation of the liner potential.

Low- frequency voltage fluctuations are corrected by adjustment of the amount of charge sprayed on the charging belt at the ground end of the accelerator. The correction signal from the VS circuit controls the potential difference between a set of charging needles and an inductor bar by varying the inductor bar potential.

This in turn controls the amount of charge sprayed onto the belt. These corrections take place with the VS circuit in the GV CONTROL mode.

This method of stabilization provides an energy stabilization of approximately ± 2 keV at 2 MeV. However, thermal expansion of the pressure vessel and the terminal support structure makes an accurate and repeatable energy calibration quite difficult. For this reason, a second system is used.

In this second system, the electron beam is momentum analyzed in the field of a 60 degree sector-field magnet designed by C. P. Browne.⁹⁴ Before entering and after exiting the field of this magnet, the electron beam passes through slits which constrain the electron trajectories to a fixed geometry. The signals from the electrically insulated LEFT and RIGHT exit slits are compared in the VS circuit (now in the SLIT CONTROL mode) and the resulting error signal is used to control the liner potential and inductor bar potential for high- and low- frequency corrections, respectively. Any drift in terminal potential with the magnetic analyzing field held constant allows the beam to move onto one or another of the energy control slits. The resulting signal imbalance in the VS circuit then produces control signals to the liner and inductor bar supplies, raising or

lowering the terminal potential as appropriate, thereby recentering the beam and zeroing the error signal.

Energy resolutions of ± 0.1 percent at 2 MeV have been attained and have been readily reproduced with this system.

APPENDIX B

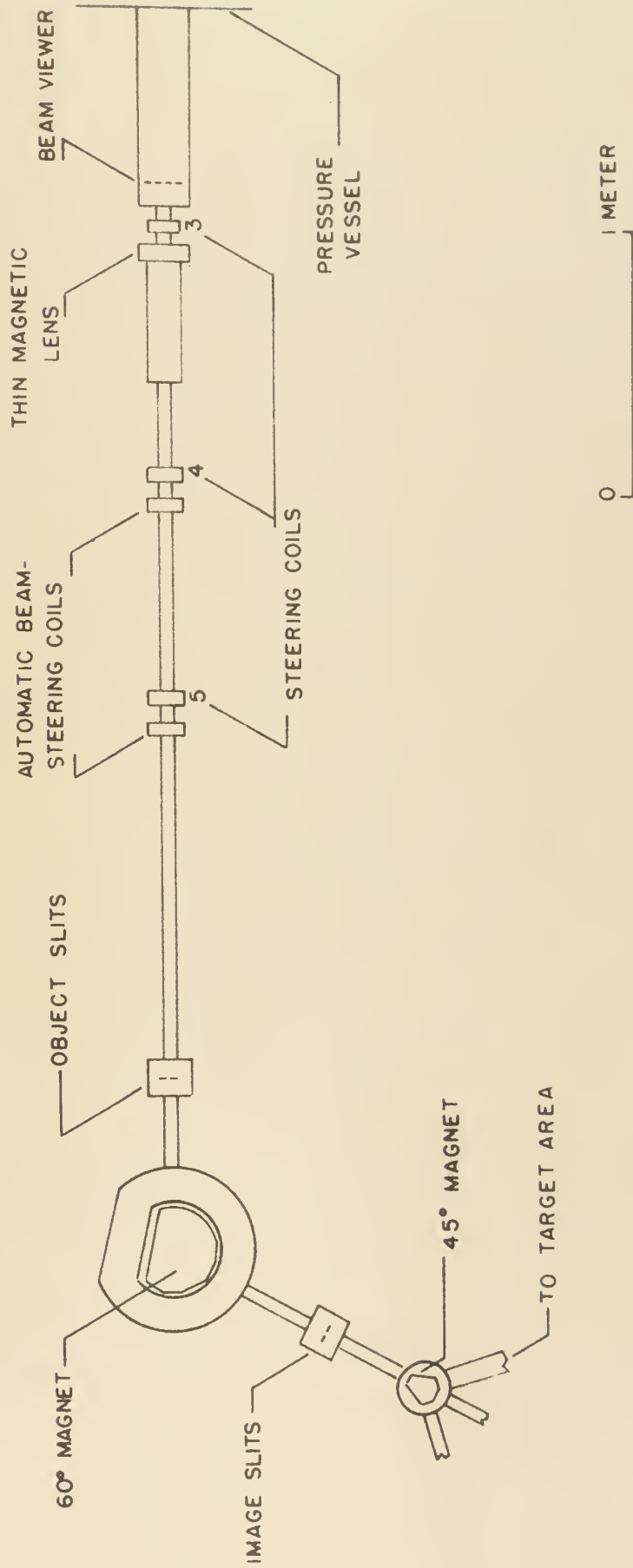
The Beam Handling System

Figure (B-1) depicts the beam handling system and the approximate location of the various devices used to steer and focus the beam. Preceding theses have discussed the beam handling system but pertinent features will be reiterated here.

The electron beam from the accelerator is focused onto a phosphor screen at a position approximately 26 inches outside the accelerator pressure vessel. This beam viewing screen is marked with two concentric circles of radii one-eighth inch and one-fourth inch, with LEFT/RIGHT and UP/DOWN reference axes. The center of the screen is aligned with the center of the beam pipe by use of a transit set on the beam line and at the proper beam altitude. The steering coils and focus coils on the gun are then used to optimize the position and size of the beam as viewed on the screen. (The screen is monitored by closed circuit television in order to avoid hazardous radiation.)

A set of steering coils (Steering 2) is located inside the pressure vessel but, in general, is only used to deflect the beam briefly for monitoring purposes. The optimumly positioned and focused beam is then directed onto the object slits of the 60 degree analyzing magnet

Figure (B-1)
The beam handling system.



by sets of steering coils (Steering 3,4, and 5) and a focus coil located immediately downstream of Steering 3. The object slits are made of .040 inch thick tantalum with each slit electrically insulated from one another. Each slit, attached by a shaft to a micrometer head, moves in a track with a range of three-quarters of an inch.⁹⁵ Slit position is repeatable to within $\pm .0005$ inches. Introduction of the movable slits obviates the necessity to remove the electron slits whenever the accelerator is operated in the positive ion mode. The slits are arranged to duplicate the fixed slits, which were previously used, in geometry and aperture size, forming a rectangle .040 inches by .050 inches. The focus coil, positioned about 36 inches outside the pressure vessel, is used to focus the beam on the object slits. In order to ensure that the beam is maintained centered at the object slits of the analyzing magnet, the electrical signals from these slits are fed into difference amplifiers. The outputs from these amplifiers are used to control the current through yet another set of steering coils (AUTO-PILOT Steering). This negative feedback system acts to keep the beam centered LEFT/RIGHT and UP/DOWN with respect to the object slits. For use with the monochromator the low-frequency cut-off of the AUTO-PILOT circuit was set below 60 Hz in order to

correct an effective 60 Hz pulsing of the beam and so provide a more uniform instantaneous current into the target foil assembly. Use of the AUTO-PILOT circuit guarantees beam centering on the object slits 100 percent of the time and allows 60 to 80 percent of the beam from the terminal to be directed onto the target foil.

The image slits of the 60 degree analyzing magnet, as well as providing energy stabilization, serve as object slits for a 45 degree bending magnet. This magnet is designed to focus the beam onto the thin foil bremsstrahlung target. Beam spot photographs taken at the foil position show the beam diameter to be less than one millimeter. As previously noted, the 45 degree deflection magnet also serves to reduce photon background and to eliminate slit scattered electrons from the beam incident on the foil. These functions have also been described in some detail by Malaker.³⁹

A set of steering coils (Steering 6) is located between the 45 degree magnet and the target foil. The purpose of this coil is to allow precise and repeatable steering of the beam onto the center of the foil. The procedure for centering has been related in the text. The beam spot photographs mentioned previously verify repeatability of centering to within half of the beam diameter (.5 millimeter).

APPENDIX C

Energy Calibration

An accurate determination of the energy of the monochromatic photons requires an accurate knowledge of both the incident electron and post-bremsstrahlung electron energies. The momentum of the incident beam is analyzed in a 60 degree deflecting magnet while the momentum of the degraded post-bremsstrahlung electrons is analyzed in a 120 degree bending magnet in the monochromator.

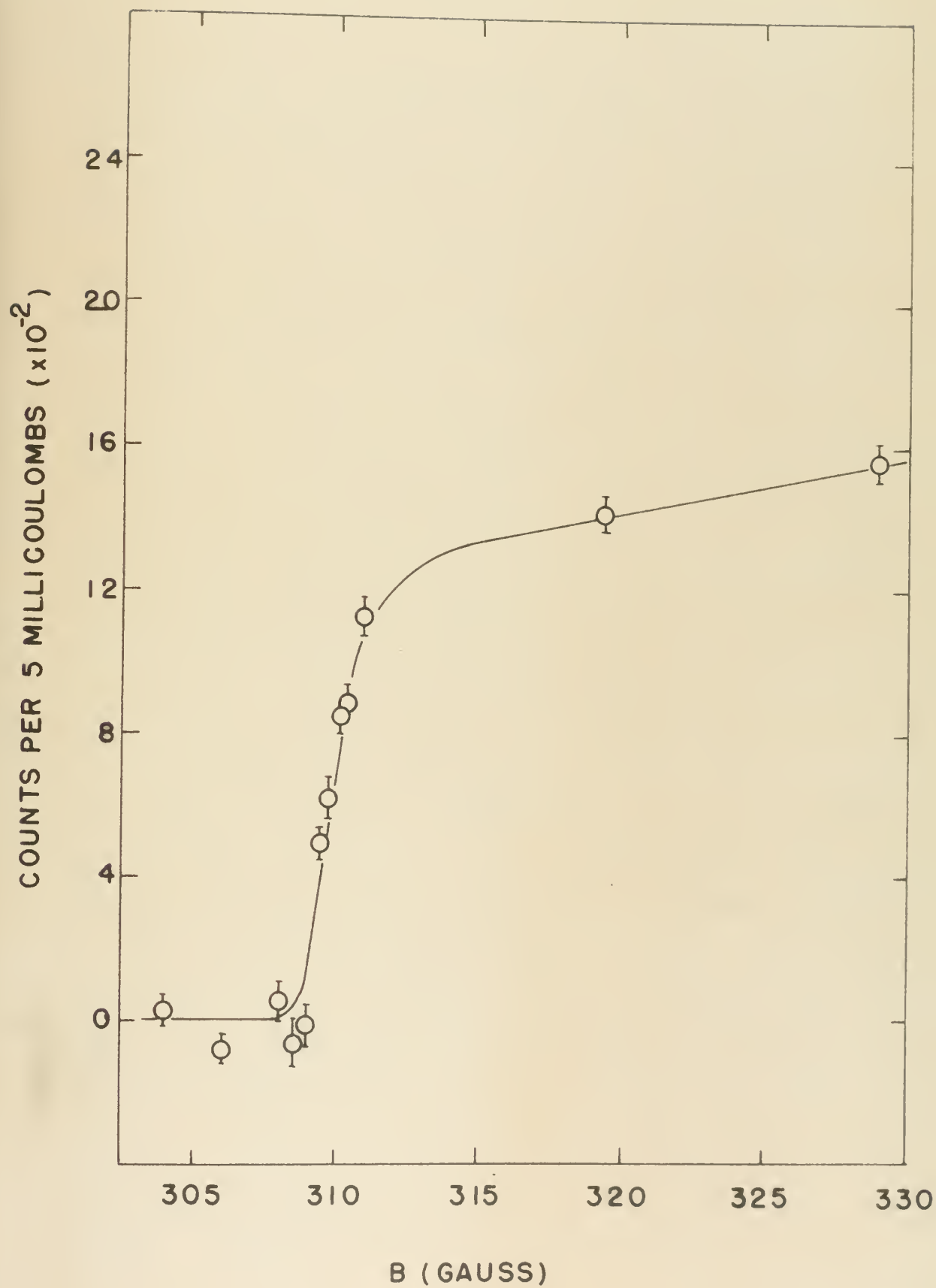
1. The 60 Degree Analyzing Magnet

The momentum of the incident beam is proportional to $B\rho$, the magnetic rigidity, and the energy of the electrons can be related as a function of this quantity. Since the ρ , radius of curvature, of the electron beam passing through this magnet is constant for fixed slit geometry, a measurement of the energy of the high-frequency limit bremsstrahlung photons using a sensitive high resolution detector will yield the energy of the electrons as a function of the field in the analyzing magnet.

A suitable high resolution detector for these photons is resonance scattering from well-known nuclear energy levels. For the present calibration the first excited state in ^{11}B and the seventh excited state in

Figure (C-1)

Isochromat for the first excited state of ^{11}B plotted versus magnetic field, B , in the analyzing magnet.



^{27}Al were used. Both levels have widths of order 100 MeV and have been measured in this laboratory to have energies of $2.125 \pm .004$ MeV and $2.985 \pm .003$ MeV, respectively.⁹⁶ These measurements have been confirmed to less accuracy in other laboratories.^{97,98,99} The measurements were made by the isochromat technique described in detail in the thesis of P. G. Loscoe.⁹⁰ In brief, the energy of the beam is set below the energy of the level being measured and is then raised in small energy steps until the incident electron energy is 50 to 100 keV above the energy of the level. The result is a yield curve which contains a step which goes from background to maximum yield in about 3 keV (the approximate energy loss for a 2 MeV electron in a thin gold foil). The energy of the level (or the corresponding value of the magnetic field) is then taken as the value corresponding to the lower "knee" of the curve. (See Figure (C-1).) The resulting isochromats were fit with the curve used by Schaller et al. in the original measurement in order to reduce subjective interpretation of the position of the isochromat "knee". These curves are plotted versus the measured field, B, in the analyzing magnet as shown in Figures (C-1) and (C-2). The B_p values for the known level energies were then used to determine the radius of curvature of the magnet. The results are presented in Table (C-1). The

Figure (C-2)

Isochromat for the seventh excited state in ^{27}Al plotted versus magnetic field, B, in the analyzing magnet.

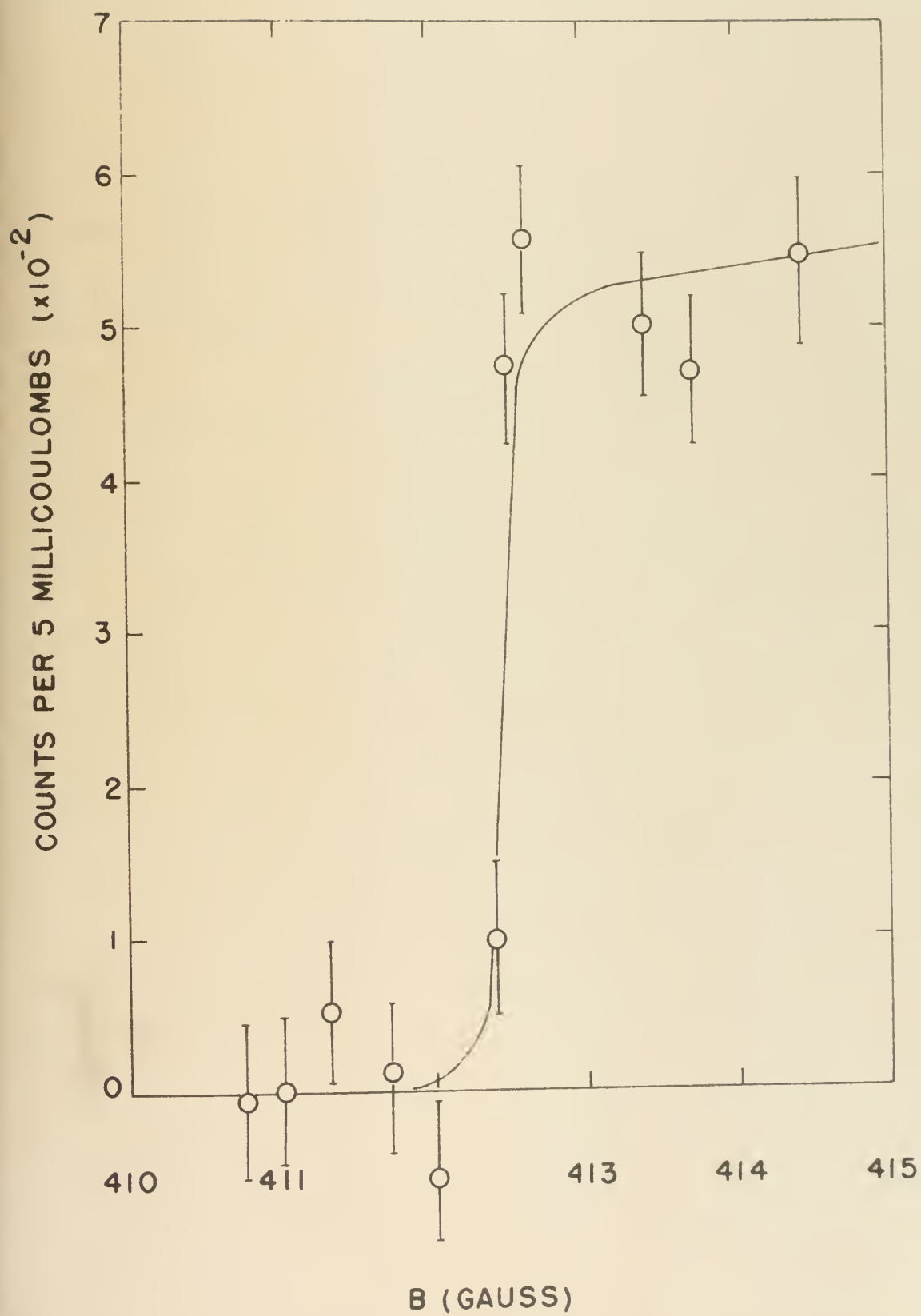


TABLE (C-1)

Results of calibration of the analyzing magnet.

Nucleus and Level Energy (MeV)		B (gauss-cm.)	B _{MEAS.} (gauss)	ρ (cm.)	ERROR (cm.)
¹¹ B	2.125	8625.9	308.2	27.98	± .05
²⁷ Al	2.985	11536.1	412.2	27.99	± .03

value of ρ was determined to be $27.98 \pm .05$ centimeters by these measurements.

The field in the momentum analyzing magnet was determined by measurement with a Rawson-Lush (Type 8245) rotating coil gaussmeter. This device is mounted through the zero degree port of the magnet. The accuracy of the gaussmeter was checked by comparison with a nuclear magnetic resonance probe which was in place in the magnetic field. The results of this comparison are presented in Table (C-2). The average difference between the NMR probe and gaussmeter measurements was 0.1 percent.

Changes in the calibration of this system took place if the magnet was not operated in a uniform manner. If the magnetic field was cycled between saturation (or near saturation) and residual field levels before each period of data collection plus making all field changes in an increasing manner, then no detectable changes in the calibration were found.

2. The Monochromator Magnet

The momentum of the degraded post-bremsstrahlung electrons was analyzed by a 120 deflection in the inclined plane pole face magnet located in the monochromator vacuum box. To calibrate this magnet, two different methods were used.

First, the K-conversion electrons from the

TABLE (C-2)

Comparison between measured magnetic fields by NMR and the Rawson
gaussmeter.

NMR PROBE

RAWSON-LUSH GAUSSMETER

Kilogauss

Kilogauss

3.2265

3.2227

5.1258

5.1247

7.0431

7.0361

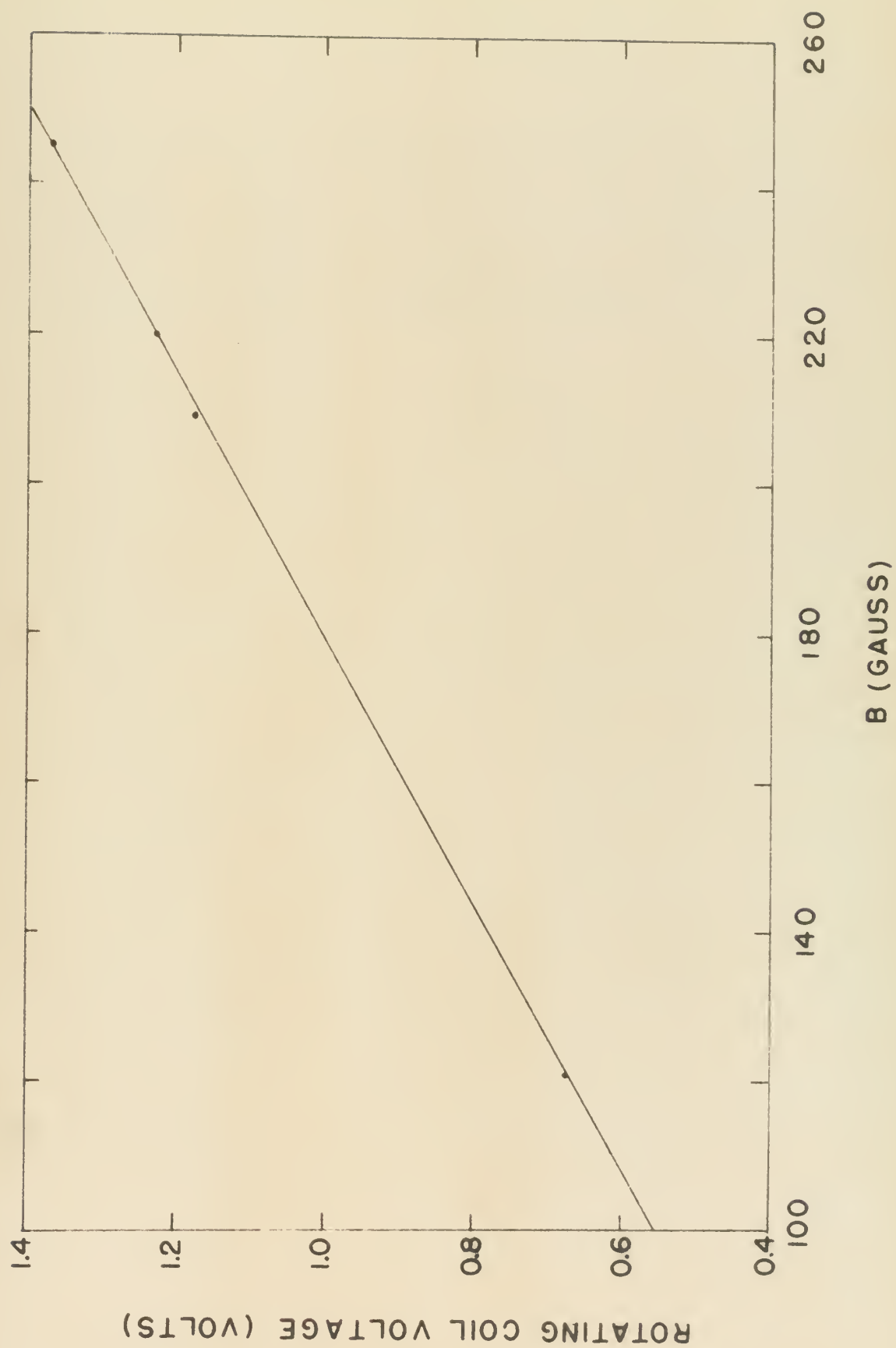
radioactive sources ^{137}Cs and ^{207}Bi , with energies 625 and 970 keV, respectively, were used to obtain rotating coil output voltages proportional to the field in the magnet. These rotating coil voltages were then plotted versus the value of magnetic field which would be necessary to bend these electrons through the radius of curvature, ρ , of the 60 degree analyzing magnet (this step was necessary in order to use these data in conjunction with the second method).

Additionally, the method developed by Malaker was used. In this procedure, the foil was removed from the foil holder. The beam was then centered using the technique described in Section (IV-B). The magnetic field in the monochromator was then varied until the beam passed through the exit slit and was collected in a Faraday cup, which replaced the electron detector. The rotating coil output voltage was recorded as well as the B field in the analyzing magnet. The incident beam energy was then changed and the process was repeated. In this manner a calibration curve, rotating coil output voltage versus field in the analyzing magnet, and therefore versus magnetic rigidity was determined. The data were fit by the method of least squares to a straight line and the results are presented in Figure (C-3).

The rotating coil consisted of a hand wound coil

Figure (C-3)

Monochromator rotating coil output
voltage plotted versus the magnetic
field, B , in the analyzing magnet.



of wire mounted on a brass shaft and driven by a 60Hz synchronous, 220 volt, 3-phase motor. The coil output voltage was measured by a Kintel Digital Voltmeter (Model 456) and was precise to within 0.5 percent.

APPENDIX D

Analog Ray Tracing Device

Referring to Figure (D-1), the analog ray tracing device, or the "Bug," is a three wheeled device with a ball-point pen centered on the rear axle at point A and has a steerable front wheel which rotates about a vertical axis through point B; with the front wheel turned at an angle α , movement of the device causes the ball-point pen to trace a curve of radius ρ , as indicated, while the front wheel moves through a curve of radius ρ' . The angle α is related to the parameters of the "Bug" through

$$\tan \alpha = \frac{L}{\rho'} .$$

However, for either small angles α or large values of ρ and ρ' , the approximation $\rho \approx \rho'$ can be made and

$$\tan \alpha = \frac{L}{\rho} .$$

From the equation

$$\frac{mv^2}{\rho} = Bev$$

we find

$$\rho = p/Be$$

where $p = mv$

and so $\tan \alpha$ can be rewritten as

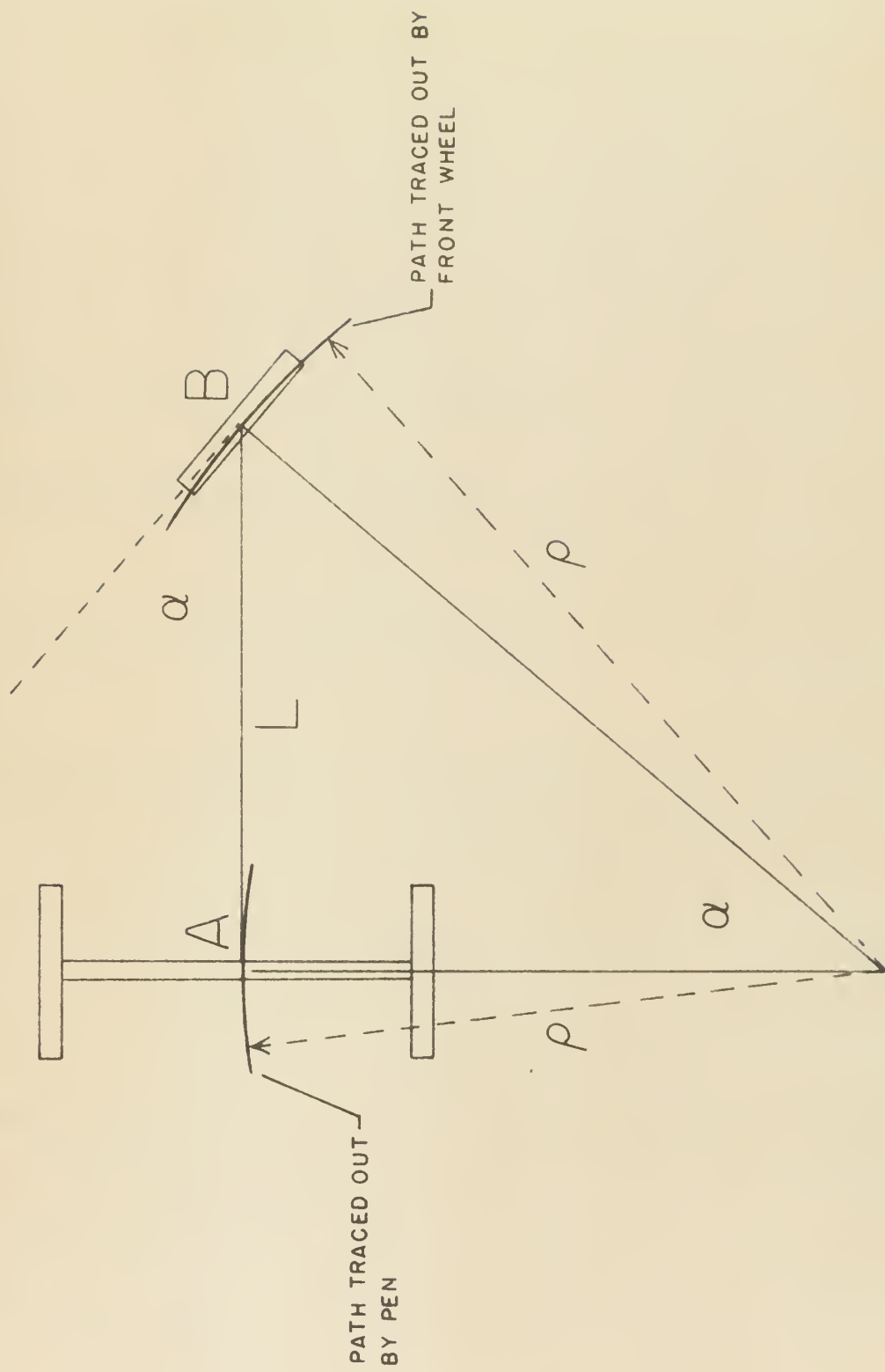
$$\tan \alpha = LBe/p$$

but for the magnet of interest here

Figure (D-1)

Schematic of the analog ray-tracing device.





$$B = \frac{B_1}{r} ; B_1 = B(r=1)$$

and so

$$\tan \alpha = \frac{LB_1e}{rp}$$

and since previous sections show that

$$K = \frac{p}{B_1e} ,$$

the expression can be written as

$$\tan \alpha = \frac{L}{Kr} ;$$

or writing $L/K = K'$, the result is

$$\tan \alpha = \frac{K'}{r}$$

and the desired trajectory can be drawn (to the proper scale set by the adjustable length L) simply by calculating the appropriate value of α . For the $1/r$ field of the monochromator, an instantaneous value of α exists at every point in the trajectory and so only an approximate curve can be drawn. The ray-tracing is completed by tabulating the values of α corresponding to penetrations r into the magnetic field. The steerable wheel is set for this angle and "driven" across the paper to the next r -value, $r + \Delta r$, where the new alpha value is set for the wheel. The procedure is repeated until the edge of the field is reached. The wheel is then set for straight travel and the trajectory completed. The angle, α , is only accurate to .5 degrees but for a large scale drawing introduces no major error. In the case of $1/r$ fields this

procedure requires many settings of the angle, α ,
(radius of curvature) and is a tedious process.

APPENDIX E

Evaluation of the Monochromatic Technique

The successful use of the monochromator in measurements of pair creation cross sections raises questions as to the efficacy of the technique for other physical measurements. As well, the inability of the present device to provide the high transmission values which were sought prompts further consideration of ways to improve the monochromator.

1. Nuclear Resonance Fluorescence

The monochromatic technique provides a high intensity flux of monoenergetic gamma-rays which can be resonantly scattered from low-lying energy levels in various nuclei. The increased transmission of the Notre Dame monochromator coupled with the measured figure of merit near unity prompted re-examination of NRF experiments. The 2.125 MeV level in ^{11}B was used in a series of experiments in order to test the usefulness of the present system in nuclear level studies. Twenty-three runs were conducted using the target nucleus. Two of these runs were successful in providing a yield with a statistical uncertainty of less than twenty-five percent. These runs were evaluated in the usual manner⁹⁰ and resulted in a measured width equal to, within the uncertainty mentioned, the value previously measured in this

laboratory. Since the energy and width of the test nucleus were both well-known, it was apparent that the present system produces a monochromatic gamma-ray flux which was both too low in intensity and not finely enough resolved in energy to conduct such measurements on narrow levels of unknown energies. (It should be pointed out that the twenty-one runs which did not produce the expected yield were determined to have failed primarily due to timing and/or energy stability difficulties.) Comparison with data taken on this level using the high frequency limit of the bremsstrahlung spectrum revealed that the photon flux of monoergic gamma-rays was approximately one-third as efficient as the tip method. Achievement of a transmission of 1 to 2 percent, while maintaining the figure of merit at unity, would allow the monochromatic technique to be as much as six times more effective than the high frequency tip method.

2. (γ ,n) Reactions

Another possible use of the monoergic photon flux is in the study of the (γ ,n) cross section in various nuclei. The details of such a study have been presented by Walter and Shea.³⁶ Briefly, the use of a monochromatic photon flux would allow determination of the detailed shape of the photodisintegration cross section near the threshold energy without unfolding the yield

from an integral photo-neutron yield curve and without the necessity of making any assumptions concerning the spectral and angular distributions of the incident bremsstrahlung radiation. A monochromator designed for use with the new Notre Dame Tandem Van de Graaff accelerator would be especially useful for the wide range of (γ, n) measurements this accelerator will make possible.

3. Bremsstrahlung Cross Section Measurements

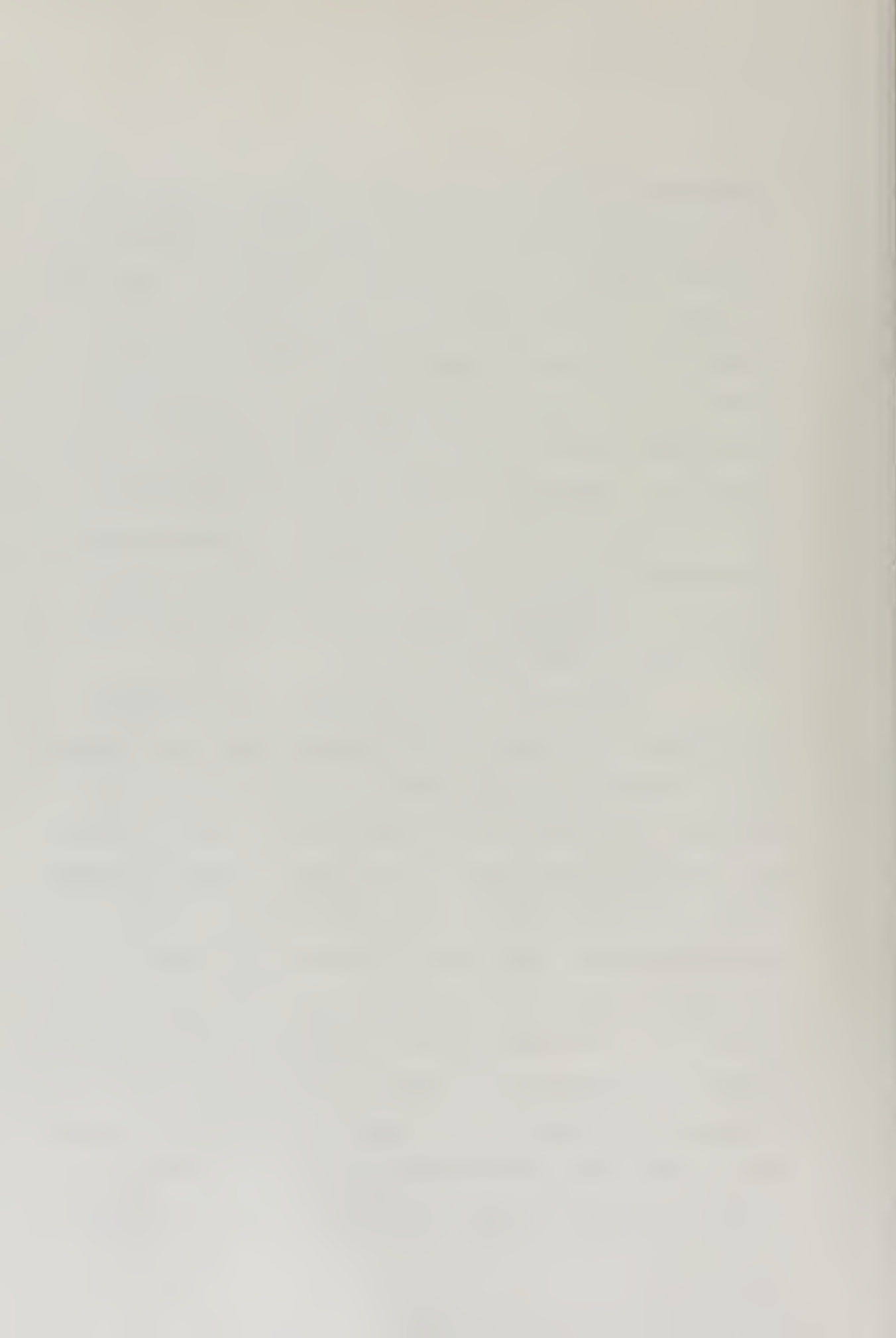
The present monochromator is suitable for use in a comprehensive series of measurements on the spectral and angular distribution of bremsstrahlung radiation for fractional photon energies up to .75. These measurements would provide values for the cross section differential in photon energy and angle and, with a monochromator set up for adjustable transmission values, would also give cross sections triply differential in photon energy, photon emission angle, and electron emission angle. Optimum measurements would require a transmission starting near two percent and with a capability of being reduced to very small values (this can be arranged using movable slit apertures). The bremsstrahlung measurements conducted in this research demonstrate the efficacy of this type of measurement.

4. Possible Technique Improvements

When the monochromator was originally conceived,

transmissions of the order of two percent were considered to be within easy reach. With such a high transmission, the monochromator would provide the experimentalist with a source of monoenergetic photons with as much as six times the available intensity using the high frequency limit of the bremsstrahlung spectrum. A transmission of one percent would provide a source comparable to the tip technique. Inability to reach the desired transmission values raises, then, the obvious question of how to improve the monochromator to attain the theoretically possible results. Some general suggestions will be made on possible methods of proceeding.

First of all, one clarifying point should be reiterated. The design of the present device was adapted from a spectrometer which used an entrance angle of 90 degrees. For use as a monochromator, the entrance angle was changed to 120 degrees in order to deflect the higher energy main beam away from the walls of the vacuum chamber and into a graphite collection box. This change reduced the available geometric solid angle of four percent of 4π to 2.24 percent in the final configuration. Since the optimum configuration of such spectrometers, as reported in the literature, allows at most fifty percent of the available geometric solid angle, the maximum value of $.265 \Omega$ GEOMETRIC achieved with the Notre Dame

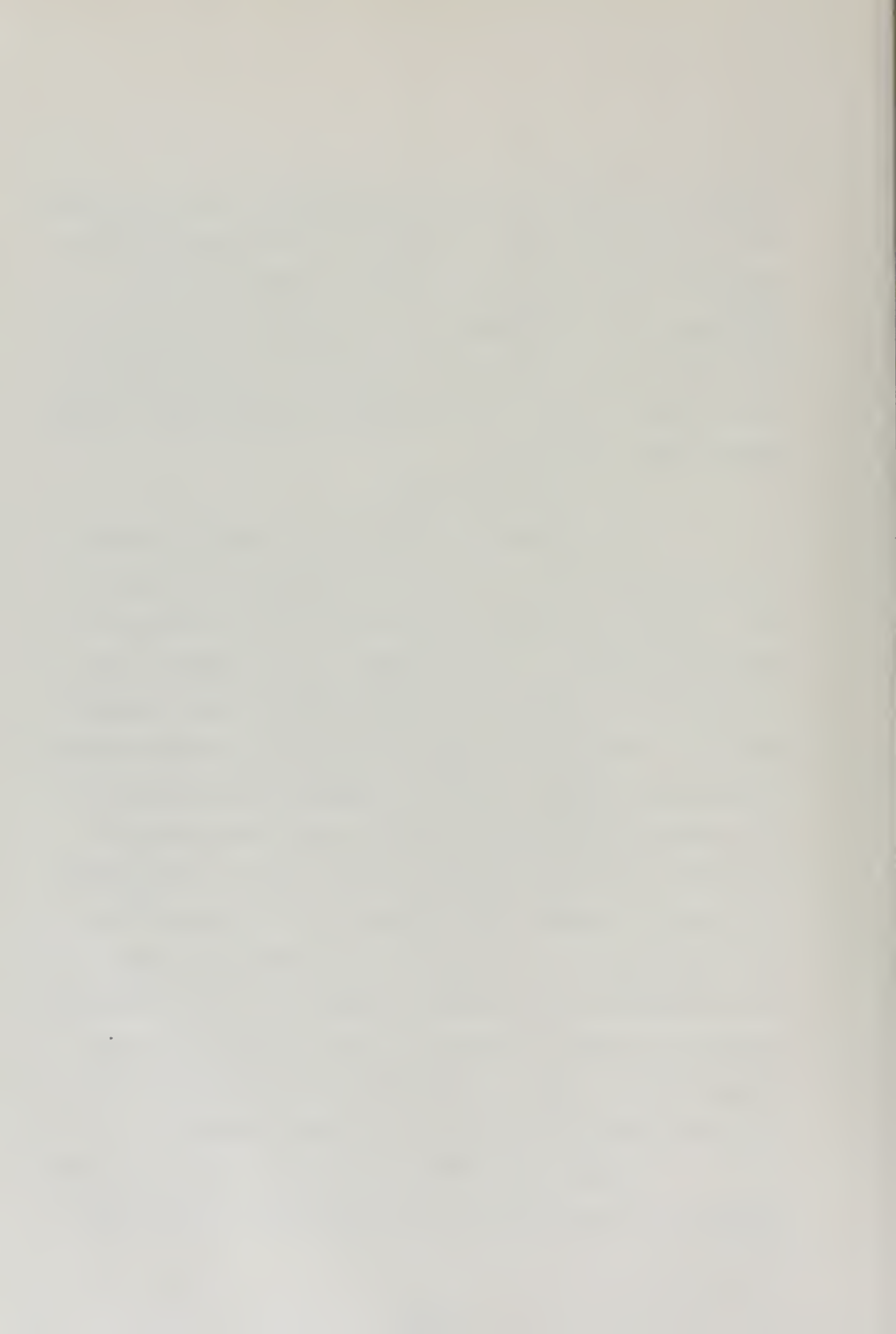


device indicates the present spectrometer may be operating at its practical limit. (Recall that 90 percent of the geometric solid angle was attained without slits or baffles with a resolution of 18 percent.) Thus, the major item to be considered in improving the monochromatic technique is raising the attainable transmission, without sacrificing resolution.

a) Pole Piece Design

The theoretical evaluation of magnetic sector spectrometers with $1/r$ fields as conducted by Jaffey et al. provides an ideal starting point for the design of a practical magnet. Close attention to the detailed consideration of fringe field effects should allow development of a theoretical design not too far removed from the optimum in reality. However, empirical determination of the final optimum profile shape is the sole practical criterion (i.e., the working version must be extensively laboratory tested). The method used by Bisgaard¹⁰⁰ in the development of a single gap beta-ray spectrometer is to be emulated (i.e., empirical shaping of the pole piece profile by study of the focal point of each ray of entrance angle, ψ_s). Though tedious, this method seems to come closest to producing an optimum magnet.

Strict attention must be paid to the pole piece profile in the vicinity of the pole piece symmetry axis



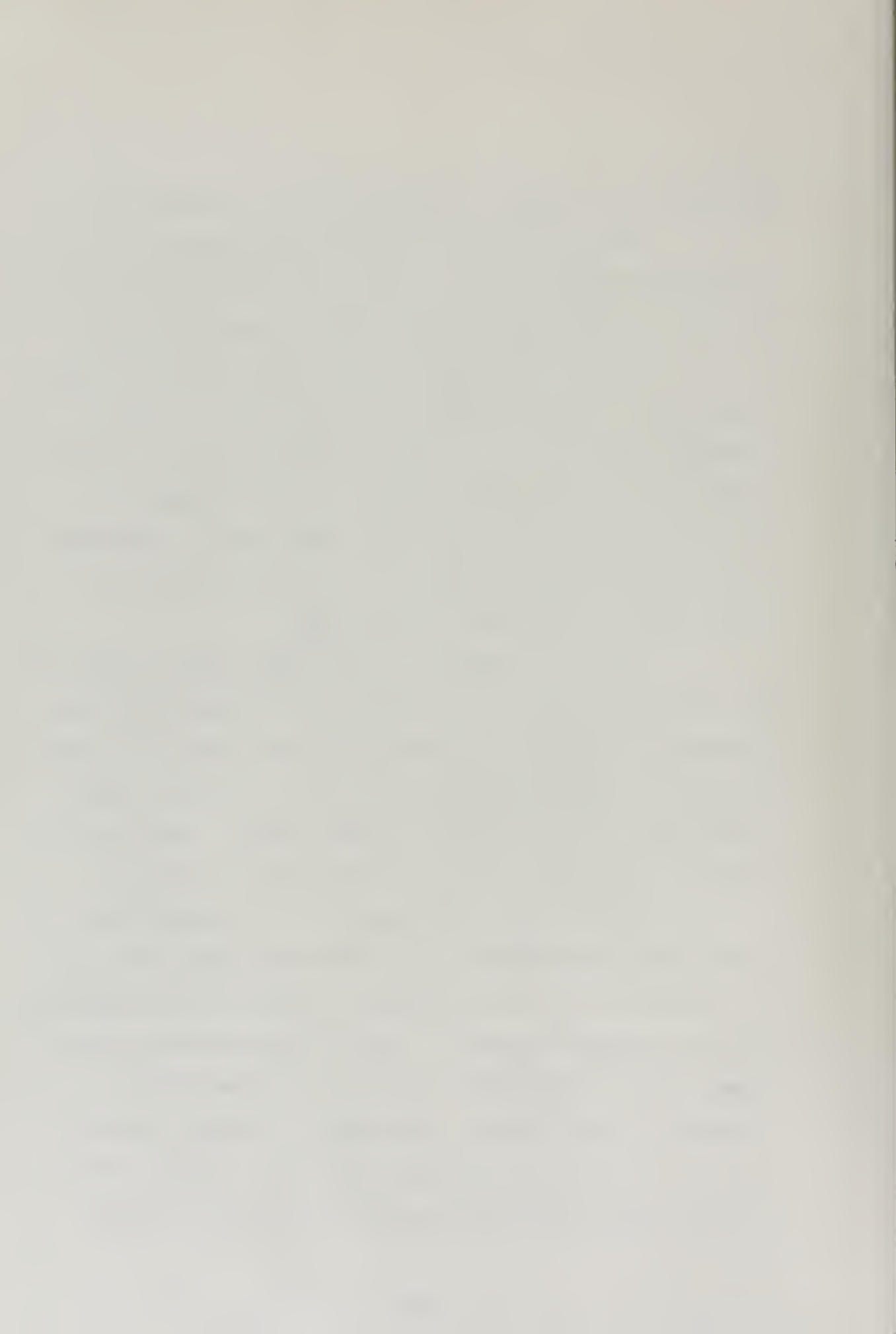
as anomolous fringe field effects arise at this point.

Use of a larger, deeper pole piece would allow a somewhat smaller entrance angle and would eliminate the necessity of passing the beam near the vertical baffle.

Bending the main electron beam through an angle less than 90 degrees would also allow use of a smaller entrance angle and, if a smaller rotating coil or a Hall probe was used as a field monitor, would increase the available geometric solid angle. Problems of background and geometry make this approach subject to severe restrictions but it is not without merit.

Use of an asymmetric pole piece design would allow the focal point of the system to be placed far from the entrance point of the main beam since the focal point could be almost arbitrarily located. A problem of maintaining sufficient distance between the main beam and the vacuum chamber is the major restriction in this case.

For a high energy beam such as is available from Tandem accelerators, the rectangular design as used by O'Connell et al. at Illinois is worthy of consideration. The small angular spread of the post-bremsstrahlung electrons tends to compensate for the low transmissions inherent in this design. Simplicity of design and construction are also meritorious features. Charge normalization poses the greatest problem since such a design



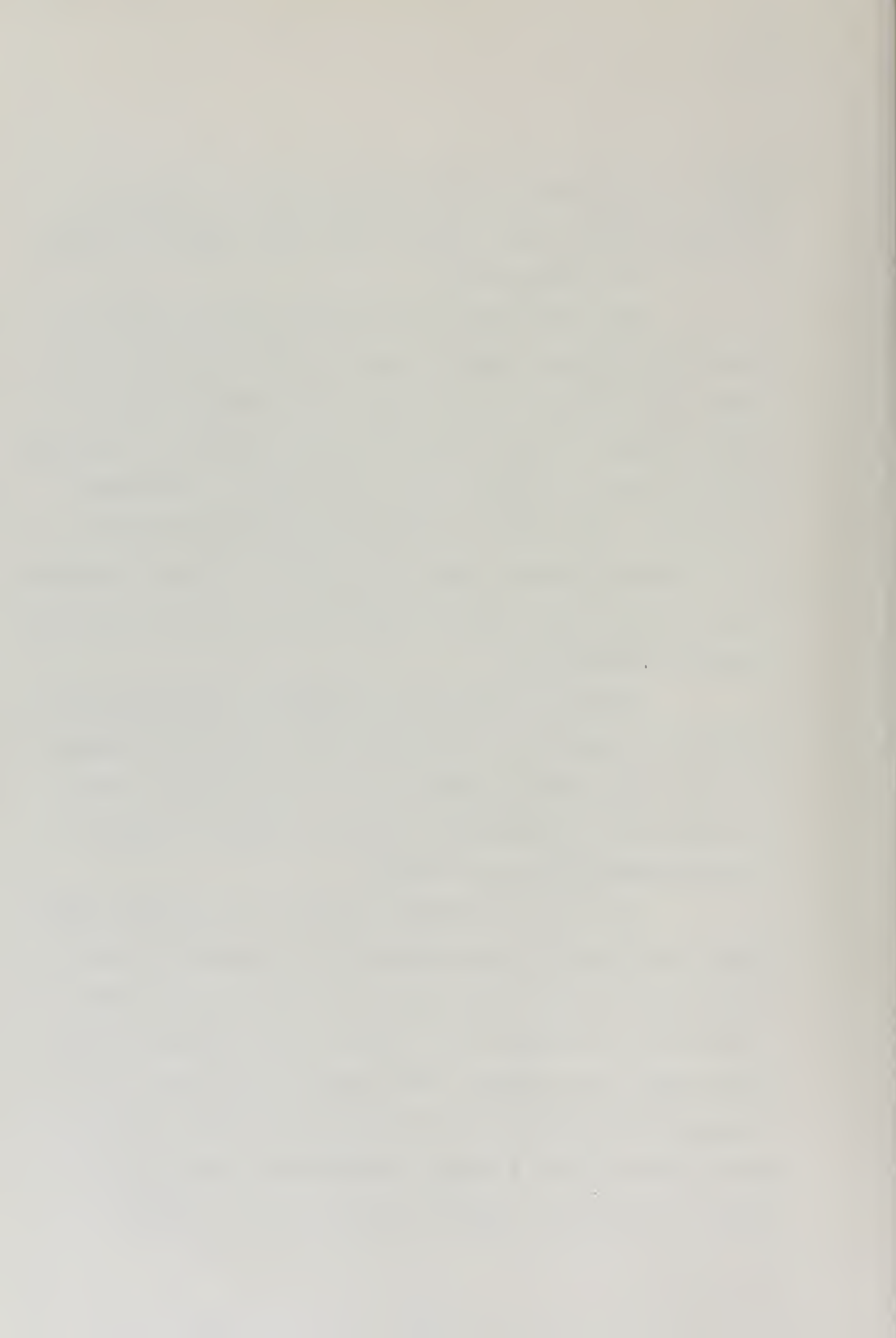
will not deflect the main beam more than a few degrees in the magnetic field unless a very large magnet is used.

b) System Size

The introduction of an exit baffle in the present monochromator played a role in reducing the anomalously large electron count rate. The placement of this baffle forced the main beam to be maintained in a position further from the electron exit slit than had previously been done. This effect contributed, at least in part, to a reduced electron count rate and was taken as evidence that the main beam should be kept as far from the electron detector as possible.

Since the effects of increasing the size of the system are linear to first order, the separation between the exit slit and the region of the vacuum box in which the main beam is monitored could be enlarged by use of a larger magnet-vacuum box system.

As well, the present design was originally used under the assumption that the full ± 15 degrees opening angle would be available for use in focusing the electrons. Due to fringe field effects, this assumption is valid only for a perfect point source. To avoid interaction between elastically scattered electrons and the pole pieces, use of a larger opening angle, say ± 20 degrees, baffled to a smaller angle, say ± 15 degrees, is

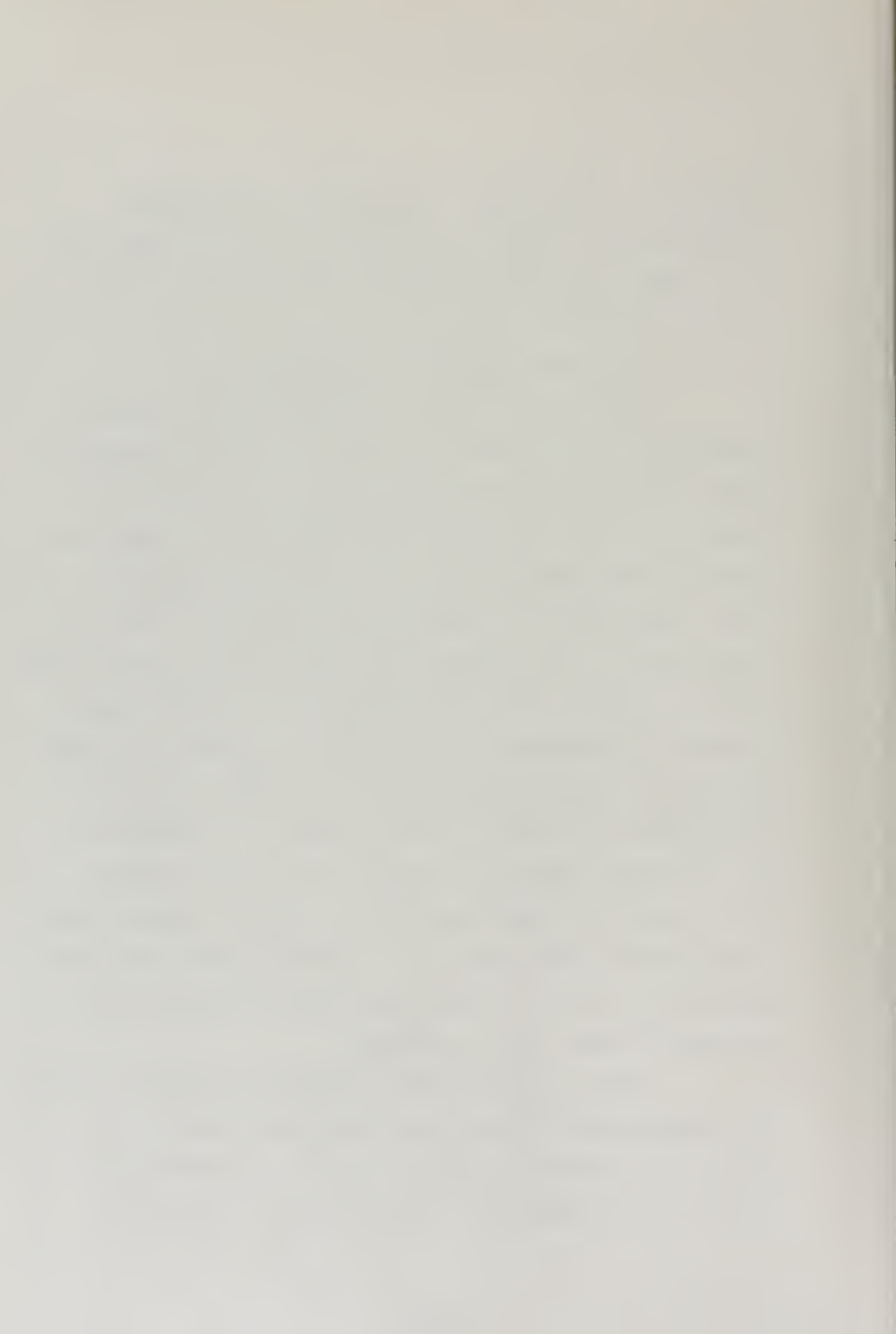


important. (Use of such a procedure on the present system gave a deleterious effect on the transmission due, most likely, to the severe restriction imposed on the available geometric solid angle.)

c) Detection System and Electronics

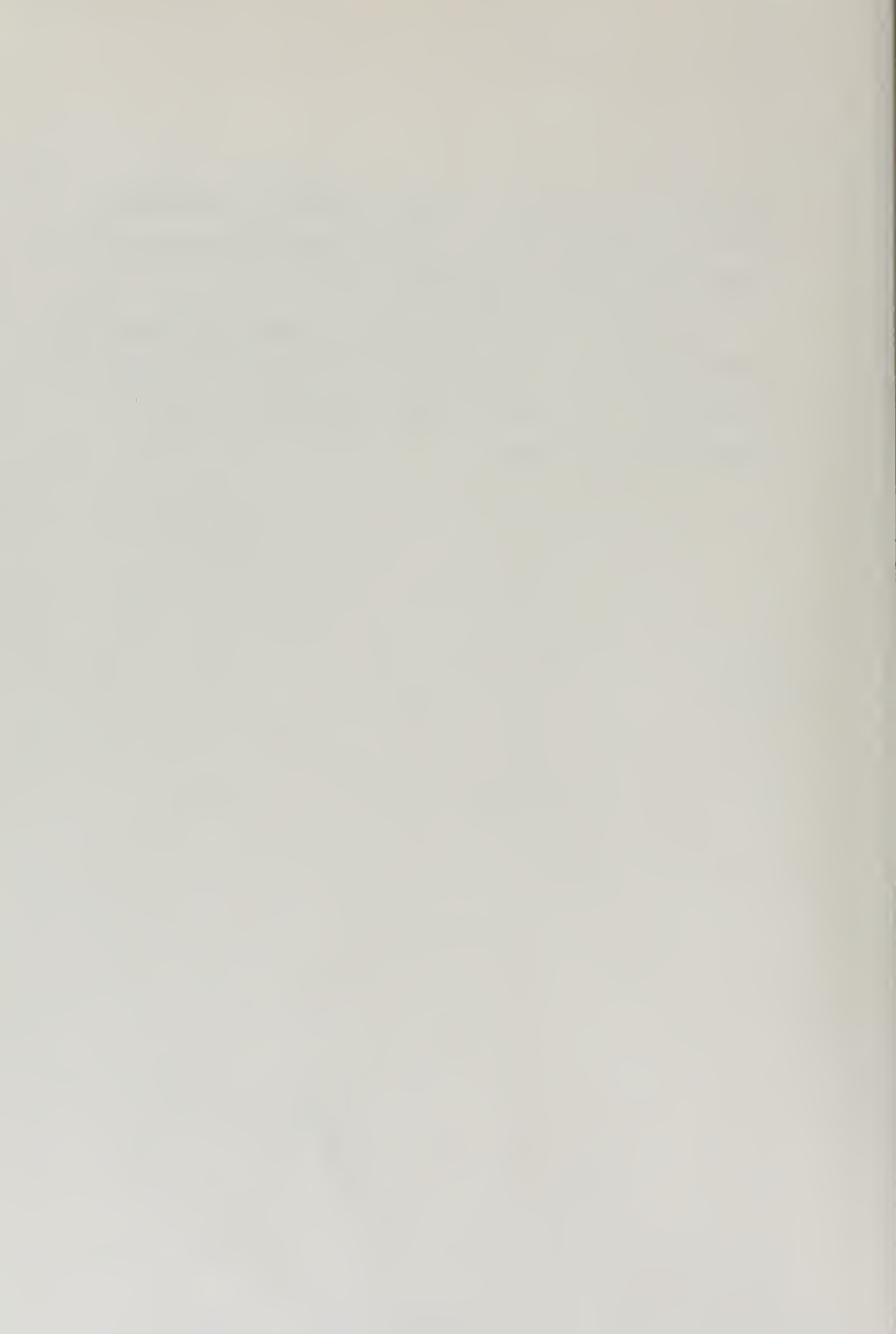
The present single electron detector could be replaced by several such detectors in the following manner. The plastic scintillator now in use would be replaced by, say, six plastic scintillators each using an optical fiber connection to its multiplier phototube. Thus, the current now carried by one phototube would be spread over six PM tubes and the total electron count rate could be raised. There are a number of problems associated with this scheme. One is the dimensions of the exit slit and, thus, the imposed size of the scintillators and light pipes. Another is the prevention of scattering of the electrons from one scintillator to another (due to their close proximity) producing, in effect, two or more coincidences rather than one. Increasing the size of the magnet would assist in reducing these problems as some increase in slit size would result.

Use of the RCA-8575 multiplier phototube in both the electron and photon detection systems would allow lower discriminator settings due to the inherently low noise characteristics of this phototube. Use of this



phototube and time-to-height conversion coincidence systems produce resolving times in the one nanosecond region using NaI(Tl) detectors.¹⁰¹

While changes in the detection and electronic systems would not improve the efficiency of the monochromator, improvement in the flexibility of the technique might result.



APPENDIX F

Transmission and Resolution

The transmission and resolution of the inclined plane pole-face spectrometer was measured using the 625 keV K-conversion electron line of ^{137}Cs . The source was centered at the bremsstrahlung foil position and the number of electron counts detected was measured as a function of the monochromator magnetic field.

The resolution is defined by

$$R = \Delta p / p$$

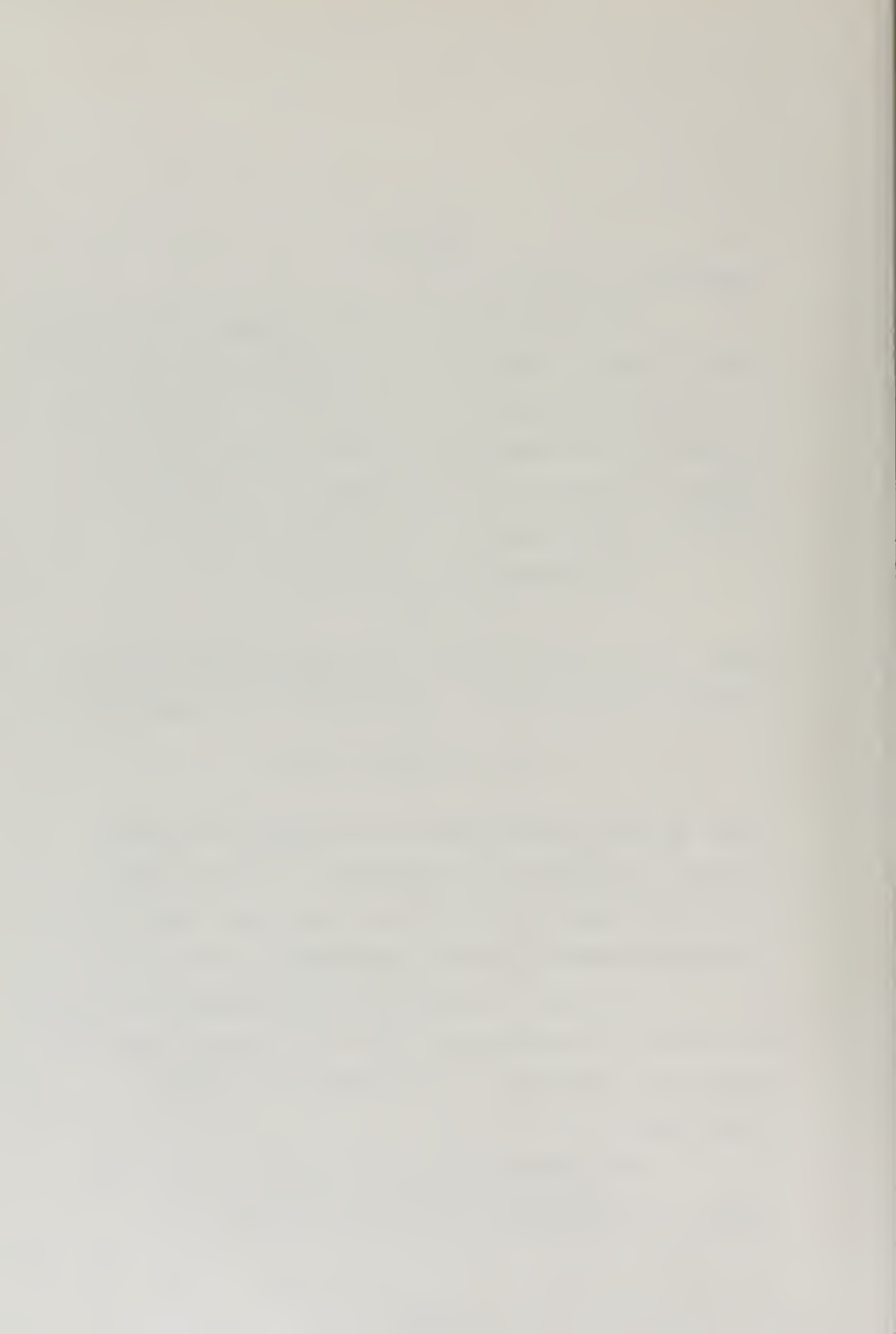
where Δp is the full width at half-maximum of the detected conversion line. The transmission is defined by

$$T = N_e(\text{peak}) / N_e(\text{total})$$

where $N_e(\text{peak})$ is the number of electrons per second counted in the electron detector at the peak of the K-conversion line and $N_e(\text{total})$ is the total number of K-conversion electrons emitted per second by the source.

$N_e(\text{total})$ is determined by measuring the strength of the 661 keV transition in the ^{137}Cs source, then multiplying this value by α_K , the known K-conversion coefficient.

The transmission can be related to the half-angle of the electron emission solid angle by the



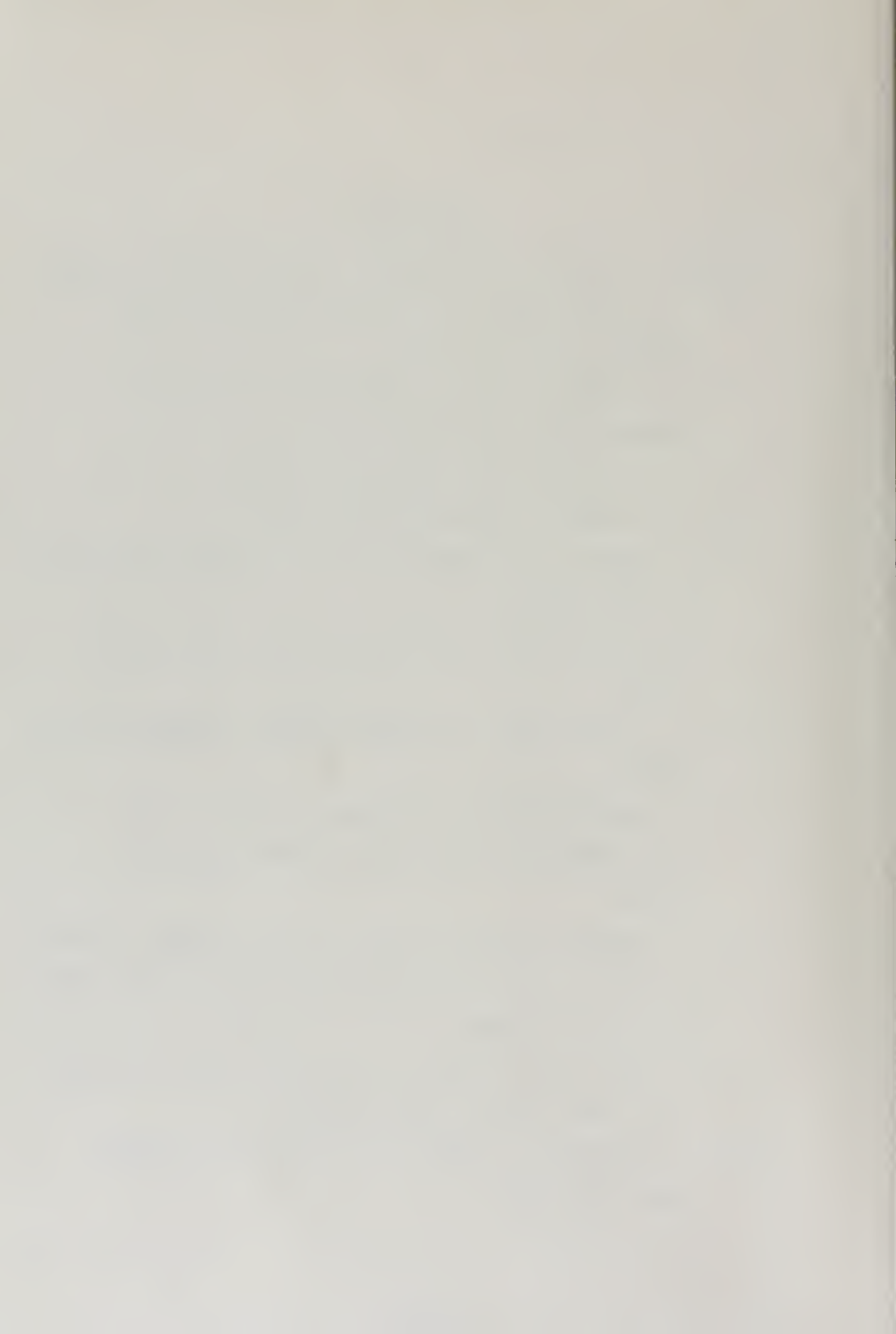
expression

$$T = \frac{1}{2} (1 - \cos \theta_p) .$$

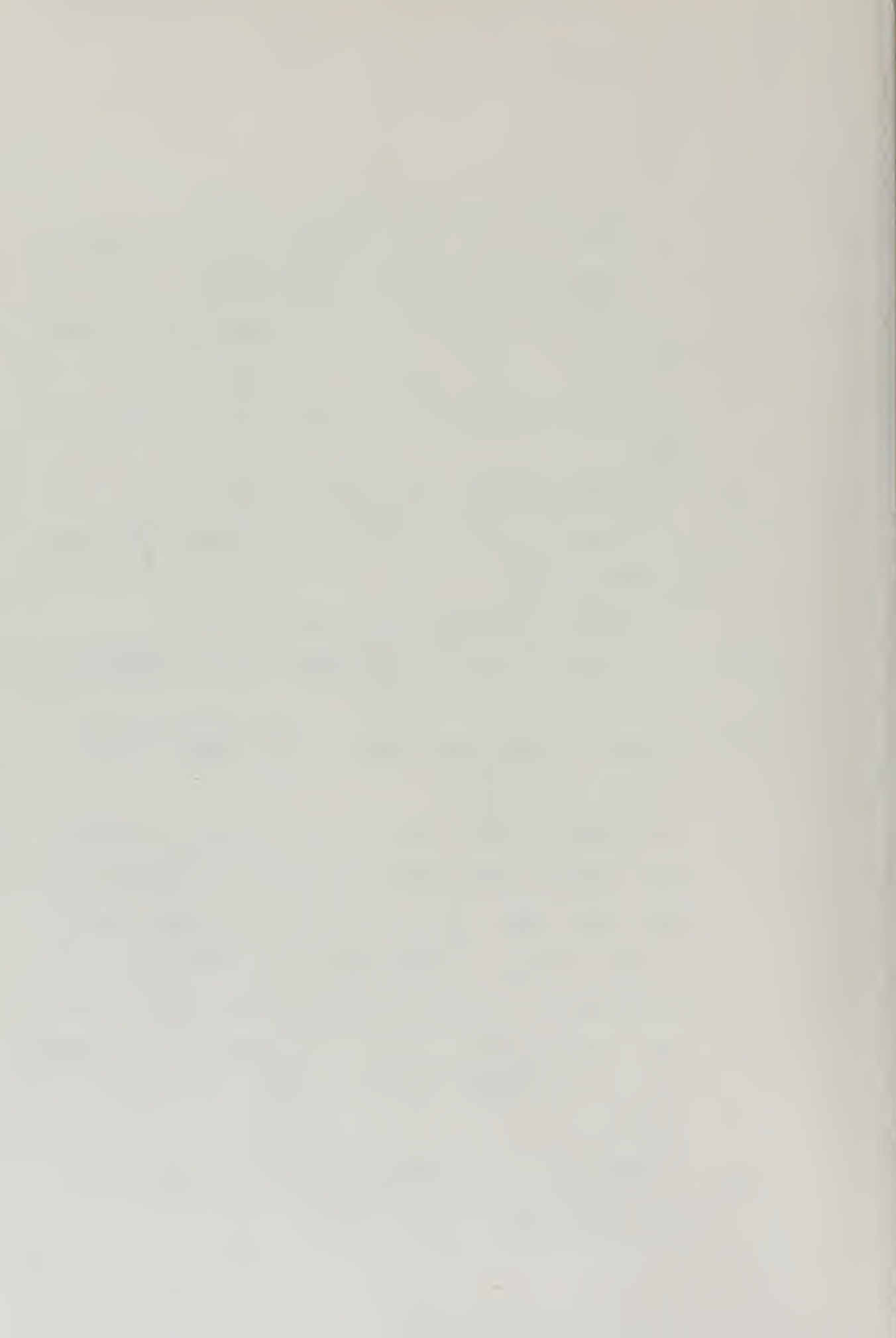


REFERENCES

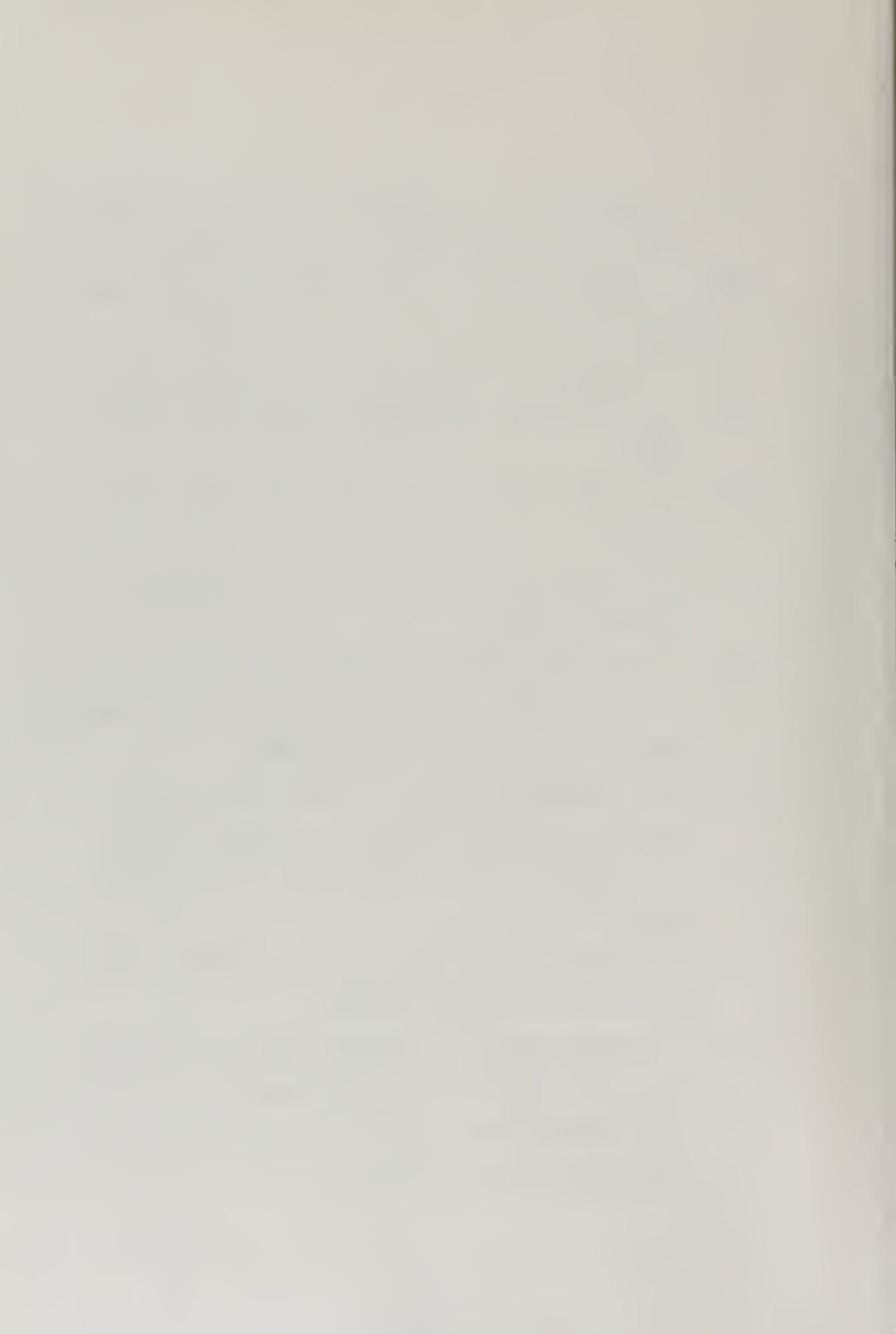
- 1) W. A. Heitler and F. Sauter, Nature 132, 892 (1933).
- 2) H. A. Bethe and W. A. Heitler, Proc. Roy. Soc. (London) A146, 83 (1934).
- 3) J. C. Jaeger and H. R. Hulme, Proc. Roy. Soc. (London) A153, 443 (1936).
- 4) J. C. Jaeger, Nature 137, 781 (1936).
- 5) J. C. Jaeger, Nature 148, 86 (1941).
- 6) H. Davies, H. A. Bethe, and L. C. Maximon, Phys. Rev. 93, 788 (1954).
- 7) H. A. Bethe and L. C. Maximon, Phys. Rev. 93, 768 (1954).
- 8) D. S. Moroi and C. L. Hammer, Nuovo Cimento 30, 1396 (1963).
- 9) J. Chadwick, P. M. S. Blackett, and G. P. S. Occhialini, Proc. Roy. Soc. (London) A144, 235 (1934).
- 10) J. Chadwick, Proc. Roy. Soc. (London) A142, 1 (1933).
- 11) L. Meitner and K. Philipp, Naturwiss. 21, 286 (1933) and 24, 486 (1933).
- 12) M. Curie and F. Joliot, C. R. Acad. Sci. Paris 196, 1105 (1933) and 196, 1581 (1933).
- 13) L. Simons and K. Zuber, Proc. Roy. Soc. (London) A159, 383 (1937).



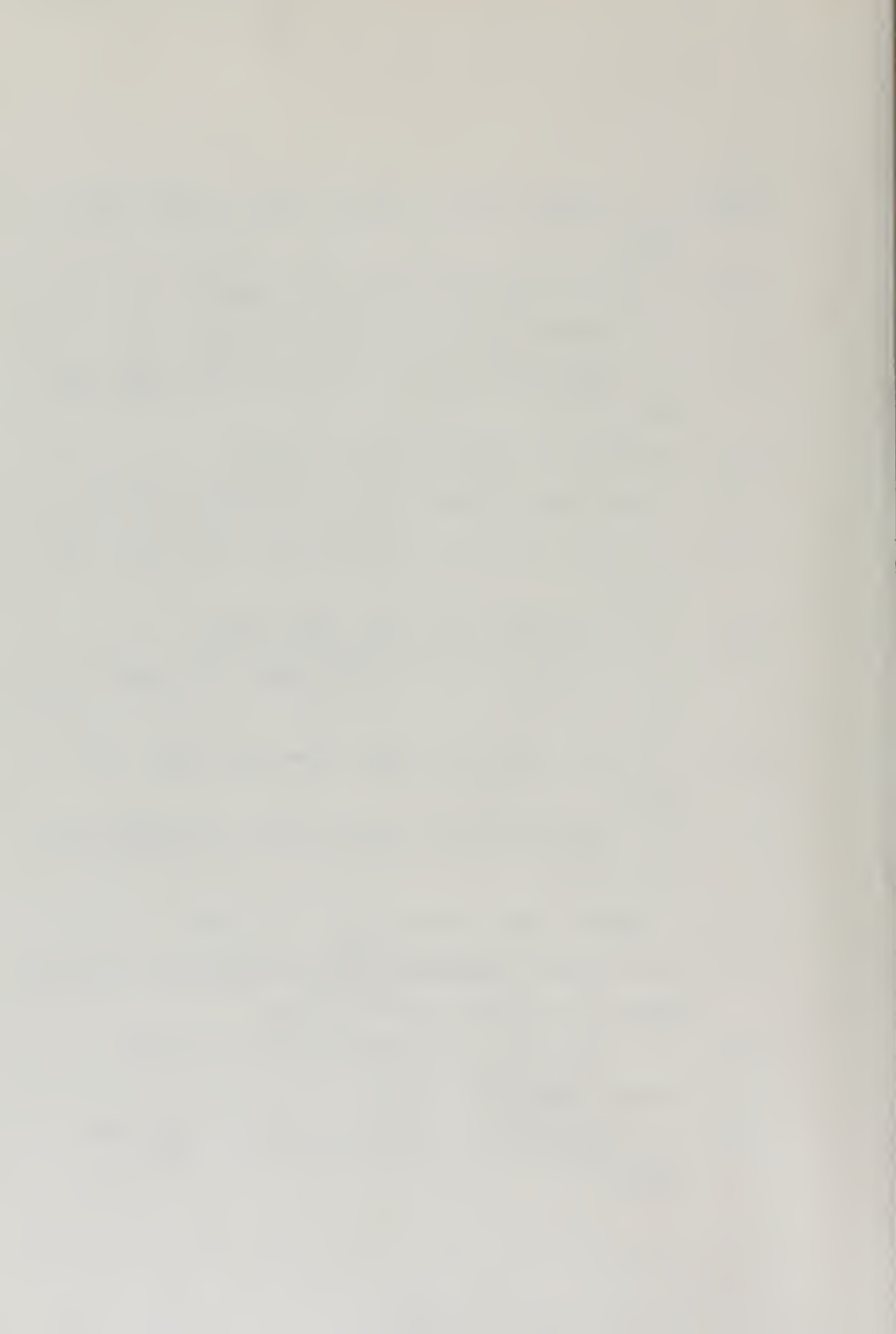
- 14) M. Immellmann, Naturwiss. 24, 61 (1936).
- 15) H. Klarman and W. Bothe, Z. Phys. 101, 489 (1936).
- 16) G. D. Adams, Phys. Rev. 74, 1707 (1948).
- 17) G. D. Adams and A. T. Nordsieck, Phys. Rev. 63, 60A (1943).
- 18) R. L. Walker, Phys. Rev. 76, 527 (1949) and 76, 1440 (1949).
- 19) J. L. Lawson, Phys. Rev. 75, 433 (1949).
- 20) J. W. Dewire, A. Ashkin, and L. A. Beach, Phys. Rev. 83, 505 (1951).
- 21) C. R. Emigh, Phys. Rev. 86, 1028 (1952).
- 22) E. S. Rosenblum, E. F. Schrader, and R. M. Warner, Phys. Rev. 88, 612 (1952).
- 23) B. Hahn, E. Baldinger, and P. Huber, Helv. Phys. Acta 25, 505 (1952).
- 24) I. E. Dayton, Phys. Rev. 89, 544 (1953); P. Schmid and P. Huber, Helv. Phys. Acta 27, 152 (1954); H. I. West, Phys. Rev. 101, 915 (1956); S. Standil and R. D. Moore, Canad. J. Phys. 34, 1126 (1956); S. Standil and V. Shkolnik, Canad. J. Phys. 35, 1156 (1957) and 36, 1154 (1958); P. P. Singh, H. W. Dasso, and G. M. Griffiths, Canad. J. Phys. 37, 1055 (1959).
- 25) J. Rama Roa, V. Lakshminarayna, and S. Jnanananda, Proc. Phys. Soc. 81, 949 (1963).



- 26) J. Rama Roa, V. Lakshminarayna, and S. Jnanananda,
Indian Jour. Appl. Phys. 1, No. 6, 199 (1963).
- 27) T. Yamazaki and J. M. Hollander, Phys. Rev. 140,
B630 (1965).
- 28) C. E. Dick, Ph.D. Thesis, Univ. of Notre Dame (1961).
- 29) J. W. Weil and B. D. McDaniel, Phys. Rev. 86, 582
(1952).
- 30) J. W. Weil and B. D. McDaniel, Phys. Rev. 92, 391
(1953).
- 31) R. Cence, Ph.D. Thesis, Univ. of California,
UCRL-8921 (1959).
- 32) J. Goldemberg, Phys. Rev. 93, 1426 (1954).
- 33) J. S. O'Connell, P. A. Tipler, and P. Axel, Technical
Report 21, Univ. of Illinois (1961).
- 34) P. A. Tipler, P. Axel, N. Stein, and D. Sutton,
Technical Report 33, Univ. of Illinois (1962).
- 35) F. T. Kuchnir, Ph.D. Thesis, Univ. of Illinois
(1965).
- 36) R. L. Walter, M. S. Shea, and W. C. Miller, Bull.
Am. Phys. Soc. 5, 479 (1960).
- 37) O. Kofoed-Hansen, J. Lindhard, and O. B. Nielsen,
Mat. Fys. Medd. Dan. Vid. Selsk 25, No. 16 (1950).
- 38) O. B. Nielsen and O. Kofoed-Hansen, Mat. Fys. Dan.
Vid. Selsk 29, No. 6 (1955).



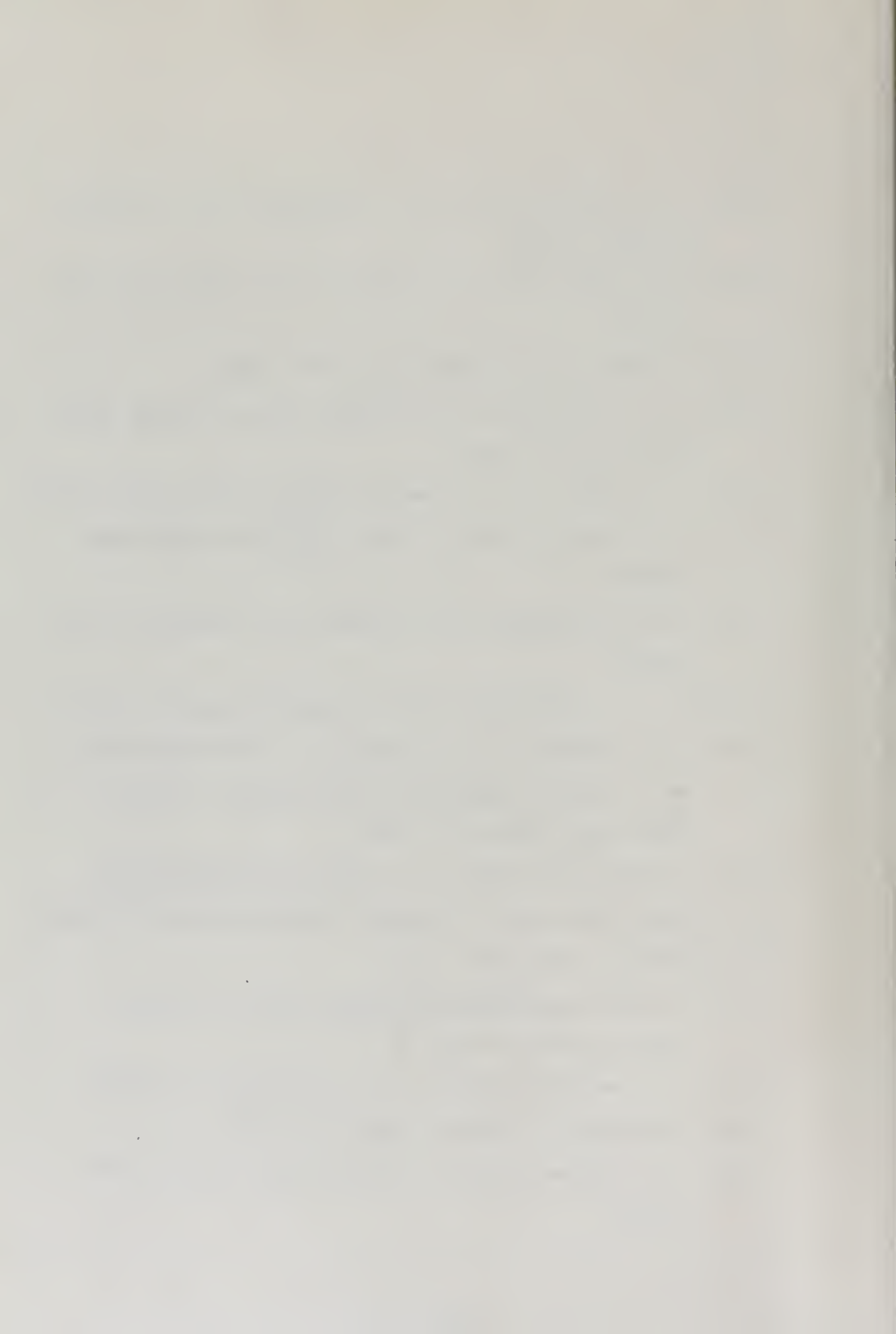
- 39) D. L. Malaker, Ph. D. Thesis, Univ. of Notre Dame (1963).
- 40) F. Sauter, Ann. Physik, 20, 404 (1934).
- 41) L. I. Schiff, Phys. Rev. 83, 252 (1951).
- 42) R. L. Gluckstern and M. H. Hull Jr., Phys. Rev. 90, 1030 (1953).
- 43) H. Amrehn, Z. Physik 144, 529 (1956).
- 44) D. Ross, Ph.D. Thesis, Univ. of Wurtzberg (1957).
- 45) J. W. Motz and R. C. Placious, Phys. Rev. 109, 235 (1958).
- 46) J. W. Motz, Phys. Rev. 100, 1560 (1955).
- 47) D. H. Rester and W. E. Dance, Phys. Rev. 161, 85 (1967).
- 48) N. Starfelt and H. W. Koch, Phys. Rev. 102, 1598 (1956).
- 49) E. V. Weinstock and J. Halpern, Phys. Rev. 100, 1293 (1955).
- 50) J. Pervin, Compt. rend. 197, 1100 (1933).
- 51) W. A. Heitler, Quantum Theory of Radiation, Third Ed., Oxford Univ. Press, London (1954).
- 52) J. C. Jaeger and H. R. Hulme, Proc. Roy. Soc. (London) A148, 708 (1935).
- 53) H. A. Bethe, Proc. Cambridge Phil. Soc. 30, 524 (1934).



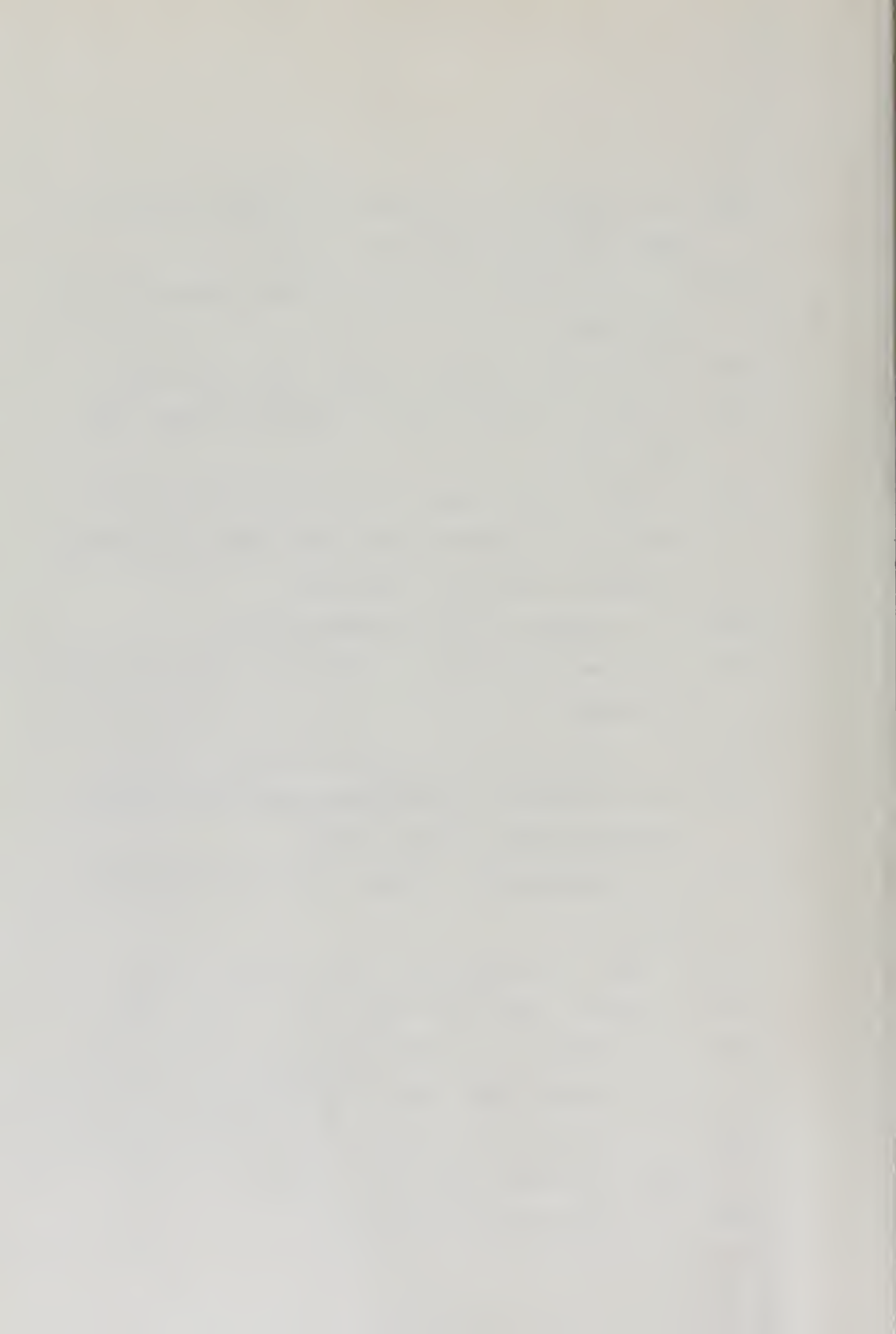
- 54) H. A. Bethe and J. Ashkin, Experimental Nuclear Physics, Vol 1, Ed. by E. Segre, J. C. Wiley and Sons, New York (1953).
- 55) P. V. C. Hough, Phys. Rev. 73, 266 (1948).
- 56) G. Racah, Nuovo Cimento 13, 69 (1936).
- 57) R. Jost, J. M. Luttinger, and M. Slotnik, Phys. Rev. 80, 189 (1950).
- 58) C. D. Zerby and H. S. Moran, Technical Report Oak Ridge National Laboratory, ORNL-CF-56-124 (1956).
- 59) O. Klein and Y. Nishina, Z. Physik 52, 853 (1929).
- 60) W. Franz, Z. Physik 98, 314 (1935).
- 61) P. Debye, Phys. Z. 31, 419 (1930).
- 62) G. E. Brown, R. E. Peirels, and J. B. Woodward, Proc. Roy. Soc. A227, 51 (1954).
- 63) J. J. Thomson, Conduction of Electricity Through Gases, Third Ed., Cambridge Univ. Press, Cambridge (1933).
- 64) C. M. Davissan in α . β . γ Ray Spectroscopy, Vol. 1, Ed. by K. Siegbahn, North Holland Publishing Co., Amsterdam (1965).
- 65) W. Zernik, Phys. Rev. 120, 549 (1960); F. Rohrllich and R. L. Gluckstern, Phys. Rev. 86, 1 (1952); H. A. Bethe and F. Rohrllich, Phys. Rev. 86, 10 (1952); P. Kessler, J. Phys. Radium 19, 739 (1958).



- 66) K. G. Standing and J. V. Jovanovich, Can. J. Phys. 40, 622 (1962).
- 67) H. W. Koch and J. W. Motz, Rev. Mod. Phys. 31, 920 (1959).
- 68) G. Racah, Nuovo Cimento 11, 476 (1934).
- 69) P. T. McCormick, D. G. Kiefer, and G. Parzen, Phys. Rev. 103, 29 (1956).
- 70) J. J. Kepes, Ph.D. Thesis, Univ. of Notre Dame (1957).
- 71) D. R. Connors, Ph.D. Thesis, Univ. of Notre Dame (1956).
- 72) H. W. Richardson, Proc. Phys. Soc. (London) 59, 791 (1947).
- 73) H. O. W. Richardson, Phil. Magazine 40, 233 (1949).
- 74) A. H. Jaffey, C. A. Mallmann, J. Suarez-Etchepare, and T. Suter, Technical Report Argonne National Laboratory, ANL-6222 (1960).
- 75) G. Knop and W. Paul in α - β - γ Ray Spectroscopy, Vol. 1, Ed. by K. Siegbahn, North-Holland Publishing Company, Amsterdam (1965).
- 76) W. Bothe, Handbuch der Physik, 22/2, Springer-Verlag, Berlin (1932) p. 1.
- 77) E. J. Williams, Proc. Roy. Soc. A169, 531 (1950).
- 78) G. Moliere, Z. Naturf. 3a, 78 (1948).
- 79) H. S. Snyder and W. T. Scott, Phys. Rev. 76, 220 (1949).



- 80) A. O. Hanson, L. H. Lanzl, E. M. Lyman, and M. B. Scott, Phys. Rev. 84, 634 (1951).
- 81) L. A. Kulchitsky and G. D. Latyshev, Phys. Rev. 61, 254 (1942).
- 82) W. Paul and H. Reich, Z. Phys. 127, 429 (1950).
- 83) G. Knop, A. Minton, and B. Nellen, Z. Phys. 165, 533 (1961).
- 84) A. Febel and G. Knop, Z. Phys. 174, 257 (1963).
- 85) RCA Electron Tube Handbook, HB3, Radio Corporation of America, Harrison, New Jersey.
- 86) P. R. Chagnon, Private Communication.
- 87) C. M. Davisson and R. D. Evans, Rev. Mod. Phys. 24, 79 (1952).
- 88) R. L. Heath, A. E. C. Report IDO-16408 (1957).
- 89) C. E. Crouthamel, Applied Gamma-Ray Spectroscopy, Pergamon Press, London (1960).
- 90) P. G. Loscoe, Ph.D. Thesis, Univ. of Notre Dame (1966).
- 91) J. Huck, C. R. Acad. Sc. Paris 6, 260 (1965).
- 92) T. Jenkins, Bull. Am. Phys. Soc. 1, 167 (1956).
- 93) C. P. Browne, A. L. Schaller, W. C. Miller, and S. E. Darden, Nucl. Inst. and Methods 30, 145 (1964).
- 94) C. P. Browne, J. A. Caley, J. E. Erskine, and K. L. Worsh, Phys. Rev. 120, 905 (1960).
- 95) R. J. Foust, (to be published).



- 96) A. L. Schaller and W. C. Miller, (to be published).
- 97) E. C. Booth and K. A. Wright, Nucl. Phys. 35, 472
(1962).
- 98) E. C. Booth, B. Chasan, and K. A. Wright, Nucl. Phys.
57 (1964).
- 99) P.M. Endt and C. Van der Leun, Nucl. Phys. 34, 1
(1962).
- 100) K. M. Bisgård, Nucl. Inst. and Methods 29, 213
(1964).
- 101) J. P. Hurley, V. L. Dagragnano, and J. M. Mathiesen,
Nucl. Inst. and Methods 51, 299 (1967).





thesG22

Absolute pair creation cross sections us



3 2768 002 01077 9

DUDLEY KNOX LIBRARY